Centimeter-Level Accuracy Path Tracking Control of Tractors and Actively Steered Implements

Vom Fachbereich Maschinenbau und Verfahrenstechnik

der Technischen Universität Kaiserslautern zur Verleihung des akademischen Grades

DOKTOR-INGENIEUR (DR.-ING.)

genehmigte Dissertation

von

DIPL.-ING. ROLAND WERNER

aus Erlangen

Berichterstatter:	Prof. Dr.-Ing. Steffen Müller
	Prof. Dr.-Ing. Jörg Seewig
Vorsitzender:	Prof. Dr.-Ing. Bernd Sauer
Dekan:	Prof. Dr.-Ing. Christian Schindler

Veröffentlichung als vom Fachbereich Maschinenbau und Verfahrenstechnik der Technischen Universität Kaiserslautern genehmigte Dissertation.

Kaiserslautern, 21.05.2015.

Acknowledgments

Abstract

Sustainable and efficient agricultural practices lay the foundation for feeding a growing world population from limited resources. For that reason, the focus of agriculture is now shifting from methods based on large area uniform treatment towards methods considering actual needs on a local scale down to single plant treatment. Key enabler for these new practices is accurate control of agricultural machinery. Within the last decade Global Positioning System (GPS) based path tracking control of tractors, in particular, became a widely used technology in agriculture. Highly sophisticated tractor path tracking control, however, revealed that control of the implement, performing the actual task, is equally or even more important. To address this increasing interest this work focuses on accurate path tracking control of both tractors and implements. The latter, as an prerequisite for improved control, are equipped with steering actuators like steerable wheels or a steerable drawbar, i.e. the implements are considered to be actively steered. Since it was only recently that steerable implements sparked interest, this work contributes both new plant models and new control approaches for those kinds of tractor-implement combinations.

Modeling faces challenges from the numerous variants of implements and actuator types that need to be accounted for. For that reason derivation of all plant models was performed in a systematic way allowing for automation using computer algebra software. A tractor towing an implement with steerable wheels and a steerable drawbar was used as an example throughout the work. Plant models of different complexity have been developed. All variants, however, are stated as explicit differential equations to allow for further analysis. For controller and estimator design simple kinematic models based on geometric properties and wheel velocity constraints have been developed. Those models can be parameterized without difficulties in order to account for variants. For simulation and further analysis more detailed dynamic models of tractor-implement combinations have been derived. Those models account for forces and moments causing the vehicle motion and allow the depiction of disturbances resulting e.g. from gravity on slopes. As a downside, however, those models require tire and inertial parameters which are difficult to obtain for a large set of variants. Parameterization therefore was only carried out for a single experimental hardware setup. Dynamic modeling of steerable implements in particular faces challenges from actuators between tractor and implement. Within this work it was proposed to consider them as time dependent or rheonomic constraints, assuming an underlying steering controller is in place. This assumption, together with a systematic derivation using Lagrangian mechanics and some well-chosen intermediate coordinate transformations, made it possible to handle the resulting lengthy equations and to obtain the associated explicit differential equations.

Control of combinations of tractors and steerable implements is not only required to be accurate up to centimeter level, but must also support a multitude of different implement

and actuator variants. At the same time robustness or adaption is required to cope with uncertainties and disturbances, e.g. resulting from changing tire-soil interaction. In addition, the final setup, performed by the operator, must remain simple and intuitive. Last but not least the resulting controller is required to run on an Electronic Control Unit (ECU) with limited computational capacity. In order to meet those requirements an extensive survey and comparison of path tracking control approaches for passenger cars, tractor-trailer and tractor-implement combinations has been performed. A Linear-Quadratic Regulator (LQR) was considered as the most promising starting point. To reduce both tuning and implementation effort, LQR state feedback control was approximated by means of static output feedback using measured angular and positional deviations (heading and lateral errors of tractor and implement) from a desired path. The output feedback was designed to approximate the dominant eigenvalues of the LQR state feedback closed loop system. Controller tuning was based on choosing weights for steering inputs as well as heading and lateral errors. The individual error weights allowed emphasizing particular objectives for a given task, focusing e.g. on implement lateral position and orientation control. The relative weight between inputs and tracking errors served as an overall gain, which was the only parameter that had to be found in experiments in the field. Experiments revealed that additional measures are required to account for disturbances resulting from wheel side-slip on slopes and in curves. Two variants have been implemented to account for that. The first variant extended LQR using integral control (LQR w. I). The second variant invoked disturbance feedforward based on Extended Kalman Filter (EKF) wheel-side slip estimates using an extended kinematic model (LQR w. EKF). For all variants an additional feedforward control law based on the path curvature was found to be advantageous. The respective control laws for steerable implements have been newly derived in this work.

As the final part of this work, numerous simulations and experiments have been carried out. The latter relied on a mid-size tractor towing a custom built implement with numerous steering actuators. Simulations utilized a non-linear dynamic model which was parameterized to depict the experimental setup. Initial condition responses in simulations and experiments indicated that LQR w. I in particular is prone to overshooting behavior and windup resulting from steering actuator absolute and rate limits. Absolute limits had been considered in anti-windup measures already. Including rate limits still might offer room for improvement. Simulations on slopes and experiments on circular paths showed that both LQR w. I and LQR w. EKF are effective measures to reduce steady-state tracking errors resulting from wheel side-slip. To consider a numerical example, experiments have been performed on a level field of dry loam, which was tilled and slightly compacted due to multiple passes. The path was circular with 20 m radius and the tractor forward velocity was 3 m/s. In those circumstances LQR w. I with tractor wheel steering only resulted in 3.3 cm, 5.5 cm, and 1.0° standard deviation (SD) as well as 0 cm, -27.7 cm,

and -0,7° mean for tractor lateral error, implement lateral error, and implement heading error. By using only one steering input it is generally possible to achieve zero steady-state error for only one controlled variable if constant disturbances are present. The tractor lateral error was chosen to be this controlled variable in the example above. In contrast, using LQR w. I with tractor wheel steering as well as implement drawbar and wheel steering resulted in 3.2 cm, 2.0 cm, and 0.7° SD with zero mean for tractor lateral error, implement lateral error, and implement heading error. In this scenario three actuators were available and tractor and implement lateral error as well as implement heading error could be chosen as controlled variables. Similarly LQR w. EKF using three actuators resulted in 3.2 cm, 2.2 cm, and 0.3° SD with -2.0 cm, 1.3 cm, and -0.4° mean. Experiments considering transient conditions while tracking paths consisting of straights, clothoids and arc segments resulted in similar tracking errors as long as curvature change rates were moderate ($0.1°/\text{m}^2$). Increased curvature change rates resulted in larger deviations from the assumption of constant disturbances due to wheel side-slip and hence also resulted in slightly increased tracking errors. Finally, a parameter variation study has been carried out. Experiments with different tractor velocities indicated that LQR w. I in particular must account for velocity changes. Gain scheduling was proposed as a possible solution. Implementation, however, is still pending. Simulations have been performed with tire and inertial parameters varied by $\pm50\%$. Closed loop systems for both LQR w. I and LQR w. EKF remained stable during parameter variation. Tire cornering stiffness parameters, however, unsurprisingly exhibited a strong influence on path tracking accuracy in transient conditions.

Kurzfassung

Nachhaltigkeit und Effizienz in der Landwirtschaft bilden die Grundlage der Ernährung einer wachsenden Weltbevölkerung mittels begrenzter Ressourcen. Das Interesse im Bereich landwirtschaftlicher Anbauformen verlagert sich daher vermehrt von großflächig einheitlichen Praktiken zu bedarfsgerechteren lokalen Bearbeitungsformen bis hin zur Einzelpflanzenbehandlung. Genaue Regelung und Steuerung landwirtschaftlicher Geräte stellt hierbei eine Schlüsseltechnologie dar. Insbesondere Global Positioning System (GPS) basierte Lenksysteme zur automatischen Querführung von Traktoren auf vordefinierten Pfaden erfuhren in den letzten 10 Jahren eine weite Verbreitung. Hochgenaue Traktorlenksysteme offenbarten dabei, dass die genaue Querführung der Anbaugeräte selbst von mindestens ebenso großer Bedeutung ist. Um dem gesteigerten Interesse gerecht zu werden widmet sich diese Arbeit der Querführung von sowohl Traktoren als auch Anbaugeräten. Als Voraussetzung zur verbesserten Querführung verfügen die betrachten Anbaugeräte selbst über Lenkaktorik, wie z.B. gelenkte Räder oder eine gelenkte Knickdeichsel. Da das gesteigerte Interesse an gelenkten Anbaugeräten selbst recht neu ist, finden sich die Beiträge dieser Arbeit sowohl im Bereich Regelung und Steuerung als auch im Bereich einer vorhergehenden Modellbildung der Traktor-Anbaugeräte-Kombinationen.

Hinsichtlich der Modellierung von Traktor-Anbaugeräte-Kombinationen ist insbesondere die große Vielfalt an Geräten und Lenkaktoren eine Herausforderung. Zur Herleitung der beschreibenden Differentialgleichungen wurde daher stets eine systematische Vorgehensweise gewählt, welche sich durch Computer-Algebra-Software großteils automatisieren lässt und mit nur kleinen Veränderungen an Varianten angepasst werden kann. Im Rahmen der Arbeit wurde exemplarisch eine Kombination aus einem an den Vorderrädern gelenkten Traktor und einem gezogenen einachsigen Anbaugerät, welches sowohl über Radlenkung als auch Knickdeichsellenkung verfügt, näher betrachtet. Die resultierende Regelstrecke wurde in verschieden Detaillierungsgraden modelliert. Alle Varianten wurden jedoch durch explizite gewöhnliche Differentialgleichungen beschrieben, um eine weitergehende Analyse zu ermöglichen. Zum Zwecke des Regler- und Beobachter/Schätzfilterentwurfs wurden einfache kinematische Beschreibungen der Strecke basierend auf Geometrieparametern und Zwangsbedingungen der Radgeschwindigkeitsvektoren entwickelt. Der Vorteil dieser Streckenbeschreibungen liegt in ihrer einfachen Parametrierbarkeit durch die Bestimmung von Geräteabmessungen, wodurch sich Varianten von Anbaugeräten sehr leicht berücksichtigen lassen. Zum Zwecke der numerischen Simulation und weitergehenden Streckenanalyse wurden detailliertere dynamische Fahrzeugmodelle entwickelt. Diese Modelle berücksichtigen der Bewegung zugrundeliegende Kräfte und Momente und erlauben es beispielsweise Störungen durch Kräfte am Hang genauer darzustellen. Nachteilig an diesen Streckenbeschreibungen ist, dass diese auf Reifen- sowie Massenträgheitsparameter zurückgreifen, welche für eine große Zahl von Gerätevarianten nur mit erheblichem Aufwand bestimmbar sind. Die Parametrierung wurde deshalb nur für einen

experimentellen Geräteaufbau durchgeführt. Die Beschreibung lenkbarer Anbaugeräte durch dynamische Fahrzeugmodelle stellt insbesondere dann eine Herausforderung dar, wenn sich die Aktorik, wie im Fall einer Knickdeichsellenkung, zwischen Traktor und Anbaugerät befindet. Im Rahmen dieser Arbeit wurde vorgeschlagen die Aktorik als unterlagert winkel-/positionsgeregelt anzunehmen und sie anschließend lediglich als zeitveränderliche bzw. holonom-rheonome Zwangsbedingung zu berücksichtigen. Durch diese Vorgehensweise sowie eine systematische Herleitung anhand des Lagrange-Formalismus zweiter Art und einiger geschickt gewählter Koordinatentransformationen war es dennoch möglich die sehr langen resultierenden Gleichungen zu handhaben und die beschreibenden Differentialgleichungen in expliziter Form anzugeben.

Die Anforderungen an eine automatische Querführung von Traktoren und lenkbaren Anbaugeräten beschränken sich nicht nur auf eine Genauigkeit im Zentimeter-Bereich. Insbesondere die Variantenvielfalt bei Geräten und Aktoren muss berücksichtigt werden. Darüber hinaus ist es nötig mit Unsicherheiten und Störungen, wie sie beispielsweise durch wechselnde Reifen-Boden-Interaktion entstehen können, umzugehen. Mögliche adaptive oder robuste Regelungsansätze sind hier in Betracht zu ziehen. Daneben muss die abschließende Parametrierung des Reglers durch den Bediener in allen Fällen einfach und intuitiv gehalten werden. Eine weitere Anforderung ist schließlich, dass der entworfene Regler auf einem Traktorsteuergerät mit begrenzten Ressourcen zum Einsatz kommen soll. Um die beschriebenen Anforderungen zu erfüllen, wurde zunächst eine umfassende Literaturrecherche zum aktuellen Stand der automatischen Querführung von PKW und Nutzfahrzeugen sowohl auf als auch abseits von Straßen durchgeführt. Ausgehend von einer ersten Bewertung wurde ein Linear-Quadratic Regulator (LQR) als vielversprechender Ausgangspunkt gewählt. Um den Parametrierungs- und Umsetzungsaufwand zu reduzieren wurde auf eine beobachter-/schätzfilterbasierte Zustandsschätzung verzichtet. Stattdessen wurde der resultierende Zustandsregler durch eine statische Ausgangsrückführung approximiert. Diese wurde derart entworfen, dass sie die dominanten Eigenwerte des geschlossenen Kreises mit Zustandsrückführung gut nachbildet. Die Reglereinstellung basierte auf der Gewichtung von Stellgrößen sowie gemessenen Positions- und Winkelabweichungen des Traktors und Anbaugerätes von einem vorgegebenen Pfad. Die relative Gewichtung der Abweichungen erlaubte es bestimmte Ziele der Anwendung zu betonen, um z.B. eine Positions- und Orientierungsregelung des Anbaugerätes zu realisieren. Das relative Gewicht von Abweichungen und Stellgrößen diente als Parameter zur Einstellung der Reglergesamtverstärkung und wurde als einziger Parameter im Feld ermittelt. Versuche offenbarten, dass zusätzliche Maßnahmen nötig sind um mit Radschräglauf und bleibenden stationären Positionsabweichungen umzugehen. Hierzu wurden zwei Varianten betrachtet. Die erste Variante basiert auf einer Erweiterung des LQR Reglers um einen Integralanteil (kurz: LQR m. I). Die zweite Variante basiert auf einer Störgrößenaufschaltung unter Zuhilfenahme geschätzter Schräglaufwinkel an allen Rädern. Die Schätzung

erfolgte hierbei mittels eines Extended Kalman Filter (EKF) und einem erweiterten kinematischen Streckenmodell (kurz: LQR m. EKF). In allen Fällen stellte sich heraus, dass eine Vorsteuerung basierend auf Krümmungsinformation des Sollpfades vorteilhaft ist. Die Gleichungen zur Vorsteuerung von gelenkten Anbaugeräten wurden hierzu in dieser Arbeit erstmals hergeleitet.

Den abschließenden Teil der Arbeit bildeten zahlreiche Simulationen und Fahrversuche. Letztere erfolgten unter Verwendung eines mittelgroßen Traktors und eines speziell für diese Arbeit entworfenen Anbaugeräts mit einer Vielzahl von Lenkaktoren. Die Simulationen basieren auf einem nichtlinearen dynamischen Fahrzeugmodell, welches so parametriert wurde, dass es den Versuchsaufbau nachbildet. Durch Betrachtung des Einschwingverhaltens der automatische Querführung sowohl in Simulationen als auch in Versuchen wurde deutlich, dass insbesondere LQR m. I im Falle von Stellgrößen- oder Stellratenbeschränkungen zu Überschwingen und Windup neigt. Stellgrößenbeschränkungen wurden bereits in Anti-Windup Maßnahmen berücksichtigt. Eine Berücksichtigung der Stellratenbeschränkungen könnte eine weitere Verbesserungsmöglichkeit darstellen. Simulationen von Fahrten am Seitenhang und Versuche mit Kreisfahrten zeigten, dass sowohl LQR m. I als auch LQR m. EKF in der Lage sind Störungen und bleibende Abweichungen aufgrund des Schräglaufs der Räder zu unterdrücken. Als Zahlenbeispiel seien Kreisfahrten mit 20 m Radius und 3 m/s Trakorlängsgeschwindigkeit genannt. Die Versuche erfolgten auf trockenem Lehm, der zuvor mit einem Grubber bearbeitet wurde und durch mehrfache Überfahrten leicht verfestigt war. Im Falle von LQR m. I und einer Beschränkung auf Traktorlenkaktorik resultierten Standardabweichungen SD von 3.3 cm, 5.5 cm und 1.0° sowie Mittelwerte von 0 cm, -27.7 cm und -0,7° für die seitliche Positionsabweichungen des Traktors und des Anbaugeräts, sowie die Winkelabweichung des Anbaugeräts. Durch die Beschränkung auf eine Stellgröße lässt sich im Allgemeinen nur für eine einzige Regelgröße stationäre Genauigkeit erzielen, falls konstante Störungen auf das System wirken. Im Zahlenbeispiel wurde die seitliche Positionsabweichung des Traktors gewählt. Im Gegensatz dazu ließen sich für LQR m. I bei Verwendung von Radlenkung an Traktor und Anbaugerät sowie Knickdeichsellenkung am Anbaugerät Genauigkeiten von 3.2 cm, 2.0 cm und 0.7° SD mit verschwindenden mittleren Fehlern erzielen. Gleichermaßen ergaben sich für LQR m. EKF Genauigkeiten von 3.2 cm, 2.2 cm und 0.3° SD mit Mittelwerten von -2.0 cm, 1.3 cm und -0.4° für die seitliche Positionsabweichungen des Traktors und des Anbaugeräts, sowie die Winkelabweichung des Anbaugeräts. Versuche zum instationären Verhalten auf Pfaden bestehend aus Geraden-, Klothoiden- und Kreisstücken lieferten ähnliche Ergebnisse, so lange die Krümmungsänderungsrate des Pfades moderat war ($0.1°/m^2$) und die Annahme einer konstanten Störung näherungsweise erfüllt blieb. Erhöhte Krümmungsänderungsraten resultierten in leicht erhöhten Abweichungen. Abschließende Untersuchungen zum Einfluss von Parameterschwankungen offenbarten, dass Geschwindigkeitsänderungen insbesondere für LQR m. I berücksichtigt werden müssen.

Gain Scheduling wurde als mögliche Lösung vorgeschlagen, eine Implementierung steht jedoch noch aus. Simulationen mit um $\pm 50\%$ veränderten Trägheits- und Reifenparametern hatten sowohl für LQR m. I als auch LQR m. EKF keinen Einfluss auf die Stabilität des Regelkreises, jedoch offenbarte sich der erwartungsgemäß hohe Einfluss der Reifenschräglaufsteifigkeit auf die erzielbare Genauigkeit.

Stichworte: Traktor, gelenktes Anbaugerät, kinematisches Fahrzeugmodell, dynamisches Fahrzeugmodell, Querführung, Linear-Quadratic Regulator (LQR), Ausgangsrückführungsapproximation, Extended Kalman Filter (EKF), Radschräglaufwinkelschätzung

Contents

Terms and Definitions

Dynamic Vehicle Model: Vehicle model accounting for the forces and moments causing the vehicle motion.

Guidance System: System calculating the vehicle steering/speed commands based on a desired path/trajectory and vehicle position information.

Kinematic Vehicle Model: Vehicle model not accounting for the forces and moments causing the vehicle motion which is based on simplified assumptions constraining the wheel velocity vector directions.

Path Tracking: Following a given curve without time requirements, i.e. a particular position on the curve may be reached at any time.

Trajectory Tracking: Following a given curve with time requirements, i.e. a particular position on the curve must be reached at a specified time.

Abbreviations

ARE Algebraic Riccati Equation

CAN Controller Area Network

c.g. center of gravity

DoF Degree of Freedom

ECU Electronic Control Unit

EKF Extended Kalman Filter

FLC Fuzzy Logic Control

GPS Global Positioning System

IMU Inertial Measurement Unit

LMS Least Mean Squares

LQG Linear-Quadratic Gaussian

LQR Linear-Quadratic Regulator

MIMO Multiple Input Multiple Output

MPC Model Predictive Control

MRAC Model Reference Adaptive Control

ODE Ordinary Differential Equation

PD Proportional-Derivative

PI Proportional-Integral

PID Proportional-Integral-Derivative

RTK Real-Time Kinematic

SD standard deviation

SISO Single Input Single Output

SMC Sliding Mode Control

STC Self-Tuning Controller

TCM Terrain Compensation Module

TIA Tractor Implement Automation

Symbols

This section lists all symbols used throughout the document in an alphabetical order. Scalars are denoted using lower and upper case italic letters. Units use lower and upper case non-italic letters. Vectors are lower case bold with exceptions for variables that are commonly upper case (e.g. forces and moments). Matrices are described using upper case bold letters. The transpose of a vector or matrix is indicated by 'T' as an upper right superscript. Matrix upper right superscripts '-1' and '$\ddagger$' denote the inverse and the Moore-Penrose Pseudo-Inverse [BIT03]. In addition upper right superscripts are used to specify coordinates and coordinate systems. $r^{x,t}$ for instance is the x coordinate of vector $\mathbf{r}$ in a tractor-fixed coordinate system. Subscripts specify the variable more precisely. The frequent subscripts t and $r1$ in particular relate properties to the tractor and the first rear mounted implement. Time or frequency dependencies of variables are stated only if required to avoid ambiguity. In this case (t) and $[k]$ are used to denote continuous and discrete time dependencies. (s) outlines a dependency on the complex Laplace variable $s = \sigma + j\omega$ in the frequency domain. Angular expressions may be given in rad or °. The first is used for all internal calculations, the latter may be used to present parameters and results in a more comprehensible way.

Symbol	Description	Unit
Latin letters		
$\mathbf{A}$	System matrix of a linear system in continuous time state-space representation	
$\mathbf{A}_d$	System matrix of a linear system in discrete time state-space representation	
$\mathbf{A}_e$	System matrix of an extended linear system in continuous time state-space representation	
$\hat{\mathbf{a}}$	Estimated parameter vector	
$\hat{\mathbf{a}}_c$	Estimated controller parameter vector	
$\hat{\mathbf{a}}_p$	Estimated plant parameter vector	
$\tilde{a}_1, \ldots, \tilde{a}_n$	Coefficients of closed-loop characteristic polynomial	
$\mathbf{B}$	Input matrix of a linear system in continuous time state-space representation	
$\mathbf{B}_d$	Input matrix of a linear system in discrete time state-space representation	
$\mathbf{B}_e$	Input matrix of an extended linear system in continuous time state-space representation	
B	Magic Formula tire model stiffness factor	
$b(y, \dot{y})$	Unknown input function of nonlinear controllable canonical form	
b_{min}, b_{max}	Lower and upper bound for $b(y, \dot{y})$	
$\hat{b}(y, \dot{y})$	Known estimate of input function of nonlinear controllable canonical form	
$\mathbb{C}$	Set of all complex numbers	
$\mathbf{C}$	Output matrix for measured outputs of a linear system in continuous time state-space representation	
$\mathbf{C}_c$	Output matrix for controlled outputs of a linear system in continuous time state-space representation	
$\mathbf{C}_d$	Output matrix for measured outputs of a linear system in discrete time state-space representation	
$\mathbf{C}_e$	Output matrix for measured outputs of an extended linear system in continuous time state-space representation	
C	Magic Formula tire model shape factor	
$C_{sx,w}$	Individual wheel longitudinal stiffness	kN
$C_{\alpha,r1r}$	Combined implement wheel cornering stiffness	kN/rad
$C_{\alpha,tf}$	Combined tractor front wheel cornering stiffness	kN/rad
$C_{\alpha,tr}$	Combined tractor rear wheel cornering stiffness	kN/rad
$C_{\alpha,w}$	Individual wheel cornering stiffness	kN/rad
$C_{\gamma,w}$	Individual wheel camber stiffness	kN
D	Magic Formula tire model peak value factor	
D_{r1d}	Implement drawbar steering actuator damping constant	
D_{r1r}	Implement wheel steering actuator damping constant	
D_{tf}	Tractor front wheel steering actuator damping constant	
d_{ah}	Look-ahead distance	m
$\hat{\mathbf{d}}$	Estimated disturbance vector	
$\mathbf{e}_r$	Vector of reference output error	

Symbol	Description	Unit
$\mathbf{e}_{x,e}$, $\mathbf{e}_{y,e}$, $\mathbf{e}_{z,e}$	Unit vectors of earth-fixed coordinate system	
$\mathbf{e}_{x,r1}$, $\mathbf{e}_{y,r1}$, $\mathbf{e}_{z,r1}$	Unit vectors of implement-fixed coordinate system	
$\mathbf{e}_{x,r1r}$, $\mathbf{e}_{y,r1r}$, $\mathbf{e}_{z,r1r}$	Unit vectors of implement wheel-fixed coordinate system	
$\mathbf{e}_{x,t}$, $\mathbf{e}_{y,t}$, $\mathbf{e}_{z,t}$	Unit vectors of tractor-fixed coordinate system	
$\mathbf{e}_{x,tf}$, $\mathbf{e}_{y,tf}$, $\mathbf{e}_{z,tf}$	Unit vectors of tractor front wheel-fixed coordinate system	
$\mathbf{e}_{x,tr}$, $\mathbf{e}_{y,tr}$, $\mathbf{e}_{z,tr}$	Unit vectors of tractor rear wheel-fixed coordinate system	
$\mathbf{e}_{x,w}$, $\mathbf{e}_{y,w}$, $\mathbf{e}_{z,w}$	Unit vectors of wheel-fixed coordinate system	
$\mathbf{e}_{\perp,r1r}$	Vector perpendicular to implement wheel velocity vector and $\mathbf{e}_{z,e}$	
$\mathbf{e}_{\perp,tf}$	Vector perpendicular to tractor front wheel velocity vector and $\mathbf{e}_{z,e}$	
$\mathbf{e}_{\perp,tr}$	Vector perpendicular to tractor rear wheel velocity vector and $\mathbf{e}_{z,e}$	
E	Magic Formula tire model curvature value factor	
$E\{\mathbf{x}\}$	Expectation of a random vector $\mathbf{x}$	
e_{r1l}	Implement lateral error	m
e_{r1h}	Implement heading error	rad
e_{tl}	Tractor lateral error	m
e_{th}	Tractor heading error	rad
$\mathbf{F}$	$\mathbf{f}_d(\mathbf{x}, \mathbf{u})$ linearized about $\mathbf{x}$	
$\mathbf{f}(\mathbf{x}, \mathbf{u})$	System and input function of a nonlinear system in continuous time state-space representation	
$\mathbf{f}_d(\mathbf{x}, \mathbf{u})$	System and input function of a nonlinear system in discrete time state-space representation	
$\mathbf{f}_u(\mathbf{x})$	Nonlinear state feedback control law	
F	Estimation error bound for $\left|\hat{f}(y,\dot{y}) - f(y,\dot{y})\right|$	
$F_{r1}^{x,e}$, $F_{r1}^{y,e}$	Applied forces on implement c.g. in earth-fixed coordinates	N
$F_{r1}^{x,r1}$, $F_{r1}^{y,r1}$	Applied forces on implement c.g. in implement-fixed coordinates	N
$F_{r1r}^{x,r1r}$, $F_{r1r}^{y,r1r}$	Longitudinal and lateral ground reaction forces at implement wheel in implement wheel-fixed coordinates	N
$F_t^{x,e}$, $F_t^{y,e}$	Applied forces on tractor c.g. in earth-fixed coordinates	N
$F_t^{x,t}$, $F_t^{y,t}$	Applied forces on tractor c.g. in tractor-fixed coordinates	N
$F_{tf}^{x,tf}$, $F_{tf}^{y,tf}$	Longitudinal and lateral ground reaction forces at tractor front wheel in tractor front wheel-fixed coordinates	N
$F_{tr}^{x,tr}$, $F_{tr}^{y,tr}$	Longitudinal and lateral ground reaction forces at tractor front wheel in tractor rear wheel-fixed coordinates	N
$F_w^{x,w}$, $F_w^{y,w}$, $F_w^{z,w}$	Ground reaction forces in wheel-fixed coordinates	N
f	Frequency	Hz
$f(y,\dot{y})$	Unknown system function of nonlinear controllable canonical form	
$\hat{f}(y,\dot{y})$	Known estimate of system function of nonlinear controllable canonical form	
$\mathbf{G}(s)$	Laplace transfer function matrix of plant	
$G(s)$	Laplace transfer function of plant	
G_{u_k,y_l}	Laplace transfer function from input u_k to output y_l	
$\mathbf{H}$	$\mathbf{h}_d(\mathbf{x})$ linearized about $\mathbf{x}$	
$\mathbf{h}(\mathbf{x})$	Output function of a nonlinear system in continuous time state-space representation	

Symbol	Description	Unit
$\mathbf{h}_d(\mathbf{x})$	Output function of a nonlinear system in discrete time state-space representation	
$\mathbf{I}$	Identity matrix	
I_{r1}	Implement moment of inertia about $\mathbf{e}_{z,r1r}$	kg m^2
I_t	Tractor moment of inertia about $\mathbf{e}_{z,t}$	kg m^2
J	Performance index of an optimization problem	
$\mathbf{K}$	Static state feedback matrix	
$\mathbf{K}$	EKF Kalman gain matrix	
$\mathbf{K}(s)$	Laplace transfer function matrix of dynamic controller	
$\mathbf{K}_y$	Static output feedback matrix	
$\mathbf{k}_i$	EKF Kalman gain vector for measurement update of output vector element y_i	
L	Lagrangian function	J
l_{r1}	Implement distance between drawbar joint and axle	m
l_{r1d}	Implement distance between drawbar joint and hitch point	m
l_{r1f}	Implement distance between drawbar joint and c.g.	m
l_{r1r}	Implement distance between c.g. and axle	m
l_t	Tractor wheel base	m
l_{tf}	Distance between tractor c.g. and front axle	m
l_{thr}	Distance between tractor rear axle and rear hitch point	m
l_{tr}	Distance between tractor c.g. and rear axle	m
$\mathbf{M}$	Generalized mass matrix in nonlinear dynamic equations of motion	
$\mathbf{M}_R$	Spherical region with radius R	
$M_w^{x,w}$, $M_w^{y,w}$, $M_w^{z,w}$	Ground reaction moments in wheel-fixed coordinates	Nm
$M_{r1}^{z,e}$	Applied moment on implement in earth-fixed coordinates	Nm
$M_{r1}^{z,r1}$	Applied moment on implement in implement-fixed coordinates	Nm
$M_t^{z,e}$	Applied moment on tractor in earth-fixed coordinates	Nm
$M_t^{z,t}$	Applied moment on tractor in tractor-fixed coordinates	Nm
m_{r1}	Implement mass	kg
m_t	Tractor mass	kg
N_p	MPC prediction horizon	
$\mathbf{P}$	Unknown matrix in ARE	
$\mathbf{P}(s)$	Laplace transfer function matrix of extended plant for H$_\infty$ control	
$p_{i,w}$	Wheel inflation pressure	bar
$\hat{\mathbf{P}}^-$	EKF a priori estimate of error covariance matrix	
$\hat{\mathbf{P}}^+$	EKF a posteriori estimate of error covariance matrix	
$\hat{\mathbf{P}}_i^{\pm}$	EKF intermediate estimate of error covariance matrix after measurement update for output vector element y_i has been performed	
$\mathbf{Q}$	LQR or MPC weighting matrix for system states or outputs	
$\mathbf{Q}$	Process noise covariance matrix	
$Q_1, \ldots, Q_4$	Generalized forces	
$q_1, \ldots, q_4$	Generalized coordinates	
$q_{1,1}, \ldots, q_{n,n}$	Diagonal elements of process noise covariance matrix $\mathbf{Q}$	

Symbol	Description	Unit
$\mathbb{R}$	Set of all real numbers	
$\mathbf{R}$	LQR or MPC weighting matrix for system inputs	
$\mathbf{R}$	Measurement noise covariance matrix	
$\mathbf{r}$	Reference input vector	
$\mathbf{r}$	Remainder vector in nonlinear dynamic equations of motion	
$\mathbf{r}_{r1}$	Implement c.g. position vector	m
$\mathbf{r}_{r1r}$	Implement wheel position vector	m
$\mathbf{r}_t$	Tractor c.g. position vector	m
$\mathbf{r}_{tr}$	Tractor rear wheel position vector	m
R	Radius	
$r_{1,1}, \ldots, r_{n,n}$	Diagonal elements of measurement noise covariance matrix $\mathbf{R}$	
$r_{d,w}$	Dynamic rolling radius	m
$r_{r1}^{x,e}, r_{r1}^{y,e}$	Implement c.g. position in earth-fixed coordinates	m
$r_{r1r}^{x,e}, r_{r1r}^{y,e}$	Implement wheel position in earth-fixed coordinates	m
$r_t^{x,e}, r_t^{y,e}$	Tractor c.g. position in earth-fixed coordinates	m
$r_{tr}^{x,e}, r_{tr}^{y,e}$	Tractor rear wheel position in earth-fixed coordinates	m
$S(t)$	Sliding surface	
S_h	Magic Formula tire model horizontal shift	
S_v	Magic Formula tire model vertical shift	
s	Complex Laplace variable $s = \sigma + j\omega$	1/s
$s(y, \dot{y})$	Function defining sliding surface	
$s_w^{x,w}, s_w^{y,w}$	Longitudinal and lateral wheel slip	
$\mathbf{T}_{r1,e}$	Transformation matrix from implement-fixed to earth-fixed coordinates	
$\mathbf{T}_{t,e}$	Transformation matrix from tractor-fixed to earth-fixed coordinates	
$\mathbf{T}_{yu}(s)$	Laplace transfer function matrix after upper fractional transformation of extended plant $\mathbf{P}(s)$ for H_∞ control	
$\mathbf{T}_{zw}(s)$	Laplace transfer function matrix after lower fractional transformation of extended plant $\mathbf{P}(s)$ for H_∞ control	
T	Kinetic energy	J
T_{r1d}	Implement drawbar steering actuator time constant	s
T_{r1r}	Implement wheel steering actuator time constant	s
T_{tf}	Tractor front wheel steering actuator time constant	s
$T_{\alpha,w}$	Wheel relaxation time constant	s
$\mathbf{U}(s)$	Laplace transform of system input vector	
$\mathbf{u}$	System input vector	
$\mathbf{u}^*(t)$	Optimal control law	
$\mathbf{u}_{min}, \mathbf{u}_{max}$	System input constraints	
$\bar{u}$	New input of linearized system	
$\mathbf{V}_i$	Matrix of closed loop eigenvectors obtained using state feedback	
$\mathbf{v}$	Measurement noise vector	
$\mathbf{v}_i$	Closed loop eigenvector obtained using state feedback	
$\mathbf{v}_{r1}$	Implement c.g. velocity vector	m/s
$\mathbf{v}_{r1r}$	Implement wheel velocity vector	m/s
$\mathbf{v}_t$	Tractor c.g. velocity vector	m/s

Symbol	Description	Unit
$\mathbf{v}_{tf}$	Tractor front wheel velocity vector	m/s
$\mathbf{v}_{tr}$	Tractor rear wheel velocity vector	m/s
$\mathbf{v}_w$	Velocity vector of wheel center	m/s
V	Potential energy	J
$V(\mathbf{x})$	Lyapunov function candidate	
$v_{r1r}^{x,t}$, $v_{r1r}^{y,t}$	Implement wheel horizontal velocity in tractor-fixed coordinates	m/s
$v_t^{x,e}$, $v_t^{y,e}$	Tractor c.g. horizontal velocity in earth-fixed coordinates	m/s
$v_t^{x,t}$, $v_t^{y,t}$	Tractor c.g. horizontal velocity in tractor-fixed coordinates	m/s
$v_{tf}^{x,t}$, $v_{tf}^{y,t}$	Tractor front wheel horizontal velocity in tractor-fixed coordinates	m/s
$v_{tr}^{x,t}$, $v_{tr}^{y,t}$	Tractor rear wheel horizontal velocity in tractor-fixed coordinates	m/s
$v_w^{x,w}$, $v_w^{y,w}$	Wheel horizontal velocity in wheel-fixed coordinates	m/s
$v_{w,0}^{x,w}$	Freely rolling wheel longitudinal velocity	m/s
$\mathbf{W}$	Weighting matrix for closed loop eigenvalues λ_i ($i = 1 \ldots n$) obtained using state feedback	
$\mathbf{W}_1(s)$, $\mathbf{W}_2(s)$	Extended plant weighting transfer function matrices for H$_\infty$ control	
$\mathbf{w}$	Weighted input of extended plant $\mathbf{P}(s)$ for H$_\infty$ control	
$\mathbf{w}$	Process noise vector	
w_i	Weight for closed loop eigenvalue λ_i obtained using state feedback	
$\mathbf{X}(s)$	Laplace transform of state vector	
$\mathbf{x}$	System state vector	
$\mathbf{x}_e$	System state vector of extended plant	
$\mathbf{x}_{min}$, $\mathbf{x}_{max}$	System state constraints	
$\hat{\mathbf{x}}$	Estimate of system state vector	
$\hat{\mathbf{x}}^-$	EKF a priori estimate of system state vector	
$\hat{\mathbf{x}}^+$	EKF a posteriori estimate of system state vector	
$\hat{\mathbf{x}}_i^\pm$	EKF intermediate estimate of system state vector after measurement update for output vector element y_i has been performed	
$\mathbf{Y}(s)$	Laplace transform of measured output vector	
$\mathbf{y}$	Vector of measured outputs	
$\mathbf{y}_c$	Vector of controlled outputs	
$\mathbf{y}_e$	Vector of measured outputs of extended plant	
$\mathbf{y}_r$	Vector of reference outputs	
$\hat{\mathbf{y}}$	Estimate of measured outputs	
$\mathbf{z}$	Weighted output of extended plant $\mathbf{P}(s)$ for H$_\infty$ control	
Greek letters		
$\alpha_{R_k,l}$	FLC degree of match of condition l of rule R_k	
α_{R_k}	FLC firing strength of rule R_k	
$\alpha_{re,r1r}$	Transient implement wheel side-slip angle	rad
$\alpha_{re,tf}$	Transient tractor front wheel side-slip angle	rad
$\alpha_{re,tr}$	Transient tractor rear wheel side-slip angle	rad
$\alpha_{re,w}$	Transient wheel side-slip angle	rad
α_{r1r}	Implement wheel side-slip angle	rad
α_{tf}	Tractor front wheel side-slip angle	rad

Symbol	Description	Unit
α_{tr}	Tractor rear wheel side-slip angle	rad
α_w	Wheel side-slip angle	rad
$\hat{\alpha}_{r1r}$	Estimated implement wheel side-slip angle	rad
$\hat{\alpha}_{tf}$	Estimated tractor front wheel side-slip angle	rad
$\hat{\alpha}_{tr}$	Estimated tractor rear wheel side-slip angle	rad
$\beta_{r1,i}^{z,e}$	Implement angular velocity coefficient	
$\beta_{t,i}^{z,e}$	Tractor angular velocity coefficient	
β_t	Tractor side-slip angle at tractor c.g.	rad
β_{tf}	Tractor side-slip angle at tractor front wheel location	rad
$\boldsymbol{\Delta}(s)$	Unstructured uncertainty transfer function matrix	
δ_{r1d}	Implement drawbar steering angle	rad
$\delta_{r1d,d}$	Desired implement drawbar steering angle	rad
$\delta_{r1d,d,cff}$	Desired implement drawbar steering angle part from curvature feedforward	rad
$\delta_{r1d,d,dff}$	Desired implement drawbar steering angle part from disturbance feedforward	rad
$\delta_{r1d,d,fb}$	Desired implement drawbar steering angle part from feedback control	rad
$\delta_{r1d,min}$, $\delta_{r1d,max}$	Implement drawbar steering angle limits	rad
δ_{r1r}	Implement wheel steering angle	rad
$\delta_{r1r,d}$	Desired implement wheel steering angle	rad
$\delta_{r1r,d,cff}$	Desired implement wheel steering angle part from curvature feedforward	rad
$\delta_{r1r,d,dff}$	Desired implement wheel steering angle part from disturbance feedforward	rad
$\delta_{r1r,d,fb}$	Desired implement wheel steering angle part from feedback control	rad
$\delta_{r1r,min}$, $\delta_{r1r,max}$	Implement wheel steering angle limits	rad
δ_{tf}	Tractor front wheel steering angle	rad
$\delta_{tf,d}$	Desired tractor front wheel steering angle	rad
$\delta_{tf,d,cff}$	Desired tractor front wheel steering angle part from curvature feedforward	rad
$\delta_{tf,d,dff}$	Desired tractor front wheel steering angle part from disturbance feedforward	rad
$\delta_{tf,d,fb}$	Desired tractor front wheel steering angle part from feedback control	rad
$\delta_{tf,min}$, $\delta_{tf,max}$	Tractor front wheel steering angle limits	rad
$\dot{\delta}_{r1d,min}$, $\dot{\delta}_{r1d,max}$	Implement drawbar steering angle rate limits	rad
$\dot{\delta}_{r1r,min}$, $\dot{\delta}_{r1r,max}$	Implement wheel steering angle rate limits	rad
$\dot{\delta}_{tf,min}$, $\dot{\delta}_{tf,max}$	Tractor front wheel steering angle rate limits	rad
$\gamma_{r1,i}^{x,e}$, $\gamma_{r1,i}^{y,e}$	Implement linear velocity coefficients	
$\gamma_{t,i}^{x,e}$, $\gamma_{t,i}^{y,e}$	Tractor linear velocity coefficients	
γ_w	Wheel camber angle	rad
κ	Desired path curvature	rad/m
κ_{r1}	Implement desired path curvature	rad/m
κ_t	Tractor desired path curvature	rad/m
λ	Strictly positive constant	

Symbol	Description	Unit
$\bar{\lambda}_i$	Closed loop eigenvalue obtained using state feedback	
$\mu_{x,w}$	Longitudinal wheel force coefficient	
$\mu_A(x)$	Membership function of a fuzzy set A over elements x	
η	Strictly positive constant	
Ω_w	Wheel's speed of revolution	rad/s
$\Omega_{w,0}$	Freely rolling wheel's speed of revolution	rad/s
ω	Angular frequency	rad/s
$\omega_t^{z,e}$	Tractor vertical angular velocity in earth-fixed coordinates	rad/s
$\omega_{r1}^{z,e}$	Implement vertical angular velocity in earth-fixed coordinates	rad/s
Ψ_d	Heading angle of desired path tangent	rad
Ψ_{r1}	Implement heading angle	rad
Ψ_t	Tractor heading angle	rad
$\sigma\left(\mathbf{G}(j\omega)\right)$	Singular value of $\mathbf{G}(j\omega)$	
$\sigma_{\alpha,r1r}$	Implement wheel relaxation length	m
$\sigma_{\alpha,tf}$	Tractor front wheel relaxation length	m
$\sigma_{\alpha,tr}$	Tractor rear wheel relaxation length	m
$\sigma_{\alpha,w}$	Wheel relaxation length	m
$\overline{\sigma}\left(\mathbf{G}(j\omega)\right)$	Largest singular value of $\mathbf{G}(j\omega)$	
$\underline{\sigma}\left(\mathbf{G}(j\omega)\right)$	Smallest singular value of $\mathbf{G}(j\omega)$	
Other		
$\in$	Set membership 'is element of'	
$\exists$	Existential quantifier 'there exists'	
$\forall$	Universal quantifier 'for all'	

1 Introduction

1.1 Motivation

Today's agriculture feeds a growing world population with decreasing arable land per capita [Bru11] using chemical fertilizers from limited natural deposits or energy intensive synthesis. In order to keep up with future demand agricultural methods are now shifting from large area uniform treatment towards more efficient and sustainable techniques. Core to those techniques is accuracy, which allows to e.g. work, seed, plant, weed, spray, or apply fertilizer based on a location's actual demand.

Accurate GPS based path tracking control in particular became a key technology for this new approach to agriculture. Using GPS and Real-Time Kinematic (RTK) correction signals allows for position measurements that are accurate up to a centimeter level. Those position measurements are input to a vehicle guidance system calculating the vehicles deviation from a previously defined path on a field. The path tracking controller within that guidance system subsequently ensures accurate path following by actuating the vehicles steering system.

Today most tractor manufacturers offer solutions for accurate tractor path tracking either directly or by suppliers [Dee12, Tri01, Top12, Aut12]. Increasingly sophisticated tractor path tracking control, however, revealed that accurate positioning of the actual implement is equally or even more important. Applications like bedded crops, row crops, strip-till fields, controlled traffic farming, drip irrigation, or simply sloped or curved fields still require improvements in implement control. For that reason attention is now drawn to steerable implements, i.e. implements with steering actuators like steerable wheels or a steerable drawbar.

Controlling the resulting tractor-implement Multiple Input Multiple Output (MIMO) system, however, is still a challenge. One reason is that there is not a single tractor-implement combination but a multitude of combinations for different crops and different tasks within a particular crop. Performing only one of those tasks accurately is of little use and hence the challenge is to support a multitude of implements while maintaining the final in field controller setup intuitive and user friendly. As a further challenge the system is placed in an imprecisely defined natural environment and therefore needs to cope with uncertainties and disturbances, e.g. resulting from varying soil, without requiring the operator to constantly adjust the controller.

1.2 Objectives

Motivated by an exemplary application to agriculture this work focuses on accurate path tracking control of vehicle combinations with particular emphasis on MIMO systems. A survey on the current state of research on off-road as well as on-road path tracking control of tractor-implement or tractor-trailer combinations is performed. An assessment of those approaches provides the basis for further research in this work.

The desired path tracking control approach is particularly required to be:

- *accurate* up to centimeter level,

- *systematic*, to support a multitude of implements and steering actuators,

- *intuitive* regarding the user's setup,

- *robust/adaptive* with regard to possible uncertainties and disturbances,

- *computationally simple* to run on a vehicle's ECU.

Modeling tractor-implement combinations is an important part of this work as well. The developed models may be of different complexity in order to serve system analysis, controller design, or numerical simulation. The first two of those applications require the models to be derived:

- *explicitly* to allow for analysis of the underlying differential equations,

- *systematically* to support a multitude of implements and steering actuators.

In addition to simulation an experimental tractor-implement combination will be setup. This hardware together with a rapid control prototyping system is used to validate the developed control approaches in real world conditions.

1.3 Structure of this Work

This work is divided into five major parts. Following this introduction, Chapter 2 summarizes the current state of the art in terms of modeling of lateral vehicle motion and in terms of vehicle path tracking control. A tractor without implement is used to define all relevant properties in a concise form. Models of lateral vehicle motion with different levels of detail are outlined. Compared to passenger cars or trucks, modeling of farm tractors is only considered on rare occasions. Therefore, particular emphasis is put on outlining the previous works on farm tractor modeling and parameter identification. As a second part of Chapter 2, an extensive survey on path tracking control of passenger cars as well as tractor-trailer combinations both in the on-road and off-road domain is provided. Each approach is briefly outlined using a concise example. In addition, a discussion is provided for each approach in order to outline the advantages and disadvantages regarding

this work's objectives. These discussions give rise to a comparison of existing approaches which is presented as a conclusion at the end of Chapter 2.

Chapter 3 ties in with the modeling approaches discussed in the previous chapter. At this point, however, the full tractor-implement combination is considered and new models are derived in order to depict actively steered implements. Models of different levels of detail are considered. Simple kinematic models are developed to allow for model based controller and estimator design. More detailed dynamic models are developed to allow for further analysis and more detailed numerical simulation. Model parameters are chosen to depict the behavior of an experimental setup consisting of a mid-size tractor and a custom built implement with a multitude of steering actuators. Chapter 3 concludes with a comparison of the different models developed.

Chapter 4 picks up the results of the comparison of path tracking control approaches in Chapter 2. The most promising approach from literature is used as a starting point. Further developments in this chapter are made to address the objectives of intuitive setup, computational simplicity, and robustness. Further developments address the particular needs arising from actively steered implements.

Chapter 5 summarizes the results of numerous simulations and experiments carried out using the newly developed control approaches. Experiments are performed, again using the mid-size tractor and the custom built actively steered implement. Initial condition responses, slopes, steady-state cornering conditions as well as transient behavior on paths consisting of straights, clothoids and arc segments are considered. Chapter 5 concludes with a parameter variation study.

Chapter 6 finally summarizes all previous chapters and provides an outlook on subsequent steps that might follow this work.

2 State of the Art

2.1 Models of Lateral Vehicle Motion

Vehicle modeling is widely used throughout the entire development process with applications ranging from those in basic research to those in final system validation. As a consequence there are numerous models which may be categorized by modeling detail or range of validity. Using the definitions of Figure 2.1 less detailed models might be solely focused on lateral, longitudinal, or vertical motion in order to asses cornering, drive train, or driving comfort properties. More complex models arise from considering interactions between different system parts, e.g. roll motion and wheel load transfer during cornering, or by including detailed descriptions of particular system parts like suspensions or tires. Regarding the range of validity one can distinguish between normal operation, e.g. turning or lane keeping, and operation close to the vehicle's limits, which typically emphasizes safety aspects like the prevention of instability, rollover, or jack-knifing.

In terms of path tracking control modeling the lateral behavior of tractor-trailer or tractor-implement combinations during normal operation is of particular interest. The main purpose of this section is to provide an overview of past and present research done on those models. This is done distinguishing between dynamic, kinematic, and identified models.
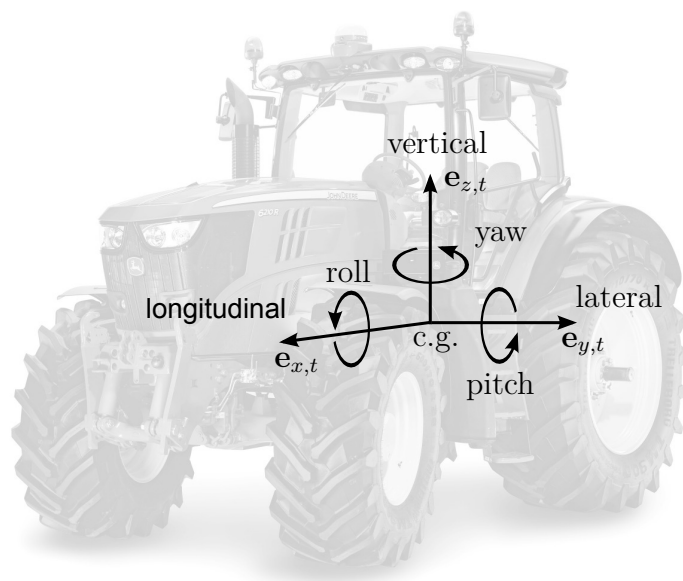

Figure 2.1: Linear and angular motion of a tractor chassis defined using a tractor-fixed coordinate system ($\mathbf{e}_{x,t}$, $\mathbf{e}_{y,t}$, $\mathbf{e}_{z,t}$) located at the tractor center of gravity (c.g.) (Photo: John Deere).

Unfortunately analysis of tractor-implement or tractor-trailer models suffers from lengthy equations due to constraints relating both vehicle parts. This is particularly true for models with steering actuators between the tractor and the implement which are newly derived in this work. For that reason, the principles of each modeling approach are introduced using a tractor without trailer or implement. Particularities of vehicle combinations will be addressed subsequently.

2.1.1 Dynamic Models

Dynamic models are derived from physical laws governing the system, i.e. these models account for forces and moments causing the vehicle's motion. This section outlines the assumptions typically made for dynamic models of lateral vehicle motion. The equations of motion resulting from those assumptions are first stated accounting for forces and moments in a general manner. Subsequently, wheel forces are considered with a particular focus on tractor tires. Combining wheel forces and equations of motion results in a nonlinear model for simulation purposes. A linearized description is provided to allow further analysis. Finally the current state of dynamic tractor-trailer or tractor-implement models is addressed in particular.

Modeling Assumptions

From a very general perspective, a vehicle can be seen as an assembly of numerous flexible bodies. The first assumption is made by lumping model elements together using rigid bodies connected by joints, springs, and dampers. For a passenger car [MW04] starts with a simplified description assuming the chassis and the 4 wheels to be rigid bodies, hence resulting in 30 Degrees of Freedom (DoFs). Including a drive train model increases this number even further. The DoFs entail a similar number of coupled Ordinary Differential Equations (ODEs) describing the system's behavior. Such a description may be suitable for multibody dynamics simulation software. However, model based controller design and further analysis are hardly possible. A common simplification is to neglect weak couplings of system parts and to assume a more restricted vehicle movement. Path tracking control similar to a driver steering the vehicle is mostly influencing a vehicle's lateral motion. Lateral motion is strongly coupled with yaw motion and less strongly coupled with roll motion of a vehicle [MW04]. The respective motions are excited by steering, asymmetric wheel forces, and external disturbances resulting from wind or slopes. Based on these considerations a simplified system description can be obtained by restricting the vehicle to plane motion in $\mathbf{e}_{x,t}$ and $\mathbf{e}_{y,t}$ direction. This model may still be coupled with a simple model of roll motion to account for wheel load transfer. If neither wheel load transfer nor asymmetric wheel forces are of importance, a further simplification can be made by combining all wheels of an axle to a single wheel summarizing all of their properties. The
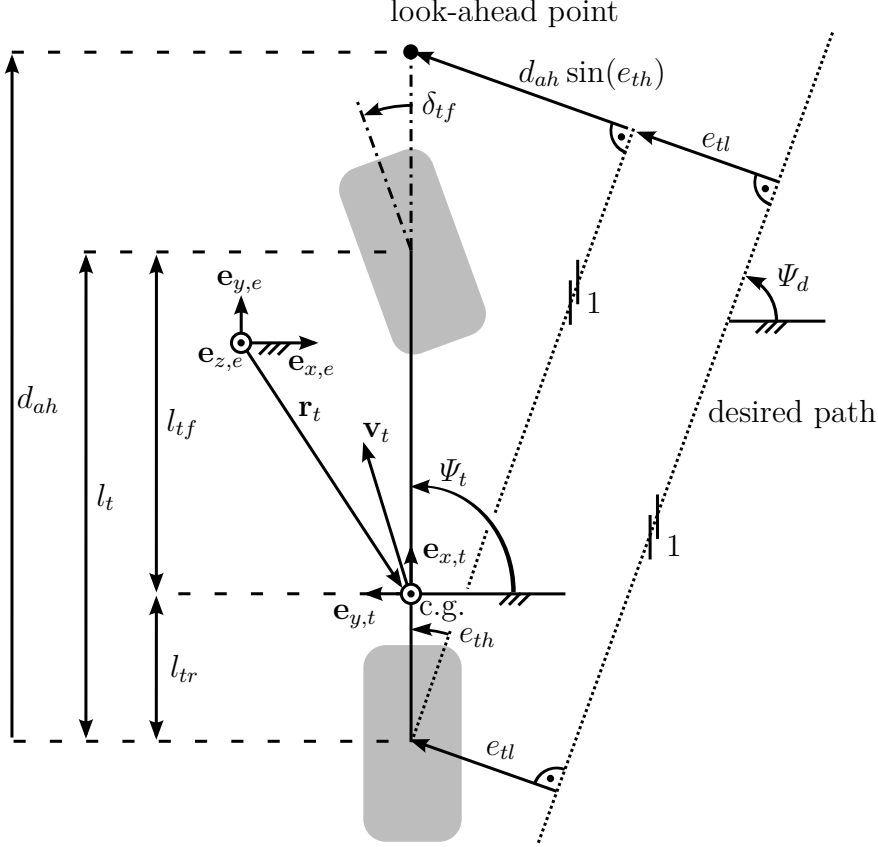
Figure 2.2: Tractor single track model with earth-fixed ($\mathbf{e}_{x,e}$, $\mathbf{e}_{y,e}$, $\mathbf{e}_{z,e}$) and tractor-fixed ($\mathbf{e}_{x,t}$, $\mathbf{e}_{y,t}$, $\mathbf{e}_{z,t}$) coordinate system, tractor center of gravity (c.g.) position $\mathbf{r}_t$, tractor c.g. velocity $\mathbf{v}_t$, tractor wheel steering angle δ_{tf}, tractor heading angle Ψ_t, orientation of the desired path Ψ_d, tractor lateral error e_{tl}, tractor heading error e_{th}, look-ahead distance d_{ah}, tractor wheel base l_t, and c.g. location given by l_{tf} and l_{tr}.

resulting description is a single track model [MW04, Pac06] as shown in Figure 2.2. The model is assumed to be a rigid body in plane motion with a mass m_t and a moment of inertia I_t about $\mathbf{e}_{z,t}$. It retains 3 DoFs which may be expressed using tractor heading Ψ_t and tractor position $\mathbf{r}_t$, the latter, for instance, given in earth-fixed coordinates $r_t^{x,e}$ and $r_t^{y,e}$. The desired path and the respective tracking errors are introduced for later use.

Equations of Motion

There is no difficulty in applying Newton's laws of motion to the single track model of Figure 2.2. Assuming arbitrary forces $F_t^{x,e}$ and $F_t^{y,e}$ acting on the tractor c.g. in $\mathbf{e}_{x,e}$ and $\mathbf{e}_{y,e}$ direction as well as a moment $M_t^{z,e}$ in $\mathbf{e}_{z,e}$ direction the equations of motion are:

$$\ddot{r}_t^{x,e} = \frac{1}{m_t} F_t^{x,e}, \tag{2.1}$$

$$\ddot{r}_t^{y,e} = \frac{1}{m_t} F_t^{y,e}, \tag{2.2}$$

$$\ddot{\Psi}_t = \frac{1}{I_t} M_t^{z,e}. \tag{2.3}$$

Introducing tractor-fixed coordinates $v_t^{x,t}$ and $v_t^{y,t}$ of $\mathbf{v}_t$ as well as tractor-fixed forces ($F_t^{x,t}$, $F_t^{y,t}$) and moments ($M_t^{z,t}$) those equations can be rewritten (see Section A.1.1) as:

$$\dot{v}_t^{x,t} = \frac{1}{m_t} F_t^{x,t} + \dot{\Psi}_t v_t^{y,t}, \tag{2.4}$$

$$\dot{v}_t^{y,t} = \frac{1}{m_t} F_t^{y,t} - \dot{\Psi}_t v_t^{x,t}, \tag{2.5}$$

$$\ddot{\Psi}_t = \frac{1}{I_t} M_t^{z,t}, \tag{2.6}$$

noting that $\dot{v}_t^{x,t}$ and $\dot{v}_t^{y,t}$ are only part of the vehicle's absolute acceleration:

$$\ddot{r}_t^{x,t} = \dot{v}_t^{x,t} - \dot{\Psi}_t v_t^{y,t}, \tag{2.7}$$

$$\ddot{r}_t^{y,t} = \dot{v}_t^{y,t} + \dot{\Psi}_t v_t^{x,t}, \tag{2.8}$$

with $\ddot{r}_t^{x,t}$ and $\ddot{r}_t^{y,t}$ as seen from an earth-fixed reference frame, stated, however, in tractor-fixed coordinates. The additional terms depict the centripetal acceleration resulting from the tractor-fixed coordinate system's motion.

In case of tractor-implement combinations multiple rigid bodies have to be considered. Those rigid bodies are subject to constraints imposed by the connecting drawbar. Applying Newton's laws of motion in case of constraints ranges form tedious to impractical. This is particularly true for steering actuators between those rigid bodies causing the constraints to become time-dependent or rheonomic [Gre88]. A practical straightforward way to consider constraints invokes Lagrange's equations of motion. The corresponding equations however are normally obtained in earth-fixed coordinates. Deriving those equations in vehicle-fixed coordinates, as required for further analysis, involves some thoughtfully chosen steps. A particularly advantageous approach has been presented by [Gen97] considering tractors and unsteered trailers. A generalized version of this approach will be used in this work to derive the equations of motion of a tractor and a steered implement. To illustrate the approach a concise example deriving the above equations (2.4) to (2.6) is provided in Section A.1.1.

Wheel Forces and Moments

Tire-road or tire-soil interaction and the resulting wheel forces and moments are core to dynamic vehicle modeling. Again, longitudinal, lateral, and vertical tire properties closely relate to a vehicle's driving/braking, handling, and ride characteristics. This section therefore focuses on the modeling of horizontal properties. Tires on roads have been extensively studied for decades and there are numerous models for this purpose. An overview given in [Pac06] distinguishes empirical, semi-empirical, simple physical, and complex physical models. Empirical models are based on measurements and curves fitted to those measurements. Semi-empirical models interpolate and extrapolate measured data relying on

Top View   Rear View
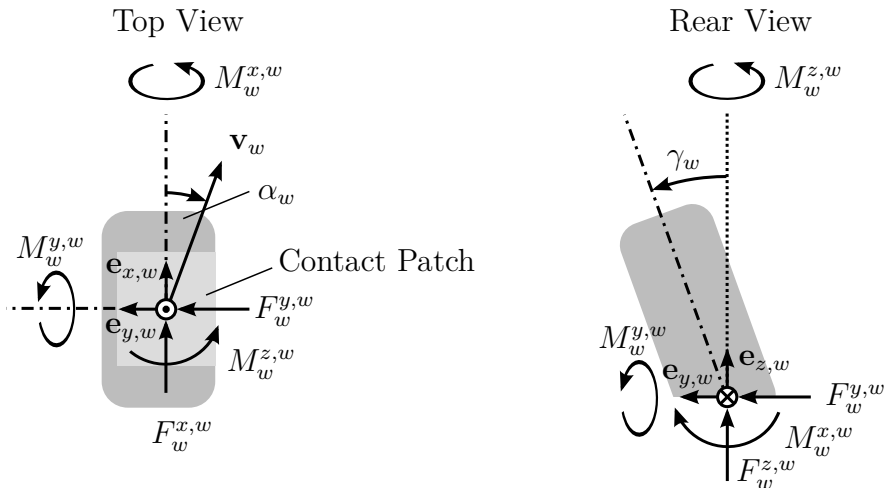
Figure 2.3: Definition of wheel related properties: wheel-fixed coordinate system ($\mathbf{e}_{x,w}$, $\mathbf{e}_{y,w}$, $\mathbf{e}_{z,w}$), ground reaction force components (longitudinal force $F_w^{x,w}$, lateral force $F_w^{y,w}$, vertical force $F_w^{z,w}$), ground reaction moment components (overturning moment $M_w^{x,w}$, rolling moment $M_w^{y,w}$, aligning moment $M_w^{z,w}$), slip angle α_w, camber angle γ_w, and velocity of the wheel center $\mathbf{v}_w$. Definitions according to [DIN94] except for α_w and γ_w which are chosen to obtain positive cornering and camber force gradients.

similarity methods and basic physical principles. [Pac06] provides the Magic Formula tire model as an example. Simple physical models may use mechanical analogies, e.g. brush tire model [Pac06], and may still have a closed form solution. Complex physical models may, for instance, rely on finite element methods and extensive computer simulations. Tires off roads operate in a less defined environment and physical models in particular require a closer look at the terrain including its elastic and plastic properties. An introduction to this vehicle-terrain interaction or terramechanics is provided by [Won08]. For tractor tires in particular, soil compaction, traction and suspension characteristics are of importance, which is also reflected in existing research. The lateral tire properties of modern tractor tires are a subject of recent studies by [GAP$^+$05] and [Sch05]. Both provide a comprehensive overview of previous research. They independently obtained measurements with custom tractor tire test rigs and proposed tractor tire models. Following some general definitions this section will focus mostly on their results.

Tire Properties: Figure 2.3 outlines the basic definitions of wheel related properties. The wheel-fixed coordinate system's origin is placed on ground level at the contact patch's center. The ground reaction force components ($F_w^{x,w}$, $F_w^{y,w}$, $F_w^{z,w}$) are assumed to act on the origin and are used to summarize normal and horizontal forces on the contact patch. The ground reaction moment components ($M_w^{x,w}$, $M_w^{y,w}$, $M_w^{z,w}$) account for possible asymmetric force distributions on the contact patch. The rolling moment $M_w^{y,w}$ typically arises from larger vertical forces at the contact patch's front. The aligning moment $M_w^{z,w}$ usually is caused by larger lateral forces at the contact patch's rear and may be alternatively

represented by shifting $F_w^{y,w}$ backwards by a distance commonly referred to as pneumatic trail [Pac06].

As a consequence of elastic tire properties and limited static friction both tire deformation and partial sliding in the contact patch will occur if horizontal wheel forces have to be developed. From a overall perspective both deformation and sliding of particular tire elements contribute to wheel slip. Wheel slip therefore is crucial for describing horizontal tire forces. To define wheel slip more precisely some auxiliary variables are required. Ω_w denotes the wheel's speed of revolution which is defined positive for a forward rolling wheel. Note, Ω_w may only be part of the wheel's entire angular velocity [Pac06]. Assuming $\alpha_w = 0$ and $\gamma_w = 0$ as well as $v_{w,0}^{x,w}$ and $\Omega_{w,0}$ to be measured on a freely rolling (i.e. undriven) wheel allows to introduce the dynamic rolling radius:

$$r_{d,w} = \frac{v_{w,0}^{x,w}}{\Omega_{w,0}}. \tag{2.9}$$

Following [Pac06] and assuming forward motion, i.e. $v_{w,0}^{x,w} \geq 0$ and $\Omega_{w,0} \geq 0$, the longitudinal $s_w^{x,w}$ and lateral slip $s_w^{y,w}$ may be defined as:

$$s_w^{x,w} = \frac{r_{d,w}\Omega_w - v_w^{x,w}}{\max\left(v_w^{x,w}, r_{d,w}\Omega_w\right)} = \begin{cases} \frac{r_{d,w}\Omega_w - v_w^{x,w}}{r_{d,w}\Omega_w} & \text{for } r_{d,w}\Omega_w \geq v_w^{x,w} \text{ (driving)}, \\ \frac{r_{d,w}\Omega_w - v_w^{x,w}}{v_w^{x,w}} & \text{for } r_{d,w}\Omega_w < v_w^{x,w} \text{ (braking)}, \end{cases} \tag{2.10}$$

$$s_w^{y,w} = \frac{-v_w^{y,w}}{v_w^{x,w}} = \tan\left(\alpha_w\right) \approx \alpha_w. \tag{2.11}$$

With these definitions horizontal forces in steady-state rectilinear motion in general are functions [Pac06]:

$$F_w^{x,w} = F_w^{x,w}\left(s_w^{x,w}, \alpha_w, \gamma_w, F_w^{z,w}\right), \tag{2.12}$$

$$F_w^{y,w} = F_w^{y,w}\left(s_w^{x,w}, \alpha_w, \gamma_w, F_w^{z,w}\right). \tag{2.13}$$

Varying either $s_w^{x,w}$ with $\alpha_w = 0$, or α_w with $s_w^{x,w} = 0$ with both cases assuming $\gamma_w = 0$ and constant $F_w^{z,w}$ yields the characteristic curves as shown in Figures 2.4, 2.5, and 2.6. Both lateral and longitudinal characteristics for tractor tires exhibit close similarities to those for passenger cars found e.g. in [MW04, Pac06]. Both $F_w^{x,w}$ vs. $s_w^{x,w}$ and $F_w^{y,w}$ vs. α_w are approximately linear for small slip. With increasing slip the increase in lateral and longitudinal force diminishes. A large longitudinal slip in particular may be accompanied by a decrease in longitudinal force due to a behavior dominated by sliding [MW04]. [Sch05] considers both driving and braking scenarios and notices differences in the longitudinal force-slip gradient with smaller values for braking wheels. He argues that this might be due to angled lugs. For passenger cars the longitudinal force coefficient $\mu_{x,w} = F_w^{x,w}/F_w^{z,w}$ varies little with changing wheel loads $F_w^{z,w}$. [Sch05] in contrast notices an increase of
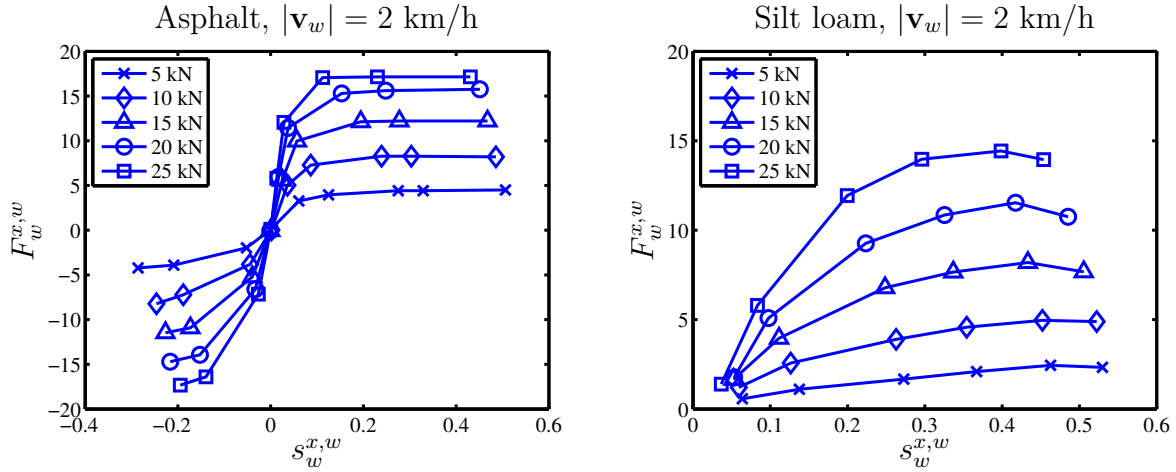
Figure 2.4: Longitudinal force $F_w^{x,w}$ vs. longitudinal slip $s_w^{x,w}$ from measurements with varying wheel load $F_w^{z,w}$. Tire: 520/70 R34, inflation pressure $p_{i,w} = 0.8$ bar. Note: Definition of $s_w^{x,w} = 0$ for driven wheel compensating rolling moment $M_w^{y,w}$ deviates slightly from this work's definition. (from [Sch05])
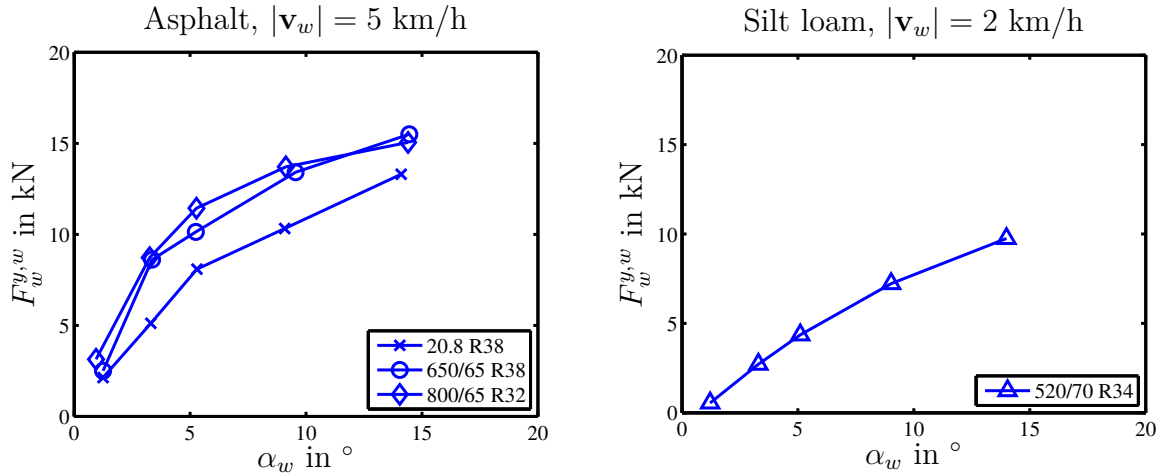
Figure 2.5: Lateral force $F_w^{y,w}$ vs. slip angle α_w from measurements with inflation pressure $p_{i,w} = 0.5$ bar, wheel load $F_w^{z,w} = 20$ kN, and varying tires. (from [Sch05])

$\mu_{x,w}$ with wheel load on loose soil and supposes an increased soil compaction contributing to improved traction. Similar to passenger cars [MW04] measurements both on asphalt and loose soil by [Sch05] exhibit a lateral force $F_w^{y,w}$ increasing with wheel load yet with decreasing increments. [Sch05] performed measurements with combined slip conditions, i.e. both $s_w^{x,w} \neq 0$ and $\alpha_w \neq 0$. The results resembled the behavior of passenger car tires, i.e. with a constant slip angle α_w applying a longitudinal force $F_w^{x,w}$ resulted in a decreased lateral force $F_w^{y,w}$. In contrast to passenger cars the asymmetry in $F_w^{y,w}$ vs. $F_w^{x,w}$ was more pronounced, with largest lateral forces not obtained for $F_w^{x,w} = 0$ but for small braking forces. The influence of camber was neither studied by [Sch05] nor [GAP$^+$05]. For passenger cars a camber angle γ_w approximately causes a vertical shift in the $F_w^{y,w}$ vs. α_w characteristic. A camber angle towards the curve's center results in a reduced α_w for a constant lateral force [MW04].
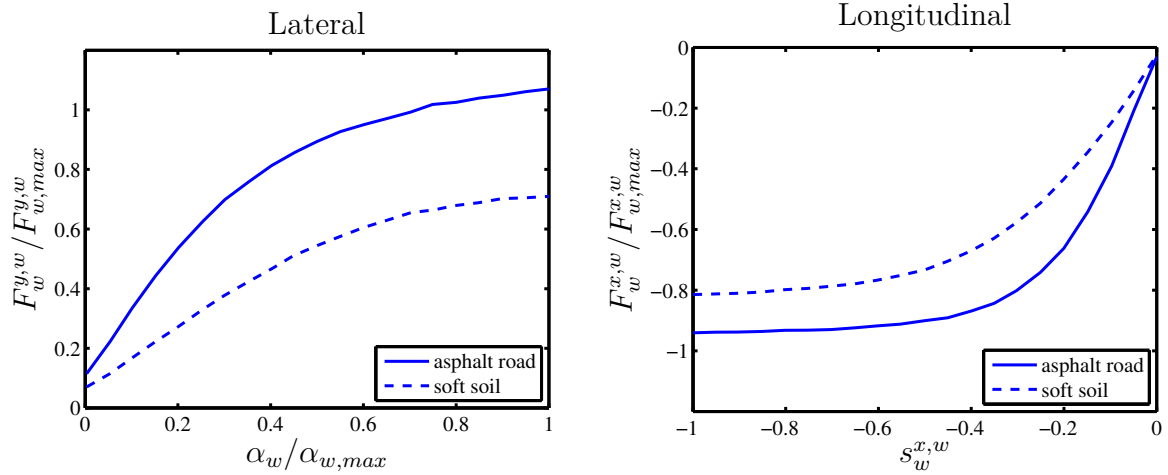
Figure 2.6: Magic Formula curve fits of measured tractor wheel lateral force $F_w^{y,w}$ vs. slip angle α_w and longitudinal force $F_w^{x,w}$ vs. longitudinal slip $s_w^{x,w}$. $F_w^{y,w}$ and $F_w^{x,w}$ are normalized to maximum values $F_{w,max}^{y,w}$ and $F_{w,max}^{x,w}$ obtained during measurements on asphalt. α_w is normalized to a reference slip angle $\alpha_{w,max}$. Tire: Pirelli TM700 300/70 R20, inflation pressure $p_{i,w} = 1.5$ bar. (from [GAP$^+$05])

Linearizing (2.12) and (2.13) about zero slip and zero camber angle as well as assuming a constant wheel load yields [Pac06]:

$$F_w^{x,w} = C_{sx,w} s_w^{x,w}, \tag{2.14}$$

$$F_w^{y,w} = C_{\alpha,w} \alpha_w + C_{\gamma,w} \gamma_w, \tag{2.15}$$

with longitudinal slip stiffness $C_{sx,w}$, cornering stiffness $C_{\alpha,w}$ and camber stiffness $C_{\gamma,w}$. The cornering stiffness in particular is an important parameter in terms of vehicle handling and stability.

Steady-State Tire Models: Numerous models have been proposed to depict (2.12) and (2.13). A common semi-empirical approach is based on fitting curves to measured data and using similarity methods to obtain results for situations not covered by measurements.

For tractor tires [GAP$^+$05] use the popular Magic Formula tire model [Pac06]. Core to this model is a curve fit [Pac06]

$$x = \tan(\alpha_w) + S_h, \tag{2.16}$$

$$F_w^{y,w} = D \sin\left(C \arctan\left(Bx - E\left(Bx - \arctan(Bx)\right)\right)\right) + S_v, \tag{2.17}$$

with similar expressions for $F_w^{x,w}$ and $M_w^{z,w}$. B, C, D, and E are factors affecting stiffness, shape, peak value and curvature. S_h and S_v account for possible horizontal and vertical shifts. The factors are obtained for pure longitudinal or lateral slip as well as nominal wheel load and camber angle. Deviations from these conditions are considered using similarity methods. Figure 2.6 depicts examples for curves obtained by [GAP$^+$05]. Unfortunately,

they just present normalized curves and do not state the quite numerous tire model parameters.

[Sch05] considers several steady-state tire models. A simple model of lateral tire forces using only two important tire parameters is:

$$F_w^{y,w} = F_{w,max}^{y,w} \left(1 - \exp \left(-\frac{\alpha_w C_{\alpha,w}}{F_{w,max}^{y,w}} \right) \right) \tag{2.18}$$

with $F_{w,max}^{y,w}$ denoting the maximum tire force. [Sch05] conducted experiments with various tires, wheel loads, speeds, and tire pressures. He used a fit of (2.18) to obtain $F_{w,max}^{y,w}$ and $C_{\alpha,w}$ as shown in Table 2.1. The purely empiric tire model (2.18) is not used with similarity methods, yet the wide range of scenarios covered by Table 2.1 proved to be a useful source of otherwise scarce information on cornering properties of tractor tires.

The second tire model parameterized by [Sch05] is a Fiala tire model. This is a simple physical model assuming the tire to be a spring-bedded ring. With one particular set of parameters the model approximately resembles a third order polynomial in terms of α_w and is capable of depicting lateral forces for a particular wheel load. Hence the advantage is rather in analyzing tire principles than in comprehensive modeling.

The last steady-state tire model considered by [Sch05] is a Slip-Drift model proposed by Grečenko. It is intended to model combined slip conditions on loose soil. This physical model is motivated by combined tire and soil deformation and the associated shear stress.

Table 2.1: Tire parameters' influence on cornering stiffness $C_{\alpha,w}$ based on test rig measurements on asphalt. (from [Sch05])

	Tire	Wheel load	Inflation pressure	Speed	Max. lateral force	Cornering stiffness
		$F_w^{z,w}$ in kN	$p_{i,w}$ in bar	$|\mathbf{v}_w|$ in km/h	$F_{w,max}^{y,w}$ in kN	$C_{\alpha,w}$ in kN/°
Varying wheel load	20.8 R38	10	0.8	2	10.14	1.71
		15			13.11	2.41
		20			15.15	2.66
		25			16.51	3.35
Varying pressure	20.8 R38	10	0.8	2	10.14	1.71
			1.2		13.24	1.50
			1.6		14.15	1.22
Varying speed	20.8 R38	20	0.8	2	15.15	2.66
				5	17.67	2.84
				10	18.04	2.11
Varying tire	20.8 R38	20	0.5	5	15.94	1.98
	650/65 R38				16.05	3.20
	800/65 R32				15.21	3.58

The model relies on four parameters for a particular wheel load comprising the maximum lateral and longitudinal force coefficient and two parameters modeling deformation. [Sch05] uses measurements with pure or combined slip conditions to parameterize the Slip-Drift model and finds that the obtained parameters differ to a noticeable degree.

Transient Tire Models: The previous tire models were based on static functions relating slip with tire forces. A changing wheel steering angle in this case results in an immediate side-slip angle change and an immediate change of the lateral tire force. In order to obtain a more realistic description of transient behavior additional measures are necessary.

For passenger cars transient lateral tire behavior is commonly introduced by using the tire relaxation length $\sigma_{\alpha,w}$ [MW04]. This is based on measurements indicating that lateral tire force generation is not time dependent but dependent on the distance a tire rolls. In measurements with tractor tires [Sch05] found a similar distance dependent behavior. In a test setup he enforced sinusoidal side-slip angles and measured the resulting lateral tire forces. Analyzing either amplitude ratio or phase shift and assuming a linear transient tire model

$$\underbrace{T_{\alpha,w}}_{\frac{\sigma_{\alpha,w}}{v_w^{x,w}}} \dot{F}_w^{y,w} + F_w^{y,w} = C_{\alpha,w}\alpha_w. \tag{2.19}$$

[Sch05] determined the time constants $T_{\alpha,w}$ as shown in Table 2.2 and calculated the relaxation lengths

$$\sigma_{\alpha,w} = T_{\alpha,w}v_w^{x,w}. \tag{2.20}$$

A second experiment was conducted to obtain $T_{\alpha,w}$ using step responses. The determined values exhibited some variation depending on the chosen approach. Typical relaxation length values obtained by [Sch05] range from slightly below the wheel's radius to the wheel's diameter. For passenger cars [MW04] provides 2/3 of a wheel's circumference as a typical value. [Sch05] performed a small number of tests in a soil bin with silt loam. The results obtained are depicted in Table 2.3. He found a decrease in cornering stiffness and, interestingly, a decrease in relaxation length, as well.

The delay in tire force buildup described by the linear transient tire model (2.19) may be combined with nonlinear steady-state models. This is done by introducing a transient side-slip angle $\alpha_{re,w}$ and the ODE

$$\frac{\sigma_{\alpha,w}}{v_w^{x,w}}\dot{\alpha}_{re,w} + \alpha_{re,w} = \alpha_w \tag{2.21}$$

$\alpha_{re,w}$ then replaces α_w in the former steady-state tire force models.

Table 2.2: Tire parameters' influence on lateral force generation first order lag time constant $T_{\alpha,w}$ based on test rig measurements on asphalt. $T_{\alpha,w}$ is either based on phase or amplitude of measurements. (from [Sch05])

	Tire	Wheel load	Inflation pressure	Speed	Time from amplitude	Time from phase
		$F_w^{z,w}$ in kN	$p_{i,w}$ in bar	$|\mathbf{v}_w|$ in km/h	$T_{\alpha,w}$ in s	$T_{\alpha,w}$ in s
Varying tire	20.8 R38	20	0.5	5	0.63	1.20
	650/65 R38				1.37	1.65
	800/65 R32				1.15	1.07
Varying pressure	800/65 R32	20	0.5	2	1.15	1.07
			0.8		0.98	0.85
			1.2		1.11	0.84
			1.6		0.76	0.53
Varying speed	20.8 R38	20	0.8	2	2.33	1.85
				5	0.80	0.95
				10	0.26	0.47

Table 2.3: Influence of terrain on cornering stiffness $C_{\alpha,w}$ and tire relaxation length $\sigma_{\alpha,w}$. Tire: 520/70 R34, inflation pressure $p_{i,w} = 0.8$ bar. (from [Sch05])

Terrain	Wheel load	Speed	Cornering stiffness	Relaxation length
	$F_w^{z,w}$ in kN	$|\mathbf{v}_w|$ in km/h	$C_{\alpha,w}$ in kN/°	$\sigma_{\alpha,w}$ in m
Silt loam	10	2	0.94	0.46
Silt loam		4	0.84	0.38
Asphalt		5	1.73	0.62
Silt loam	20	2	0.98	0.47
Silt loam		3.5	1.14	0.65
Asphalt		5	1.87	0.89

Dynamic Tractor Model

The properties discussed for an individual wheel and the single track model given in Figure 2.2, as well as (2.4), (2.5), and (2.6) are now combined. Figure 2.7 depicts the relevant properties of a tractor front wheel. Definitions for tractor rear wheel and possible implement wheels are similar. The subscript $_w$ is omitted to avoid lengthy double subscripts. By combining all wheels of an axle the properties of a single track model's wheel differ from individual wheel properties discussed previously. Nevertheless it is common to use the same variables. The cornering stiffness $C_{\alpha,tf}$ for instance describes a combined cornering stiffness of all tractor front wheels. In this work no dual tires have been considered, hence the combined cornering stiffness is approximately twice the cornering stiffness of a single wheel. For vehicle handling or path tracking the focus is on lateral vehicle motion.
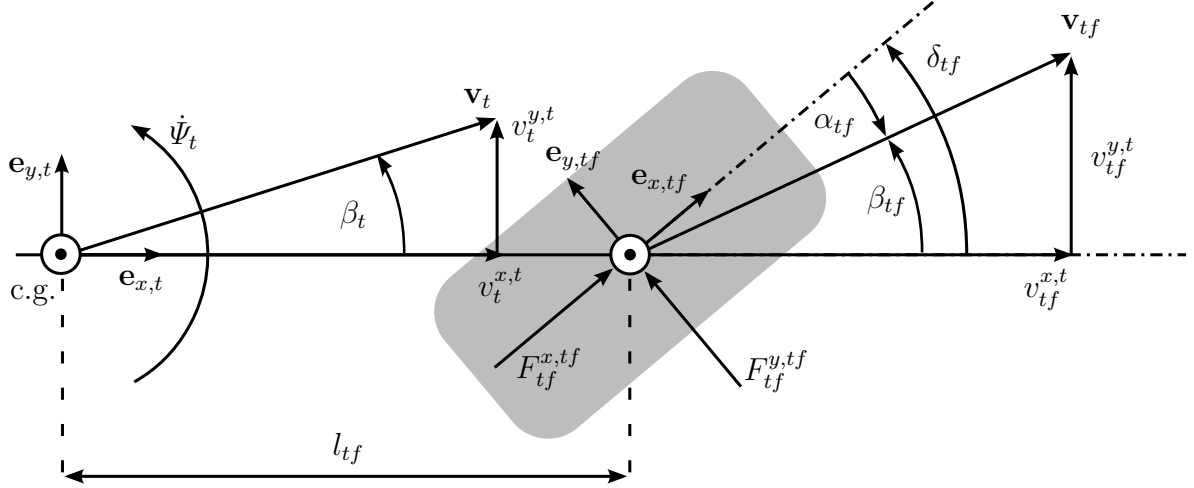
Figure 2.7: Definition of tractor front wheel related properties: wheel-fixed coordinate system ($\mathbf{e}_{x,tf}$, $\mathbf{e}_{y,tf}$, $\mathbf{e}_{z,tf}$), longitudinal wheel force $F_{tf}^{x,tf}$, lateral wheel force $F_{tf}^{y,tf}$, and wheel side-slip angle α_{tf}. β_t denotes the commonly used tractor side-slip angle located at the tractor c.g. Similarly β_{tf} defines the tractor side-slip angle at the tractor front wheel location. Rear wheel and implement properties are defined analogously.

Common assumptions therefore are that the tractor longitudinal velocity $v_t^{x,t}$ is constant or slowly changing. Hence, it is assumed to be an additional plant parameter in vehicle lateral motion. The influence of longitudinal wheel slip and forces is initially neglected within the describing equations. Nevertheless, the influence can be studied subsequently by varying lateral tire parameters. Similarly, different wheel loads and soil conditions may be studied using parameter variation. With tractor path tracking being part of vehicle normal operation away from vehicle limits a linear tire model is chosen to describe lateral tire forces.

With these assumptions the overall dynamic tractor model can be stated using the front and rear wheels side-slip angels α_{tf} and α_{tr}, which can be found to be (cf. Figure 2.7):

$$\alpha_{tf} = \delta_{tf} - \arctan\left(\frac{v_{tf}^{y,t}}{v_{tf}^{x,t}}\right) = \delta_{tf} - \arctan\left(\frac{l_{tf}\dot{\Psi}_t + v_t^{y,t}}{v_t^{x,t}}\right), \tag{2.22}$$

$$\alpha_{tr} = -\arctan\left(\frac{v_{tr}^{y,t}}{v_{tr}^{x,t}}\right) = -\arctan\left(\frac{-l_{tr}\dot{\Psi}_t + v_t^{y,t}}{v_t^{x,t}}\right). \tag{2.23}$$

The resulting tire forces are modeled transient by introducing front and rear wheel tire relaxation lengths $\sigma_{\alpha,tf}$ and $\sigma_{\alpha,tr}$. With (2.21) the transient side-slip angles $\alpha_{re,tf}$ and $\alpha_{re,tr}$ are given by ODEs:

$$\dot{\alpha}_{re,tf} = \frac{\cos\left(\delta_{tf}\right) v_t^{x,t} + \sin\left(\delta_{tf}\right)\left(l_{tf}\dot{\Psi}_t + v_t^{y,t}\right)}{\sigma_{\alpha,tf}}\left(\alpha_{tf} - \alpha_{re,tf}\right), \tag{2.24}$$

$$\dot{\alpha}_{re,tr} = \frac{v_t^{x,t}}{\sigma_{\alpha,tr}}\left(\alpha_{tr} - \alpha_{re,tr}\right). \tag{2.25}$$

Using the combined cornering stiffnesses $C_{\alpha,tf}$ and $C_{\alpha,tr}$ to describe lateral tire forces the equations of motion (2.5) and (2.6) may be rewritten:

$$\dot{v}_t^{y,t} = \frac{1}{m_t} \left(\cos\left(\delta_{tf}\right) C_{\alpha,tf} \alpha_{re,tf} + C_{\alpha,tr} \alpha_{re,tr} \right) - \dot{\Psi}_t v_t^{x,t}, \tag{2.26}$$

$$\ddot{\Psi}_t = \frac{1}{I_t} \left(l_{tf} \cos\left(\delta_{tf}\right) C_{\alpha,tf} \alpha_{re,tf} - l_{tr} C_{\alpha,tr} \alpha_{re,tr} \right). \tag{2.27}$$

In a next step, one may introduce earth-fixed coordinates describing the vehicle position for simulation purposes. This is done using e.g. ODEs for the tractor rear wheel position $r_{tr}^{x,e}$ and $r_{tr}^{y,e}$:

$$\dot{r}_{tr}^{x,e} = \cos\left(\Psi_t\right) \left(v_t^{x,t}\right) - \sin\left(\Psi_t\right) \left(-l_{tr}\dot{\Psi}_t + v_t^{y,t}\right), \tag{2.28}$$

$$\dot{r}_{tr}^{y,e} = \sin\left(\Psi_t\right) \left(v_t^{x,t}\right) + \cos\left(\Psi_t\right) \left(-l_{tr}\dot{\Psi}_t + v_t^{y,t}\right). \tag{2.29}$$

Alternatively the vehicle position may be stated in terms of deviations from a desired path. Referring to the straight path of Figure 2.2 the associated ODEs are:

$$\dot{e}_{th} = \dot{\Psi}_t - \dot{\Psi}_d, \tag{2.30}$$

$$\dot{e}_{tl} = \sin\left(e_{th}\right) \left(v_t^{x,t}\right) + \cos\left(e_{th}\right) \left(-l_{tr}\dot{\Psi}_t + v_t^{y,t}\right). \tag{2.31}$$

The latter description is particularly suitable for controller design as well as further analysis. Having put emphasis on using tractor-fixed variables the system given by (2.22) to (2.27) as well as (2.30) and (2.31) allows for linearization. Defining the system state vector $\mathbf{x}$, input vector $\mathbf{u}$, and output vector $\mathbf{y}$ as:

$$\mathbf{x} = \left[e_{tl}, e_{th}, v_t^{y,t}, \dot{\Psi}_t, \alpha_{re,tf}, \alpha_{re,tr}\right]^{\mathrm{T}}, \tag{2.32}$$

$$\mathbf{u} = \delta_{tf}, \tag{2.33}$$

$$\mathbf{y} = \left[e_{tl}, e_{th}\right]^{\mathrm{T}} \tag{2.34}$$

the system linearized about $\mathbf{x} = \mathbf{0}$ and $\mathbf{u} = \mathbf{0}$ is:

$$\dot{\mathbf{x}} = \mathbf{A}\mathbf{x} + \mathbf{B}\mathbf{u}, \tag{2.35}$$

$$\mathbf{y} = \mathbf{C}\mathbf{x}, \tag{2.36}$$

$$\mathbf{A} = \begin{bmatrix} 0 & v_t^{x,t} & 1 & -l_{tr} & 0 & 0 \\ 0 & 0 & 0 & 1 & 0 & 0 \\ 0 & 0 & 0 & -v_t^{x,t} & \frac{C_{\alpha,tf}}{m_t} & \frac{C_{\alpha,tr}}{m_t} \\ 0 & 0 & 0 & 0 & \frac{l_{tf}C_{\alpha,tf}}{I_t} & \frac{l_{tr}C_{\alpha,tr}}{I_t} \\ 0 & 0 & \frac{-1}{\sigma_{\alpha,tf}} & \frac{-l_{tf}}{\sigma_{\alpha,tf}} & \frac{-v_t^{x,t}}{\sigma_{\alpha,tf}} & 0 \\ 0 & 0 & \frac{-1}{\sigma_{\alpha,tr}} & \frac{l_{tr}}{\sigma_{\alpha,tr}} & 0 & \frac{-v_t^{x,t}}{\sigma_{\alpha,tr}} \end{bmatrix}, \qquad \mathbf{B} = \begin{bmatrix} 0 \\ 0 \\ 0 \\ 0 \\ \frac{v_t^{x,t}}{\sigma_{\alpha,tf}} \\ 0 \end{bmatrix}, \qquad (2.37)$$

$$\mathbf{C} = \begin{bmatrix} 1 & 0 & 0 & 0 & 0 & 0 \\ 0 & 1 & 0 & 0 & 0 & 0 \end{bmatrix}. \qquad (2.38)$$

Optionally, this may be further simplified for steady-state cornering without relaxation length using:

$$\mathbf{x} = \left[e_{tl}, e_{th}, v_t^{y,t}, \dot{\Psi}_t \right]^{\mathrm{T}}, \qquad (2.39)$$

$$\mathbf{u} = \delta_{tf}, \qquad (2.40)$$

$$\mathbf{y} = \left[e_{tl}, e_{th} \right]^{\mathrm{T}}, \qquad (2.41)$$

yielding a system description given by:

$$\mathbf{A} = \begin{bmatrix} 0 & v_t^{x,t} & 1 & -l_{tr} \\ 0 & 0 & 0 & 1 \\ 0 & 0 & \frac{-C_{\alpha,tf}-C_{\alpha,tr}}{m_t v_t^{x,t}} & \frac{-m_t\left(v_t^{x,t}\right)^2 - l_{tf}C_{\alpha,tf} + l_{tr}C_{\alpha,tr}}{m_t v_t^{x,t}} \\ 0 & 0 & \frac{-l_{tf}C_{\alpha,tf} + l_{tr}C_{\alpha,tr}}{I_t v_t^{x,t}} & \frac{-l_{tf}^2 C_{\alpha,tf} - l_{tr}^2 C_{\alpha,tr}}{I_t v_t^{x,t}} \end{bmatrix}, \qquad \mathbf{B} = \begin{bmatrix} 0 \\ 0 \\ \frac{C_{\alpha,tf}}{m_t} \\ \frac{l_{tf}C_{\alpha,tf}}{I_t} \end{bmatrix},$$
$$(2.42)$$

$$\mathbf{C} = \begin{bmatrix} 1 & 0 & 0 & 0 \\ 0 & 1 & 0 & 0 \end{bmatrix}. \qquad (2.43)$$

For passenger cars the differential equations describing $\dot{v}_t^{y,t}$ and $\ddot{\Psi}_t$, given by the last two rows of (2.42), are of fundamental importance for vehicle handling and stability. Properties of these equations are widely studied by [MW04, Pac06].

Conditions encountered during path tracking with agricultural tractors deviate from typical conditions for passenger cars or trucks. Both vehicle parameters and operating speeds are different. Using this work's tractor parameters of Appendix A.5, Figure 2.8 depicts the eigenvalues of system matrices $\mathbf{A}$ given by (2.37) and (2.42) for various tractor speeds. Both systems, regardless of a particular speed, exhibit two eigenvalues at 0. Examining the block triangular form of (2.37) and (2.42) allows to trace those eigenvalues to (2.30) and (2.31). Both lateral error e_{tl} and heading error e_{th} are not fed back into other system parts. With a typically small lateral tractor rear wheel velocity $\left(-l_{tr}\dot{\Psi}_t + v_t^{y,t} \right)$ the tracking error dynamics may be seen as the yaw rate $\dot{\Psi}_t$ being integrated twice yielding
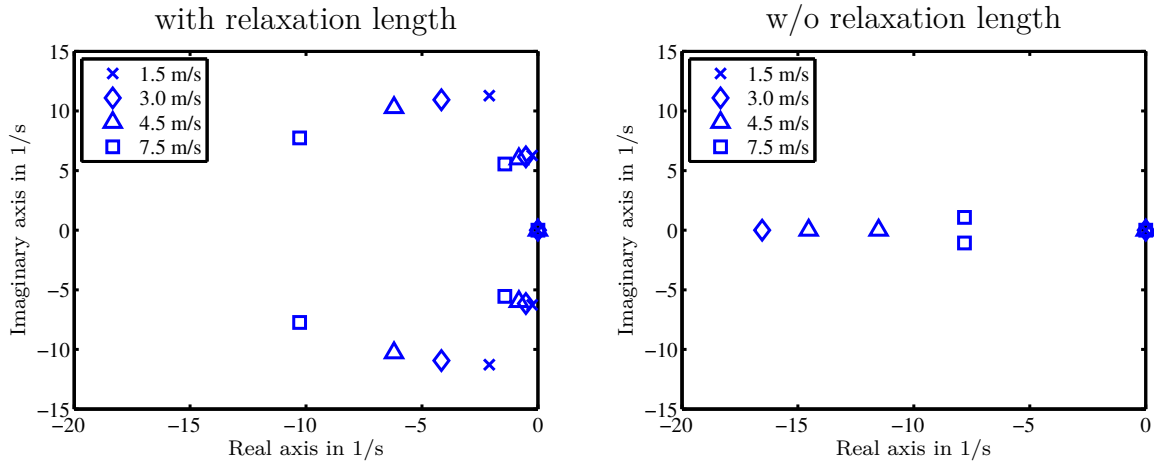
Figure 2.8: Eigenvalues of system matrix **A** either considering relaxation length (2.37) or neglecting it (2.42). Parameters are chosen as stated in Appendix A.5 and tractor lateral velocity $v_t^{x,t}$ is varied.

approximately e_{tl}. This double integrator however exhibits a velocity dependent gain as seen in (2.31). The remaining parts of (2.37) and (2.42) are different. For low speeds the simple system without relaxation length given by differential equations for $\dot{v}_t^{y,t}$ and $\ddot{\Psi}_t$ yields two real eigenvalues. At higher speeds these eigenvalues become conjugate complex. This resembles the behavior found for passenger cars with positive understeer gradients [Pac06]. Considering the tire relaxation length immediately results in two conjugate complex eigenvalue pairs. Having described the tracking error dynamics approximately by two integrators with input $\dot{\Psi}_t$, the remaining system parts may be further analyzed considering the transfer function from steering angle input δ_{tf} to yaw rate $\dot{\Psi}_t$, i.e.:

$$\frac{\mathscr{L}\left\{\dot{\Psi}_t(t)\right\}}{\mathscr{L}\left\{\delta_{tf}(t)\right\}} = G_{\delta_{tf},\dot{\psi}_t}(s) \tag{2.44}$$

with $\mathscr{L}\left\{\cdot\right\}$ denoting the Laplace transform [Foe94]. The corresponding Bode diagrams are depicted in Figure 2.9, using again the tractor parameters of Appendix A.5. Magnitude and phase for both indicate an upper limit for steering frequencies the vehicle is capable to follow. This however is without delays due to hydraulic tractor steering actuators. The simple case neglecting tire relaxation length is extensively studied for passenger cars [Pac06]. For small speeds the steady-state gain increases almost linearly with speed. The peak in $\left|G_{\delta_{tf},\dot{\psi}_t}(s)\right|$, as found for some passenger cars [Pac06], can be found for the given parameters as well yet at tractor speeds beyond typical values. In case relaxation length is considered, $\left|G_{\delta_{tf},\dot{\psi}_t}(s)\right|$ exhibits a peak for small speeds also. It is worth noting that both cases with and without relaxation length are in agreement with research by [KS10] using a different tractor and different parameters. In particular their transfer function $G_{\delta_{tf},\dot{\psi}_t}(s)$ accounting for relaxation length has been found to resemble their measurements remarkably well.
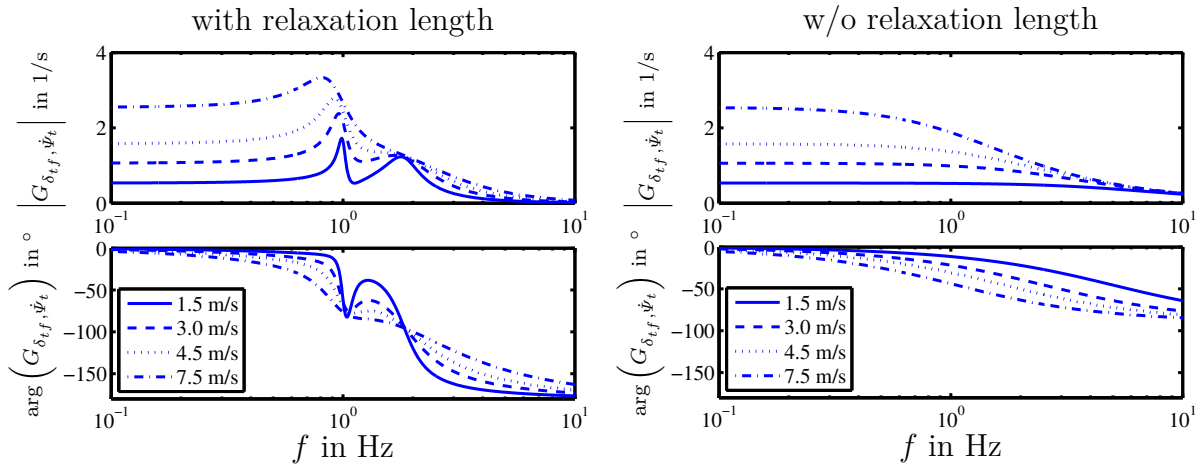
Figure 2.9: Steering angle to yaw rate transfer function $G_{\delta_{tf}, \dot{\psi}_t}(s)$ either considering relaxation length (2.37) or neglecting it (2.42). Parameters are chosen as stated in section Appendix A.5 and tractor lateral velocity $v_t^{x,t}$ is varied.

Dynamic Tractor-Trailer and Tractor-Implement Models

Having outlined the principal idea of dynamic vehicle modeling this, section now provides an overview of related work modeling tractor-implement or tractor-trailer combinations.

On-road tractor-trailer combinations have been subject to research for quite a while and fundamentals on modeling and lateral stability can be found in [Ell94] and [Gen97]. Both derive the describing ODEs explicitly, but consider unsteered trailers only. [Gen97] uses a very systematic approach to modeling invoking Lagrangian mechanics and some well-considered coordinate transformations. [Ell94] and [Gen97] use linear tire models for vehicle handling analysis and provide an outlook on using nonlinear tire models for detailed simulations. [CT95a, CT00] derive a dynamic tractor-trailer model for path tracking control on automated highways and use trailer brakes as additional inputs. To account for asymmetric forces due to braking, individual wheels are considered. Simulations are performed using a dedicated nonlinear truck tire model from literature. Controller design relies on tires modeled by longitudinal and cornering stiffness parameters. [TWH+98] extend this model by adding multiple trailers. [RT07] model a tractor with three trailers placing steerable front wheels on all or a subset of those trailers. The objective is to minimize the rearward amplification of the trailers' lateral accelerations. A single track model, with cornering stiffnesses being the only tire parameters, is used for both controller design and simulation. [Wag10] uses dynamic modeling for path tracking control of train-like tractor-trailer combinations with all-wheel-steering. The tire model used is based on cornering stiffnesses only. All approaches so far have stated the underlying ODEs in an explicit form in order to allow for comprehensive system analysis and subsequent controller design. If the focus was mostly on simulation without the need of explicit ODEs, a multibody dynamics simulation software would be a further modeling option. Common tractor-trailer combinations are supported by commercial software like Adams/Car Truck [MSC12], IPG TruckMaker [WOS+10], and Simpack Automotive [SIM11].

Off-road tractor-trailer or tractor-implement combinations are usually operated at lower speeds, which is accompanied by lower lateral accelerations and smaller wheel side-slip while cornering on solid ground. Despite that, on loose or slippery soil as well as on slopes wheel side-slip might still be prominent. A dynamic vehicle model might in this case be a reasonable choice to depict the real world behavior. [PKE07] have derived a single track model for a tractor towing an implement with steerable wheels under the influence of lateral disturbances. [SKEP09] have extended this model by attaching an unsteered trailer to the implement. In both cases lateral tire forces are modeled using cornering stiffnesses. Longitudinal tire forces are divided into traction forces and rolling resistances. Traction forces are inputs to the system. The rolling resistances exhibit a velocity and a wheel load dependent term. [KS10] modeled a tractor and an unsteered towed implement using a single track description. The model is used for path tracking controller design and simulation. They consider two linear tire model variants, which are a simple model using cornering stiffnesses as only parameters and a second model accounting for tire relaxation length. [GB08, DB09] consider the special case of a three-point hitch mounted implement which, in contrast to a towed implement, is not pivotable and forms a single rigid body with the tractor. They use a single track description and model both lateral tire forces as well as lateral forces caused by the ground engaging implement tools via cornering stiffnesses.

2.1.2 Kinematic Models

Kinematic models, as for instance discussed in introductory literature [Raj06], describe vehicle motion in a simplified manner without considering forces and moments causing the movement. This section outlines the modeling assumptions made and derives a simple concise kinematic tractor model. Related work regarding kinematic models of tractor-trailer or tractor-implement combinations is addressed subsequently.

Modeling Assumptions
Starting with Figure 2.2 and the assumptions made for a dynamic single track vehicle model, the kinematic model is assumed to be in plane motion with all wheel properties combined into a single wheel per axle as well. In addition to those premises, the kinematic model is further restricted. The model is based on geometric properties and the assumption of purely rolling wheels. In other words, side-slip is neglected and the wheels' velocities are assumed to point in wheel forward direction. The kinematic model does not account for forces and moments causing the motion and dynamic model parameters like mass and moment of inertia are not required. The model exhibits 3 DoFs which may be defined using tractor heading Ψ_t and the tractor rear wheel position $r_{tr}^{x,e}$ and $r_{tr}^{y,e}$ in earth-fixed coordinates for instance. The tractor c.g. position is not used, because there is no need to determine the c.g. position at all. The tractor's lateral velocity $v_{tr}^{x,t} = v_t^{x,t}$ is assumed to be a parameter of the system.

Kinematic Tractor Model

Core to kinematic modeling is the assumption of restricted wheel velocity directions. Considering Figure 2.2 these constraints can be formalized as follows:

$$\underbrace{\left[-\sin\left(\delta_{tf}\right), \cos\left(\delta_{tf}\right) \right]}_{\mathbf{e}_{\perp,tf}^{\mathrm{T}}} \begin{bmatrix} v_{tf}^{x,t} \\ v_{tf}^{y,t} \end{bmatrix} = 0, \tag{2.45}$$

$$\underbrace{\begin{bmatrix} 0, 1 \end{bmatrix}}_{\mathbf{e}_{\perp,tr}^{\mathrm{T}}} \begin{bmatrix} v_{tr}^{x,t} \\ v_{tr}^{y,t} \end{bmatrix} = 0, \tag{2.46}$$

with $\mathbf{e}_{\perp,tf}$ and $\mathbf{e}_{\perp,tr}$ denoting vectors perpendicular to the respective wheel velocity vectors $\mathbf{v}_{tf}$ and $\mathbf{v}_{tr}$. $\mathbf{e}_{\perp,tf}$ and $\mathbf{e}_{\perp,tr}$ are chosen to depict the zero side-slip constraint. From (2.46) immediately follows $v_{tr}^{y,t} = 0$, i.e. the lateral rear wheel velocity vanishes. Using

$$\begin{bmatrix} v_{tf}^{x,t} \\ v_{tf}^{y,t} \end{bmatrix} = \begin{bmatrix} v_{tr}^{x,t} \\ v_{tr}^{y,t} \end{bmatrix} + \begin{bmatrix} 0 \\ \dot{\Psi}_t l_t \end{bmatrix} = \begin{bmatrix} v_{tr}^{x,t} \\ \dot{\Psi}_t l_t \end{bmatrix} \tag{2.47}$$

and (2.45) allows to solve for $\dot{\Psi}_t$ yielding

$$\dot{\Psi}_t = \frac{v_{tr}^{x,t}}{l_t} \tan\left(\delta_{tf}\right). \tag{2.48}$$

In contrast to the transfer functions found for the previously discussed dynamic tractor models, the kinematic model exhibits a simple static function relating steering angle δ_{tf} and yaw rate $\dot{\Psi}_t$.

Introducing earth-fixed coordinates describing the vehicle position for simulations may be done similar to (2.28) and (2.29) using:

$$\dot{r}_{tr}^{x,e} = \cos\left(\Psi_t\right) v_{tr}^{x,t} - \sin\left(\Psi_t\right) \underbrace{v_{tr}^{y,t}}_{0}, \tag{2.49}$$

$$\dot{r}_{tr}^{y,e} = \sin\left(\Psi_t\right) v_{tr}^{x,t} + \cos\left(\Psi_t\right) \underbrace{v_{tr}^{y,t}}_{0}. \tag{2.50}$$

Similar to (2.30) and (2.31) the vehicle position in terms of deviations from a straight path as shown in Figure 2.2 can be stated as:

$$\dot{e}_{th} = \underbrace{\frac{v_{tr}^{x,t}}{l_t} \tan\left(\delta_{tf}\right)}_{\dot{\Psi}_t} - \dot{\Psi}_d \tag{2.51}$$

$$\dot{e}_{tl} = \sin\left(e_{th}\right) v_{tr}^{x,t} + \cos\left(e_{th}\right) \underbrace{v_{tr}^{y,t}}_{0}. \tag{2.52}$$

Defining the system state vector $\mathbf{x}$, input vector $\mathbf{u}$, and output vector $\mathbf{y}$ as:

$$\mathbf{x} = [e_{tl}, e_{th}]^{\mathrm{T}}, \tag{2.53}$$

$$\mathbf{u} = \delta_{tf}, \tag{2.54}$$

$$\mathbf{y} = [e_{tl}, e_{th}]^{\mathrm{T}} \tag{2.55}$$

the system linearized about $\mathbf{x} = \mathbf{0}$ and $\mathbf{u} = \mathbf{0}$ is

$$\dot{\mathbf{x}} = \mathbf{A}\mathbf{x} + \mathbf{B}\mathbf{u}, \tag{2.56}$$

$$\mathbf{y} = \mathbf{C}\mathbf{x}, \tag{2.57}$$

with

$$\mathbf{A} = \begin{bmatrix} 0 & v_t^{x,t} \\ 0 & 0 \end{bmatrix}, \qquad \mathbf{B} = \begin{bmatrix} 0 \\ \frac{v_t^{x,t}}{l_t} \end{bmatrix}, \qquad \mathbf{C} = \begin{bmatrix} 1 & 0 \\ 0 & 1 \end{bmatrix}. \tag{2.58}$$

The linearized system possesses only two eigenvalues at zero and the transfer function from steering input δ_{tf} to lateral error e_{tl} is:

$$\frac{\mathscr{L}\{e_{tl}(t)\}}{\mathscr{L}\{\delta_{tf}(t)\}} = G_{\delta_{tf},e_{tl}}(s) = \frac{\left(v_t^{x,t}\right)^2}{l_t}\frac{1}{s^2}. \tag{2.59}$$

Kinematic Tractor-Trailer and Tractor-Implement Models

Kinematic modeling of on-road tractor-trailer combinations is not very common due to the fact that wheel side-slip normally has to be considered at higher vehicle speeds. However, geometric properties might be useful to assess the turning radii of those combinations [Gen97].

Off-road tractor-trailer or tractor-implement combinations are more frequently described using kinematic models. [Bel99, Bev01, CLTM10, KS10] each modeled a tractor towing an unsteered implement. [BOV12] modeled a towed seed drill with a steerable drawbar. Although kinematic models lack the ability to include side-slip based on physical principles, [CLTM10, BOV12] try to include this effect by adding bias parameters to the kinematic model. Using those extended models in an estimator which is computed parallel to the real tractor-implement combination allows them to capture the differences between kinematic model and real system. Those differences are then considered within the control laws.

2.1.3 Identified Models

Kinematic and dynamic models are the result of a theoretical modeling approach considering physical laws and the actual structure of the system. Identified models or black-box models [Ise07] in contrast assume a certain class of models, e.g. a transfer function with still undefined coefficients, without knowing the system's internal structure. The black-box model parameters are identified using information from input and output measurements only.

[Bev01] used this approach and created a black-box model for the major part of a tractor towing an unsteered implement. Only the lateral tracking error calculation required some geometric parameters to be measured.

Identification of entire models relies on test drives in order to obtain sufficient measurements for identification. These test drives have to be performed for each particular tractor-implement combination. Requiring an operator to do these drives in possibly planted fields was seen as a major drawback over e.g. measuring geometric properties required to obtain a kinematic model. Hence, identified models have not been considered in this work.

2.2 Path Tracking Control

Research interest in vehicle path tracking control is driven by numerous applications. In the on-road domain examples range from automated highways to autonomous cars in urban environments. In the off-road domain path tracking control of agricultural machinery in particular aroused interest due to the possibilities resulting from automation, repeatability, and accuracy.

This chapter provides an overview of past and present research on path tracking control. In case a particular approach has been applied to passenger cars as well as tractor-trailer or tractor-implement combinations the overview focuses on combinations. An additional tabular summary of tractor-trailer and tractor-implement path tracking research is given in Table A.9 of Appendix A.8. A survey on passenger car path tracking control in particular is given by [Sni09]. For each approach a brief introduction to the underlying theory is included in this section. The simple kinematic tractor model of Section 2.1.2 is used to illustrate the principle idea of each approach. The approaches' particular advantages and disadvantages regarding this work's objectives are discussed for later use.

2.2.1 Kinematic Tractor Example Prerequisites

Depending on the particular control approach different representations describing the kinematic tractor model of Section 2.1.2 are required. The measured output of the system is always assumed to be

$$\mathbf{y} = [e_{tl}, e_{th}]^{\mathrm{T}} \tag{2.60}$$

The controlled output may be a subset of (2.60) or the weighted sum

$$y = e_{tl} + d_{ah}\sin(e_{th}) \approx e_{tl} + d_{ah}e_{th}, \tag{2.61}$$

which has a geometric interpretation as shown in Figure 2.2. d_{ah} is denoted as look-ahead distance. The output in this case can be seen as the distance of the look-ahead point from the desired path.

In case a control approach is based on a nonlinear system description which is tailored towards a particular system structure the description given by (2.51) and (2.52) is used directly. In case the approach is not tailored towards a particular system structure the nonlinear system may be denoted more generally

$$\dot{\mathbf{x}} = \mathbf{f}(\mathbf{x}, \mathbf{u}), \tag{2.62}$$

$$\mathbf{y} = \mathbf{h}(\mathbf{x}), \tag{2.63}$$

with $\mathbf{u} = \delta_{tf}$ and $\mathbf{x} = [e_{tl}, e_{th}]^{\mathrm{T}}$.

Controller design based on a linear continuous-time system description may use the general time domain representation given by (2.56) and (2.57) or the respective frequency domain representation relating the input and output signal Laplace transforms $\mathbf{U}(s)$ and $\mathbf{Y}(s)$ by using the transfer function matrix $\mathbf{G}(s)$ [Lun10]

$$\mathbf{Y}(s) = \mathbf{G}(s)\mathbf{U}(s) = \mathbf{C}\left(s\mathbf{I} - \mathbf{A}\right)^{-1}\mathbf{B}\mathbf{U}(s). \tag{2.64}$$

Using output (2.61) in particular results in a simple Single Input Single Output (SISO) transfer function

$$G(s) = \frac{\left(v_{tr}^{x,t}\right)^2}{l_t} \frac{s\frac{d_{ah}}{v_{tr}^{x,t}} + 1}{s^2}. \tag{2.65}$$

In some cases a discrete time representation of (2.56) and (2.57) is advantageous, which can be found to [Lun10]

$$\mathbf{x}[k+1] = \mathbf{A}_d\mathbf{x}[k] + \mathbf{B}_d\mathbf{u}[k], \tag{2.66}$$

$$\mathbf{y}[k] = \mathbf{C}_d\mathbf{x}[k], \tag{2.67}$$

with sample time T_s and numerically calculated matrices:

$$\mathbf{A}_d = \mathrm{e}^{\mathbf{A}T_s}, \quad \mathbf{B}_d = \int_0^{T_s} \mathrm{e}^{\mathbf{A}\tau}d\tau\,\mathbf{B}, \quad \mathbf{C}_d = \mathbf{C}. \tag{2.68}$$

2.2.2 PID Control

Proportional-Integral-Derivative (PID) control of a vehicle with front wheel steering input and the distance between look-ahead point and desired path as an output is a classical approach to path tracking control found in introductory literature [Raj06]. The rather simple linearized kinematic vehicle model given by its transfer function (2.65) allows an outline of this control approach. With (2.65) the control problem can be interpreted as asymptotic stabilization [SL91] of a double integrator system with a zero at $s_{0,1} = -v_{tr}^{x,t}/d_{ah}$. The look-ahead distance d_{ah} might be either predetermined by the type of sensor used, e.g. a camera detecting the center of a lane some distance ahead, or might be chosen freely, e.g. with a GPS receiver allowing to determine the lateral error e_{tl} and heading error e_{th} separately. The look-ahead distance's influence can be seen from the open-loop Bode diagrams [Foe94] and the closed loop root locus plots [Foe94] of Figure 2.10. The root locus plots depict the system's closed loop poles for proportional control with a controller gain varying from 0 to $+\infty$. For a look-ahead distance of $d_{ah} = 0$ it is impossible to asymptotically stabilize the resulting system using proportional control. With a positive look-ahead distance d_{ah} proportional control stabilizes the system and larger values of d_{ah} result in an increased damping. However, d_{ah} may not be chosen
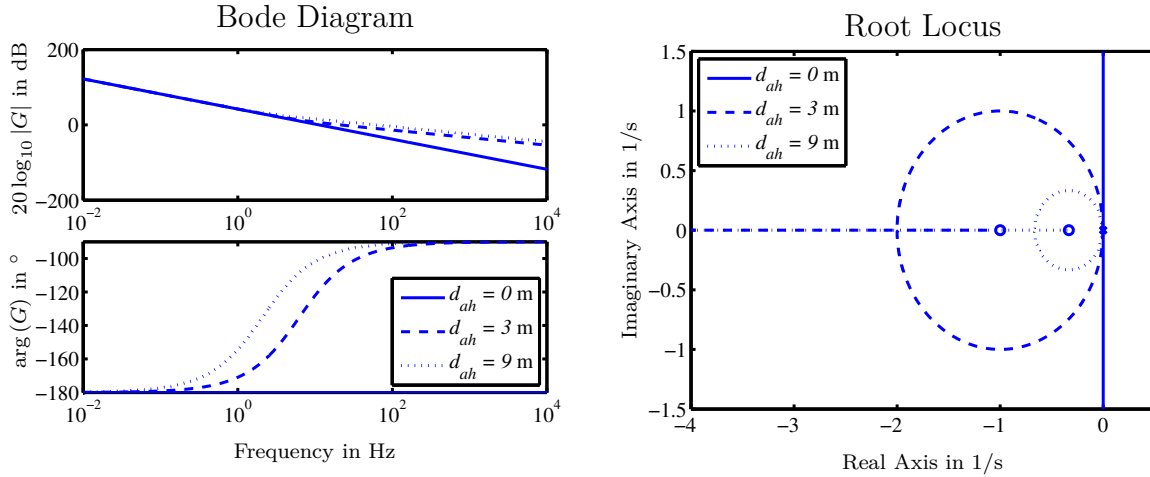
Figure 2.10: Open-loop bode diagram and closed loop proportional control root locus for tractor kinematic model with wheel base $l_t = 2.8$ m, longitudinal velocity $v_{tr}^{x,t} = 3$ m/sec and several look-ahead distances d_{ah}.

arbitrarily large for practical applications. For curved paths an increase of d_{ah} results in an increased cutting of corners. Up to a certain limit this cutting of corners is acceptable for less demanding applications like lane keeping. For accurate path tracking, however, this is undesirable. If the look-ahead distance is fixed, e.g. by sensor design, using Proportional-Derivative (PD) control with an additional zero and phase lead might be necessary to allow for sufficient damping of the closed loop system.

In order to include path tracking control of a steerable trailer or implement a decentralized control approach may be used. This means that the tractor is controlled ignoring the implement and using the SISO control approach described above. Subsequently, the resulting system is controlled using an implement steering input and the implement lateral or heading error as a controlled output. Alternatively one could try to apply tuning rules for MIMO Proportional-Integral (PI) controllers, as given by [Lun10] for instance. An initial guess for a controller gain matrix is typically found by inverting the plant's steady-state gain. In case of tractor-implement control this inversion requires the plant to be stabilized in a previous step. Stabilization could be done by first controlling the tractor only using a SISO PID controller as outlined.

Literature Survey

Besides [Raj06], applying the described approach to passenger car lane keeping, [TWH+98, TT03] use the sketched combination of a look-ahead distance and PD control for a tractor with an unsteered trailer. [Wag10] uses decentralized PD control for a tractor towing multiple single-axle trailers with steerable wheels. The lateral error of each unit is a controlled variable. [GB08] use PD lateral error control of a tractor with a three-point hitched implement without looking ahead, i.e. $d_{ah} = 0$. They adapt the controller gain according to an EKF estimate of the steering angle to yaw rate steady-state gain in order to account for changed cornering properties with ground engaging tools on the

implement. For the same task [DB09] use PID lateral position control and an adapted feedforward gain which is calculated using a reference model. [Dee13, Aut08, Tri07] are dedicated commercial systems for decentralized implement lateral error control which are meant to be used in combination with commercial tractor path tracking controllers like [Dee12, Aut12, Tri01]. Details on their control approaches are not publicized, their setup however relies on some user adjusted gain parameters.

Discussion

Pro: The main advantages of PID control are its computational simplicity and the limited system information required for the controller setup. It is possible to set up the controller by tuning without prior knowledge of the system. Using integral control in particular increases the chance of obtaining a controller that is rather robust with regard to slowly changing system parameters or disturbances.

Contra: As a drawback, the control approach is not systematic and depends very much on the actual input-output combination of an implement. Several controllers are required to control e.g. tractor lateral error, implement lateral and heading error. This approach neglects any possible coupling between those control loops. Similarly, the controller setup is little intuitive because different input-output combinations and hence different transfer functions react differently on controller gain tuning.

2.2.3 Linear-Quadratic Regulator

A Linear-Quadratic Regulator (LQR) [Nai02] is a popular optimal control approach for linear systems. Instead of using auxiliary means like bode and root locus diagrams LQR design is based on weighting the time course of a system's input and state (or output) variables directly. Keeping the notation of (2.56) and (2.57) for a continuous time infinite horizon problem this is done by introducing the performance index

$$J = \int_0^\infty \left(\mathbf{x}^{\mathrm{T}}(t)\mathbf{Q}\mathbf{x}(t) + \mathbf{u}^{\mathrm{T}}(t)\mathbf{R}\mathbf{u}(t) \right) dt. \tag{2.69}$$

The constant symmetric weighting matrices $\mathbf{Q}$ (positive semi-definite) and $\mathbf{R}$ (positive definite) are normally chosen to be diagonal and the performance index in this case simply weights the squares of inputs and states. The idea of optimal control is to find an optimal control law $\mathbf{u}^*(t)$ that minimizes (2.69) subject to (2.56). Interestingly, this optimal control law for the inifinite horizon LQR problem (2.69) has a very simple structure. Considering a few prerequisites [Nai02] it is simply given by a time invariant state feedback

$$\mathbf{u}^*(t) = -\underbrace{\mathbf{R}^{-1}\mathbf{B}^{\mathrm{T}}\mathbf{P}}_{\mathbf{K}}\mathbf{x}(t). \tag{2.70}$$

The matrix $\mathbf{P}$ is found by numerically solving the Algebraic Riccati Equation (ARE)

$$\mathbf{A}^{\mathrm{T}}\mathbf{P} + \mathbf{P}\mathbf{A} - \mathbf{P}\mathbf{B}\mathbf{R}^{-1}\mathbf{B}^{\mathrm{T}}\mathbf{P} + \mathbf{Q} = \mathbf{0}. \tag{2.71}$$

The solution has to be computed during the controller setup using numerical representations of $\mathbf{Q}$, $\mathbf{R}$, $\mathbf{A}$, and $\mathbf{B}$. The term optimal control is slightly misleading. The controller is optimal for a particular choice of weighting matrices $\mathbf{Q}$ and $\mathbf{R}$. The important feature of LQR, however, is not this optimality but the straightforward controller design based on the weighting of input and state (or output) variables. LQR results in a state feedback controller and therefore additional effort might be necessary to estimate states that are not measured. A popular choice is to combine LQR with a Kalman filter for state estimation which is referred to as Linear-Quadratic Gaussian (LQG) control [Lun10]. There is an interesting frequency domain interpretation considering both LQR and LQG special cases of H_2 optimal control [Mac04]. The related H_∞ control however is a more common frequency domain approach and will be discussed below. Besides the stated continuous time infinite horizon LQR problem (2.69) there are numerous variants considering discrete or time varying system descriptions, finite or receding horizon performance indices, as well as time varying weighting matrices [BGW90, Nai02].

Literature Survey

LQR control is used for both passenger car path tracking [Sni09] as well as tractor-trailer or tractor-implement path tracking. [Bel99], [Bev01], and [KS10] used LQR for a tractor towing an unsteered implement. [Bel99] and [KS10] briefly simulate tractor and towed implement control assuming all states are measured. [Bev01] conducts experiments combining LQR control with EKF based full state feedback and focuses on accurate implement lateral control. [CT95b] state simulation results for lateral LQR control of an on-road tractor trailer-combination with the tractor steering as an input and all states being measured. They present a frequency shaping LQR variant in order to penalize large lateral accelerations e.g. during lane change maneuvers. [RT07] simulate LQR control of a manually steered tractor and three trailers with automatically steered front wheels. The weights are chosen to minimize the rearward amplification of the trailers' lateral accelerations. They only consider ideal state feedback with all states being measured.

Discussion

Pro: LQR control based on weighting matrices for inputs, states or outputs in most cases turns out to be very intuitive in terms of controller design. MIMO systems with different input-output combinations can be handled systematically and the resulting controller is computationally simple.

Contra: LQR results in a state feedback controller and most practical problems therefore require additional effort for state estimation. Furthermore, LQR is MIMO proportional control only and hence may result in a large steady-state error in case of uncertainties or disturbances. For that reason additional measures like error integral states or disturbance feedforward might be necessary.

2.2.4 Model Predictive Control

Model Predictive Control (MPC) is an optimization based control approach characterized by using a plant model and the model's predicted behavior over a receding (i.e. moving fixed length) horizon [Mac02]. During each controller time step an optimal control signal sequence is found in order to minimize a performance index over the receding horizon. Only the first control signal values of that sequence are applied to the plant. The remaining control sequence is discarded, the horizon is shifted, and the optimization is restarted during the next time step. There is a multitude of historical approaches with different terminology describing the idea of MPC [Mac02] and LQR with a receding horizon can be interpreted as a special case of MPC [BGW90]. MPC in general, however, is a more powerful approach, because it is particularly tailored towards optimization with constraints. Those constraints might be for example limits on inputs, input slew rates, or system states.

Using the discrete system description (2.66) and (2.67) a MPC optimization problem for the simple example could be stated using the performance index

$$J[k] = \sum_{i=1}^{N_p} \mathbf{x}^{\mathrm{T}}[k+i|k]\mathbf{Q}[i]\mathbf{x}[k+i|k] + \sum_{i=0}^{N_p-1} \Delta\mathbf{u}^{\mathrm{T}}[k+i|k]\mathbf{R}[i]\Delta\mathbf{u}[k+i|k] \tag{2.72}$$

which is assumed to be subject to constraints

$$\mathbf{x}_{min} \leq \mathbf{x}[k+i|k] \leq \mathbf{x}_{max} \qquad \text{for } i = 1, \ldots, N_p, \tag{2.73}$$

$$\mathbf{u}_{min} \leq \mathbf{u}[k+i|k] \leq \mathbf{u}_{max} \qquad \text{for } i = 0, \ldots, N_p - 1, \tag{2.74}$$

$$\Delta\mathbf{u}_{min} \leq \Delta\mathbf{u}[k+i|k] \leq \Delta\mathbf{u}_{max} \qquad \text{for } i = 0, \ldots, N_p - 1. \tag{2.75}$$

$\mathbf{Q}[i]$ and $\mathbf{R}[i]$ are (time variant) symmetric positive semi-definite weighting matrices. N_p states the prediction horizon. $\mathbf{u}[k+i|k]$ denotes a future value of $\mathbf{u}$ as it is assumed at step k. Similarly $\mathbf{x}[k+i|k]$ denotes a predicted future state vector $\mathbf{x}$ which is calculated using the assumed future input values up to $\mathbf{u}[k+i-1|k]$ and (2.66). $\Delta\mathbf{u}[k+i|k] = \mathbf{u}[k+i|k] - \mathbf{u}[k+i-1|k]$ is the difference between subsequent input values.

This MPC problem can be rewritten as Quadratic Programming optimization problem with linear inequality constraints, which is convex and can be solved using numerical approaches like active set or interior point method [Mac02]. Numerical optimization yields the optimal control signal sequence at step k:

$$[\Delta\mathbf{u}^*[k|k], \ldots, \Delta\mathbf{u}^*[k+N_p-1|k]]^{\mathrm{T}} = \underset{[\Delta\mathbf{u}[k|k],\ldots,\Delta\mathbf{u}[k+N_p-1|k]]^{\mathrm{T}}}{\operatorname{argmin}} J[k] \tag{2.76}$$

Only $\mathbf{u}^*[k|k] = \Delta\mathbf{u}^*[k|k] + \mathbf{u}[k-1]$ is applied to the plant and the entire optimization is repeated during the next time step.

Prediction of future system states using (2.66) so far has assumed knowledge of the current state $\mathbf{x}[k]$. In practical applications the current state is often estimated.

In order to apply MPC to nonlinear systems a straightforward approach is to replace the linear difference equation (2.66) predicting the system's behavior by a more accurate nonlinear difference equation. The resulting nonlinear MPC optimization problem is not convex in general and the solution therefore might only be a local optimum. Optimization might take an unpredictably long time or might never terminate. For that reason, measures must be taken to stop the optimization and use a suboptimal yet stabilizing input signal [Mac02].

Literature Survey

Path tracking using MPC has been subject to research in mobile robotics, automotive, and agricultural applications and [Bac13] summarizes these approaches. All of them have not considered a trailer or an implement attached to the vehicle. [BOV09, Bac13] in contrast focus on MPC of a tractor towing a seed drill with a steerable drawbar. For prediction they use a kinematic model of tractor and implement and include a multiplicative factor accounting for tractor front wheel side-slip. Both tractor and implement lateral error are controlled variables. [BOV09] started with linear MPC and realized that a linear model was not sufficient. Therefore nonlinear MPC was used in subsequent publications [Bac13]. In the simple example above, a performance index (2.72) for a straight path tracking problem was given. In more general applications MPC is naturally tailored towards trajectory tracking, i.e. following a series of desired positions given as a function of time. For path tracking in contrast desired positions are stated independently of time, i.e the time a particular position is reached is irrelevant. [Bac13] proposed a modified performance index to replace trajectory tracking by path tracking for curved paths. [Bac13] in addition combines path tracking control with collision avoidance by augmenting the MPC performance index. Estimation of system states and the front wheel side-slip factor was done using an Extended Kalman Filter (EKF). The nonlinear MPC was implemented using a very capable computer (Intel Core 2 Duo E8600 2x3.3GHz, 2GB memory). Despite this fact the nonlinear MPC with a sample time of 100 ms was too demanding to maintain the desired prediction horizon of 30 steps. The prediction horizon, therefore, was reduced during runtime depending on the current computational load.

Discussion

Pro: Similar to LQR setup of MPC is based on weighting of inputs, states or outputs and is normally very intuitive. The approach is easily extended to MIMO systems with different input-output combinations, as well. In contrast to LQR it allows to consider actuator, actuator rate, and system state limits. This is an advantage in case limits are either reached frequently or in case optimized performance at those limits is crucial.

Contra: The major drawback of MPC is the computational load due to numerical optimization performed at each time step. A measurement or estimate of all system states is required. To obtain a small steady-state error in presence of uncertainties or disturbances additional measures, like including disturbance estimates or error integral states, may be necessary.

2.2.5 Robust H$_\infty$ Control

Classical controller design for linear SISO systems makes excessive use of a plant's frequency domain description given by the complex transfer function $G(s)$ (2.65). A frequency domain description for a MIMO system is given by the complex transfer function matrix $\mathbf{G}(s)$ (2.64). Unfortunately, the simple interpretation of an input signal's gain given by the transfer function's magnitude $|G(j\omega)|$ is not applicable to MIMO systems. Following the strict but lengthy definitions of [Mac04] a useful alternative for MIMO systems is the use of singular values $\sigma\left(\mathbf{G}(j\omega)\right)$ [Mac04]. They at least allow to state frequency dependent upper and lower bounds for an input signal vector's gain, which are given by:

$\overline{\sigma}\left(\mathbf{G}(j\omega)\right)$: the largest singular value of $\mathbf{G}(j\omega)$, and

$\underline{\sigma}\left(\mathbf{G}(j\omega)\right)$: the smallest singular value of $\mathbf{G}(j\omega)$.

In addition, the supremum of the largest singular value is used to define the H$_\infty$ norm:

$$\|\mathbf{G}\|_\infty = \sup_{\omega \in \mathbb{R}} \overline{\sigma}\left(\mathbf{G}(j\omega)\right). \tag{2.77}$$

An interesting property of $\|\mathbf{G}\|_\infty$ is that it can be interpreted as an upper bound for the ratio between output and input signal vector energy.

The main idea of robust H$_\infty$ control is to design a dynamic output feedback controller $\mathbf{K}(s)$ that stabilizes not only a nominal plant $\mathbf{G}(s)$ but every plant belonging to an entire set of uncertain plants, i.e. the controller robustly stabilizes this set of uncertain plants. Again following the strict definitions of [Mac04], Fig. 2.11 outlines the general framework of robust H$_\infty$ control. The nominal plant $\mathbf{G}(s)$ models the assumed plant behavior. This is a simplified description of reality neglecting e.g. high-frequency dynamics or parameter uncertainties. In order to deal with uncertainty during controller design the nominal plant model is extended introducing new weighted inputs $\mathbf{w}$ and outputs $\mathbf{z}$ resulting in an extended plant $\mathbf{P}(s)$. Uncertainty is introduced by closing the upper loop with an unknown unstructured model of uncertainties denoted by the transfer function matrix $\mathbf{\Delta}(s)$. The only assumption is that $\mathbf{\Delta}(s)$ is a real-rational transfer function matrix without poles on the imaginary axis and in the right half-plane of s. With $\mathbf{P}(s)$ of Fig. 2.11 the uncertainty is assumed to be output multiplicative as an example. The uncertain plant model is found by

only closing the upper loop and calculating the resulting transfer function matrix $\mathbf{T}_{yu}(s)$ from $\mathbf{u}$ to $\mathbf{y}$:

$$\mathbf{T}_{yu}(s) = (\mathbf{I} + \mathbf{W}_1(s)\boldsymbol{\Delta}(s)\mathbf{W}_2(s))\mathbf{G}(s). \tag{2.78}$$

The stable weighting transfer functions matrices $\mathbf{W}_1(s)$ and $\mathbf{W}_2(s)$ may be used to normalize signals of different magnitudes or to emphasize particular frequency ranges with uncertainties.

Closing just the lower loop yields the transfer function matrix $\mathbf{T}_{zw}(s)$ from $\mathbf{w}$ to $\mathbf{z}$:

$$\mathbf{T}_{zw}(s) = \mathbf{W}_2(s)\mathbf{G}(s)\mathbf{K}(s)\left(\mathbf{I} - \mathbf{G}(s)\mathbf{K}(s)\right)^{-1}\mathbf{W}_1(s). \tag{2.79}$$

$\mathbf{T}_{zw}(s)$ plays a crucial role in robust stability analysis and controller design. Assuming the nominal feedback loop, i.e. the loop as shown in Fig. 2.11 with $\boldsymbol{\Delta}(s) = \mathbf{0}$, is internally stable [Mac04] and $\gamma > 0$, then the following holds as a result of the Small Gain Theorem [Mac04]:

If and only if $\|\mathbf{T}_{zw}\|_\infty \leq \gamma$ then the uncertain feedback loop as depicted in Fig. 2.11 is well-posed [Mac04] and internally stable *for all* uncertainties fulfilling the assumptions on $\boldsymbol{\Delta}(s)$ stated above and $\|\boldsymbol{\Delta}\|_\infty < \frac{1}{\gamma}$.

As a consequence, the robust stabilization problem is translated into a general optimal H$_\infty$ problem, i.e. finding all controllers $\mathbf{K}(s)$ that minimize $\|\mathbf{T}_{zw}\|_\infty$. Solving the optimal H$_\infty$ problem is a difficult task, and practical approaches only approximately minimize
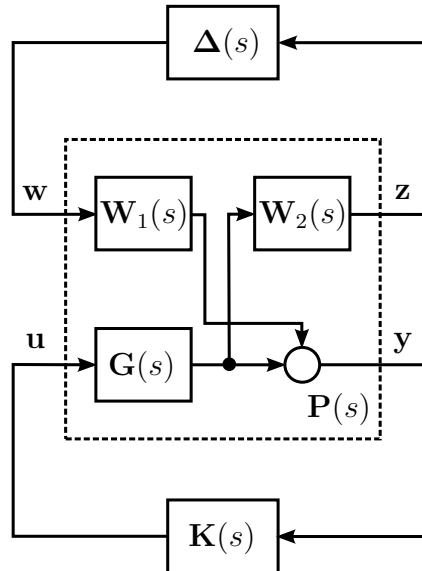

Figure 2.11: Uncertain feedback system considered for robust H$_\infty$ control, with nominal plant $\mathbf{G}(s)$, extended plant $\mathbf{P}(s)$, controller $\mathbf{K}(s)$, unknown unstructured uncertainty $\boldsymbol{\Delta}(s)$, as well as weighting matrices $\mathbf{W}_1(s)$ and $\mathbf{W}_2(s)$. As an example $\mathbf{P}(s)$ is chosen to model an output multiplicative uncertainty.

$\|\mathbf{T}_{zw}\|_{\infty}$. Algorithms solving this general suboptimal H_{∞} problem may either rely on iterated solutions of two Algebraic Riccati Equations (AREs) or may be based on solving a Linear Matrix Inequalities problem [Mac04]. [MG90] in contrast consider a special case relying on a particular plant factorization using coprime factors. As a consequence the two AREs have to be solved only once. The resulting dynamic controllers $\mathbf{K}(s)$ and in particular those found by solving two AREs exhibit close structural similarities to LQG control (i.e. LQR plus Kalman filter) and the more general H_2 control [DGKF89].

So far robust stability was the only objective during controller design. There are several possibilities to specify performance objectives. For the general suboptimal H_{∞} problem [MG90] propose to consider additional weighted inputs and outputs in $\mathbf{w}$ and $\mathbf{z}$ in order to represent important closed-loop transfer functions, e.g. from a disturbance to the plant output. The minimization of the extended $\|\mathbf{T}_{zw}\|_{\infty}$ results in a tradeoff between different objectives stated as closed-loop transfer functions, which is denoted as mixed sensitivity weighting [Mac04]. For the special case based on coprime factorization [MG90] propose a two-step approach. They first shape the open-loop nominal plant $\mathbf{G}(s)$ by attaching shaping transfer function matrices to its inputs and outputs. Those matrices are chosen to specify a desired performance. In a subsequent step this shaped plant is robustly stabilized. The overall controller then consists of the robustly stabilizing controller combined with the shaping transfer function matrices.

Uncertainties $\mathbf{\Delta}(s)$ were assumed to be unstructured during controller H_{∞} synthesis. In some control problems there is more information regarding the structure of uncertainties. $\mathbf{\Delta}(s)$ might be a block diagonal matrix for example. In this case, H_{∞} synthesis might result in a very conservative controller performance. Robust control can be refined in this case by defining structured uncertainties, structured singular values, and using the D-K iteration algorithm for controller synthesis [Mac04].

Literature Survey

Research on robust H_{∞} path tracking control has been carried out for passenger cars [OIU96], buses [Mam96] and on-road tractor-trailer combinations [HWTT03]. They all used the two-step approach proposed by [MG90] which is based on open-loop shaping and subsequent robust stabilization. [HWTT03] in particular used a dynamic tractor-trailer model with tractor front wheel steering as an input and the tractor lateral error at a look-ahead distance as an output. Uncertainties due to varying road conditions, trailer mass, and tractor velocity have been considered. Controller validation was based on simulations and experiments. [MM03] consider a tractor-trailer combination very similar to [HWTT03]. They also claim to use H_{∞} control based on open-loop shaping and subsequent robust stabilization, yet do not provide any details on the variant and weighting functions used. Validation was done in experiments. In order to improve performance and robustness with varying velocity [HWTT03] consider further variants combining H_{∞} control with velocity dependent gain scheduling.

Discussion

Pro: Robust H_∞ control is well suited for MIMO control problems. The requirement of robust stability is a part of controller design and can be achieved not only for vaguely defined slightly perturbed plants but for every uncertain plant of a well-defined set. This is a great advantage in case there is only one attempt in controller design, e.g. if an unstable closed-loop system has catastrophic consequences and there are little testing and tuning possibilities. The computational requirements of a H_∞ controller are rather low and comparable to state feedback with observer.

Contra: In order to not sacrifice performance to robust stability a closer look at possible uncertainties as well as the system's frequency domain description is required. Choosing the weighting transfer function matrices is a task for an engineer rather than an operator. This is a major drawback for the given problem of controlling a multitude of tractor-implement combinations which are chosen and set up by the customer.

2.2.6 Nonlinear Lyapunov Based Control

The basic idea of this approach is to utilize Lyapunov's theory of stability to find a (nonlinear) control law. Following the definitions of [SL91] and starting with the nonlinear system (2.62) the first step is to choose a control law

$$\mathbf{u} = \mathbf{f}_u(\mathbf{x}) \tag{2.80}$$

that possibly stabilizes the equilibrium point $\mathbf{x} = \mathbf{0}$ of the resulting autonomous system

$$\dot{\mathbf{x}} = \mathbf{f}(\mathbf{x}, \mathbf{f}_u(\mathbf{x})). \tag{2.81}$$

In a second step a scalar Lyapunov function candidate $V(\mathbf{x})$ with continuous first partial derivatives is chosen so that

$$V(\mathbf{0}) = 0 \text{ and } \mathbf{x} \neq \mathbf{0} \Rightarrow V(\mathbf{x}) > 0 \text{ for } \mathbf{x} \in \mathbf{M}_R = \{\mathbf{x} \mid \|\mathbf{x}\| < R\}, \tag{2.82}$$

i.e. $V(\mathbf{x})$ is locally positive definite in a spherical region $\mathbf{M}_R$ with radius R.

Finally with the Lyapunov theorem for local stability [SL91], if

$$\dot{V}(\mathbf{x}) = \frac{\partial V(\mathbf{x})}{\partial \mathbf{x}} \dot{\mathbf{x}} = \frac{\partial V(\mathbf{x})}{\partial \mathbf{x}} \mathbf{f}(\mathbf{x}, \mathbf{f}_u(\mathbf{x})) \tag{2.83}$$

is locally negative semi-definite in $\mathbf{M}_R$, i.e.

$$\dot{V}(\mathbf{0}) = 0 \text{ and } \mathbf{x} \neq \mathbf{0} \Rightarrow \dot{V}(\mathbf{x}) \leq 0 \text{ for } \mathbf{x} \in \mathbf{M}_R \tag{2.84}$$

then the equilibrium point $\mathbf{x} = \mathbf{0}$ is stable in the sense of Lyapunov [SL91], meaning

$$\forall R > 0, \exists\, r > 0, \|\mathbf{x}(0)\| < r \;\Rightarrow\; \forall t \geq 0, \|\mathbf{x}(t)\| < R. \tag{2.85}$$

This definition requires $\|\mathbf{x}(t)\|$ to be less than an arbitrarily small R. However, it does not imply asymptotic stability ($\mathbf{x}(t) \to 0$ as $t \to \infty$). Demanding $\dot{V}(\mathbf{x})$ to be locally negative definite or ensuring the requirements of La Salle's invariant set theorem [SL91] are met allows to account for asymptotic stability. If the test for negative semi-definiteness of $\dot{V}(\mathbf{x})$ fails a modified control law (2.80) has to be chosen and the described steps have to be repeated. This makes the Lyapunov based control approach an iterative task that requires some educated guessing for the control law and the Lyapunov function candidate.

For the kinematic single track tractor example (2.52) and (2.51) in particular possible choices (following [ABL04]) for the control law (2.80) and the Lyapunov function candidate $V(\mathbf{x})$ could be

$$\delta_{tf} = \arctan\left(-k_1 \tanh(e_{tl})\frac{\sin(e_{th})}{e_{th}} - k_2 \tanh\left(\frac{e_{th}}{k_2}\right)\right), \;\; \text{with } k_1 > 0, k_2 > 0, \tag{2.86}$$

$$V(e_{tl}, e_{th}) = \frac{k_1}{l_t} \log\left(\cosh(e_{tl})\right) + \frac{1}{2}e_{th}^2. \tag{2.87}$$

Using (2.52) and (2.51) this results in

$$\dot{V}(e_{tl}, e_{th}) = \frac{\partial V}{\partial e_{tl}}\dot{e}_{tl} + \frac{\partial V}{\partial e_{th}}\dot{e}_{th} = -\frac{v_{tr}^{x,t} k_2}{l_t}\, e_{th} \tanh\left(\frac{e_{th}}{k_2}\right). \tag{2.88}$$

With $v_{tr}^{x,t} > 0$ the derivative $\dot{V}(e_{tl}, e_{th})$ is negative semi-definite in $\mathbb{R}^2$ and $[e_{tl}, e_{th}]^{\mathrm{T}} = \mathbf{0}$ therefore is a stable equilibrium point. Further investigation shows that $V(e_{tl}, e_{th})$ is radially unbounded, i.e. $V(e_{tl}, e_{th}) \to \infty$ as $\left\|[e_{tl}, e_{th}]^{\mathrm{T}}\right\| \to \infty$, and the application of La Salle's global invariant set theorem [SL91] finally allows to conclude that the chosen control law results in a globally asymptotic stable equilibrium point $[e_{tl}, e_{th}]^{\mathrm{T}} = \mathbf{0}$, i.e. for all initial conditions in $\mathbb{R}^2$ this point is reached with $t \to \infty$.

Literature Survey

[ABL04] apply the control approach of this example to a tractor and an unsteered trailer in forward and backward motion. [CLTM10] use Lyapunov based control for a similar system in off-road applications. However, the control law in their case is the result of a two-step approach. They first stabilize the trailer motion by considering it a virtual vehicle with the trailer's direction of travel at the hitch point as an input. In a second step a tractor control law ensuring this direction of travel is conceived. Finally, stability is proven by using Lyapunov's theory. In order to cope with the uncertainties resulting from tire-soil interaction [CLTM10] combine this control law with a nonlinear observer estimating the wheel side-slip angles.

Discussion

Pro: Lyapunov based control allows to account for the nonlinearity of the actual system and provides at least a lower bound estimate for the domain of attraction [SL91] within the system's state space. The computational demand of the control approach depends on the actual system, however, with application to path tracking control in [ABL04] and [CLTM10], it turns out to be simple. MIMO systems are supported without any changes to the approach.

Contra: The major drawback of Lyapunov based control is that finding a control law and a Lyapunov function candidate, as shown in the example, is not systematic and requires some educated guessing. This makes an application to a multitude of implements with different input-output combinations impractical. Similarly choosing the controller gain (k_1 and k_2 in the example) is far from intuitive. The control law itself results in a nonlinear state feedback which is very likely to require additional measures in order to make it robust or adaptive. [CLTM10] therefore added an estimation of the wheel side-slip angle to their observer and used the estimates in their control law.

2.2.7 Feedback Linearization

Feedback linearization may be grouped in two categories depending on the resulting system [SL91]. Input-state linearization is based on finding a nonlinear state feedback and a nonlinear state transformation that result in an equivalent linear system described by a linear system matrix $\mathbf{A}$ and a linear input matrix $\mathbf{B}$. In contrast to Jacobian linearization this transformation maintains an exact description of the original system. Input-output linearization aims for a nonlinear state feedback resulting in linear differential equations relating inputs and outputs. In both cases the resulting linear system is subsequently stabilized by using a linear controller.

Considering the example (2.52) and (2.51) with output $y = e_{tl}$, an input-output linearizing control law can be found by first calculating

$$y = e_{tl}, \tag{2.89}$$

$$\dot{y} = \dot{e}_{tl} = v_{tr}^{x,t} \sin(e_{th}), \tag{2.90}$$

$$\ddot{y} = v_{tr}^{x,t} \cos(e_{th}) \dot{e}_{th} = \frac{\left(v_{tr}^{x,t}\right)^2}{l_t} \cos(e_{th}) \tan(\delta_{tf}) \tag{2.91}$$

where $v_{tr}^{x,t}$ is assumed to be positive and constant or slowly changing. The relative degree $r = 2$ at $[e_{tl}, e_{th}]^{\mathrm{T}} = \mathbf{0}$ equals the number of system states, hence there is no internal dynamics that might affect stability [SL91].

Solving (2.89) and (2.90) for e_{tl} and e_{th} and substituting them in (2.91) yields

$$\ddot{y} = \underbrace{0}_{f(y,\dot{y})} + \underbrace{\frac{\left(v_{tr}^{x,t}\right)^2}{l_t} \cos\left(\arcsin\left(\frac{\dot{y}}{v_{tr}^{x,t}}\right)\right)}_{b(y,\dot{y})} \underbrace{\tan(\delta_{tf})}_{u}, \tag{2.92}$$

which is a system representation in terms of y and time derivatives referred to as nonlinear controllable canonical form [Ada09]. Having transformed the system into this canonical form a possible input-output linearizing state feedback is found to be

$$u = \frac{1}{b(y,\dot{y})} \left(-f(y,\dot{y}) + \bar{u}\right), \tag{2.93}$$

with $\bar{u}$ denoting a new input. Linearity can be verified by inserting (2.93) in (2.92). The resulting linearized system is a chain of two integrators with input $\bar{u}$ and output y, which can be stabilized by the linear control law

$$\bar{u} = -\tilde{a}_1\dot{y} - \tilde{a}_0 y \tag{2.94}$$

with $\tilde{a}_1$ and $\tilde{a}_0$ denoting the coefficients of an arbitrarily chosen desired closed loop characteristic polynomial. To implement (2.93) and (2.94) y and $\dot{y}$ are calculated using the transformations given by (2.89) and (2.90). Input-output linearization in case of a relative degree lower than the number of system states is very similar. This, however, requires using the Byrnes-Isidori canonical form [Ada09] and checking the internal dynamics for stability.

Literature Survey

The sketched feedback input-output linearization approach is not limited to SISO systems and [CT95b, CT00] apply it to a tractor-trailer combination using the tractor front wheel steering angle and the trailer's differential braking force to control the tractor lateral error and the trailer hitch angle. [Wag10] considers a slightly modified approach to input-output linearization: instead of linearizing feedback he uses linearizing feedforward calculated from desired system states. This is done with the assumption of rather small differences between desired and actual system states. The result is a set of almost linear differential equations which are stabilized using linear controllers. He applies his approach to a tractor with two trailers. Tractor and trailer wheels are the steering inputs and the tractor lateral position and the trailer hitch angles are the controlled variables.

Discussion

Pro: Feedback linearization, similar to Lyapunov based control, allows accounting for the system's nonlinearities and hence tends to result in a large domain of attraction.

The computational load of calculating nonlinear state feedback and state transformations depends on the particular system. Path tracking control for the stated approaches, though, is still rather computationally simple.

Contra: A linearizing state feedback can be found more systematically compared to iterative guessing with Lyapunov based control. However, it is still tailored towards a particular input-output combination. For each variant a transformation into one of the described canonical forms has to be found analytically which is a task difficult to automate. In addition to this, the linearizing state feedback and state transformations tend to be sensitive to modeling errors and uncertainties [SL91]. In case of larger, more complex systems it is not easy to find a physical interpretation of the transformed system states or high order derivatives of particular outputs. This makes the subsequent design of a linear stabilizing controller for the linearized system less intuitive.

2.2.8 Sliding Mode Control

Sliding Mode Control (SMC) is a robust control approach particularly addressing nonlinear systems with parametric uncertainties or unmodeled dynamics. Robustness is achieved by using a switching control law. The principal idea of the approach is to divide the control of a nth order nonlinear system into two control tasks. One considering a first order nonlinear system and a second considering a $(n-1)^{th}$ order linear system. This is done by choosing a surface $S(t)$ in $\mathbb{R}^n$ in a way which makes it possible to find a switching controller that forces the system's trajectories onto this surface within finite time. Once on the surface the system's trajectories are forced to remain on the surface. The system's behavior on this surface is called sliding mode [SL91] and with an appropriate choice of $S(t)$ this behavior will be of order $(n-1)$, linear, and asymptotically stable.

In order to apply SMC to the example given by (2.52) and (2.51) it is again transformed into the nonlinear controllable canonical form (2.92) and hence given by:

$$\ddot{y} = \underbrace{0}_{f(y,\dot{y})} + \underbrace{\frac{\left(v_{tr}^{x,t}\right)^2}{l_t} \cos\left(\arcsin\left(\frac{\dot{y}}{v_{tr}^{x,t}}\right)\right)}_{b(y,\dot{y})} \underbrace{\tan(\delta_{tf})}_{u}. \tag{2.95}$$

Following [SL91] the above functions f and b are assumed to be unknown and $\hat{f}$ and $\hat{b}$ denote their known estimates. The estimation errors are assumed to be bounded by

$$\left|\hat{f} - f\right| \leq F, \tag{2.96}$$

$$0 < b_{min} \leq b \leq b_{max}. \tag{2.97}$$

Choosing $\hat{b} = \sqrt{b_{min}b_{max}}$ the latter can be rewritten as

$$\beta^{-1} \leq \frac{\hat{b}}{b} \leq \beta, \text{ with } \beta = \sqrt{\frac{b_{max}}{b_{min}}}. \tag{2.98}$$

The first step in SMC is to define a sliding surface S(t) in $\mathbb{R}^2$. [SL91] proposes the definition $s(y, \dot{y}) = 0$ with

$$s(y, \dot{y}) = \dot{y} + \lambda y \tag{2.99}$$

and λ being a strictly positive constant. With this definition the condition a switching controller needs to fulfill in order to force the system's trajectory $[y, \dot{y}]^{\mathrm{T}}$ onto $S(t)$ can be formalized by introducing the sliding condition

$$\frac{1}{2}\frac{d}{dt}s^2 \leq -\eta\,|s|\,, \text{ i.e. } \begin{cases} \dot{s} \leq -\eta & \text{for } s > 0, \\ \dot{s} = 0 & \text{for } s = 0, \\ \dot{s} \geq +\eta & \text{for } s < 0 \end{cases} \tag{2.100}$$

with η being a strictly positive constant. s^2 can be interpreted as a measure for the distance of the system's trajectory from the sliding surface $S(t)$. Requiring η to be strictly positive implies the sliding surface is reached in finite time. Once on the surface the sliding condition requires the trajectory $[y, \dot{y}]^{\mathrm{T}}$ to remain on the surface, i.e. s remains 0. With (2.99) this results in a reduced order linear system which is asymptotically stable due to the choice of λ.

With the previous definitions [SL91] derives a robust controller

$$u = \frac{1}{\hat{b}}\left(-\hat{f} - \lambda\dot{y} - k\,\mathrm{sgn}(s)\right) \tag{2.101}$$

satisfying the sliding condition (2.100) if k is chosen to fulfill

$$k \geq \beta\,(F + \eta) + (\beta - 1)\left|-\hat{f} - \lambda\dot{y}\right|. \tag{2.102}$$

In case of $\hat{b} = b$ and $\hat{f} = f$ this control law may be interpreted as input-output linearizing state feedback (2.93) with the resulting chain of integrators being subsequently stabilized using the new input $\bar{u} = -\lambda\dot{y} - k\,\mathrm{sgn}(s)$. In case of model uncertainties (2.101) provides approximate input-output linearization only. The sign function

$$\mathrm{sgn}(s) = \begin{cases} +1 & \text{for } s > 0, \\ 0 & \text{for } s = 0, \\ -1 & \text{for } s < 0 \end{cases} \tag{2.103}$$

results in a discontinuous control law being switched at the surface $S(t)$. The factor k is chosen considering the upper bounds of the model's uncertainties. The larger those uncertainties are the larger the switched part of the control signal has to be in order to overcome the uncertainties. In practice switching is not instantaneous and the system's trajectory therefore will not slide perfectly on the surface but will chatter across both sides of the surface. Consequence is a very high control switching frequency. Only few applications are suitable for high frequency switching and that is why the sign function is normally replaced by a saturation function [SL91]

$$\text{sat}\left(\frac{s}{\Phi}\right) = \begin{cases} +1 & \text{for } \frac{s}{\Phi} > 1, \\ \frac{s}{\Phi} & \text{for } \left|\frac{s}{\Phi}\right| \leq 1, \\ -1 & \text{for } \frac{s}{\Phi} < -1. \end{cases} \tag{2.104}$$

The strictly positive boundary layer thickness Φ is a tuning parameter used to smooth the control signal. The price of smoothing the control signal is a weakened robustness and a remaining steady-state error, which is however kept within guaranteed limits [SL91]. Keeping (2.99) in mind the saturation function within the boundary layer Φ only resembles PD control.

Literature Survey

[TT03] use several variants of SMC for a tractor-trailer combination. Tractor front wheel steering serves as an input and the lateral error at a look-ahead distance as an output. Besides the approach sketched above, they combine SMC with an adaption of tire cornering stiffness parameters. In addition, they state a slightly different switching control law not requiring the introduction of a sliding surface. The term SMC is used throughout the entire work. This, however, is misleading, because in most simulations and all experiments [TT03] use an infinite boundary layer thickness Φ resulting in a degenerated SMC which actually is PD control only.

Discussion

Pro: SMC is very similar to feedback linearization. It is able to account for a system's nonlinearities and is computationally simple for the given problem. In contrast to feedback linearization SMC is designed to cope with parameter uncertainties and unmodeled system dynamics. This robustness is achieved by introducing a switching control law.

Contra: SMC may perform extremely well in applications that allow for switching controllers. Tractor and implement steering actuators unfortunately are not intended for switching control and in addition exhibit a steering rate limitation imposed by the maximum hydraulic valve flow. Either this rate limit or the necessary smoothing boundary layer at the switching surface will deteriorate the controller's robustness. As a conse-

quence the steady-state error can be kept within certain limits, but will not necessarily vanish. Deriving SMC is tailored towards particular input-output combinations for the same reasons as feedback linearization, i.e. controller design involves transforming each system variant into an appropriate canonical form. The bounds F, β, the sliding surface s, and the boundary layer thickness Φ depend on the actual implement and have to be tuned by the user.

2.2.9 Geometric Path Tracking

The main idea of geometric path tracking is to use geometric properties of the vehicle and the desired path to derive a (heuristic) control law. From a multitude of variants [Sni09] states some that are particularly popular in mobile robotics. His pure pursuit control approach is given as an example. Figure 2.12 depicts the approach and the required geometric properties. The approach comprises several steps with the objective to calculate a steering angle that results in driving a circular arc to a particular point on the desired path ahead. The first step is to draw a circle with radius d_{ah} around the tractor's rear axle. d_{ah} here denotes a look-ahead distance with a definition slightly different from the
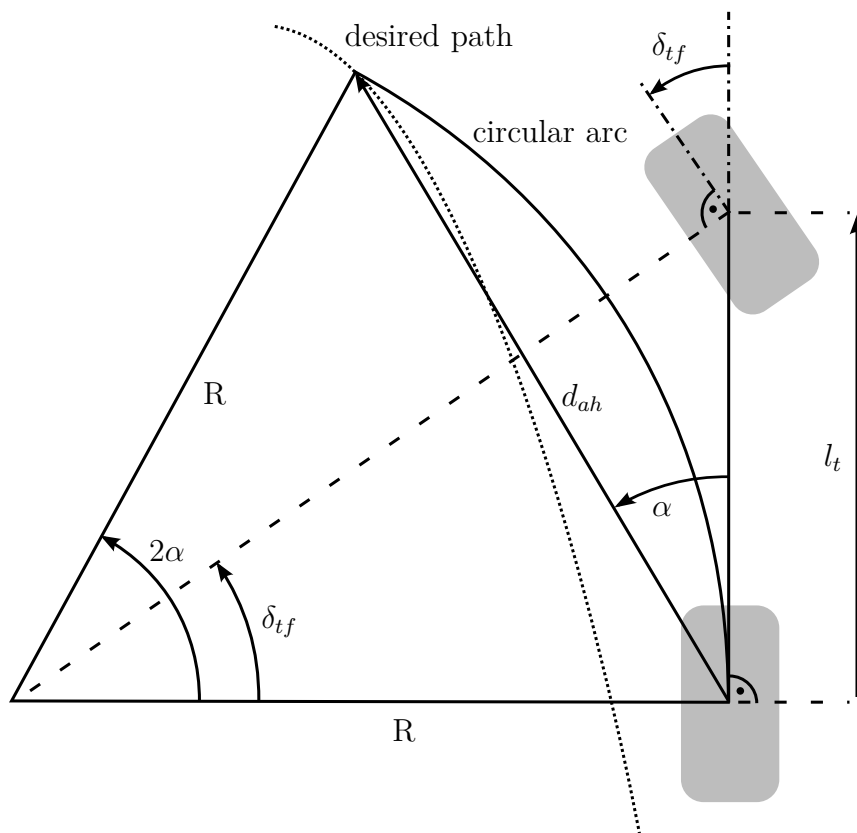

Figure 2.12: Geometric path tracking control of a tractor using a pure pursuit approach. The instantaneous steering angle δ_{tf} is calculated to bring the tractor's rear axle back on track by following the depicted circular arc which intersects the desired path at a chosen look-ahead distance d_{ah}.

previous one used for PID control. In a next step the point of intersection between this circle and the desired path ahead is calculated. In a third step a circular arc is placed between this intersection and the tractor rear axle. With α defined as shown in Figure 2.12 the arc's radius R and the chord length d_{ah} are related by

$$d_{ah} = 2R\sin(\alpha). \tag{2.105}$$

Assuming no wheel side-slip and using the Ackermann steering angle (from Figure 2.12)

$$\delta_{tf} = \arctan\left(\frac{l_t}{R}\right), \tag{2.106}$$

the instantaneous pure pursuit steering angle is

$$\delta_{tf} = \arctan\left(\frac{2\,l_t sin(\alpha)}{d_{ah}}\right). \tag{2.107}$$

This steering angle is applied to the tractor at the current controller time step. During the next time step the previous result is discarded and a new circular arc as well as a new pure pursuit steering angle are calculated. Controller tuning can be achieved by introducing a multiplicative tuning parameter within equation (2.107).

Literature Survey

The second geometric approach stated by [Sni09] and denoted as the Stanley method is based on a weighted sum of the vehicle heading error and the distance between the vehicle front axle and the desired path. [Sni09] applies both the pure pursuit and the Stanley method to passenger cars only. In order to control a tractor towing an implement with steerable drawbar [BOV12], besides their proposed MPC control approach, introduce a simple comparative approach which is based on a variant of pure pursuit and an additional geometric control law for the drawbar.

Discussion

Pro: Geometric approaches offer a straightforward solution to path tracking control without requiring any knowledge of control systems, which might be one reason for their popularity. In addition to this, the resulting control laws turn out to be computationally simple.

Contra: As a drawback the straight forward yet heuristic approaches impede analysis regarding stability and performance. The geometric control laws are tailored to a particular implement and actuator and this complicates application to a multitude of different combinations. The considered control laws furthermore do not account for parameter uncertainties or disturbances making controller retuning during field work rather likely.

2.2.10 Fuzzy Logic Control

Numerous control problems are concerned with the automation of tasks that have been previously performed by skilled operators. The idea of Fuzzy Logic Control (FLC) is to use human expert knowledge directly for controller design. Human knowledge however is seldom expressed mathematically but in most cases given as a set of linguistic rules. Considering the simple path tracking example of Figure 2.2 such a rule could look like "IF the lateral error is positive AND the heading error is positive THEN the steering angle is negative".

Fuzzy logic provides means to translate human knowledge into a mathematical form. To outline this connection the concepts of fuzzy sets and linguistic variables are required, which are introduced following the strict definitions of [Bot93]. An ordinary (crisp) set may either contain or not contain an element. The idea of fuzzy sets in contrast is to specify a degree to which a certain element is member of a fuzzy set. For a fuzzy set A this is done using a membership function μ_A taking values in the interval $[0, 1]$, with 1 and 0 denoting full membership and no membership respectively. The fuzzy set A may then be defined using ordered pairs of elements x and their respective degrees of membership $\mu_A(x)$, i.e. $A = \{(x, \mu_A(x))|x \in X\}$, with X generally being a collection of objects denoted as universe of discourse [Lee90a]. In the following section X is assumed to be a set of real numbers given by the interval $[x_{min}, x_{max}]$. Omitting some technicalities [Bot93] linguistic variables are characterized by a variable name, e.g "lateral error", and linguistic values taken from a set of linguistic terms, e.g. {"positive", "zero", "negative"}.

Using those definitions fuzzy logic associates linguistic values with fuzzy sets and linguistic operators (e.g. AND, OR, IF-THEN) with operations on those fuzzy sets and their membership functions. With FLC this link between linguistic and mathematical expressions is used to design a controller based on linguistic rules. A fuzzy logic controller may be divided into a fuzzification interface, a knowledge base, an inference engine, and a defuzzification interface [Bot93]. The knowledge base comprises a collection of linguistic rules specifying the controller behavior. The inference engine uses those rules and linguistic controller input values to obtain linguistic controller output values. Actual calculations are performed using the corresponding fuzzy sets. The theoretical basis of decision making within the inference engine is approximate reasoning [Bot93]. The key idea is an extension of Boolean logic allowing not only for expressions like "IF A is true THEN B is true" but also for "IF A is true to a certain degree THEN B is true to certain degree". The fuzzification interface is used to express controller input values, e.g. measured process variables, their integrals, and their derivatives, in linguistic terms and their corresponding fuzzy sets. The defuzzification interface is used to calculate a crisp controller output value from a linguistic controller output value given as a fuzzy set.
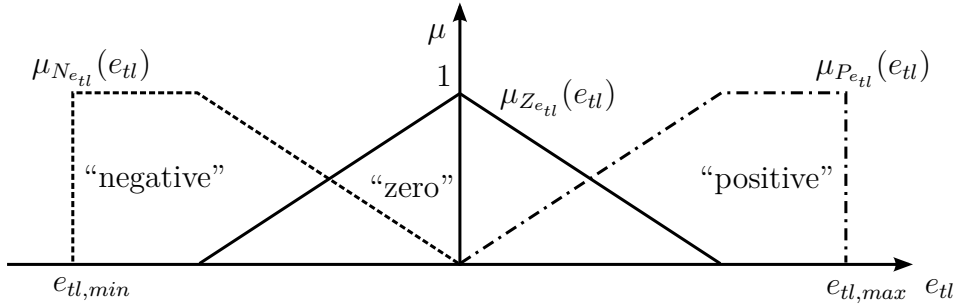
Figure 2.13: Membership functions $\mu_{P_{e_{tl}}}(e_{tl})$, $\mu_{Z_{e_{tl}}}(e_{tl})$, and $\mu_{N_{e_{tl}}}(e_{tl})$ numerically representing the linguistic values "positive", "zero", and "negative". Values of e_{tl} are assumed to be within a suitable universe of discourse given by the interval $[e_{tl,min}, e_{tl,max}]$. For e_{th} and δ_{tf} membership functions and linguistic values are chosen similarly.

There are numerous variants of FLC using different fuzzy sets and operators on fuzzy sets [Bot93, Lee90a, Lee90b]. In order to illustrate FLC a particular variant using triangular and trapezoidal membership functions as well as Mamdani's Max-Min-Inference method [Bot93] is applied to the simple path tracking example of Figure 2.2. The controller inputs are e_{tl} and e_{th} with the corresponding linguistic variables "lateral error" and "heading error". Similarly, the controller output is δ_{tf} with the linguistic variable "steering angle". The universes of discourse for e_{tl}, e_{th}, and δ_{tf} are chosen to be suitable intervals in $\mathbb{R}$. The universe of discourse of each input and output is partitioned by defining membership functions as depicted in Figure 2.13. Considering e.g. the linguistic value "zero", the idea of fuzzy sets becomes apparent. The fuzzy set denoted by $Z_{e_{tl}}$ and defined using the membership function $\mu_{Z_{e_{tl}}}(e_{tl})$ comprises not only the numerical value 0 but also small values close to 0 reflecting an imprecise linguistic definition. The choice of suitable membership functions as well as their shapes and sizes is part of controller design. The choice is based on human expert knowledge. The exemplary partition using three membership functions is rather coarse and there are finer partitions e.g. distinguishing between "large positive" and "small positive" etc. [Bot93].

The second important part of controller design is the creation of a linguistic rule base. A possible rule base for the simple path tracking example is stated in Table 2.4. The rule base depicts human expert knowledge and implicitly considers their knowledge of the controlled plant.

Table 2.4: Fuzzy path tracking control rule base.

R_1:	IF lateral error is positive	AND	heading error is positive	THEN steering angle is negative
R_2:	IF lateral error is positive	AND	heading error is zero	THEN steering angle is negative
R_3:	IF lateral error is positive	AND	heading error is negative	THEN steering angle is zero
R_4:	IF lateral error is zero	AND	heading error is positive	THEN steering angle is negative
R_5:	IF lateral error is zero	AND	heading error is zero	THEN steering angle is zero
...				
R_9:	IF lateral error is negative	AND	heading error is negative	THEN steering angle is positive

The remaining choices during controller design are more technical and comprise fuzzification, decision making, and defuzzification strategies. Fuzzification of controller input values is achieved by representing them using fuzzy sets. Using e.g. $e_{tl,m}$ to denote the current measured lateral error a simple representation is given by defining the fuzzy set $M_{e_{tl}}$ with membership function:

$$\mu_{M_{e_{tl}}}(e_{tl}) \text{ with } \begin{cases} \mu_{M_{e_{tl}}}(e_{tl}) = 1 & \text{for } e_{tl} = e_{tl,m}, \\ \mu_{M_{e_{tl}}}(e_{tl}) = 0 & \text{for } e_{tl} \neq e_{tl,m}. \end{cases} \tag{2.108}$$

Using Mamdani's Max-Min-Inference method [Bot93] to set up the inference engine a particular mathematical interpretation of the rules of Table 2.4 is given as follows. The first condition of rule R_1, i.e. "lateral error is positive", is interpreted as

$$\alpha_{R_{1,1}} = \sup_{e_{tl} \in [e_{tl,min}, e_{tl,max}]} \left(\min \left(\mu_{M_{e_{tl}}}(e_{tl}), \mu_{P_{e_{tl}}}(e_{tl}) \right) \right). \tag{2.109}$$

For the special case (2.108) $\alpha_{R_{1,1}}$ is

$$\alpha_{R_{1,1}} = \mu_{P_{e_{tl}}}(e_{tl,m}). \tag{2.110}$$

$\alpha_{R_{1,1}}$ may be seen as the degree to which the first condition of rule R_1 is fulfilled. Calculating $\alpha_{R_{1,2}}$ for the second condition of R_1 in a similar way the combined condition "lateral error is positive AND heading error is positive" is interpreted as

$$\alpha_{R_1} = \min \left(\alpha_{R_{1,1}}, \alpha_{R_{1,2}} \right). \tag{2.111}$$

The implication "IF lateral error is positive AND heading error is positive THEN steering angle is negative" is implemented by weighting the conclusion's membership function $\mu_{N_{\delta_{tf}}}(\delta_{tf})$, i.e:

$$\mu_{R_1}(\delta_{tf}) = \min \left(\alpha_{R_1}, \mu_{N_{\delta_{tf}}}(\delta_{tf}) \right). \tag{2.112}$$

α_{R_1} defines an upper limit for $\mu_{R_1}(\delta_{tf})$ and is denoted as firing strength [Lee90b] of rule R_1. Performing similar calculations for all rules allows to combine the result in one membership function

$$\mu_R(\delta_{tf}) = \max \left(\mu_{R_1}(\delta_{tf}), \ldots, \mu_{R_9}(\delta_{tf}) \right). \tag{2.113}$$

Defuzzification finally yields the controller output value. Using the center of area method [Bot93] as an example, the controller output value applied to the plant is

$$\delta_{tf,coa} = \frac{\int\limits_{\delta_{tf,min}}^{\delta_{tf,max}} \delta_{tf}\mu_R(\delta_{tf})d\delta_{tf}}{\int\limits_{\delta_{tf,min}}^{\delta_{tf,max}} \mu_R(\delta_{tf})d\delta_{tf}}. \tag{2.114}$$

The entire procedure is repeated for each controller time step. The FLC has no internal states and results in a nonlinear function relating controller inputs and outputs. For that reason it may be interpreted as a lookup table [Bot93] which is parametrized using linguistic expressions.

Literature Survey

In literature FLC was considered in remotely related path tracking applications for mobile robots [ACF07] as well as in applications for passenger cars on automated highways [HT94]. The latter designed fuzzy logic controllers with rule bases comprising feedback control, curvature preview, and velocity based gain scheduling. Feedback control compared to the simple example above relies on a finer partition of the universes of discourse, hence resulting in numerous (125) rules. The fuzzy logic controller was tuned manually mimicking a driver's behavior and using an existing LQR to aid the initial choice of parameters. An experimental comparison with LQR and PID indicated that a well-tuned fuzzy logic controller is capable of achieving a similar performance without using an explicit plant model. In a later publication [HT95] tried to reduce the tuning effort of their fuzzy logic controller by combining it with model reference adaption techniques.

Discussion

Pro: FLC allows for controller design based on linguistic rules and expert knowledge. This is a great advantage for plants that are difficult to model or not completely understood. The approach can be applied to MIMO systems without difficulties. With a moderate number of rules the approach is computationally simple.

Contra: The advantage of FLC in case of vaguely known plants turns into a drawback in case of plant models that can be stated easily. In this situation both the tuning parameters of membership functions and the rules within the knowledge base quickly outnumber the parameters required for e.g. PID or LQR control. FLC is a nonlinear proportional control law only and additional measures might be necessary to cope with changing parameters and disturbances.

2.2.11 State, Parameter, and Disturbance Estimation

Many of the control approaches mentioned above require full state feedback. In most cases, however, some states are either unmeasurable or measurable only with great effort. Therefore, numerous ways of estimating unmeasurable system states have been developed. Figure 2.14 depicts the principle idea of state estimation. A plant model is computed parallel to the actual plant. This model is fed with the plant input signals $\mathbf{u}$. The computed estimated output $\hat{\mathbf{y}}$ is compared with the actual plant output $\mathbf{y}$. The difference between both is fed back to the plant model. The associated output estimation error feedback is designed such that the plant model states follow the plant states. If the plant model states $\hat{\mathbf{x}}$ track the plant states $\mathbf{x}$ reasonably fast they can be used as a substitute for the plant states within a controller for the plant. Besides the system states considered for plant control, the plant model may include additional (uncontrolled) states modeling disturbances [Foe94, Lun10] or slowly changing plant parameters [GKN+74]. The plant model used within the estimator may be linear or nonlinear. Estimator design is motivated using either deterministic [FPEN10, Foe94, Lun10, Ada09] or stochastic [GKN+74, May82] system descriptions. For linear deterministic plants the Luenberger observer [Foe94, Lun10] is very common. Research on state estimation for linear stochastic plants produced the celebrated Kalman filter [GKN+74] which, with some assumptions regarding the system's noise [GKN+74], is an optimal filter. This means it provides a minimum error covariance system state estimate for linear systems. Nonlinear estimation problems have led to numerous estimator variants and it is impractical to provide a comprehensive list within this section. Only a relevant selection of approaches is briefly discussed. For deterministic
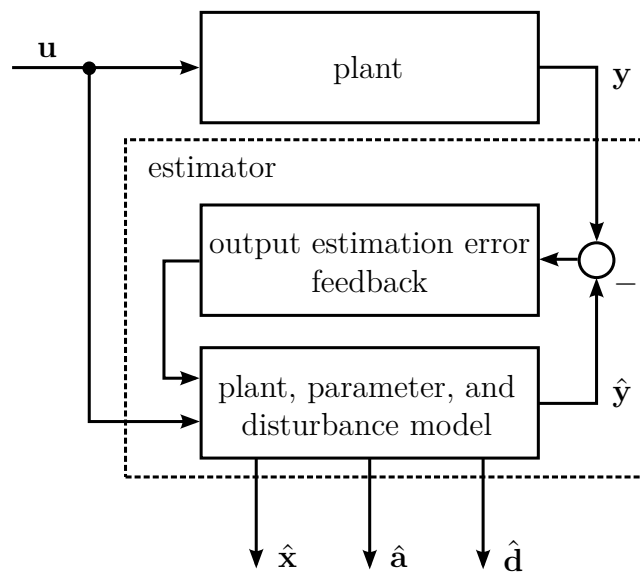
Figure 2.14: State estimation based on a plant model computed parallel to the plant. The output estimation error feedback is designed to have the plant model states follow the plant states. The plant model may include additional disturbance and parameter models. $\mathbf{y}$ and $\hat{\mathbf{y}}$ denote plant output and output estimate. $\hat{\mathbf{x}}$, $\hat{\mathbf{a}}$, and $\hat{\mathbf{d}}$ are state, parameter, and disturbance estimates.

system descriptions [Ada09] states estimators that closely resemble the ideas of nonlinear controllers, using feedback linearization for instance. For nonlinear stochastic systems numerous generalizations of the linear Kalman filter have been developed. The very popular Extended Kalman Filter (EKF) [GKN+74, May82] is a straightforward generalization that includes a nonlinear plant description. Partly however it is still based on a first order Taylor series expansion of the nonlinear system. For systems exhibiting stronger nonlinearities two alternatives are common. The first one is a second-order filter [GKN+74] that simply relies on a higher order Taylor series expansion. The second is the more recent Sigma-Point Kalman Filter [Mer04] which sparked interest because it allows to avoid plant linearization and the calculation of the respective Jacobian matrices. This estimation approach, instead, relies on statistical analysis of carefully chosen state space sample points which are propagated using the nonlinear system description. Besides the mentioned estimators, which allow for parameter estimation in a state estimation framework there are related methods focusing on parameter estimation only. Among those the Least Squares Estimator [SL91] and its variants are common.

Besides those universally applicable state estimation methods some particularities regarding state estimation combined with parameter and disturbance estimation for path tracking control applications are noteworthy. [CLTM10] add side-slip parameters for all wheels to a kinematic tractor-trailer model and use a deterministic observer to estimate those. [BOV12] in contrast capture side-slip properties of a tractor-trailer combination by multiplying the tractor front wheel steering angle with an estimated factor. An EKF is used for state and parameter estimation. [Bel99] considers two variants. The first variant uses a kinematic tractor model with two parameters accounting for side-slip and calibration errors. Those parameters are an additive steering angle bias and a multiplicative factor affecting the tractor yaw rate ODE. An EKF and a more accurate second order nonlinear filter have been used to estimate those parameters. Simulations showed relative small performance differences between both. The second order nonlinear filter however could not be computed in real-time and was not considered in experiments. The second variant of [Bel99] is a slope adjusted parameter estimation approach. In this case the influence of two parameters accounting for steering angle and yaw angle bias is modeled to be proportional to the tractor's roll angle. Due to this choice changing slope angles do not perturb settled bias parameter estimates. The tractor's roll angle was measured and provided to the estimator. [Rek01] focuses on parameter estimation for a dynamic tractor model. He combines multiple physical model parameters to a reduced number of parameters and proposes two estimator variants for those. The first variant is an EKF including additional states to model slowly changing parameters. The second variant uses an EKF for state estimation only which is combined with an outer loop Least Mean Squares (LMS) parameter identification algorithm. This variant allows maintaining a lower number of system states and results in a considerably reduced computational effort.

2.2.12 Adaptive Control

Dynamic systems often exhibit parameters that are uncertain or slowly changing. If the mismatch between parameters assumed for controller design and actual plant parameters deteriorates the performance of the controlled system, then the controller may be improved by changing the control law during runtime based on recent more accurate parameter estimates. This is the main idea of adaptive control. [SL91] distinguishes two adaptive control concepts which are depicted in Figure 2.15 and Figure 2.16. The remaining section briefly summarizes the detailed explanations in [SL91]. The Self-Tuning Controller (STC) is a straightforward approach using current plant parameter estimates to recalculate the controller parameters. This approach may be combined with many control approaches stated before. A STC is quite simple to design. The convergence properties of the resulting system, however, are difficult to analyze. Model Reference Adaptive Control (MRAC) in contrast uses a reference model specifying the desired closed loop plant behavior. The tracking error between reference model output and controlled plant output is fed into an adaption law modifying some controller parameters until the tracking error converges to zero. MRAC can be interpreted as estimation of uncertain controller parameters in contrast to plant parameter estimation with STC. With MRAC controller design normally is based on trial and error. Convergence analysis however is rather simple. Both adaptive control approaches share a crucial requirement. Sufficient excitation of the controlled system is needed in order guarantee stability and parameter convergence. Measurement noise in particular may cause a drift of parameters in case there is a lack of excitation.

Regarding research on path tracking control [GB08] considers a tractor with a three-point hitched ripper. The steady-state gain of the steering angle to yaw rate transfer function in this setup was shown to vary with velocity and working depth of the ripper. To achieve a consistently good controller performance they derived a PD lateral position controller with
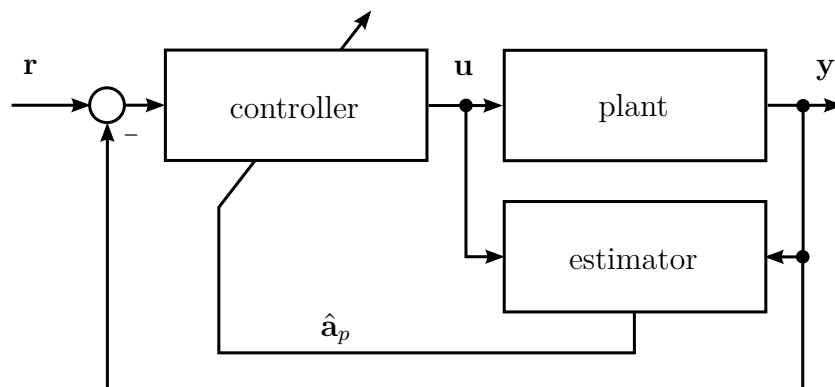

Figure 2.15: Principle of a Self-Tuning Controller (STC) (following [SL91]). An estimator is used to obtain plant parameter estimates $\hat{\mathbf{a}}_p$. Subsequently these estimates are used to recalculate the controller. The reference signal $\mathbf{r}$ must provide sufficient excitation.
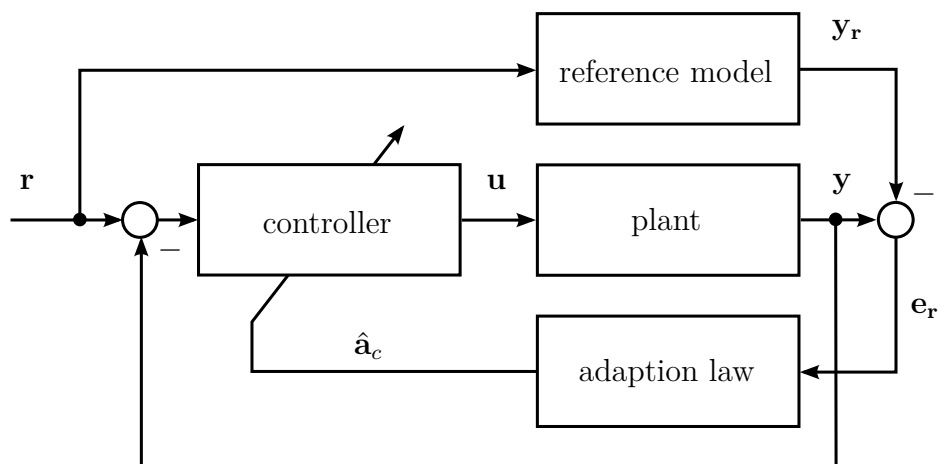
Figure 2.16: Principle of Model Reference Adaptive Control (MRAC) (following [SL91]). A reference model specifies the desired closed loop behavior. The reference output error $\mathbf{e_r}$ between actual output $\mathbf{y}$ and reference output $\mathbf{y_r}$ is used to adapt the estimated controller parameters $\hat{\mathbf{a}}_c$ until $\mathbf{e_r}$ converges to $\mathbf{0}$. The reference signal $\mathbf{r}$ must provide sufficient excitation.

a precalculated controller gain lookup table considering the tractor velocity and a second parameter accounting for changes in the ripper's working depth. This second parameter was estimated using an EKF. Data analysis was included in order stop estimation in case the yaw dynamics excitation becomes insufficient. [Der08, DB09] as well used a tractor and a three-point hitched ripper. They presented a PID path tracking controller with two MRAC variants adapting an inner loop yaw rate controller. The first variant adapted the feedback gain of the yaw rate controller. This controller however suffered from fluctuations in the adaption response and system oscillations. Therefore, a second variant introducing and adapting a feedforward gain for the yaw rate controller was derived. Both controllers were used for straight path tracking and the adaption was only performed during the initial path acquisition. [Rek01] considered a tractor with a three-point hitched cultivator on curved paths. He combined LQR with his EKF/LMS parameter estimator described in the previous section. He performed experiments on curved paths and recommended using headland turns for identification in case paths do not provide sufficient excitation. In order to improve their nonlinear MPC prediction in the presence of wheel side-slip [BOV12] include an EKF estimation based factor affecting the tractor steering angle. [CLTM10] used tractor and unsteered implement wheel side-slip estimates to enhance their nonlinear control law based on a kinematic vehicle description. [TT03] considered a dynamic model description of an on-road tractor-trailer combination with uncertain cornering stiffness parameters for all wheels. They combined adaptive with sliding mode control and utilize estimates of the uncertain cornering stiffness parameters to improve the linearizing part of the sliding mode control law. Special emphasis was on keeping the estimated parameters within a specified interval. This allowed maintaining a formal upper bound for model uncertainties which is needed to motivate sliding mode control.

2.2.13 Overview and Comparison

The numerous path tracking control approaches outlined within the previous sections are intended for various applications. Objectives, requirements, and surrounding conditions may differ for those applications. In order to identify solutions suiting this work's objectives of Section 1.2 a discussion outlining advantages and disadvantages has been provided for each approach. This section compiles the results of those discussions in order to narrow down the wide choice of approaches to a smaller number of promising solutions. This rather coarse assessment however does not exclude the possibility that other choices might be modified to meet this work's objectives as well.

Table 2.5 lists possible control approaches and this work's objectives which can be considered prior to actually implementing an approach. In addition to this, the need for state estimation was included as a criterion depicting increased effort. This effort arises namely for two reasons. The first is implement specific estimator parameterization which is possibly done in the field. The second stems from state feedback control on curved paths requiring a nonlinear reference variable generator to obtain desired system states (e.g. desired hitch angle) matching the desired path.

Considering variants of implements and actuator combinations, nonlinear Lyapunov based control, feedback linearization as well as SMC in particular rely on control laws tailored

Table 2.5: Comparison of path tracking control approaches.

	Variants systematic	MIMO	Robust w/o additional measures	Tuning intuitive	Computation simple	State estimation unnecessary
Classical PID Control			✓		✓	✓
Linear-Quadratic Regulator	✓	✓		✓	✓	
Model Predictive Control	✓	✓		✓		
Robust H_∞ Control	✓	✓	✓		✓	✓
Nonlinear Lyapunov		✓			✓	
Feedback Linearization		✓			✓	
Sliding Mode Control		✓	✓		✓	
Geometric Path Tracking					✓	✓
Fuzzy Logic Control		✓		✓	✓	✓

towards a particular system input-output configuration. Classical PID control as well as FLC do not require reformulation of the entire control law. However, they still respond differently depending on the particular input-output behavior. LQR, MPC, and robust H_∞ control share the advantage that the underlying numerical algorithms are applicable to (controllable) linear systems in general regardless of a particular structure. Most stated control approaches are directly applicable to MIMO systems. Only geometric path tracking as considered in literature [BOV12] and most classical PID controller design approaches require multiple SISO control loops to be closed and therefore neglect coupling. Robustness of a control approach must be further distinguished due to different definitions. Robust controllers as precisely defined by [DG75] (see Appendix A.7) exhibit zero steady-state error despite particular types of disturbances and uncertain plant parameters. The allowed parameter perturbations are finite and not just arbitrarily small, provided that the closed loop system remains stable. PID is such a robust controller for constant disturbances. Robustness as defined for SMC is in a sense that for specified upper bounds of parametric uncertainties the steady state error remains within defined limits. The achievable limits result from a trade-off considering unmodeled dynamics, a finite switching frequency, and possibly smoothed switching using a boundary layer [SL91]. Robust stability as defined by [Mac04] while considering robust H_∞ control achieves closed loop stability for an entire set of well-defined uncertain plants. The closed loop however does not necessarily exhibit good a performance and small steady-state errors. In terms of tuning LQR and MPC share the advantage that those rely on choosing weights for input signals as well as state or output signals. Choosing weights for steering inputs and tracking error outputs in particular allows for intuitive interpretation. FLC is meant to depict expert knowledge and can therefore be quite intuitive. This is in case the number of rules remains limited. From previous work MPC was the only one being rather computationally demanding due to numerical optimization at each time step. Considering additional effort due to state estimation PID, FLC, and geometric path tracking could rely on measured outputs only. H_∞ controller design immediately results in a dynamic output feedback law and designing a separate state estimator is not necessary.

3 Models of Lateral Tractor-Implement Motion

Tying in with the general introduction on models of vehicle lateral motion provided in Section 2.1 the present section is used to derive the tractor and implement models needed throughout the remainder of this work. Both dynamic and kinematic models of lateral motion are considered. A combination studied in particular comprises a front wheel steered tractor and a towed implement with steerable wheels and steerable drawbar. Regarding this combination variants using either all or subsets of the available actuators are taken into account. The models are given in two representations with the first one being based on earth-fixed coordinates for simulation purposes. The second representation, in terms of deviations from a desired path, allows for linearization, further analysis, and model based controller design. While deriving all models particular emphasis is put on using approaches that can be easily extended to other implement variants. For both kinematic and dynamic models the approaches require constraints of a particular implement to be stated up-front. Subsequently, equations of motion are found using automated procedures and computer algebra software. Within this section each model is parameterized in order to resemble the experimental setup described in Appendix A.3. Finally, an analysis and comparison is given to outline the capabilities and limitations of each model.

3.1 Dynamic Models

The first models to be considered are dynamic models of tractor-implement combinations. The basic ideas regarding modeling assumptions, equations of motion, as well as wheel forces and moments can be transferred directly from Section 2.1.1. The introduction of an implement with steerable drawbar in particular, however, deviates from all previous work on dynamic vehicle modeling. Wheel steering, as considered before, causes a change in the external force vector acting on one of the rigid bodies. This is without immediate influence on the rigid bodies' position and orientation. Drawbar steering in contrast requires the connected rigid bodies to move in order obtain a desired steering angle. As a consequence, drawbar steering compared to wheel steering exhibits a closer coupling with rigid body dynamics. This section proposes a new solution of how to include drawbar steering and similar types of actuators in a convenient way.

3.1.1 Modeling Assumptions

For the given task of path tracking control a simulation model as well as a possibly linearized and simplified model for further analysis and controller design have to be found. The considered steering inputs do not result in asymmetric wheel forces. Hence, as in most previous research stated in Section 2.1.1, all wheel properties of an axle are combined and a single track model as depicted in Figure 3.1 is used to describe the tractor-implement combination. The model is assumed to be in plane motion, while wheel load transfer as well as roll and pitch movement are neglected. The influence of slopes, however, may be included by adding lateral or longitudinal disturbing forces. Tractor and implement are modeled as two rigid bodies with masses m_t and m_{r1} as well as moments of inertia I_t and I_{r1}. The rigid bodies exhibit 3 DoFs each, which are further reduced due to constraints imposed by the drawbar. Steering of tractor and implement is achieved using the tractor front wheel steering angle δ_{tf} as well as the implement drawbar and wheel steering angles δ_{r1d} and δ_{r1r}. These steering angles are typically enforced by a steering angle controller and hydraulic actuators. The desired straight path and the associated tracking errors are introduced to obtain a linear system description in terms of path deviations.

3.1.2 Equations of Motion

The introductory example of Section 2.1.1 considered a tractor and hence a single rigid body with simple equations of motion. Tractor-implement combinations described by multiple rigid bodies, which are subject to constraints, in contrast result in lengthy equations. To obtain those equations in a systematic manner [Gen97] proposes a particularly useful approach using Lagrangian mechanics as well as some well-considered intermediated coordinate transformations. [Gen97] uses this approach to derive the equations of motion for a tractor with an arbitrary number of trailers. As a concise example an extended version of his approach has been used in Appendix A.1.1 to derive the equations of motion of a tractor. The extensions made comprise the introduction of arbitrary forces and moments acting on the c.g. allowing the inclusion of disturbing forces for instance.

In this section the approach as stated in Appendix A.1.1 shall be applied to tractors and steerable implements. First however the particular case of actuators between two rigid bodies, such as a steerable drawbar for instance, has to be addressed. There are two approaches to consider the steerable drawbar. In a first approach one could try to model the moment applied by the drawbar steering actuators, for instance by including a model of the underlying hydraulics and a steering angle controller enforcing a desired steering angle. In a second approach one could assume that some arbitrary kind of actuator and steering angle controller is in place and that this actuator is capable of providing any moment required to steer the drawbar. With this second option it is not possible to
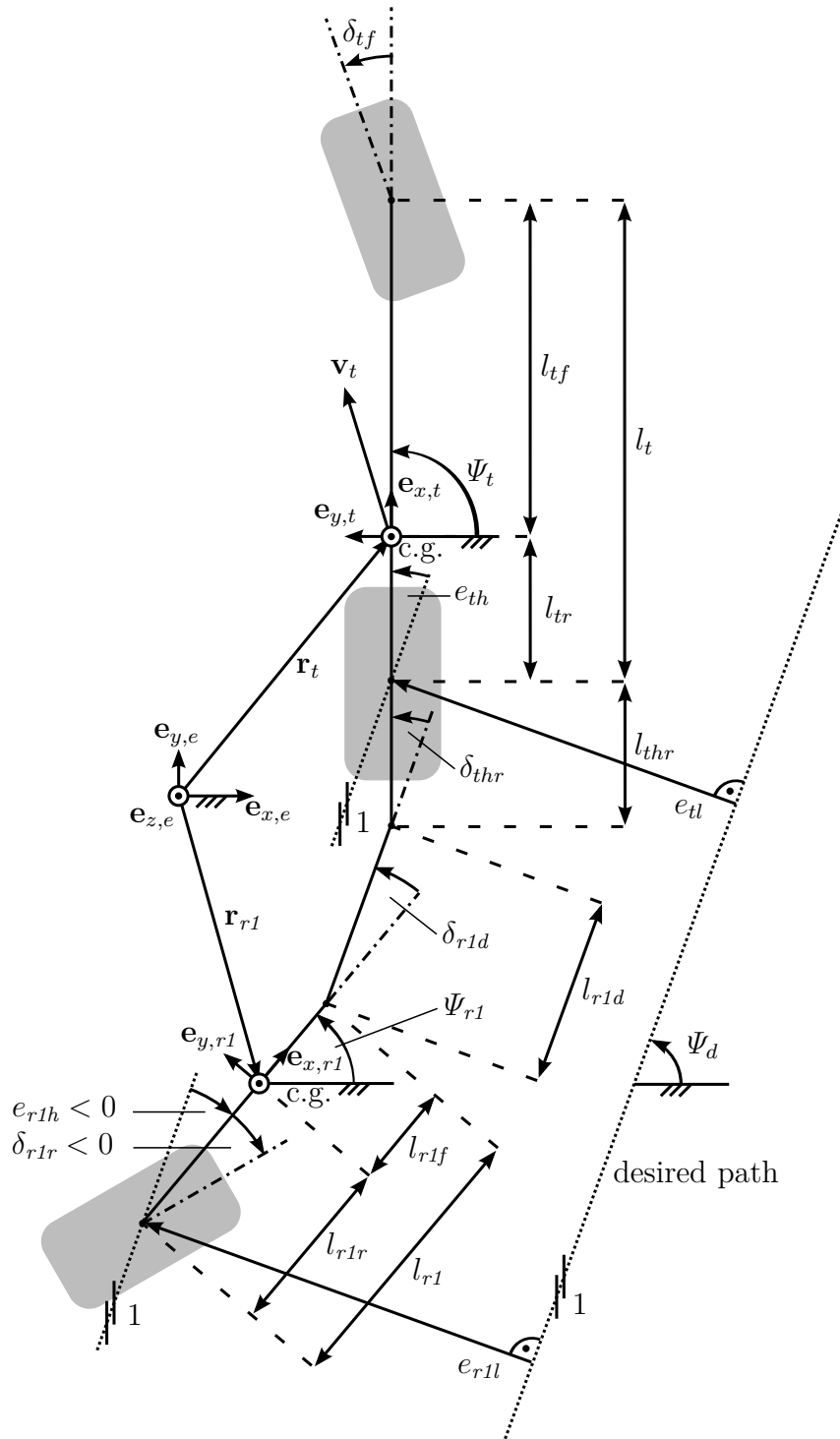
Figure 3.1: Tractor (subscript *t*) and steerable implement (subscript *r1*, i.e. first rear-mounted implement) single track model with earth-fixed ($\mathbf{e}_{x,e}$, $\mathbf{e}_{y,e}$, $\mathbf{e}_{z,e}$), tractor-fixed ($\mathbf{e}_{x,t}$, $\mathbf{e}_{y,t}$, $\mathbf{e}_{z,t}$), implement-fixed ($\mathbf{e}_{x,r1}$, $\mathbf{e}_{y,r1}$, $\mathbf{e}_{z,r1}$) coordinate systems, tractor wheel steering angle δ_{tf}, implement wheel steering angle δ_{r1r}, drawbar steering angle δ_{r1d}, hitch angle δ_{thr}, tractor heading angle Ψ_t, implement heading angle Ψ_{r1}, orientation of the desired path Ψ_d, tractor lateral error e_{tl}, tractor heading error e_{th}, implement lateral error e_{r1l}, implement heading error e_{r1h}, and geometric parameters $l_{...}$. $\mathbf{r}_t$ and $\mathbf{r}_{r1}$ specify the tractor and implement c.g. positions relative to the earth-fixed origin.

model a blocked actuator, e.g. due to tractor and implement being immovable. Modeling however is simplified and reduced to the introduction of a time dependent or rheonomic constraint, independent of a particular actuator. The second approach has been chosen in this work.

Referring to Figure 3.1 the two rigid bodies in plane motion are subject to two constraints imposed by the steerable drawbar. Hence four generalized coordinates are introduced to describe for the remaining DoFs. The generalized coordinates are chosen to be:

$$q_1 = r_t^{x,e}, \qquad q_2 = r_t^{y,e}, \qquad q_3 = \Psi_t, \qquad q_4 = \delta_{thr}. \qquad (3.1)$$

Tractor and implement position and orientation in terms of generalized coordinates are:

$$r_t^{x,e} = q_1, \qquad (3.2)$$
$$r_t^{y,e} = q_2, \qquad (3.3)$$
$$\Psi_t = q_3, \qquad (3.4)$$
$$r_{r1}^{x,e} = q_1 - (l_{tr} + l_{thr}) \cos(q_3) - l_{r1d} \cos(q_3 - q_4) - l_{r1f} \cos(q_3 - q_4 - \delta_{r1d}), \qquad (3.5)$$
$$r_{r1}^{y,e} = q_2 - (l_{tr} + l_{thr}) \sin(q_3) - l_{r1d} \sin(q_3 - q_4) - l_{r1f} \sin(q_3 - q_4 - \delta_{r1d}), \qquad (3.6)$$
$$\Psi_{r1} = q_3 - q_4 - \delta_{r1d}. \qquad (3.7)$$

The system's kinetic energy is [Gre88]:

$$T = \frac{1}{2} I_t \dot{\Psi}_t^2 + \frac{1}{2} m_t \left((\dot{r}_t^{x,e})^2 + (\dot{r}_t^{y,e})^2 \right) + \frac{1}{2} I_{r1} \dot{\Psi}_{r1}^2 + \frac{1}{2} m_{r1} \left((\dot{r}_{r1}^{x,e})^2 + (\dot{r}_{r1}^{y,e})^2 \right). \qquad (3.8)$$

With potential energy $V = 0$ the Lagrangian function is:

$$L = T - V = T. \qquad (3.9)$$

Lagrange's equations of motion are [Gre88]:

$$\frac{d}{dt} \left(\frac{\partial L}{\partial \dot{q}_i} \right) - \frac{\partial L}{\partial q_i} = Q_i, \quad i = 1, 2, 3, 4, \qquad (3.10)$$

with generalized forces Q_i introduced to account for arbitrary applied forces and moments. With $F_t^{x,e}$, $F_t^{y,e}$, $F_{r1}^{x,e}$, and $F_{r1}^{y,e}$ denoting applied forces on tractor and implement c.g. as well as $M_t^{z,e}$ and $M_{r1}^{z,e}$ denoting applied moments acting on tractor and implement the respective generalized forces are:

$$Q_i = F_t^{x,e} \gamma_{t,i}^{x,e} + F_t^{y,e} \gamma_{t,i}^{y,e} + M_t^{z,e} \beta_{t,i}^{z,e} + F_{r1}^{x,e} \gamma_{r1,i}^{x,e} + F_{r1}^{y,e} \gamma_{r1,i}^{y,e} + M_{r1}^{z,e} \beta_{r1,i}^{z,e}, \qquad (3.11)$$

with linear and angular velocity coefficients [Gre88]:

$$\gamma_{t,i}^{x,e} = \frac{\partial \dot{r}_t^{x,e}}{\partial \dot{q}_i} = \frac{\partial r_t^{x,e}}{\partial q_i}, \qquad \gamma_{t,i}^{y,e} = \frac{\partial \dot{r}_t^{y,e}}{\partial \dot{q}_i} = \frac{\partial r_t^{y,e}}{\partial q_i}, \qquad \beta_{t,i}^{z,e} = \frac{\partial \dot{\Psi}_t}{\partial \dot{q}_i}, \tag{3.12}$$

$$\gamma_{r1,i}^{x,e} = \frac{\partial \dot{r}_{r1}^{x,e}}{\partial \dot{q}_i} = \frac{\partial r_{r1}^{x,e}}{\partial q_i}, \qquad \gamma_{r1,i}^{y,e} = \frac{\partial \dot{r}_{r1}^{y,e}}{\partial \dot{q}_i} = \frac{\partial r_{r1}^{y,e}}{\partial q_i}, \qquad \beta_{r1,i}^{z,e} = \frac{\partial \dot{\Psi}_{r1}}{\partial \dot{q}_i}. \tag{3.13}$$

Vehicle-Fixed Coordinates

Evaluating (3.1) to (3.13) already allows one to state the system's equations of motion for simulation purposes. The resulting description however is in earth-fixed coordinates and not suitable for linearization. A more suitable description is found by introducing vehicle-fixed coordinates, using:

$$\mathbf{T}_{t,e} = \begin{bmatrix} \cos(\Psi_t) & -\sin(\Psi_t) \\ \sin(\Psi_t) & \cos(\Psi_t) \end{bmatrix}, \tag{3.14}$$

$$\mathbf{T}_{r1,e} = \begin{bmatrix} \cos(\Psi_t - \delta_{thr} - \delta_{r1d}) & -\sin(\Psi_t - \delta_{thr} - \delta_{r1d}) \\ \sin(\Psi_t - \delta_{thr} - \delta_{r1d}) & \cos(\Psi_t - \delta_{thr} - \delta_{r1d}) \end{bmatrix}, \tag{3.15}$$

$$\begin{bmatrix} \dot{r}_t^{x,e} \\ \dot{r}_t^{y,e} \end{bmatrix} = \begin{bmatrix} v_t^{x,e} \\ v_t^{y,e} \end{bmatrix} = \mathbf{T}_{t,e} \begin{bmatrix} v_t^{x,t} \\ v_t^{y,t} \end{bmatrix}, \tag{3.16}$$

$$\begin{bmatrix} F_t^{x,e} \\ F_t^{y,e} \end{bmatrix} = \mathbf{T}_{t,e} \begin{bmatrix} F_t^{x,t} \\ F_t^{y,t} \end{bmatrix}, \qquad\qquad M_t^{z,e} = M_t^{z,t}, \tag{3.17}$$

$$\begin{bmatrix} F_{r1}^{x,e} \\ F_{r1}^{y,e} \end{bmatrix} = \mathbf{T}_{r1,e} \begin{bmatrix} F_{r1}^{x,r1} \\ F_{r1}^{y,r1} \end{bmatrix}, \qquad\qquad M_{r1}^{z,e} = M_{r1}^{z,r1}. \tag{3.18}$$

Equations of motion in vehicle-fixed coordinates can be obtained by following the procedure described below. The required steps are similar to those given in the concise example of Appendix A.1.1. Intermediate results in this section are very lengthy and therefore omitted. All steps have been performed using computer algebra software.

1. Insert (3.12), (3.13), and (3.11) in (3.10).

2. Calculate partial derivatives of (3.10). Time derivatives are considered later.

3. Reintroduce original coordinates by using (3.1).

4. Replace earth-fixed coordinates by tractor and implement-fixed coordinates using (3.14) to (3.18).

5. Calculate time derivatives of (3.10).

6. Combine equations (3.10) for $i = 1, 2$ to column vectors and multiply with $\mathbf{T}_{t,e}^{-1}$.

7. Perform a multitude of (automated) trigonometric simplifications.

The result is:

$$\left[\dot{v}_t^{x,t}, \dot{v}_t^{y,t}, \ddot{\Psi}_t, \ddot{\delta}_{thr}\right]^{\mathrm{T}} = -\mathbf{M}^{-1}\mathbf{r}, \tag{3.19}$$

with

$$\mathbf{M} = \mathbf{M}(\delta_{thr}, \delta_{r1d}), \tag{3.20}$$

$$\mathbf{r} = \mathbf{r}(v_t^{x,t}, v_t^{y,t}, \dot{\Psi}_t, \dot{\delta}_{thr}, \delta_{thr}, \ddot{\delta}_{r1d}, \dot{\delta}_{r1d}, \delta_{r1d}, F_t^{x,t}, F_t^{y,t}, M_t^{z,t}, F_{r1}^{x,r1}, F_{r1}^{y,r1}, M_{r1}^{z,r1}). \tag{3.21}$$

The full matrix $\mathbf{M}$ and vector $\mathbf{r}$ are shown in Appendix A.1.2. Most important to note is that $q_3 = \Psi_t$ is part of the constraints (3.5) to (3.7) but not part of the final result. Hence (3.19) became independent of earth-fixed references. This is not surprising but in agreement with expectations, i.e. ODEs for vehicle velocities, yaw rate and hitch angle are independent of the vehicles' actual position and orientation. Another look at (3.19) reveals that the result depends not only on the drawbar steering angle δ_{r1d} but also on its first and second time derivative $\dot{\delta}_{r1d}$ and $\ddot{\delta}_{r1d}$. This depicts the closer coupling of drawbar steering and rigid body dynamics requiring the rigid bodies to move in order to enforce a desired steering angle. A proposal to obtain $\dot{\delta}_{r1d}$ and $\ddot{\delta}_{r1d}$ is provided in Section 3.1.4.

3.1.3 Wheel Forces and Moments

With a focus on path tracking control, vehicle lateral motion during normal operation away from wheel force limits is of particular interest. For that reason a linear, yet transient tire model is chosen by introducing combined cornering stiffness and relaxation length parameters. Influence of longitudinal slip as well as varying soil properties is considered subsequently by parameter variation.

By extending the introductory example of Section 2.1.1 the side-slip angles of the considered tractor-implement combination are:

$$\alpha_{tf} = \delta_{tf} - \arctan\left(\frac{v_{tf}^{y,t}}{v_{tf}^{x,t}}\right), \ \alpha_{tr} = -\arctan\left(\frac{v_{tr}^{y,t}}{v_{tr}^{x,t}}\right), \ \alpha_{r1r} = \delta_{r1r} - \arctan\left(\frac{v_{r1r}^{y,r1r}}{v_{r1r}^{x,r1r}}\right), \tag{3.22}$$

with velocities found from time derivatives of (3.2), (3.3), (3.5), and (3.6) considering (3.1), (3.14), and (3.15).

Similarly, tire forces are modeled to account for transient behavior by introducing tire relaxation lengths for all wheels. This results in:

$$\dot{\alpha}_{re,tf} = \frac{\cos\left(\delta_{tf}\right) v_{tf}^{x,t} + \sin\left(\delta_{tf}\right)\left(v_{tf}^{y,t}\right)}{\sigma_{\alpha,tf}} \left(\alpha_{tf} - \alpha_{re,tf}\right), \tag{3.23}$$

$$\dot{\alpha}_{re,tr} = \frac{v_{tr}^{x,t}}{\sigma_{\alpha,tr}} \left(\alpha_{tr} - \alpha_{re,tr}\right). \tag{3.24}$$

$$\dot{\alpha}_{re,r1r} = \frac{\cos\left(\delta_{r1r}\right) v_{r1r}^{x,r1} + \sin\left(\delta_{r1r}\right) \left(v_{r1}^{y,r1}\right)}{\sigma_{\alpha,r1r}} \left(\alpha_{r1r} - \alpha_{re,r1r}\right). \tag{3.25}$$

Lateral wheel forces in wheel-fixed coordinates (cf. Figure 2.7) then are:

$$F_{tf}^{y,tf} = C_{\alpha,tf}\alpha_{re,tf} \qquad\qquad F_{tr}^{y,tr} = C_{\alpha,tr}\alpha_{re,tr} \qquad\qquad F_{r1r}^{y,r1r} = C_{\alpha,r1r}\alpha_{re,r1r} \tag{3.26}$$

Transforming them to vehicle-fixed coordinates and considering the lever arms to the respective center of gravity (c.g.) yields $F_t^{x,t}$, $F_t^{y,t}$, $F_{r1}^{x,r1}$, and $F_{r1}^{y,r1}$ as well as $M_t^{z,t}$ and $M_{r1}^{z,r1}$ required for (3.19).

3.1.4 Steering Actuator Dynamics

Within the introductory example of Section 2.1.1 the tractor steering angle δ_{tf} was used as an input. This steering angle therefore could be altered arbitrarily fast. In reality hydraulic steering, however, introduces some delay, which will be considered in the remainder of this work. It is assumed that a underlying steering angle controller is in place and enforces a desired steering angle. The resulting closed loop behavior is approximated by a delay. In order to satisfy the requirement of an existing second order drawbar steering angle derivative $\ddot{\delta}_{r1d}$ in (3.19) this delay is modeled to be of second order.

Defining the desired steering angle inputs $\delta_{tf,d}$, $\delta_{r1d,d}$, and $\delta_{r1r,d}$ the respective ODEs are:

$$\ddot{\delta}_{tf} = \frac{1}{T_{tf}^2} \left(-2D_{tf}T_{tf}\dot{\delta}_{tf} - \delta_{tf} + \delta_{tf,d}\right) \tag{3.27}$$

$$\ddot{\delta}_{r1d} = \frac{1}{T_{r1d}^2} \left(-2D_{r1d}T_{tr}\dot{\delta}_{r1d} - \delta_{r1d} + \delta_{r1d,d}\right) \tag{3.28}$$

$$\ddot{\delta}_{r1r} = \frac{1}{T_{r1r}^2} \left(-2D_{r1r}T_{tf}\dot{\delta}_{r1r} - \delta_{r1r} + \delta_{r1r,d}\right) \tag{3.29}$$

In addition, lower and upper steering angle limits $\delta_{tf,min}$ and $\delta_{tf,max}$ as well as positive and negative steering angle rate limits $\dot{\delta}_{tf,min}$ and $\dot{\delta}_{tf,max}$ are considered (similar for δ_{r1d} and δ_{r1r}).

3.1.5 Tracking Errors and Earth-Fixed Positions

Similar to Section 2.1.1 the tractor position in earth-fixed coordinates may be introduced by stating ODEs for the tractor rear wheel position:

$$\dot{r}_{tr}^{x,e} = \cos\left(\Psi_t\right)\left(v_t^{x,t}\right) - \sin\left(\Psi_t\right)\left(-l_{tr}\dot{\Psi}_t + v_t^{y,t}\right), \tag{3.30}$$

$$\dot{r}_{tr}^{y,e} = \sin\left(\Psi_t\right)\left(v_t^{x,t}\right) + \cos\left(\Psi_t\right)\left(-l_{tr}\dot{\Psi}_t + v_t^{y,t}\right). \tag{3.31}$$

The implement's orientation and wheel position can be found from Figure 3.1:

$$\Psi_{r1} = \Psi_t - \delta_{thr} - \delta_{r1d}, \tag{3.32}$$

$$r_{r1r}^{x,e} = r_{tr}^{x,e} - l_{thr}\cos(\Psi_t) - l_{r1d}\cos(\Psi_t - \delta_{thr}) - l_{r1}\cos(\Psi_t - \delta_{thr} - \delta_{r1d}), \tag{3.33}$$

$$r_{r1r}^{y,e} = r_{tr}^{y,e} - l_{thr}\sin(\Psi_t) - l_{r1d}\sin(\Psi_t - \delta_{thr}) - l_{r1}\sin(\Psi_t - \delta_{thr} - \delta_{r1d}). \tag{3.34}$$

Alternatively it is again possible to introduce a description in terms of deviations from a straight desired path:

$$\dot{e}_{th} = \dot{\Psi}_t - \dot{\Psi}_d, \tag{3.35}$$

$$\dot{e}_{tl} = \sin\left(e_{th}\right)\left(v_t^{x,t}\right) + \cos\left(e_{th}\right)\left(-l_{tr}\dot{\Psi}_t + v_t^{y,t}\right), \tag{3.36}$$

with implement tracking errors (cf. Figure 3.1) given as:

$$e_{r1h} = e_{th} - \delta_{thr} - \delta_{r1d}, \tag{3.37}$$

$$e_{r1l} = e_{tl} - l_{thr}\sin(e_{th}) - l_{r1d}\sin(e_{th} - \delta_{thr}) - l_{r1}\sin(e_{th} - \delta_{thr} - \delta_{r1d}). \tag{3.38}$$

3.1.6 Dynamic Model Overview

Sections 3.1.1 to 3.1.5 provide all model parts required to describe the lateral motion of a tractor-implement combination as shown in Figure 3.1. Several variants comprising nonlinear and linear system descriptions are needed throughout the subsequent chapters. This section therefore provides an overview by compiling the required equations. For all variants $v_t^{x,t}$ is assumed to be a constant or slowly changing system parameter, i.e. the ODE describing longitudinal motion in (3.19) is omitted.

Nonlinear Model

For simulation purposes a nonlinear dynamic system description with a transient tire force model is used. This description is found by combining (3.19), (3.22), (3.23), (3.24), (3.25), (3.26), (3.27), (3.28), (3.29), (3.30), (3.31), (3.32), (3.33), and (3.34). The result is:

$$\dot{\mathbf{x}} = \mathbf{f}\left(\mathbf{x}, \mathbf{u}\right), \tag{3.39}$$

$$\mathbf{y} = \mathbf{h}\left(\mathbf{x}\right), \tag{3.40}$$

$$\mathbf{x} = \left[r_{tr}^{x,e}, r_{tr}^{y,e}, v_t^{y,t}, \Psi_t, \dot{\Psi}_t, \alpha_{re,tf}, \alpha_{re,tr}, \alpha_{re,r1r}, \delta_{thr}, \dot{\delta}_{thr}, \delta_{tf}, \dot{\delta}_{tf}, \delta_{r1d}, \dot{\delta}_{r1d}, \delta_{r1r}, \dot{\delta}_{r1r}\right]^{\mathrm{T}}, \tag{3.41}$$

$$\mathbf{u} = \left[\delta_{tf,d}, \delta_{r1d,d}, \delta_{r1r,d}\right]^{\mathrm{T}}, \tag{3.42}$$

$$\mathbf{y} = \left[r_{tr}^{x,e}, r_{tr}^{y,e}, \Psi_t, r_{r1r}^{x,e}, r_{r1r}^{y,e}, \Psi_{r1}, \delta_{tf}, \delta_{r1d}, \delta_{r1r}\right]^{\mathrm{T}}. \tag{3.43}$$

Notes:

- In contrast to passenger cars, with nonlinear models commonly referring to nonlinear tire force descriptions, nonlinearity in this work arises from large steering angles and a large hitch angle between tractor and implement.

- The actual numerical simulation model was set up retaining the individual model parts in order to allow for simple modifications.

Linear Models

To allow for further analysis, two linearized model variants in terms of path deviations have been considered. The first variant uses a transient tire model with relaxation length parameters, the second omits transient tire properties using cornering stiffness parameters only. To obtain the first variant (3.19), (3.22), (3.23), (3.24), (3.25), (3.26), (3.27), (3.28), (3.29), (3.35), (3.36), (3.37), and (3.38) are combined. System state vector $\mathbf{x}$, input vector $\mathbf{u}$, and measured output vector $\mathbf{y}$ are defined as:

$$\mathbf{x} = \left[e_{tl}, e_{th}, v_t^{y,t}, \dot{\Psi}_t, \alpha_{re,tf}, \alpha_{re,tr}, \alpha_{re,r1r}, \delta_{thr}, \dot{\delta}_{thr}, \delta_{tf}, \dot{\delta}_{tf}, \delta_{r1d}, \dot{\delta}_{r1d}, \delta_{r1r}, \dot{\delta}_{r1r} \right]^{\mathrm{T}}, \quad (3.44)$$

$$\mathbf{u} = \left[\delta_{tf,d}, \delta_{r1d,d}, \delta_{r1r,d} \right]^{\mathrm{T}}, \quad (3.45)$$

$$\mathbf{y} = \left[e_{tl}, e_{th}, e_{r1l}, e_{r1h} \right]^{\mathrm{T}}. \quad (3.46)$$

Linearization about $\mathbf{x} = \mathbf{0}$ and $\mathbf{u} = \mathbf{0}$ yields:

$$\dot{\mathbf{x}} = \mathbf{A}\mathbf{x} + \mathbf{B}\mathbf{u}, \quad (3.47)$$

$$\mathbf{y} = \mathbf{C}\mathbf{x}. \quad (3.48)$$

Matrices $\mathbf{A}$, $\mathbf{B}$, and $\mathbf{C}$ are again obtained using computer algebra software. An intermediate step requires symbolic inversion of matrix $\mathbf{M}$ in (3.19). This in particular results in very long expressions by far exceeding the size of those given for (3.19) in Appendix A.1.2. For that reason $\mathbf{A}$, $\mathbf{B}$, and $\mathbf{C}$ are not stated fully. Nevertheless, an overview outlining nonzero elements and couplings between system parts is given by the structure matrices in Appendix A.2.1.

The second simplified linear system variant does not consider transient tire forces modeled by (3.23), (3.24), and (3.25). Hence the reduced system state vector is:

$$\mathbf{x} = \left[e_{tl}, e_{th}, v_t^{y,t}, \dot{\Psi}_t, \delta_{thr}, \dot{\delta}_{thr}, \delta_{tf}, \dot{\delta}_{tf}, \delta_{r1d}, \dot{\delta}_{r1d}, \delta_{r1r}, \dot{\delta}_{r1r} \right]^{\mathrm{T}}. \quad (3.49)$$

Again structure matrices of $\mathbf{A}$, $\mathbf{B}$, and $\mathbf{C}$ outlining nonzero elements and coupling between system parts are provided in Appendix A.2.1.

3.1.7 Model Parameters

Both simulations and experiments will be used to validate this work's control approaches. Experiments are performed using the hardware setup described in Appendix A.3 comprising a John Deere 6210R tractor towing a custom built implement with multiple actuators. For model based controller design as well as simulation purposes the model parameters have to be chosen to depict this hardware setup. The chosen parameters are summarized in Appendix A.5. This section outlines the methods used to obtain these parameters.

Geometric parameters have been found using total station measurements (Leica TS15). In a first step a set of adhesive target marks has been placed on tractor and implement allowing to set up body-fixed coordinate systems for both. In a second step additional measurements have been performed to obtain relevant vehicle vertices and sensor locations within those body-fixed coordinate systems.

Mass parameters and c.g. locations have been calculated from axle load measurements on a vehicle scale.

Steering actuator time constants and damping ratios have been found from step responses with small desired steering angle steps. Steering actuator rate limits resulting from limited hydraulic flow are derived from steering angle slope measurements in large step responses.

Cornering stiffnesses, relaxation lengths, and moments of inertia have been identified within a dedicated thesis [Pfr13] supporting this work. The task has been divided into several parameter identification problems solved consecutively. Part of this division was to first consider tractor parameter identification only. Subsequently, implement parameter identification was performed with known tractor parameters. The finally chosen identification method used iterative optimization methods based on the comparison of measurements and nonlinear system simulations. Special attention was given to choosing multiple initial conditions to avoid finding a local minimum only. All measurements have been performed on asphalt. Similar measurements on a test field of dry loam have been attempted yet suffered from large noise in Inertial Measurement Unit (IMU) data due to increased vehicle vibration.

Combined cornering stiffness parameters in particular have been identified using quasi steady-state cornering maneuvers with steering angles of $\pm 10°$ and $\pm 20°$. Tractor speed was slowly varied between 0.2 m/s and 8 m/s in the first case and between 0.2 m/s and 4.2 m/s in the second. Each maneuver has been repeated three times. Identification relied on measured lateral accelerations and yaw rates, as well as calculated lateral velocities. The latter calculation was based on the differences between direction of travel and vehicle heading both obtained from accurate position measurements of two GPS receivers with RTK correction signals.

Moments of inertia and relaxation lengths have been found by performing sine sweep maneuvers using either tractor or implement wheel steering inputs. A sine sweep with 10° amplitude was used. The frequency was increased from 0.2 to 1 Hz in 30 s and tractor speed was 2.8 m/s. Each maneuver was repeated four times. Only lateral acceleration and yaw rate measurements were evaluated in this maneuver. The GPS receiver sample rate was not sufficient to allow for reasonable vehicle lateral velocity calculations. Following a common approach in vehicle handling studies [Pfr13] first considered simple tire models with cornering stiffnesses being the only parameters. In this case identification of the tractor's moment of inertia resulted in a widespread range of results for different maneuvers. With none of the identified parameters was it possible to resemble measured results above a steering input frequency of approximately 0.57 Hz. As a consequence, the tire models have been extended to explicitly account for transient behavior. Figures 3.2 and 3.3 depict measurements and simulation results with both model variants.

Parameters identified by [Pfr13] are listed in Table 3.1. Combined cornering stiffness and relaxation length parameters in particular resemble test bench results of [Sch05] provided in Section 2.1.1, keeping in mind that the combined cornering stiffness summarizes the properties of both individual wheels. In addition to results by [Pfr13] Table 3.1 outlines parameters of related research. Comparison of those reveals no major deviations, except from very large cornering stiffnesses stated by [Bev01]. Those however are contrasting test bench results by [Sch05] as well.

Discussion

A brief discussion of the parameterized model shall be given. Keeping in mind the conditions encountered in path tracking control of tractor-implement combinations the capabilities and limitations of the derived models have to be addressed. With the chosen parameters the model will be capable of providing further insight into tractor and implement behavior. Differences between simple kinematic and more detailed dynamic models may be outlined. The derived models in addition will allow to study the influence of parameter uncertainties and external disturbances, for instance resulting from disturbing forces on slopes. The models' applicability to controller design however must be seen as limited. Dynamic model parameters are subject to large uncertainties, e.g. resulting from tire-soil interaction or changing implement loads. Even with the rather small number of parameters of this work's models parameterization causes considerable effort. In contrast to on-road applications tractors will in some cases operate with very low speeds. This in addition will result in poorly conditioned system matrices causing numerical problems during controller design. For model based control it is therefore very desirable to use a simplified kinematic description. The controller in this case must, however, be able to cope with unmodeled uncertainties and disturbances.
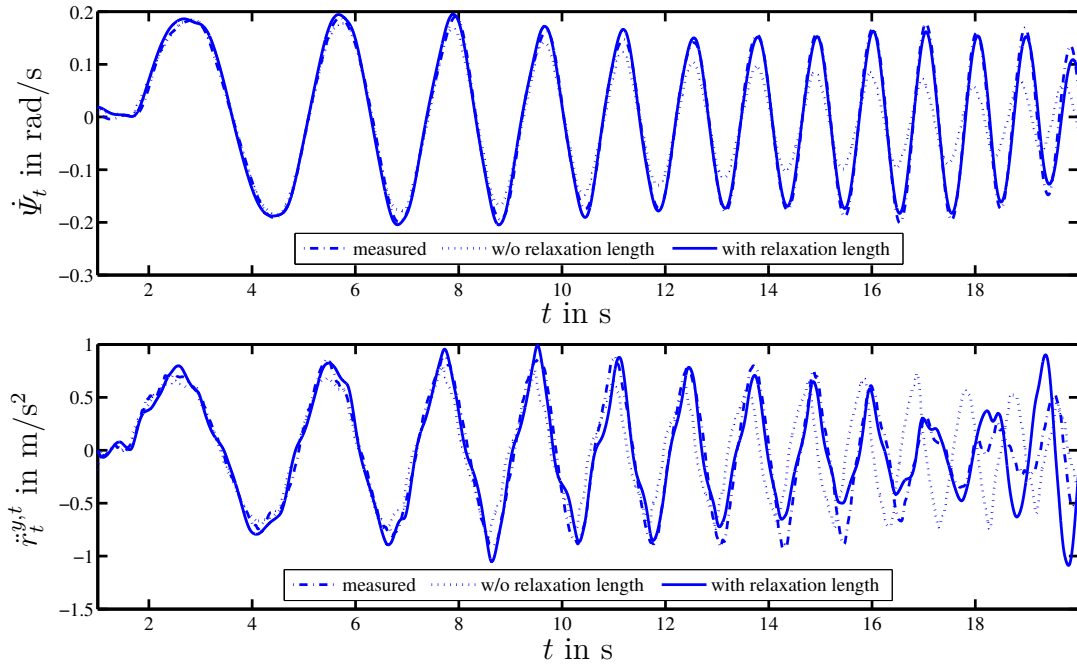
Figure 3.2: Measured and simulated tractor yaw rate $\dot{\Psi}_t$ and lateral acceleration $\ddot{r}_t^{y,t}$ in response to sine sweep tractor steering. The experimental setup used is described in Appendix A.3. Nonlinear dynamic simulation models with steady-state (cornering stiffness) and transient tire models (cornering stiffness plus relaxation length) have been used. Measured steering angles served as simulation input. (from [Pfr13])
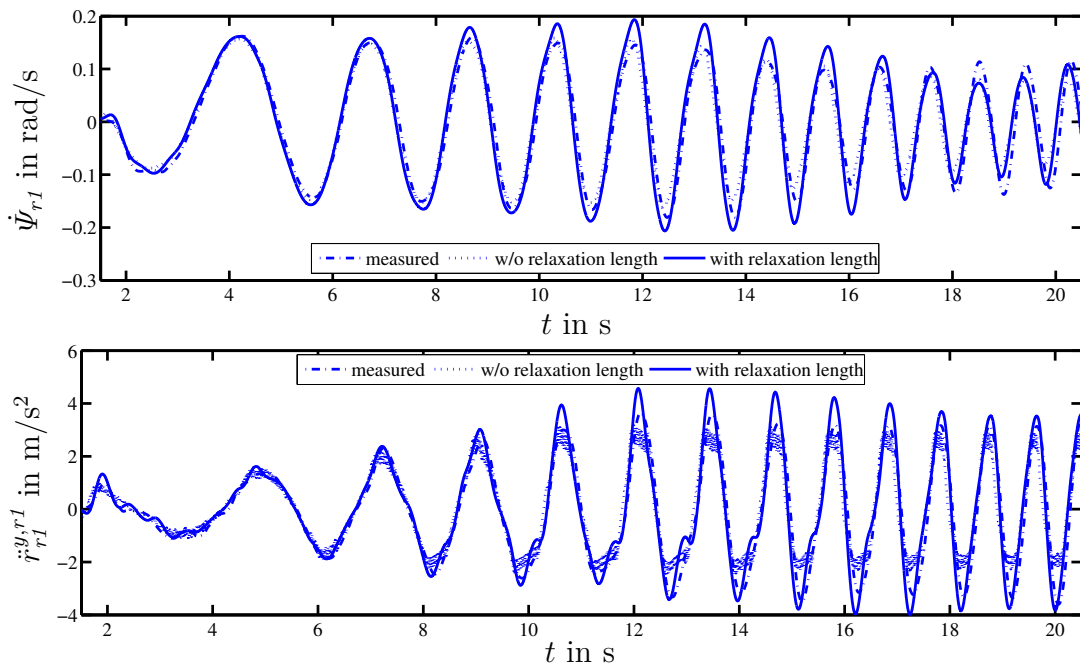
Figure 3.3: Measured and simulated implement yaw rate $\dot{\Psi}_{r1}$ and lateral acceleration $\ddot{r}_{r1}^{y,r1}$ in response to zero tractor steering angle and sine sweep implement wheel steering. The experimental setup used is described in Appendix A.3. Nonlinear dynamic simulation models with steady-state (cornering stiffness) and transient tire models (cornering stiffness plus relaxation length) have been used. Measured steering angles served as simulation input. (from [Pfr13])

Table 3.1: Comparison of parameters from literature: [Pfr13] using this works' experimental setup as described in Appendix A.3, [KS10] using a John Deere 7930 tractor with Parker 500 grain cart, and [Bev01] using a John Deere 8400 tractor.

| Parameter		Unit	[Pfr13]	[KS10]	[Bev01]
Tractor mass	m_t	kg	9088	9391	9500
Implement mass	m_{r1}	kg	2418	2127	
Tractor moment of inertia	I_t	kg m^2	21782	35709	18525
Implement moment of inertia	I_{r1}	kg m^2	5316	6402	
Tractor front wheel cornering stiffness	$C_{\alpha,tf}$	kN/$^\circ$	3.54	3.84	22.9
Tractor rear wheel cornering stiffness	$C_{\alpha,tr}$	kN/$^\circ$	7.23	8.48	49.4
Implement wheel cornering stiffness	$C_{\alpha,r1r}$	kN/$^\circ$	3.47	2.91	
Tractor front wheel relaxation length	$\sigma_{\alpha,tf}$	m	0.40	0.75	0.83
Tractor rear wheel relaxation length	$\sigma_{\alpha,tr}$	m	1.61	1.0	1.35
Implement wheel relaxation length	$\sigma_{\alpha,r1r}$	m	0.61	0.75	

3.2 Kinematic Models

Initial parameterization effort as well as remaining parameter uncertainty of dynamic tractor-implement models are a major hurdle for model based controller design considering a multitude of variants. Kinematic models relying on geometric tractor and implement properties can be obtained with significantly less effort and therefore seem to be a more reasonable choice for model based controller design. For that reason a linearized kinematic tractor-implement model will be derived. A nonlinear kinematic model is derived in order to be used as part of a disturbance estimator. The latter follows a proposal by [CLTM10] originally considering an unsteered kinematic tractor-implement description extended by disturbance models to account for side-slip at all wheels. In terms of steerable implements [BOV12] come closest by providing a model of a tractor towing a drawbar steered implement. This section will consider implements with multiple actuators using drawbar and wheel steering as an example. To allow for variants the models are derived using a procedure suitable for automation.

3.2.1 Modeling Assumptions

The modeling assumptions made for kinematic tractor-implement combinations extend those given in Section 3.1.1 for the dynamic single track model as depicted in Figure 3.1. The model is hence reduced to plane motion and wheel properties of all wheels of an axle are combined. Extended assumptions comprise further restrictions regarding the vehicle velocity vectors at the wheels' location. Kinematic modeling is normally based on the assumption of zero wheel side-slip, which means the vehicle velocity vectors located there point in wheel forward direction (during forward motion). In a generalized variant of kinematic modeling wheel side-slip may be included by considering it a disturbance. With this approach however side-slip is not based on physical principles and no model describing the cause of side-slip is given. Instead, assumptions about the disturbances' course in time are made and depicted by a signal model. In case the signal models are chosen suitably an estimator may be used to attribute measured differences between kinematic model and real plant to these modeled disturbances. Regardless of the chosen model variant the tractor longitudinal velocity $v_{tr}^{x,t}$ is assumed to be a constant or rather slowly changing plant parameter.

3.2.2 Equations of Motion

Similar to the tractor example of Section 2.1.2 kinematic modeling for tractor-implement combinations is based on the assumption of restricted vehicle velocities at the wheels' locations. In contrast to the introductory example this restriction is formulated more generally. Referring to Figure 2.7 the velocity vector is no longer assumed to point in wheel forward direction $\mathbf{e}_{x,tf}$. Hence, the assumption of zero wheel side-slip angle α_{tf} is abandoned. Instead, wheel side-slip is assumed to be an arbitrary given disturbance without asking for its actual cause. The tractor front wheel velocity $\mathbf{v}_{tf}$ of Figure 2.7 and all other wheel velocities may then be formally related to given steering angles and given side-slip angles:

$$\underbrace{\left[-\sin\left(\delta_{tf}-\alpha_{tf}\right),\cos\left(\delta_{tf}-\alpha_{tf}\right)\right]}_{\mathbf{e}_{\perp,tf}^{\mathrm{T}}}\begin{bmatrix}v_{tf}^{x,t}\\v_{tf}^{y,t}\end{bmatrix}=0,\qquad(3.50)$$

$$\underbrace{\left[-\sin\left(-\alpha_{tr}\right),\cos\left(-\alpha_{tr}\right)\right]}_{\mathbf{e}_{\perp,tr}^{\mathrm{T}}}\begin{bmatrix}v_{tr}^{x,t}\\v_{tr}^{y,t}\end{bmatrix}=0,\qquad(3.51)$$

$$\underbrace{\left[-\sin\left(\delta_{r1r}-\alpha_{r1r}-\delta_{r1d}-\delta_{thr}\right),\cos\left(\delta_{r1r}-\alpha_{r1r}-\delta_{r1d}-\delta_{thr}\right)\right]}_{\mathbf{e}_{\perp,r1r}^{\mathrm{T}}}\begin{bmatrix}v_{r1r}^{x,t}\\v_{r1r}^{y,t}\end{bmatrix}=0,\qquad(3.52)$$

with $\mathbf{e}_{\perp,tf}$, $\mathbf{e}_{\perp,tr}$, and $\mathbf{e}_{\perp,r1r}$ denoting vectors perpendicular to the respective wheel velocity vectors $\mathbf{v}_{tf}$, $\mathbf{v}_{tr}$, and $\mathbf{v}_{r1r}$.

Due to $v_{tr}^{x,t}$ being a plant parameter the tractor rear wheel velocity $\mathbf{v}_{tr}$ may be found from (3.51) to:

$$\begin{bmatrix}v_{tr}^{x,t}\\v_{tr}^{y,t}\end{bmatrix}=\begin{bmatrix}v_{tr}^{x,t}\\\tan\left(-\alpha_{tr}\right)v_{tr}^{x,t}\end{bmatrix}.\qquad(3.53)$$

Relating tractor front $\mathbf{v}_{tf}$ and rear wheel velocity $\mathbf{v}_{tr}$ yields:

$$\begin{bmatrix}v_{tf}^{x,t}\\v_{tf}^{y,t}\end{bmatrix}=\begin{bmatrix}v_{tr}^{x,t}\\v_{tr}^{y,t}\end{bmatrix}+\begin{bmatrix}0\\l_t\dot{\Psi}_t\end{bmatrix}=\begin{bmatrix}v_{tr}^{x,t}\\\tan\left(-\alpha_{tr}\right)v_{tr}^{x,t}+l_t\dot{\Psi}_t\end{bmatrix}.\qquad(3.54)$$

Inserting this equation in (3.50) and solving for $\dot{\Psi}_t$ results in:

$$\dot{\Psi}_t=\frac{v_{tr}^{x,t}}{l_t}\left(\tan\left(\delta_{tf}-\alpha_{tf}\right)-\tan\left(-\alpha_{tr}\right)\right).\qquad(3.55)$$

Relating implement wheel $\mathbf{v}_{r1r}$ and tractor rear wheel $\mathbf{v}_{tr}$ velocity produces a longish intermediate result which is omitted. This intermediate result inserted in (3.52) allows to solve for $\dot{\delta}_{thr}$:

$$\dot{\delta}_{thr} = N/D, \tag{3.56}$$

with

$$
\begin{aligned}
N = \Big(& -\cos\left(-\delta_{r1r} + \alpha_{r1r}\right) l_{r1} \dot{\delta}_{r1d} \cos\left(\alpha_{tr}\right) \cos\left(-\delta_{tf} + \alpha_{tf}\right) l_t - \left(\left(\left(l_t \left(\sin\left(\delta_{thr}\right) \cos\left(\delta_{r1d}\right)\right.\right.\right.\right. \\
& + \cos\left(\delta_{thr}\right) \sin\left(\delta_{r1d}\right)\right) \cos\left(\alpha_{tr}\right) - \left(\left(\left(l_{thr} + l_t\right) \cos\left(\delta_{thr}\right) + l_{r1d}\right) \cos\left(\delta_{r1d}\right)\right. \\
& - \sin\left(\delta_{thr}\right) \left(l_{thr} + l_t\right) \sin\left(\delta_{r1d}\right) + l_{r1}\right) \sin\left(\alpha_{tr}\right)\right) \cos\left(-\delta_{r1r} + \alpha_{r1r}\right) \\
& + \sin\left(-\delta_{r1r} + \alpha_{r1r}\right) \left(l_t \left(\cos\left(\delta_{thr}\right) \cos\left(\delta_{r1d}\right) - \sin\left(\delta_{thr}\right) \sin\left(\delta_{r1d}\right)\right) \cos\left(\alpha_{tr}\right)\right. \\
& + \sin\left(\alpha_{tr}\right) \left(\sin\left(\delta_{thr}\right) \left(l_{thr} + l_t\right) \cos\left(\delta_{r1d}\right) + \sin\left(\delta_{r1d}\right) \left(\left(l_{thr} + l_t\right) \cos\left(\delta_{thr}\right) + l_{r1d}\right)\right)\right) \\
& \cdot \cos\left(-\delta_{tf} + \alpha_{tf}\right) + \left(\left(\left(\cos\left(\delta_{thr}\right) l_{thr} + l_{r1d}\right) \cos\left(\delta_{r1d}\right) - \sin\left(\delta_{thr}\right) \sin\left(\delta_{r1d}\right) l_{thr} + l_{r1}\right)\right. \\
& \cdot \cos\left(-\delta_{r1r} + \alpha_{r1r}\right) - \sin\left(-\delta_{r1r} + \alpha_{r1r}\right) \left(\sin\left(\delta_{thr}\right) \cos\left(\delta_{r1d}\right) l_{thr}\right. \\
& + \sin\left(\delta_{r1d}\right) \left(\cos\left(\delta_{thr}\right) l_{thr} + l_{r1d}\right)\right)\right) \cos\left(\alpha_{tr}\right) \sin\left(-\delta_{tf} + \alpha_{tf}\right) v_{tr}^{x,t}\Big),
\end{aligned}
\tag{3.57}
$$

$$
\begin{aligned}
D = \cos\left(\alpha_{tr}\right) l_t \big(& \left(l_{r1} + \cos\left(\delta_{r1d}\right) l_{r1d}\right) \cos\left(-\delta_{r1r} + \alpha_{r1r}\right) \\
& - \sin\left(-\delta_{r1r} + \alpha_{r1r}\right) \sin\left(\delta_{r1d}\right) l_{r1d}\big) \cos\left(-\delta_{tf} + \alpha_{tf}\right).
\end{aligned}
\tag{3.58}
$$

The special case of zero wheel side-slip angles α_{tf}, α_{tr}, and α_{r1r} as considered in Section 2.1.2 results in simplified expressions:

$$\dot{\Psi}_t = \frac{v_{tr}^{x,t}}{l_t} \tan\left(\delta_{tf}\right) \tag{3.59}$$

$$\dot{\delta}_{thr} = N/D, \tag{3.60}$$

with

$$
\begin{aligned}
N = \big(& \left(\sin\left(\delta_{tf} + \delta_{thr} + \delta_{r1d} - \delta_{r1r}\right) - \sin\left(-\delta_{tf} + \delta_{thr} + \delta_{r1d} - \delta_{r1r}\right)\right) l_{thr} \\
& + \left(\sin\left(\delta_{tf} - \delta_{thr} - \delta_{r1d} + \delta_{r1r}\right) - \sin\left(\delta_{tf} + \delta_{thr} + \delta_{r1d} - \delta_{r1r}\right)\right) l_t \\
& + \left(\sin\left(\delta_{tf} + \delta_{r1d} - \delta_{r1r}\right) - \sin\left(-\delta_{tf} + \delta_{r1d} - \delta_{r1r}\right)\right) l_{r1d} \\
& + \left(\sin\left(\delta_{tf} + \delta_{r1r}\right) - \sin\left(-\delta_{tf} + \delta_{r1r}\right)\right) l_{r1}\big) v_t^{xt} \\
& - \left(\cos\left(-\delta_{tf} + \delta_{r1r}\right) + \cos\left(\delta_{tf} + \delta_{r1r}\right)\right) l_{r1} l_t \dot{\delta}_{r1d},
\end{aligned}
\tag{3.61}
$$

$$
\begin{aligned}
D = \big(& \left(\cos\left(-\delta_{tf} + \delta_{r1d} - \delta_{r1r}\right) + \cos\left(\delta_{tf} + \delta_{r1d} - \delta_{r1r}\right)\right) l_{r1d} \\
& + \left(\cos\left(-\delta_{tf} + \delta_{r1r}\right) + \cos\left(\delta_{tf} + \delta_{r1r}\right)\right) l_{r1}\big) l_t.
\end{aligned}
\tag{3.62}
$$

As a result, kinematic equations of motion are given as first order ODEs for yaw angle Ψ_t and hitch angle δ_{thr}, i.e. (3.55), (3.56), (3.57), and (3.58) or simplified without wheel side-slip (3.59), (3.60), (3.61), and (3.62). It should be noted that the drawbar steering angle δ_{r1d} and its time derivative $\dot{\delta}_{r1d}$ are part of the above mentioned equations. Both are assumed to result from time dependent constraints.

Note: Besides the chosen approach of modeling additive disturbances affecting the wheel velocity vector directions other possibilities have been considered. Modeling the disturbances at this location comes closest to the actual effect of wheel side-slip. Modeling yaw angle biases or steering angles biases as considered by [Bel99] attributes disturbances to other model parts increasing the risk of estimation errors. Using multiplicative disturbances instead of additive ones, as considered by [BOV12] was seen as disadvantageous due to a loss of observability properties for zero steering angles and numerical challenges close to zero steering angles. Straight path tracking on slopes, in particular, is affected by this.

3.2.3 Steering Actuator Dynamics

Similar to Section 3.1.4, altering steering angles is assumed to be subject to delays. Again underlying steering angle controllers are assumed to enforce the desired steering angles. The respective closed inner control loops are approximately modeled by delays. With a kinematic description only the first drawbar steering angle time derivative $\dot{\delta}_{r1d}$ is required. For that reason one could attempt to simplify inner loop approximations by using first order delays. This work however retains approximations using second order delays as stated in (3.27), (3.28), and (3.29), which is to allow for comparison with dynamic models described previously.

3.2.4 Tracking Errors and Earth-Fixed Positions

For later use, kinematic models are required to be given in earth-fixed coordinates as well as in terms of deviations from a desired straight path as depicted in Figure 3.1.

The tractor rear wheel position in earth-fixed coordinates may be found by integrating:

$$\dot{r}_{tr}^{x,e} = \cos(\Psi_t)v_{tr}^{x,t} + \sin(\Psi_t)\tan(\alpha_{tr})v_{tr}^{x,t}, \tag{3.63}$$

$$\dot{r}_{tr}^{y,e} = \sin(\Psi_t)v_{tr}^{x,t} - \cos(\Psi_t)\tan(\alpha_{tr})v_{tr}^{x,t}. \tag{3.64}$$

Implement position and orientation are related to tractor position and orientation as previously described in (3.32), (3.33), and (3.34).

Alternatively it is again possible to introduce a description in terms of deviations from a straight desired path:

$$\dot{e}_{th} = \frac{v_{tr}^{x,t}}{l_t} \left(\tan(\delta_{tf} - \alpha_{tf}) - \tan(-\alpha_{tr}) \right) - \dot{\Psi}_d, \tag{3.65}$$

$$\dot{e}_{tl} = \sin(e_{th}) v_{tr}^{x,t} + \cos(e_{th}) \tan(-\alpha_{tr}) v_{tr}^{x,t}. \tag{3.66}$$

Assuming zero wheel side-slip this simplifies to:

$$\dot{e}_{th} = \frac{v_{tr}^{x,t}}{l_t} \tan(\delta_{tf}) - \dot{\Psi}_d, \tag{3.67}$$

$$\dot{e}_{tl} = \sin(e_{th}) v_{tr}^{x,t}. \tag{3.68}$$

Implement heading and lateral error are again given by (3.37) and (3.38).

3.2.5 Side-Slip Angle Disturbance Model

Wheel side-slip angles α_{tr}, α_{tf}, and α_{r1r} are assumed to be disturbances affecting the plant described by a kinematic model. In order to allow for disturbance estimation as introduced in Section 2.2.11 a model describing the disturbance is required. This can be accomplished by assuming particular types of signal models with constant, ramp, or sinusoidal signals being common choices [Foe94].

Wheel side-slip angles in this work are modeled assuming constant signals with ODEs:

$$\dot{\alpha}_{tf} = 0, \qquad\qquad \dot{\alpha}_{tr} = 0, \qquad\qquad \dot{\alpha}_{r1r} = 0. \tag{3.69}$$

This choice however does not require side-slip angles to be constant. It rather expresses the way an estimator propagates side-slip angle estimates over time in case there is no difference between estimated and measured outputs. In case of differences the estimator must ensure to obtain updated side-slip angle estimates reasonably fast, as compared to actual plant dynamics.

3.2.6 Kinematic Model Overview

For later use the model variants developed in Sections 3.2.1 to 3.2.5 are compiled in an overview.

Nonlinear Model

The required nonlinear kinematic model uses an earth-fixed coordinate representation and accounts for wheel side-slip. It is given by combining (3.55), (3.56), (3.57), (3.58), (3.27), (3.28), (3.29), (3.63), (3.64), (3.32), (3.33), (3.34), and (3.69) resulting in:

$$\dot{\mathbf{x}} = \mathbf{f}(\mathbf{x}, \mathbf{u}), \tag{3.70}$$

$$\mathbf{y} = \mathbf{h}(\mathbf{x}), \tag{3.71}$$

with

$$\mathbf{x} = \left[r_{tr}^{x,e}, r_{tr}^{y,e}, \Psi_t, \delta_{thr}, \delta_{tf}, \dot{\delta}_{tf}, \delta_{r1d}, \dot{\delta}_{r1d}, \delta_{r1r}, \dot{\delta}_{r1r}, \alpha_{tf}, \alpha_{tr}, \alpha_{r1r} \right]^{\mathrm{T}}, \tag{3.72}$$

$$\mathbf{u} = \left[\delta_{tf,d}, \delta_{r1d,d}, \delta_{r1r,d} \right]^{\mathrm{T}}, \tag{3.73}$$

$$\mathbf{y} = \left[r_{tr}^{x,e}, r_{tr}^{y,e}, \Psi_t, r_{r1r}^{x,e}, r_{r1r}^{y,e}, \Psi_{r1}, \delta_{tf}, \delta_{r1d}, \delta_{r1r} \right]^{\mathrm{T}}, \tag{3.74}$$

In deviation from previously derived models, steering angles are included within the measured output vector. Those will provide additional information for the estimator being developed.

Linear Model

The linearized model is given in terms of deviations from a desired path and does not account for wheel side-slip. It is found by combining (3.59), (3.60), (3.61), (3.62), (3.27), (3.28), (3.29), (3.67), (3.68), (3.37) and (3.38).

Defining:

$$\mathbf{x} = \left[e_{tl}, e_{th}, \delta_{thr}, \delta_{tf}, \dot{\delta}_{tf}, \delta_{r1d}, \dot{\delta}_{r1d}, \delta_{r1r}, \dot{\delta}_{r1r} \right]^{\mathrm{T}}, \tag{3.75}$$

$$\mathbf{u} = \left[\delta_{tf,d}, \delta_{r1d,d}, \delta_{r1r,d} \right]^{\mathrm{T}}, \tag{3.76}$$

$$\mathbf{y} = \left[e_{tl}, e_{th}, e_{r1l}, e_{r1h} \right]^{\mathrm{T}}, \tag{3.77}$$

and linearizing the combined equations about $\mathbf{x} = \mathbf{0}$ and $\mathbf{u} = \mathbf{0}$ yields:

$$\dot{\mathbf{x}} = \mathbf{A}\mathbf{x} + \mathbf{B}\mathbf{u}, \tag{3.78}$$

$$\mathbf{y} = \mathbf{C}\mathbf{x}, \tag{3.79}$$

with matrices $\mathbf{A}$, $\mathbf{B}$, and $\mathbf{C}$ as stated in Appendix A.2.2.

3.2.7 Model Parameters

Kinematic model parameters are simply a subset of the dynamic model parameters obtained before. An overview of parameters describing this works experimental setup (Appendix A.3) is given in Appendix A.5.

3.3 Model Analysis and Comparison

Within the preceding sections several models with different levels of fidelity have been derived. This section provides a comparison and further analysis of those models using this work's parameters as stated in Appendix A.5. Linear system descriptions as given in Sections 3.1.6 and 3.2.6 will be considered more closely.

Figure 3.4 depicts the eigenvalues of system matrices $\mathbf{A}$ for a kinematic model and two dynamic models. The latter either consider or neglect transient tire behavior and therefore are modeled with or without tire relaxation length. Tractor longitudinal velocity $v_t^{x,t}$ is varied as a system parameter. All variants exhibit six conjugate complex eigenvalues not changing with tractor velocity. Those result from steering actuator dynamics modeled as second order delays (3.27), (3.28), and (3.29). Similarly, all variants exhibit two eigenvalues located at the origin resulting from tracking error dynamics (3.35), (3.36), (3.67), and (3.68), which is not fed back to other system parts. The kinematic model exhibits one additional real eigenvalue resulting from the hitch angle ODE (3.60). It is not surprising that the hitch angle rate of change $\dot{\delta}_{thr}$ exhibits a tractor velocity dependent behavior. The respective real eigenvalue moves to the left as the tractor velocity increases. Considering the simple dynamic model without relaxation length reveals four eigenvalues resulting from rigid body dynamics. Figure 3.4 only depicts them completely for a speed of 7.5 m/s. For lower speeds the missing eigenvalues are real and located further to the left. For tractor velocities above 9 m/s the four eigenvalues finally form conjugate complex pairs. Eigenvalues close to the origin typically dominate a system's behavior [Foe94]. In case of the simple dynamic model the three eigenvalues closest to the origin (remembering two of them are at $s = 0$) closely match those of the kinematic model up to speeds of 4.5 m/s. The dynamic model with relaxation length exhibits seven eigenvalues resulting from coupled rigid body dynamics and transient tire models. Again, the three eigenvalues closest to the origin match the kinematic model's up to 4.5 m/s. In addition, however, this most complex model considered exhibits weakly damped conjugate complex pairs of eigenvalues.

Figure 3.5 depicts the Bode diagrams of transfer functions from desired steering angles to implement lateral error with a tractor longitudinal velocity of 3 m/s. In case of a kinematic model the transfer functions are rather short and given as:

$$G_{\delta_{tf,d},e_{rll}} = \frac{3.2143(1 - 0.6033s_N)}{s_N^2(1 + 1.4s_N)(1 + 1.6(0.19s_N) + (0.19s_N)^2)} \frac{\text{m}}{\text{rad}}, \tag{3.80}$$

$$G_{\delta_{r1d,d},e_{rll}} = \frac{-1.76}{(1 + 1.4s_N)(1 + 1.1(0.12s_N) + (0.12s_N)^2)} \frac{\text{m}}{\text{rad}}, \tag{3.81}$$

$$G_{\delta_{r1r,d},e_{rll}} = \frac{4.2}{(1 + 1.4s_N)(1 + 0.98(0.1s_N) + (0.1s_N)^2)} \frac{\text{m}}{\text{rad}}, \tag{3.82}$$

with $s_N = s/(1/\text{s})$, i.e s is normalized to be unitless for convenience. All three exhibit a

second order lag resulting from the particular steering actuator dynamics and a first order lag from hitch angle dynamics. The first order lag time constant of $T = 1.4$ s corresponds to a corner frequency of $f = 0.11$ Hz indicating the lowest frequency with a drop in phase and magnitude as shown in Figure 3.5. Comparing kinematic and dynamic models reveals first larger deviations at approx 0.7 Hz. The detailed dynamic model exhibits some resonant behavior which will be further addressed considering the tractor and implement yaw rates. The notch in magnitude and jump in phase found for the dynamic model without relaxation length is due to a conjugate complex pair of zeros on the imaginary axis. Considering $G_{\delta_{tf,d},e_{r1l}}$ in particular, the kinematic transfer function (3.80) allows for an interesting interpretation. This transfer function describes a SISO plant with a desired tractor steering angle input and implement lateral error output. The transfer function exhibits double integrator behavior and is non-minimum phase [Foe94] due to a positive zero. As a consequence implement lateral error control with tractor steering as only input is a challenge for classical PID control and one must expect rather poor performance.

A closer look at the model differences is possible by considering the tractor and implement yaw rates, noting that those can be obtained from other system states by using (3.32) and (3.35) with $\dot{\Psi}_d \equiv 0$. Figures 3.6 and 3.7 depict the respective Bode plots and responses to a 1 rad unit step. The most notable characteristics from Figure 3.6 are the resonant peaks found for a dynamic model with transient tire models. The resonant peaks are close to the natural frequencies $f = 0.92$ Hz and $f = 1.85$ Hz of the weakly damped conjugate complex eigenvalues $s = -0.53 \pm j5.73$ and $s = -2.12 \pm j11.42$ of Figure 3.4. Considering the implement steering to tractor yaw rate Bode plots in particular, this resonant behavior is the only visible influence of implement steering on the tractor. The kinematic model does neglect any influence of implement steering on the tractor as already seen from (3.59). The unit step responses as shown in Figure 3.7 visualize the weakly damped complex eigenvalues' influence in case of a dynamic model accounting for relaxation length. The consequences are small oscillations overlaying the main response. In case of implement steering to tractor yaw rate transfer functions, those oscillations are the only influence. Considering the implement yaw rate response to a tractor front wheel steering step in particular allows to observe a response initially moving away from the final steady-state value. This is again typical for a non-minimum phase transfer function [Foe94].
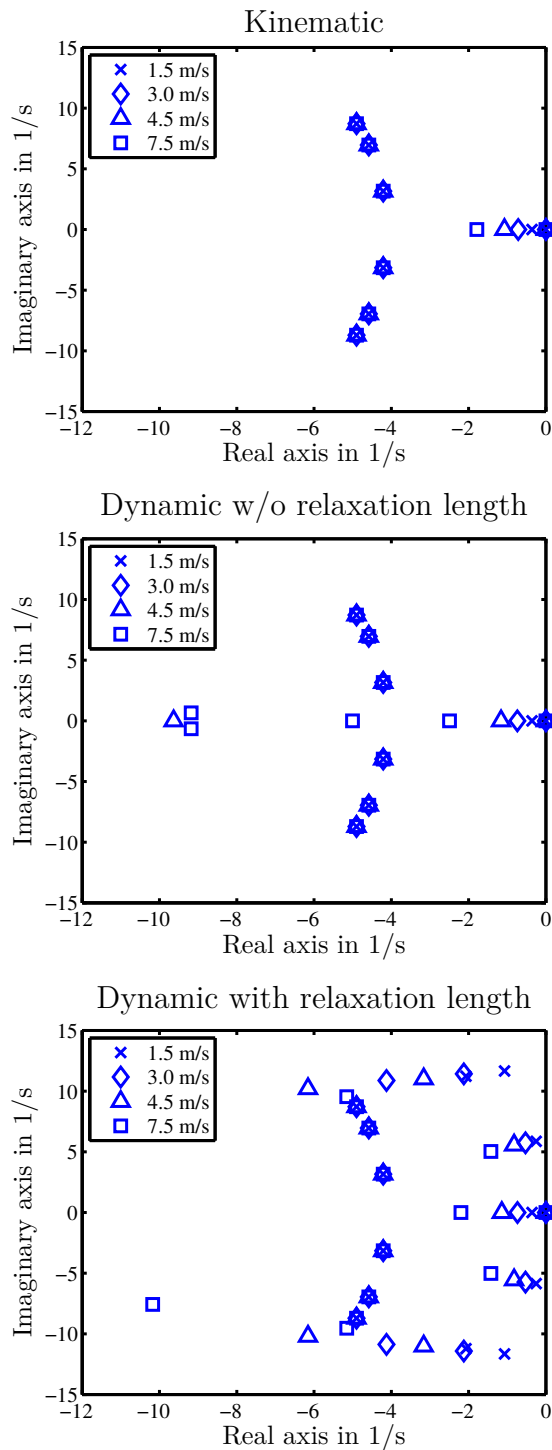
Figure 3.4: Eigenvalues of linear system matrices **A** for various tractor longitudinal velocities $v_t^{x,t}$ with kinematic model as in Section 3.2.6, dynamic models as in Section 3.1.6, parameters as in Appendix A.5.
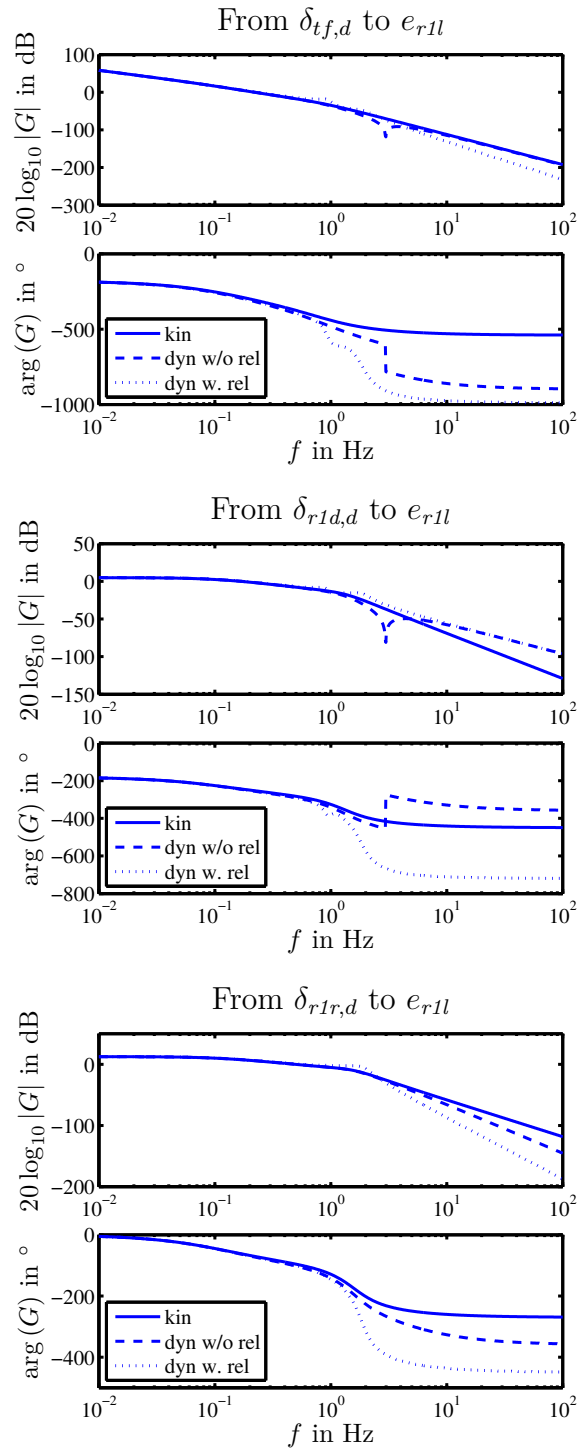
Figure 3.5: Bode diagrams for desired steering angle to implement lateral error transfer functions G using a linear kinematic model as in Section 3.2.6, linear dynamic models as in Section 3.1.6, parameters as in Appendix A.5, and $v_t^{x,t} = 3$ m/s.

Figure 3.6: Bode diagrams for all desired steering angle to yaw rate transfer functions G using a linear kinematic model as in Section 3.2.6, linear dynamic models as in Section 3.1.6, parameters as in Appendix A.5, and $v_t^{x,t} = 3$ m/s.

Figure 3.7: Unit step responses from desired steering angles to tractor and implement yaw rates using a linear kinematic model as in Section 3.2.6, linear dynamic models as in Section 3.1.6, parameters as in Appendix A.5, and $v_t^{x,t} = 3$ m/s.
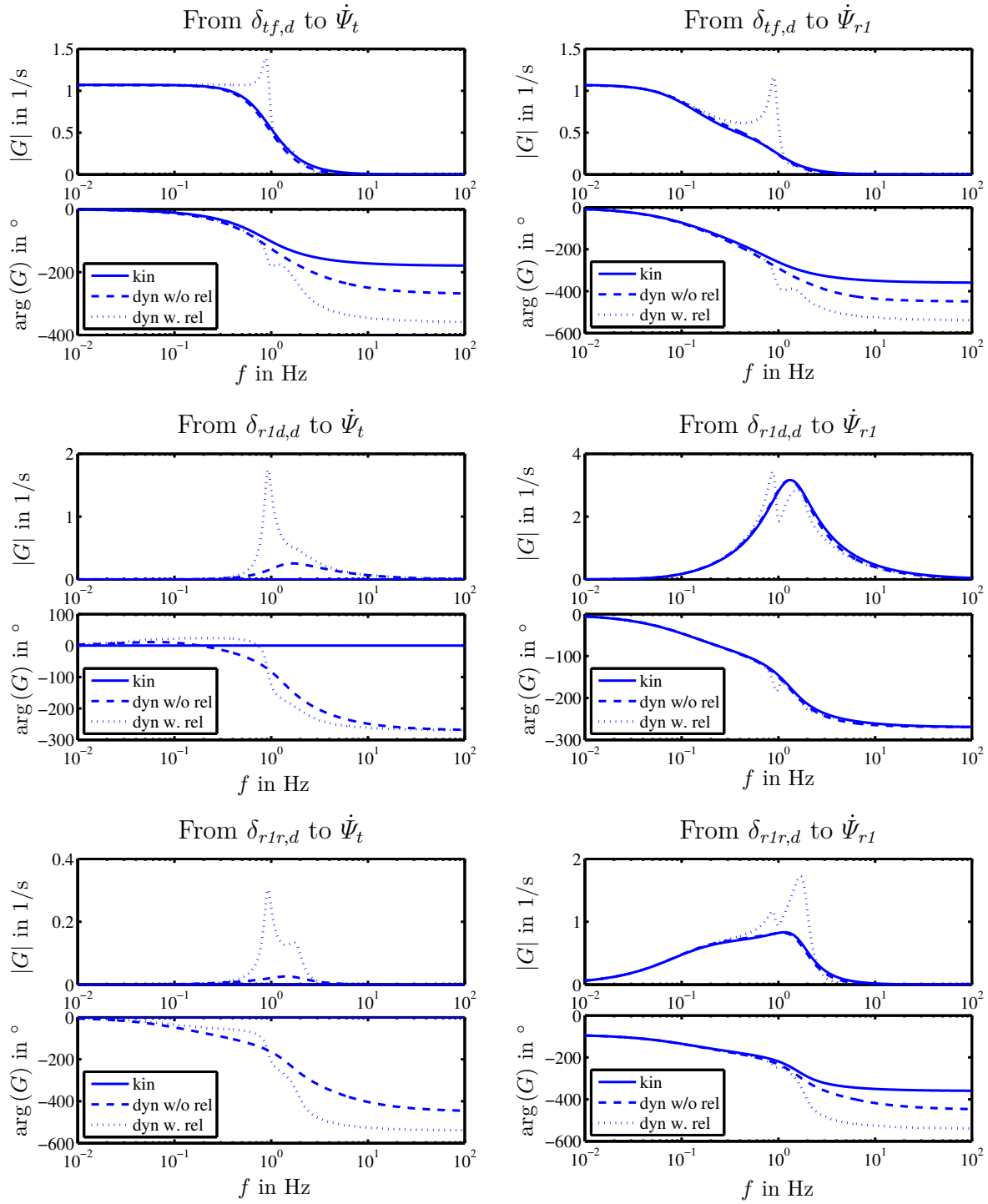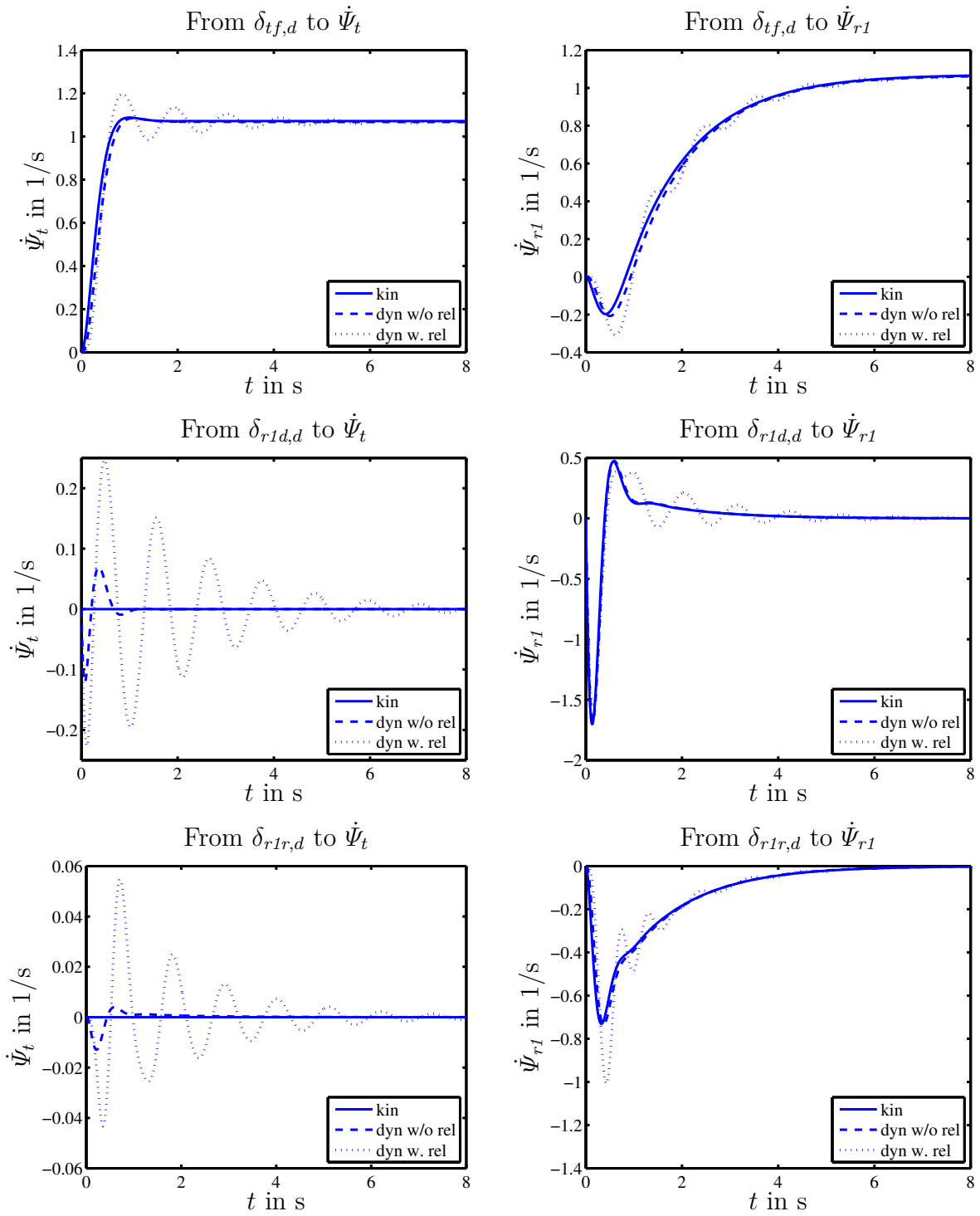
4 Path Tracking Control

Section 2.2 provided a broad overview of existing path tracking control approaches and a discussion outlining advantages and disadvantages regarding the objectives of Section 1.2. Within this section, the most promising approach is used as a starting point for controller design considering a tractor towing a wheel and drawbar steered implement. Variants of that combination are considered by using subsets of the available steering actuators. The kinematic models as derived in Section 3.2 serve as a basis for controller design. Special emphasis during controller design is placed on handling disturbances and uncertainties resulting from wheel side-slip. Two alternative approaches are conceived for that purpose. The developed feedback controllers will be complemented by feedforward control accounting for curved paths. Finally, a system overview is provided to summarize this section.

4.1 LQR Control

By considering Table 2.5 in Section 2.2.13 and omitting only poor matches one could regard PID control, MPC, SMC, LQR, robust H_∞ control, and FLC as possible choices to start with. This work uses LQR as a starting point. The problem of overcoming the remaining drawbacks of lacking robustness and the need for state estimation is addressed in the subsequent sections. Among alternative choices SISO PID control depicts the current state of commercial systems. MPC results in an increased computational load which is difficult to justify unless actually necessary, e.g. in case actuator limits are reached frequently. Frequency domain tuning for each particular tractor-implement combination using weighting transfer functions was seen as a hurdle for robust H_∞ control. Path tracking based on SMC using a switching control law was already degraded to feedback linearization plus PD in previous research [TT03]. Applying a switching control law to hydraulic actuators with limited dynamics was not seen as the most promising approach. FLC for SISO passenger car path tracking by [HT94] resulted in numerous rules (125). An extension to MIMO tractor-implement combinations therefore appeared to be very difficult to tune. The FLC considered by [HT94] was actually tuned using LQR to aid the initial choice of parameters. In general however it should be noted that the choice of LQR as the most promising approach to begin with does not necessarily exclude the possibility of tailoring other approaches to this work's objectives in future research.

An introduction on LQR was provided in Section 2.2.3. The first step of this work's controller design closely follows the outlined approach using the linear kinematic model

given by (3.78), (3.79), (3.75), (3.76), and (3.77). For the given task tractor as well as implement lateral and heading errors are measured outputs. As a consequence, choosing a performance index based on output weights rather than weights for system states allows for a very intuitive interpretation. The performance index therefore is chosen to be

$$J = \int_0^\infty \left(\mathbf{y}^{\mathrm{T}}(t)\mathbf{Q}\mathbf{y}(t) + \mathbf{u}^{\mathrm{T}}(t)\mathbf{R}\mathbf{u}(t) \right) dt \tag{4.1}$$

which can be rewritten as

$$J = \int_0^\infty \left(\mathbf{x}^{\mathrm{T}}(t)\mathbf{C}^{\mathrm{T}}\mathbf{Q}\mathbf{C}\mathbf{x}(t) + \mathbf{u}^{\mathrm{T}}(t)\mathbf{R}\mathbf{u}(t) \right) dt \tag{4.2}$$

resembling (2.69). $\mathbf{C}^{\mathrm{T}}\mathbf{Q}\mathbf{C}$ and $\mathbf{R}$ are required to be positive semi-definite and positive definite weighting matrices, with $\mathbf{Q}$ and $\mathbf{R}$ chosen to be diagonal:

$$\mathbf{Q} = \mathrm{diag}(q_{e,tl}, q_{e,th}, q_{e,r1l}, q_{e,r1h}), \tag{4.3}$$
$$\mathbf{R} = \mathrm{diag}(r_{\delta,tf}, r_{\delta,r1d}, r_{\delta,r1r}). \tag{4.4}$$

For a controllable system [Nai02] the optimal control law for the inifinite horizon LQR problem (4.1) is:

$$\mathbf{u}^*(t) = -\underbrace{\mathbf{R}^{-1}\mathbf{B}^{\mathrm{T}}\mathbf{P}}_{\mathbf{K}}\mathbf{x}(t) \tag{4.5}$$

with $\mathbf{P}$ being found by numerically solving the ARE:

$$\mathbf{A}^{\mathrm{T}}\mathbf{P} + \mathbf{P}\mathbf{A} - \mathbf{P}\mathbf{B}\mathbf{R}^{-1}\mathbf{B}^{\mathrm{T}}\mathbf{P} + \mathbf{C}^{\mathrm{T}}\mathbf{Q}\mathbf{C} = \mathbf{0}. \tag{4.6}$$

Considering the actual plant with parameters given in Appendix A.5, weighting matrices (4.3) and (4.4) have been parameterized as given in Appendix A.6.2. The elements of $\mathbf{Q}$ and $\mathbf{R}$ are normalized to typical error and steering input ranges. Different weights for elements in $\mathbf{Q}$ express the emphasis put on reducing a particular error. For the chosen weights of Appendix A.6.2 emphasis is on the tractor lateral error as well as the implement lateral and heading error. The tractor heading error was considered irrelevant and hence weighted significantly less. Choosing zero weight entries on the diagonal of $\mathbf{Q}$ was avoided in general. This would result in weighting a subset of outputs only and involves ignoring some rows in $\mathbf{C}$. As outlined by [Nai02] this might cause the system to lose its detectability property, which in turn is a necessary condition for stability of the closed-loop system. The relative size of weights in $\mathbf{R}$ and $\mathbf{Q}$ influences the overall controller gain. Hence, normalized entries of $\mathbf{R}$ have been chosen to represent an overall tuning parameter found in simulations and experiments.

4.2 Output Feedback Approximation

Numerous control concepts including LQR require either the measurement or the estimation of all system state variables. The assumption of complete state feedback allows for a systematic and mathematically exact treatment of control problems. For controllable linear time-invariant systems in particular this includes the possibility of placing closed-loop eigenvalues arbitrarily [Won67]. Considering practical applications however, state feedback in general may face some challenges, including increased effort for estimator design and implementation as well as sensitivity in terms of estimator model errors [Foe94].

Motivation

In this work state feedback is avoided for two reasons:

- All possible controlled variables (e_{tl}, e_{th}, e_{r1l}, e_{r1h}) are available from measurements and additional estimation effort is unnecessary from this point of view.

- Additional tractor-implement combination specific parameterization and implementation effort for an estimator or observer is undesirable. In case of curved path tracking in particular this effort comprises of a nonlinear estimator and a nonlinear reference variable generator to obtain estimated and desired system states without introducing model errors due to linearization.

Approaches

In order to obtain a simpler controller the assumption of full state feedback based on an estimation or measurement is abandoned. Instead, a simpler feedback based on measured outputs is considered. In terms of output feedback one may distinguish between static and dynamic output feedback [Foe94]. Static output feedback only comprises a proportional controller K_y with

$$\mathbf{u} = -\mathbf{K}_y \mathbf{y}. \tag{4.7}$$

Dynamic output feedback in contrast denotes controllers that contribute additional system states ranging from simple differentiators or integrators to a full state estimator. In terms of controller design dynamic output feedback can be reduced to static output feedback using an extended plant [Foe94].

Compared to state feedback the design of static output feedback controllers is more challenging due to the reduced number of free parameters. In contrast to state feedback no exhaustive theoretical framework exists. Instead various numerical approaches exist [Foe94], [Lun10], [SAG97] to address the problem. One may distinguish between approaches trying to approximate a previously calculated state feedback and direct methods of obtaining K_y. Most approaches presented require either numerical optimization or an iterative solution

of numerical equations. Two exceptions however allow for output feedback approximation using closed-form equations. The first method presented by [Foe94] aims to approximate state feedback by minimizing the difference between input vectors $\mathbf{u}(t)$ of both closed-loop systems as those follow a reference input step. Obtaining the output feedback approximation K_y requires solving a Lyapunov equation and performing some matrix operations. The second closed-form solution presented by [Lun10] and originally proposed by [BL74] relies on approximating a subset of eigenvalues of a closed-loop system with state feedback. K_y is found in a very concise way requiring some matrix operations and the calculation of a pseudo-inverse. From the very beginning the approach was intended to be an alternative to observers or Kalman filters developed previously. This approach is used to obtain an approximation for (4.5).

Static Output Feedback with Mode Preservation
A brief sketch of the underlying idea by [BL74] is provided in this paragraph. The eigenvalues $\bar{\lambda}_i$ $(i = 1, \ldots, n)$ and the corresponding eigenvectors $\mathbf{v}_i$ of a state feedback closed-loop system matrix $\mathbf{A} - \mathbf{BK}$ are related (by definition) as follows:

$$(\mathbf{A} - \mathbf{BK})\,\mathbf{v}_i = \bar{\lambda}_i\mathbf{v}_i. \tag{4.8}$$

With pole placement or slight changes in the performance index those eigenvalues $\bar{\lambda}_i$ can be chosen to be distinct. Hence eigenvectors $\mathbf{v}_i$ are linearly independent and form a basis:

$$\mathbf{V} = [\mathbf{v}_1, \ldots, \mathbf{v}_n]. \tag{4.9}$$

$\bar{\lambda}_i$ is also an eigenvalue of the output feedback closed-loop system matrix $\mathbf{A} - \mathbf{BK}_y\mathbf{C}$, if

$$\mathbf{K}_y\mathbf{C}\mathbf{v}_i = \mathbf{K}\mathbf{v}_i, \tag{4.10}$$

which can be seen from:

$$\mathbf{A}\mathbf{v}_i - \mathbf{BK}_y\mathbf{C}\mathbf{v}_i = \mathbf{A}\mathbf{v}_i - \mathbf{BK}\mathbf{v}_i = \bar{\lambda}_i\mathbf{v}_i. \tag{4.11}$$

Collecting all conditions (4.10) yields

$$\mathbf{K}_y\mathbf{C}\mathbf{V} = \mathbf{K}\mathbf{V}, \tag{4.12}$$

which is a matrix equation for the unknown $\mathbf{K_y}$. In case solutions exist, one is given by:

$$\mathbf{K}_y = \mathbf{K}\mathbf{V}\,(\mathbf{C}\mathbf{V})^{\ddagger}, \tag{4.13}$$

with $(\bullet)^{\ddagger}$ denoting the Moore-Penrose Pseudo-Inverse [BIT03].

If no solution exists (4.13) at least minimizes the Frobenius matrix norm $\|\mathbf{K}_y\mathbf{CV} - \mathbf{KV}\|_F$ [BIT03] with

$$\|\mathbf{M}\|_F = \sqrt{\sum_{k=1}^{m}\sum_{l=1}^{n}|m_{k,l}|^2} \qquad \text{and} \qquad \mathbf{M} \in \mathbb{C}^{m\times n}. \qquad (4.14)$$

Mode Weighting

The difference $\mathbf{K}_y\mathbf{Cv}_i - \mathbf{Kv}_i$ can be seen as a measure of the approximation of $\bar{\lambda}_i$. Emphasis on approximating particular eigenvalues can be expressed by introducing weights w_i

$$\mathbf{K}_y\mathbf{Cv}_iw_i = \mathbf{Kv}_iw_i \qquad (4.15)$$

resulting in

$$\mathbf{K}_y\mathbf{CVW} = \mathbf{KVW} \qquad \text{with} \qquad \mathbf{W} = \operatorname{diag}\left(w_1, \ldots, w_n\right). \qquad (4.16)$$

The output feedback controller considering weighted eigenvalues is found similar to (4.13) yielding the final result:

$$\mathbf{K}_y = \mathbf{KVW}\left(\mathbf{CVW}\right)^{\ddagger}. \qquad (4.17)$$

Degree of Match

So far an approximation of state feedback closed-loop eigenvalues has been provided. The success of this approximation and the degree of match however has not been considered. State feedback of a controllable plant allows for an arbitrary choice of eigenvalues [Won67]. In case of output feedback no similar statement exists and placing eigenvalues is more involved. It is worth noting two theorems regarding an approximation's possible degree of match.

State feedback $\mathbf{K}$ and output feedback $\mathbf{K}_y$ are equivalent if and only if [Lun10]:

$$\operatorname{rank}\begin{pmatrix} \mathbf{C} \\ \mathbf{K} \end{pmatrix} = \operatorname{rank}\left(\mathbf{C}\right) \qquad (4.18)$$

In this rare occasion row vectors of $\mathbf{K}$ are linear combinations of row vectors of $\mathbf{C}$. The output feedback $\mathbf{K}_y$ then is

$$\mathbf{K}_y = \mathbf{K}\left(\mathbf{C}\right)^{\ddagger}. \qquad (4.19)$$

For less restrictive cases [Dav70] provides sufficient conditions ensuring that static output feedback (4.7) is capable of bringing a limited number of rank ($\mathbf{C}$) eigenvalues arbitrarily close to preassigned values. Complex preassigned eigenvalues must appear in conjugate complex pairs. The sufficient conditions are:

- The uncontrolled system with system matrix $\mathbf{A}$ and input matrix $\mathbf{B}$ is controllable.

- Eigenvalues of $\mathbf{A}$ must be distinct or repeated in such a way that the eigenvalues of each Jordan block of the respective Jordan canonical form are distinct.

Application to Tractor-Implement Combinations

Considering this work's linear kinematic model given by equations (3.78), (3.79), (3.75), (3.76), (3.77) and parameters as stated in Appendix A.5 a LQR controller is designed using an exemplary forward velocity $v_{tr}^{x,t}$ of 3 m/s and weights as given in Appendix A.6.2. The resulting state feedback (4.5) is approximated using equation (4.17). The parameterized open-loop system is controllable and the Jordan canonical form exhibits Jordan blocks with distinct eigenvalues hence fulfilling the sufficient conditions of [Dav70] stated above. Therefore, rank ($\mathbf{C}$) = 4 eigenvalues can be brought arbitrarily close to preassigned values, remembering that complex eigenvalues must form conjugate complex pairs. Considering the open-loop system eigenvalues as shown in Figure 3.4 weights are chosen to emphasize the three real eigenvalues closest to the origin. The three conjugate complex pairs of eigenvalues resulting from steering actuator dynamics are neglected. Numeric values of weights w_i are given in Appendix A.6.3. The resulting closed-loop eigenvalues and initial condition responses using either state or output feedback are depicted in Figure 4.1. Initial condition responses are based on simulations using the linear kinematic system description
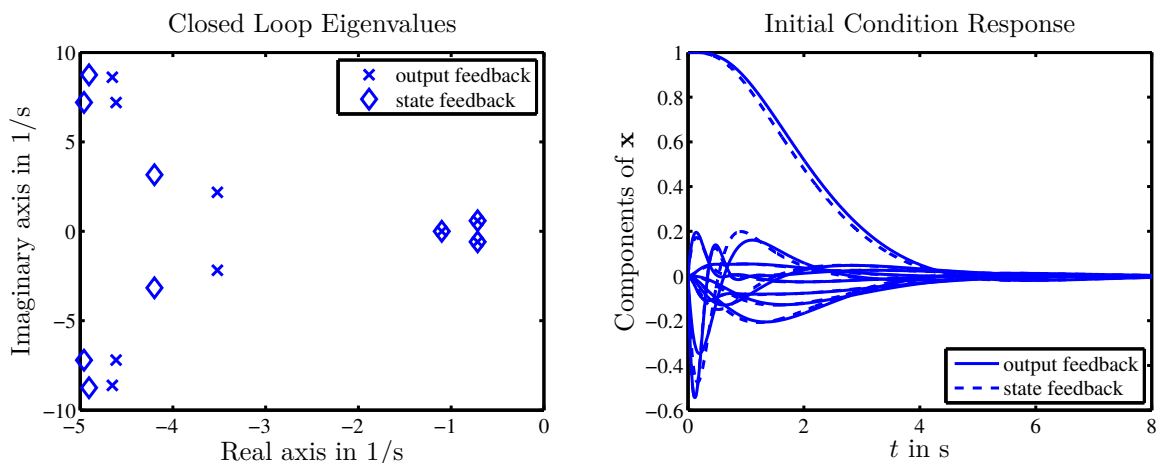
Figure 4.1: Comparison of closed-loop eigenvalues and initial condition responses obtained using state feedback and an respective static output feedback approximation. A linear kinematic model was used for LQR controller design and simulations. Parameters are as stated in Appendix A.5, and A.6. $v_{tr}^{x,t}$ is 3 m/s. The initial condition represents a scenario of tractor and implement starting with 1 m lateral error parallel to the desired path.

as used for controller design. Figure 4.1 at this point is intended to outline the differences between state feedback and output feedback approximation. A further discussion of closed loop behavior is given in Chapter 5. In agreement with original examples by [BL74] the neglected eigenvalues in case of static output feedback become more dominant and move to the right. This expresses some decrease in performance caused by the approximation. Comparing the particular initial condition responses of system states **x** the differences for the given case are marginal. In theory state feedback allows for an arbitrary choice of eigenvalues either obtained via pole placement or performance index weights. Output feedback with limited system information may not be capable to resemble this choice. In this case it was observed that some neglected eigenvalues move to the right half-plane resulting in an unstable closed-loop system. For practical applications this requires the checking of the closed-loop eigenvalues resulting from output feedback. For an unstable approximation one needs to return to LQR controller design with less demanding weights.

4.3 Integral Control

LQR control and subsequent output feedback approximation as described in the previous sections results in a proportional controller

$$\mathbf{u} = \mathbf{K}_y \mathbf{y} \tag{4.20}$$

with

$$\mathbf{y} = [e_{tl}, e_{th}, e_{r1l}, e_{r1h}]^{\mathrm{T}} \qquad \text{and} \qquad \mathbf{u} = [\delta_{tf,d}, \delta_{r1d,d}, \delta_{r1r,d}]^{\mathrm{T}}. \tag{4.21}$$

In some variants only a subset of steering angle inputs of **u** may be available. Results in Chapter 5 will show that this proportional control approach exhibits unsatisfactory steady-state errors in curves and on slopes, which is due to the neglected wheel side-slip acting as a disturbance. In addition, uncertain plant parameters might contribute to this remaining deviation. From experience with classical SISO PID control one would expect that integral control will account for uncertain plant parameters as well as for constant or slowly changing disturbances. Formally this means SISO PID is a robust controller in a sense as defined by [DG75] and as outlined in Appendix A.7. For MIMO control this raises the questions:

- Is there a similar robust controller for MIMO?

- In case of m inputs, how many controlled outputs will exhibit zero steady-state errors despite parameter uncertainties and disturbances?

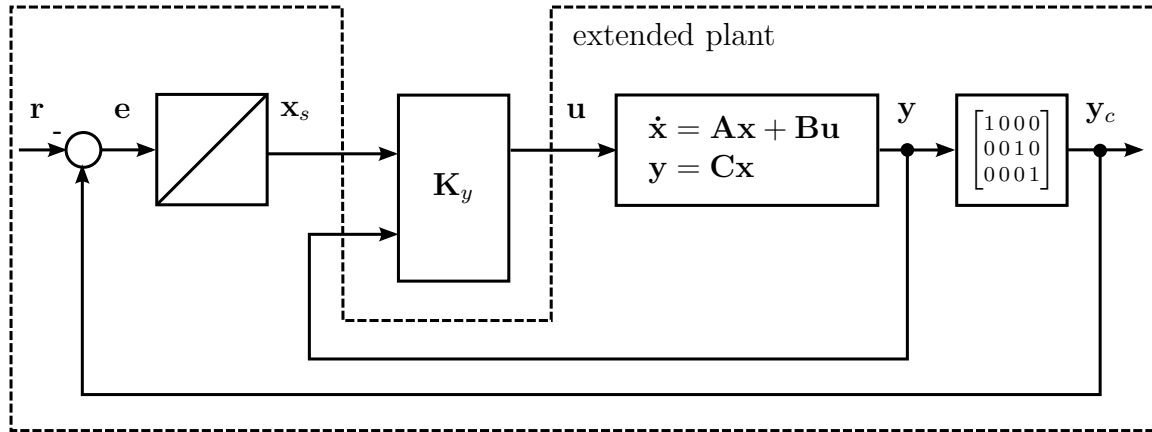- What does a suitable robust controller look like?

Figure 4.2: Extended plant considered for robust controller design in case of constant disturbances and reference inputs, with plant inputs $\mathbf{u} \in \mathbb{R}^m$, measured plant outputs $\mathbf{y} \in \mathbb{R}^r$, controlled plant outputs $\mathbf{y}_c \in \mathbb{R}^{p_c}$, reference input $\mathbf{r} \in \mathbb{R}^{p_c}$ (here: $\mathbf{r} \equiv 0$), error $\mathbf{e} \in \mathbb{R}^{p_c}$, and servo-compensator states $\mathbf{x}_s = \int \mathbf{e}$. $\mathbf{y}_c$ is obtained by selecting a subset of $\mathbf{y}$ such that $p_c \leq m$. $\mathbf{K}_y$ is a static output feedback controller for the extended plant used to stabilize the overall system.

Answers to those questions have been provided by [DG75] considering possible disturbances and reference input signals in a very general way. Results for constant disturbances and reference inputs are summarized in Appendix A.7. Core to a robust controller is the inclusion of suitable models depicting the classes of disturbances and reference input signals that need to be considered. This is now commonly known as the 'internal model principle' [FW75]. Constant disturbances and reference inputs in particular require the inclusion of integrators as depicted in Figure 4.2. For $p_c = \dim(\mathbf{y}_c)$ controlled outputs p_c integrators are required. The number of controlled outputs p_c however may not exceed the number of inputs $m = \dim(\mathbf{u})$, if all controlled outputs shall exhibit zero steady-state error despite parameter uncertainties and disturbances. Figure 4.2 indicates this requirement by distinguishing between measured outputs $\mathbf{y}$ and controlled outputs $\mathbf{y}_c$ which are a selection of the former. With those prerequisites robust controller design is a two-step approach. The first step comprises creation of the extended plant as described. The second step is stabilization of that extended plant using an arbitrary suitable controller. In Figure 4.2 this is done using a static output feedback controller $\mathbf{K}_y$.

It is worth noting that [DD11] only recently considered the case of fewer plant inputs than controlled outputs in particular. In this case zero steady-state error is normally not achieved for all outputs if disturbances are present. A controller is proposed to minimize the remaining steady-state error. This controller however requires the steady-state plant gain $-\mathbf{C}_c\mathbf{A}^{-1}\mathbf{B}$ to be unaffected by parameter uncertainties, which is a major restriction. For this work's application achieving zero steady-state errors for an equal number of inputs and controlled outputs and at the same time allowing for more general uncertainties seemed more relevant.

Application to Tractor-Implement Combinations

Considering the linear kinematic tractor-implement model given by (3.78), (3.79), (3.75), (3.76), and (3.77) in particular allows to simplify the extended plant as given in Appendix A.7 resulting in:

$$
\underbrace{\begin{bmatrix} \dot{\mathbf{x}} \\ \dot{\mathbf{x}}_s \end{bmatrix}}_{\dot{\mathbf{x}}_e} = \underbrace{\begin{bmatrix} \mathbf{A} & \mathbf{0} \\ \mathbf{C}_c & \mathbf{0} \end{bmatrix}}_{\mathbf{A}_e} \underbrace{\begin{bmatrix} \mathbf{x} \\ \mathbf{x}_s \end{bmatrix}}_{\mathbf{x}_e} + \underbrace{\begin{bmatrix} \mathbf{B} \\ \mathbf{0} \end{bmatrix}}_{\mathbf{B}_e} \mathbf{u}
\tag{4.22}
$$

$$
\underbrace{\begin{bmatrix} \mathbf{y} \\ \mathbf{x}_s \end{bmatrix}}_{\mathbf{y}_e} = \underbrace{\begin{bmatrix} \mathbf{C} & \mathbf{0} \\ \mathbf{0} & \mathbf{I} \end{bmatrix}}_{\mathbf{C}_e} \underbrace{\begin{bmatrix} \mathbf{x} \\ \mathbf{x}_s \end{bmatrix}}_{\mathbf{x}_e}.
\tag{4.23}
$$

Multiple variants with different combinations of inputs $\mathbf{u}$ and controlled outputs $\mathbf{y}_c$ are considered. This results in the slight differences in the extended plant (4.22) and (4.23). The most comprehensive plant considered uses tractor front wheel steering input $\delta_{tf,d}$ as well as implement drawbar and wheel steering inputs $\delta_{r1d,d}$ and $\delta_{r1r,d}$. The controlled outputs considered for this variant are the tractor lateral error e_{tl} as well as the implement lateral and heading error e_{r1l} and e_{r1h}. For this variant vectors $\mathbf{x}$, $\mathbf{u}$, and $\mathbf{y}$ remain as given by (3.75), (3.76), and (3.77). Similarly matrices $\mathbf{A}$, $\mathbf{B}$, and $\mathbf{C}$ remain as stated in Appendix A.2.2. $\mathbf{x}_s$ and $\mathbf{C}_c$ depict the choices made in terms of controlled outputs $\mathbf{y}_c$ resulting in:

$$
\mathbf{x}_s = \left[\int e_{tl}, \int e_{r1l}, \int e_{r1h} \right]^T,
\tag{4.24}
$$

$$
\mathbf{C}_c = \begin{bmatrix} 1 & 0 & 0 & 0 \\ 0 & 0 & 1 & 0 \\ 0 & 0 & 0 & 1 \end{bmatrix} \mathbf{C}.
\tag{4.25}
$$

A summary of all variants considered can be found in Table A.4 of Appendix A.6.2. In those cases the extended plant (4.22), and (4.23) exhibits a reduced number of states due to less steering actuators. Similarly, $\mathbf{x}_s$ comprises only of a subset of tracking error integrals due to a reduced number of controlled outputs.

The stabilization of (4.22) and (4.23) is similar for all variants considered. Again LQR control with subsequent output feedback approximation as described in Sections 4.1 and 4.2 is used. Additional performance index weights for tracking error integrals have been introduced and chosen as stated in Appendix A.6.2. To emphasize the approximation of dominant state feedback closed-loop eigenvalues the weighting rule as stated in Appendix A.6.3 is used in an unchanged manner.

Assuming a tractor forward velocity of $v_{tr}^{x,t} = 3$ m/s and parameters as outlined in Appendix A.5 the resulting closed loop eigenvalues and initial condition responses of all

variants are depicted in Figures 4.3 and 4.4. Initial condition responses have been calculated using the linear kinematic model as considered for controller design. Again a comparison of ideal state feedback and the respective static output feedback approximation is intended. Further discussion of closed-loop properties will be given in Chapter 5. In addition to directly comparing the degree of match in Figures 4.3 and 4.4 sufficient conditions of Davison's theorem [Dav70] as outlined in Section 4.2 have been evaluated. Determining rank $\mathbf{C}_e$ for each variant showed that the approximation's weighting rule of Appendix A.6.3 is not emphasizing too many eigenvalues. All sufficient conditions held for single input variants. For variants with multiple inputs the sufficient condition of distinct Jordan block eigenvalues was not fulfilled. Those cases allowed for no conclusion using Davison's theorem [Dav70].

As a final remark it should be noted that step responses with integral control typically exhibit an overshooting behavior. This is already visible in Figures 4.3 and 4.4. In case reference input steps are frequent a prefilter shaping the command response may be used [Lun08]. Here initial path acquisition is the only situation requiring particular attention. Overshooting in this situation will be addressed within the wider frame of anti-windup.

Figure 4.3: Comparison of closed-loop eigenvalues and initial condition responses obtained using state feedback and an corresponding static output feedback approximation. Variants of steering inputs $\mathbf{u}$ and controlled outputs $\mathbf{y}_c$ have been considered. Linear kinematic models were used for LQR controller design and simulations. Integral control for all $\mathbf{y}_c$ was included by using an extended plant. Parameters are as stated in Appendix A.5 and A.6. $v_{tr}^{x,t}$ is 3 m/s. The initial condition represents a scenario of tractor and implement starting with 1 m lateral error parallel to the desired path.
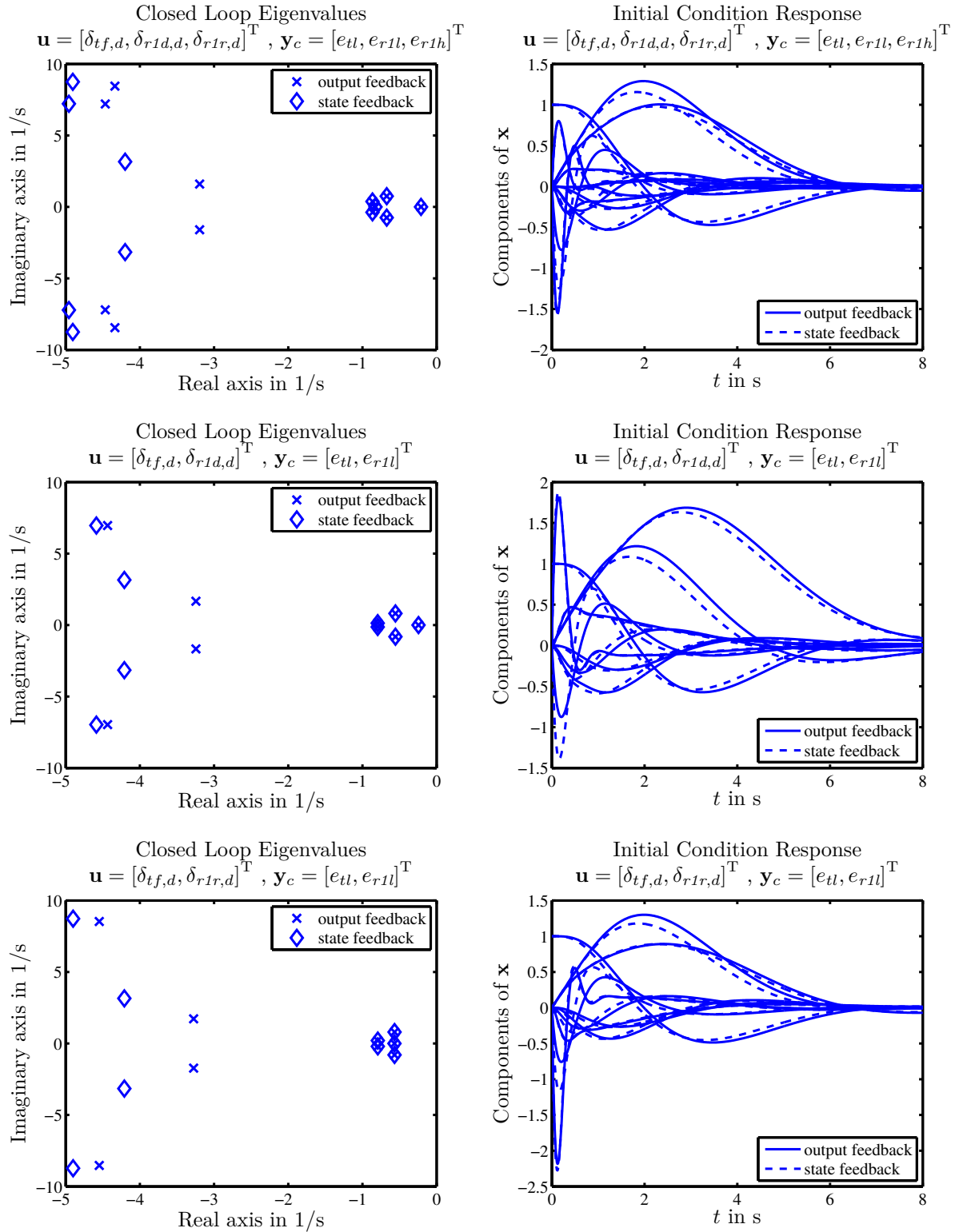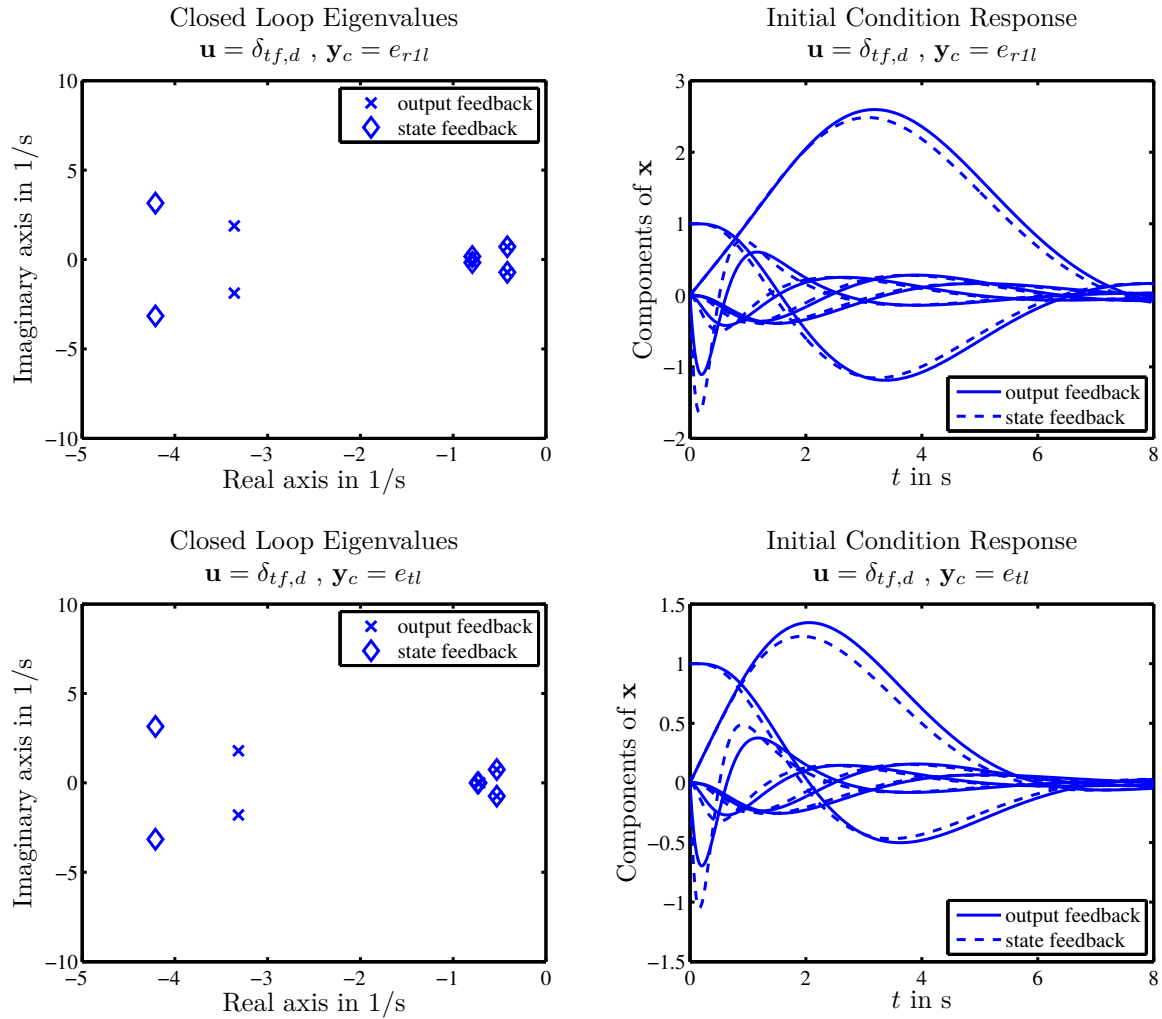
Figure 4.4: Comparison of closed-loop eigenvalues and initial condition responses obtained using state feedback and an corresponding static output feedback approximation. Variants of steering inputs $\mathbf{u}$ and controlled outputs $\mathbf{y}_c$ have been considered. Linear kinematic models were used for LQR controller design and simulations. Integral control for all $\mathbf{y}_c$ was included by using an extended plant. Parameters are as stated in Appendix A.5 and A.6. $v_{tr}^{x,t}$ is 3 m/s. The initial condition represents a scenario of tractor and implement starting with 1 m lateral error parallel to the desired path.

Controller Windup Prevention

Integral controllers (among others) [Hip06] face a challenge that arises from plant input saturation. If plant inputs $\mathbf{u}$ saturate, changes in the plant outputs $\mathbf{y}$ and tracking errors $\mathbf{e}$ remain without influence on the plant inputs. During this open-loop situation integral controller state values may increase dramatically. This is followed by an error overshoot in the opposite direction in order to decrease the error integral. The error overshoot is possibly accompanied by reaching the opposite input saturation. As a consequence a sequence of large and poorly decaying overshoots may develop. This phenomenon is known as controller windup [Hip06]. Numerous measures have been developed to prevent controller windup.

In an overview [Hip06] lists:

- Hold integrators if control inputs are outside defined limits.

- Hold integrators if tracking errors are outside defined limits.

- Feed back difference between saturated and unsaturated plant inputs to stabilize the controller during saturation.

- Use controllers given in a particular observer structure fed with saturated inputs.

The listed measures range from simple and rather pragmatic to complex and sophisticated. The latter in particular allow to address performance problems in case of frequent and rapid reference input **r** changes. Similarly some approaches are tailored towards maintaining the direction **u** for particular MIMO systems that are sensitive to such changes.

For the given task of path tracking control actuator limits are reached in very rare occasions. The only exception is the initial path acquisition while transitioning from manual to automatic steering. For that reason a rather simple method of controller windup prevention has been implemented. It uses the subsequent rules and thresholds as given in Appendix A.6.4:

- Hold all integrators if at least one desired steering angle exceeds its defined limits.

- Hold all integrators if at least one tracking error exceeds its defined limits.

- Limit a particular integration rate if values of error and error integral are both positive or both negative.

- Limit error integrals to a defined range.

During path tracking the controller exhibits linear behavior unaffected by those measures.

4.4 Disturbance Estimation and Feedforward

Integral control of Section 4.3 was introduced to account for disturbances resulting from wheel side-slip. As an alternative this section derives an estimator for wheel-side slip. The wheel side-slip estimates are used for disturbance feedforward control in order to reduce steady-state path tracking errors. This section ties in with the introduction on disturbance estimation of Section 2.2.11. A suitable nonlinear kinematic plant model accounting for wheel side-slip as additive disturbances was derived in Section 3.2. This model serves as a basis for estimator design. Estimation relies on the widely used Extended Kalman Filter (EKF) [GKN+74], [May82], [Wen11] which is motivated by (approximately) minimizing the state estimation error covariance for a plant with given sensor noise and process noise properties. The EKF will be implemented using a digital controller and therefore a discrete time system description is used throughout estimator design.

Estimator Plant Model

Starting with the nonlinear kinematic model as summarized in Section 3.2.6 a discrete time system given by difference equations can be found using forward Euler integration of (3.70) if the sample time T_s is chosen sufficiently small. Introducing additional process noise $\mathbf{w}$ and sensor noise $\mathbf{v}$ random vectors [GKN$^+$74] results in a nonlinear stochastic system:

$$\mathbf{x}[k+1] = \underbrace{\mathbf{x}[k] + T_s \mathbf{f}(\mathbf{x}[k], \mathbf{u}[k])}_{\mathbf{f}_d(\mathbf{x}[k], \mathbf{u}[k])} + \mathbf{w}[k], \tag{4.26}$$

$$\mathbf{y}[k] = \underbrace{\mathbf{h}(\mathbf{x}[k])}_{\mathbf{h}_d(\mathbf{x}[k])} + \mathbf{v}[k] \tag{4.27}$$

with

$$\mathbf{x} = \left[r_{tr}^{x,e}, r_{tr}^{y,e}, \Psi_t, \delta_{thr}, \delta_{tf}, \dot{\delta}_{tf}, \delta_{r1d}, \dot{\delta}_{r1d}, \delta_{r1r}, \dot{\delta}_{r1r}, \alpha_{tf}, \alpha_{tr}, \alpha_{r1r} \right]^{\mathrm{T}}, \tag{4.28}$$

$$\mathbf{u} = \left[\delta_{tf,d}, \delta_{r1d,d}, \delta_{r1r,d} \right]^{\mathrm{T}}, \tag{4.29}$$

$$\mathbf{y} = \left[r_{tr}^{x,e}, r_{tr}^{y,e}, \Psi_t, r_{r1r}^{x,e}, r_{r1r}^{y,e}, \Psi_{r1}, \delta_{tf}, \delta_{r1d}, \delta_{r1r} \right]^{\mathrm{T}}, \tag{4.30}$$

In the theory of optimal filtering the process noise $\mathbf{w}$ and the sensor noise $\mathbf{v}$ are assumed to be zero mean white gaussian random vectors and therefore defined by expectations $E\{\bullet\}$ [GKN$^+$74]:

$$E\{\mathbf{w}[k]\} = \mathbf{0}, \qquad E\{\mathbf{w}[k]\mathbf{w}^{\mathrm{T}}[l]\} = \begin{cases} \mathbf{Q}[k] & \text{for } k = l, \\ \mathbf{0} & \text{for } k \neq l, \end{cases} \tag{4.31}$$

$$E\{\mathbf{v}[k]\} = \mathbf{0}, \qquad E\{\mathbf{v}[k]\mathbf{v}^{\mathrm{T}}[l]\} = \begin{cases} \mathbf{R}[k] & \text{for } k = l, \\ \mathbf{0} & \text{for } k \neq l. \end{cases} \tag{4.32}$$

Obtaining statistical properties in practice is a challenge, however. The measurement noise covariance matrix $\mathbf{R}[k]$ may be obtained from sensor data sheets or measurements. The process noise covariance matrix $\mathbf{Q}[k]$ in contrast is seldom found and rather depicts a tuning parameter for the resulting filter [Wen11]. If additional information on noise spectral properties or correlation between $\mathbf{w}$ and $\mathbf{v}$ exists this may be used to enhance estimates [Wen11]. Here, due to lack of further information, $\mathbf{w}$ and $\mathbf{v}$ as well as their individual elements are assumed to be uncorrelated, resulting in:

$$E\{\mathbf{v}[k]\mathbf{w}^{\mathrm{T}}[l]\} = \mathbf{0} \text{ for all } k, l \geq 0. \tag{4.33}$$

$$\mathbf{Q}[k] = \mathrm{diag}\left(q_{1,1}[k], \ldots, q_{n,n}[k]\right), \tag{4.34}$$

$$\mathbf{R}[k] = \mathrm{diag}\left(r_{1,1}[k], \ldots, r_{p,p}[k]\right). \tag{4.35}$$

Numerical values for $\mathbf{Q}[k]$ and $\mathbf{R}[k]$ used in this work's setup are provided in Appendix A.6.5. For $\mathbf{R}[k]$ those have been obtained from sensor data sheets and sensor noise variance measurements for known sensor positions. For $\mathbf{Q}[k]$ numerical values were obtained during experiments and simulations starting from an initial guess on how large the propagation errors could become within one time step.

Note that earth-fixed coordinates instead of path deviations have been chosen for (4.26) to (4.30). This is because wheel-side slip estimation is not necessarily tied to path tracking. Keeping path information separate from this estimator model increases the flexibility in terms of possible paths for tractor and implement. Those must not necessarily be identical and could be given as a sequence of points without the need to find a describing function.

Extended Kalman Filter

The EKF is an estimator as shown in Figure 2.14. It is a nonlinear model based filter running parallel to the actual plant and its task is to provide estimates $\hat{\mathbf{x}}$ for the actual plant's system states $\mathbf{x}$. Along with those state estimates the EKF provides a measure of estimation accuracy given by the state estimation error covariance matrix

$$\hat{\mathbf{P}} = E\left\{ (\mathbf{x} - \hat{\mathbf{x}})\,(\mathbf{x} - \hat{\mathbf{x}})^{\mathrm{T}} \right\}. \tag{4.36}$$

The process of filtering can be divided into *measurement update* and *propagation*. Assuming a discrete time EKF at the beginning of each time step a measurement update is performed using available plant output measurements $\mathbf{y}$ to update the estimated system states $\hat{\mathbf{x}}$ and the state estimation error covariance $\hat{\mathbf{P}}$. Subsequently, during propagation the EKF uses system information given by a plant model to predict both the estimated system states $\hat{\mathbf{x}}$ and the state estimation error covariance $\hat{\mathbf{P}}$ for the next controller time step. The possibly time varying covariance matrices $\mathbf{Q}[k]$ and $\mathbf{R}[k]$ express uncertainty in the system model and measurements. Noisy measurements and hence large $\mathbf{R}[k]$ result in small and slow state estimate changes due to measurement updates. Perfect measurements in contrast result in quick changes to estimated system states.

For this work's discrete time plant model given by (4.26) to (4.30) the step of propagation comprises of evaluating a nonlinear difference equation depicting the propagation of the estimated states as well as a linear difference equation depicting the propagation of the estimation error covariance [Wen11]:

$$\hat{\mathbf{x}}^{-}[k+1] = \mathbf{f}_d(\hat{\mathbf{x}}^{+}[k], \mathbf{u}[k]), \tag{4.37}$$

$$\hat{\mathbf{P}}^{-}[k+1] = \mathbf{F}[k]\hat{\mathbf{P}}^{+}[k]\mathbf{F}^{\mathrm{T}}[k] + \mathbf{Q}[k], \tag{4.38}$$

$$\mathbf{F}[k] = \left.\frac{\partial \mathbf{f}_d(\mathbf{x}, \mathbf{u})}{\partial \mathbf{x}}\right|_{\mathbf{x}=\hat{\mathbf{x}}^{+}[k], \mathbf{u}=\mathbf{u}[k]} = \mathbf{I} + T_s \left.\frac{\partial \mathbf{f}(\mathbf{x}, \mathbf{u})}{\partial \mathbf{x}}\right|_{\mathbf{x}=\hat{\mathbf{x}}^{+}[k], \mathbf{u}=\mathbf{u}[k]}. \tag{4.39}$$

$(\bullet)^{-}$ and $(\bullet)^{+}$ denote *a priori* and *a posteriori* estimates, i.e. estimates before and after measurements have been considered in a particular time step.

In case all measured plant outputs $\mathbf{y}$ are obtained at the same time and with the same sample rate the EKF measurement update could be stated in the common form [Wen11]:

$$\mathbf{K}[k] = \hat{\mathbf{P}}^-[k]\mathbf{H}^{\mathrm{T}}[k]\left(\mathbf{H}[k]\hat{\mathbf{P}}^-[k]\mathbf{H}[k]^T + \mathbf{R}[k]\right)^{-1}, \tag{4.40}$$

$$\hat{\mathbf{x}}^+[k] = \hat{\mathbf{x}}^-[k] + \mathbf{K}[k]\left(\mathbf{y}[k] - \underbrace{\mathbf{h}_d(\hat{\mathbf{x}}^-[k])}_{\hat{\mathbf{y}}^-[k]}\right), \tag{4.41}$$

$$\hat{\mathbf{P}}^+[k] = \left(\mathbf{I} - \mathbf{K}[k]\mathbf{H}[k]\right)\hat{\mathbf{P}}^-[k]\left(\mathbf{I} - \mathbf{K}[k]\mathbf{H}[k]\right)^{\mathrm{T}} + \mathbf{K}[k]\mathbf{R}[k]\mathbf{K}^{\mathrm{T}}[k], \tag{4.42}$$

with $\mathbf{K}[k]$ denoted as Kalman gain and

$$\mathbf{H}[k] = \left.\frac{\partial \mathbf{h}_d(\mathbf{x})}{\partial \mathbf{x}}\right|_{\mathbf{x}=\hat{\mathbf{x}}^-[k]}. \tag{4.43}$$

In the given case several sensor signal sample rates have to be considered. As a consequence only a subset of new sensor measurements $\mathbf{y}$ is available at some time steps. If the entire vector $\mathbf{y}$ was used for measurement updates this would result in using outdated sensor measurements $\mathbf{y}$ causing an additional estimation error. To overcome this problem a proposal by [Wen11] is implemented. Instead of using a single measurement update considering all outputs $\mathbf{y}$ a sequence of measurement updates each considering a single output y_i only is performed. If y_i is a new measurement the update is performed, if it is an outdated measurement the update is omitted. For p outputs this results in:

$$\hat{\mathbf{x}}_0^{\pm}[k] = \hat{\mathbf{x}}^-[k], \tag{4.44}$$

$$\hat{\mathbf{P}}_0^{\pm}[k] = \hat{\mathbf{P}}^-[k], \tag{4.45}$$

for $i = 1, \ldots, p$ **do**

$$\mathbf{k}_i[k] = \hat{\mathbf{P}}_{i-1}^{\pm}[k]\mathbf{h}_i[k]\left(\mathbf{h}_i^{\mathrm{T}}[k]\hat{\mathbf{P}}_{i-1}^{\pm}[k]\mathbf{h}_i[k] + r_{i,i}[k]\right)^{-1}, \tag{4.46}$$

$$\hat{\mathbf{x}}_i^{\pm}[k] = \begin{cases} \hat{\mathbf{x}}_{i-1}^{\pm}[k] + \mathbf{k}_i[k]\left(y_i[k] - \underbrace{h_{d,i}(\hat{\mathbf{x}}^-[k])}_{\hat{y}_i^-[k]}\right) & \text{(update)}, \\ \hat{\mathbf{x}}_{i-1}^{\pm}[k] & \text{(no update)} \end{cases} \tag{4.47}$$

$$\hat{\mathbf{P}}_i^{\pm}[k] = \begin{cases} \left(\mathbf{I} - \mathbf{k}_i[k]\mathbf{h}_i^{\mathrm{T}}[k]\right)\hat{\mathbf{P}}_{i-1}^{\pm}[k]\left(\mathbf{I} - \mathbf{k}_i[k]\mathbf{h}_i^{\mathrm{T}}[k]\right)^{\mathrm{T}} + \mathbf{k}_i[k]r_{i,i}[k]\mathbf{k}_i^{\mathrm{T}}[k] & \text{(update)}, \\ \hat{\mathbf{P}}_{i-1}^{\pm}[k] & \text{(no update)}, \end{cases}$$

$$\tag{4.48}$$

end for

$$\hat{\mathbf{x}}^+[k] = \hat{\mathbf{x}}_p^{\pm}[k], \tag{4.49}$$

$$\hat{\mathbf{P}}^+[k] = \hat{\mathbf{P}}_p^{\pm}[k], \tag{4.50}$$

with intermediate results $\hat{\mathbf{x}}_i^{\pm}[k]$, $\hat{\mathbf{P}}_i^{\pm}[k]$, Kalman gain column vectors $\mathbf{k}_i[k]$, and the following row vectors:

$$
\begin{bmatrix} \mathbf{h}_1^{\mathrm{T}}[k] \\ \vdots \\ \mathbf{h}_p^{\mathrm{T}}[k] \end{bmatrix} = \mathbf{H}[k] = \left. \frac{\partial \mathbf{h}_d(\mathbf{x})}{\partial \mathbf{x}} \right|_{\mathbf{x}=\hat{\mathbf{x}}^-[k]}.
\tag{4.51}
$$

Initial values $\hat{\mathbf{x}}^-[0]$ and $\hat{\mathbf{P}}^-[0]$ need to be given as parameters. Those are stated in Appendix A.6.5.

Disturbance Feedfoward Control

Estimation of $\hat{\mathbf{x}}$ as in (4.28) results in wheel side-slip estimates $\hat{\alpha}_{tf}$, $\hat{\alpha}_{tr}$, and $\hat{\alpha}_{r1r}$. Disturbance feedforward is established by including additive terms $\delta_{tf,d,dff}$, $\delta_{r1d,d,dff}$, and $\delta_{r1r,d,dff}$ contributing to the desired steering angles $\delta_{tf,d}$, $\delta_{r1d,d}$, and $\delta_{r1r,d}$ used to control tractor and implement. Those additive terms are defined as:

$$
\delta_{tf,d,dff} = \hat{\alpha}_{tf},
\tag{4.52}
$$

$$
\delta_{r1r,d,dff} = \hat{\alpha}_{r1r},
\tag{4.53}
$$

$$
\delta_{r1d,d,dff} = -\arcsin\left(\frac{l_{thr}}{l_{r1d}}\sin\left(\hat{\alpha}_{tr}\right)\right).
\tag{4.54}
$$

Referring to Figure 2.7 the disturbance feedfoward terms $\delta_{tf,d,dff}$ and $\delta_{r1r,d,dff}$ are simply chosen to increase the corresponding steering angle and to compensate the influence of wheel side-slip. The tractor rear wheel is unsteered which excludes this possibility. The estimate $\hat{\alpha}_{tr}$ is used to aid the positioning of the implement instead. Therefore, the implement drawbar disturbance feedforward $\delta_{r1d,d,dff}$ is chosen in such a way that the implement straight line tracking error caused by the tractor hitch point offset due to wheel side-slip (i.e. $l_{thr}\sin\left(\hat{\alpha}_{tr}\right)$) is compensated.

Controller Windup Prevention

In case of saturated input signals $\mathbf{u}$ differences between actual plant and estimator plant model input signals might cause the estimator to attribute those differences wrongfully to system state and disturbance estimates. As a consequence controller windup might occur. A systematic way of preventing this windup is to saturate input signals to the estimator as well [Hip06]. This was implemented by limiting desired steering angles to the permissible ranges as stated in Appendix A.5.

4.5 Path Curvature Feedforward

Path tracking by means of feedback control as derived in the previous sections only takes place after a tracking error is already present. On paths with changing curvature this will result in poor performance. To account for changing path curvature prior to leaving the desired path, feedback control is supplemented by feedforward control based on the paths curvature. Feedforward control laws for both tractor and implement will be derived by relating path curvature and steering angles.

Path Curvature and Steering Angle Relations

Tractor feedforward control is found as shown in Figure 4.5. Assuming no wheel side-slip, path curvature $\kappa = 1/R$ and tractor front wheel steering angle δ_{tf} are related by simple trigonometry and l_t as only parameter. A feedforward steering angle $\delta_{tf,d,cff}$ that keeps the tractor on the depicted arc segment, if no wheel side-slip and no disturbances are present, is given by the well-known equation:

$$\delta_{tf,d,cff} = \arctan\left(l_t \kappa\right). \tag{4.55}$$

Implement feedforward control is slightly more involved, yet can be found using trigonometry and a small number of parameters as well. Figure 4.5 depicts a drawbar steered implement. Assuming that the tractor rear wheel and implement wheel are both located on an arc segment with radius R or curvature $\kappa = 1/R$ allows to relate drawbar steering angle and path curvature. Using some trigonometric laws to calculate lengths and angles of the depicted triangles between tractor rear wheel and implement wheel yields:

$$\delta_{r1d,d,cff} = \arctan\left(l_{r1}\kappa\right) + \arcsin\left(\frac{\kappa\left(l_{r1}^2 + l_{r1d}^2 - l_{thr}^2\right)}{2l_{r1d}\sqrt{1 + \kappa^2 l_{r1}^2}}\right). \tag{4.56}$$

This feedforward control law is used in case drawbar steering is available. It is preferred over feedforward control via implement wheel steering due to not causing an implement heading error. This means that path tangent and implement remain aligned at the implement rear wheel position as shown in Figure 4.5.

If only implement wheel steering is available the respective feedforward control law is:

$$\delta_{r1r,d,cff} = -\arcsin\left(\frac{\kappa\left(\left(l_{r1} + l_{r1d}\right)^2 - l_{thr}^2\right)}{2\left(l_{r1} + l_{r1d}\right)}\right). \tag{4.57}$$

It can be found as a special case of (4.56) using the substitutes $\delta_{r1d,d,cff} \rightarrow -\delta_{r1r,d,cff}$, $l_{r1} \rightarrow 0$, and $l_{r1d} \rightarrow l_{r1d} + l_{r1}$.
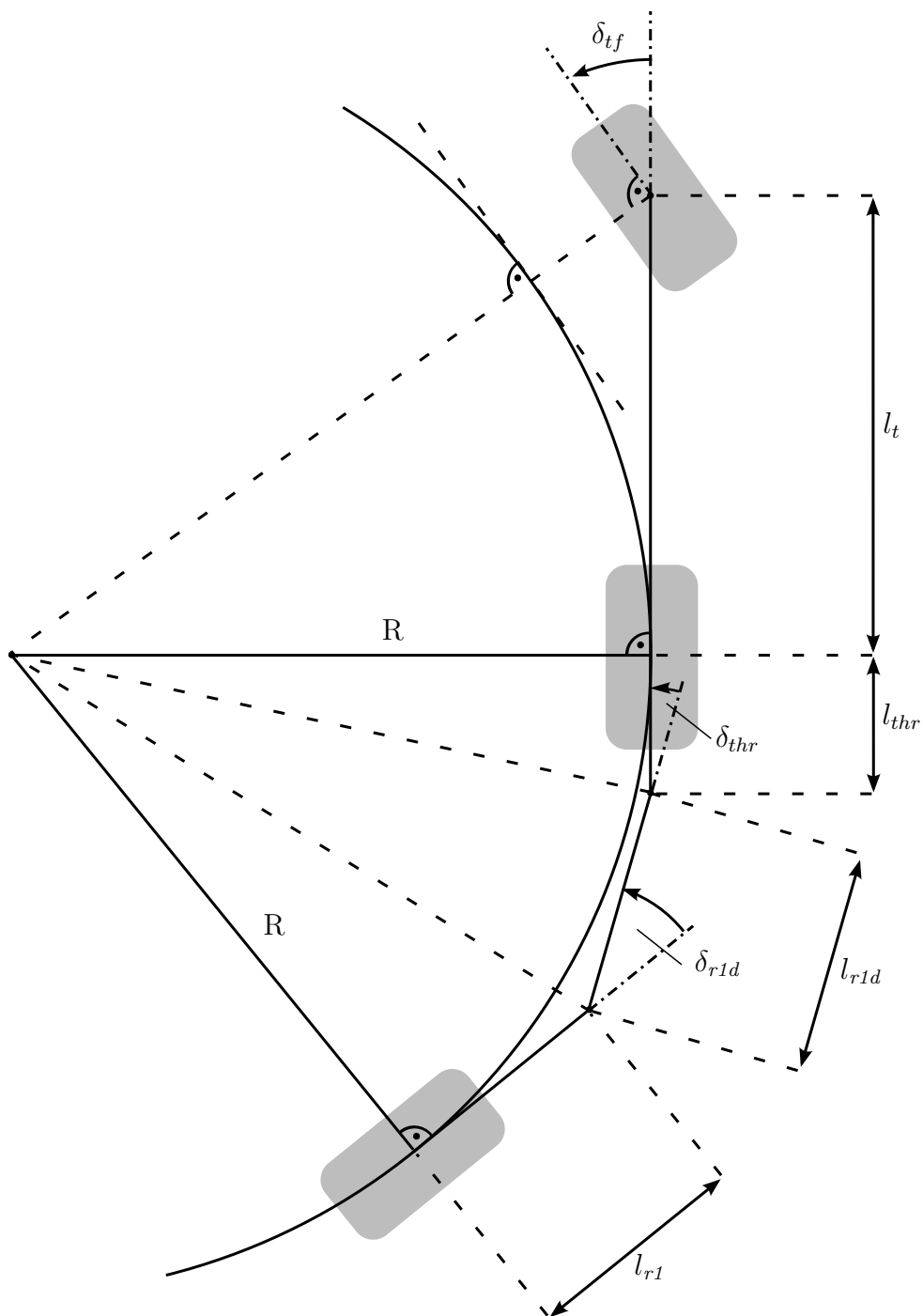
Figure 4.5: Tractor and drawbar steered implement on arc segment with radius R and curvature $\kappa = 1/R$. Steering angles and curvature are positive as drawn.

Path Curvature Look-Ahead

The curvature feedforward control laws (4.55), (4.56), and (4.57) have been derived assuming that the tractor and the implement are located on an arc segment with curvature κ. For arbitrary paths, as for instance given in Appendix A.4, the derived feedforward control laws are an approximation. To improve performance on those paths two small modifications are made. First, instead of using only one desired path curvature variable κ, two separate variables κ_t and κ_{r1} are obtained from the desired path information. Second, to account for delays due to steering actuator dynamics the curvatures obtained are taken from points slightly ahead of the tractor rear wheel and implement wheel respectively. The corresponding distances are found by multiplying a time constant with current tractor and implement speed to account for different distances traveled while the steering actuation takes place. Numerical values of those time constants are given in Appendix A.6.6. Those have been chosen to depict the delay until a small steering angle step response reaches 63% of its final value.

4.6 Tracking Error and Curvature Calculation

Feedback controller design was based on a linearized bicycle model in terms of deviations from a desired straight path as shown in Figure 3.1. Lateral errors e_{tl}, e_{r1l} and heading errors e_{th}, e_{r1h} were assumed to be measured plant outputs. This choice of outputs was motivated by the possibility of applying the controller to arbitrary paths without introducing large errors due to linearization. However, regardless of the chosen desired path no details on obtaining e_{tl}, e_{r1l}, e_{th}, and e_{r1h} have been provided so far. The same holds for the path curvature κ_t and κ_{r1} required for curvature feedforward. This section will sketch the basic idea of this work's underlying calculations. The chosen approach is not core to this work and may be replaced by arbitrary suitable alternatives.

Calculation Inputs

Inputs to error calculation are tractor and implement positions as well as a desired path given by a sequence of points. All of them are given in local earth-fixed coordinates. The sequence of points defining the desired path is assumed to be the result of an arbitrary form of path planning. By choosing a sequence of points over e.g. parameterized curves path planning and path tracking error calculation share a very general interface and can be designed independently. The desired paths as described in Appendix A.4 have been obtained by connecting different types of curves (e.g. straights, curves, clothoids). Sampling points have been taken with an approximate distance of 15 cm.

Algorithm

In order to obtain heading errors and desired path curvature, an at least two times differentiable parameterized curve describing the desired path is required. The key idea of the chosen approach is to interpolate the given sequence of points using a cubic spline

moving with tractor and implement. This is regardless of the original curve used during path planning.

The implemented steps are:

- Find the points in the desired path point sequence that are closest to tractor rear axle and implement axle.

- Interpolate the desired path by using a moving cubic spline with the arc length s_d as curve parameter (algorithm cf. [PTVF07]).

- Find the points on the interpolated curve that are closest to tractor rear axle and implement axle. The corresponding distances yield e_{tl} and e_{r1l}.

- Obtain the desired path curve tangents at those points. The angles between those and tractor/implement heading yield e_{th} and e_{r1h}.

- Obtain the desired path curvatures κ_t and κ_{r1} at short distances ahead of those closest points, as described in Section 4.5.

Notes:

- By choosing sufficiently short distances between the sampling points it was ensured that the differences between derivatives of the original curves and the cubic splines became negligible.

- In order to use this method with desired paths obtained from measurements a combined interpolation and approximation method smoothing the noisy measurements is probably advisable.

4.7 Controller Overview

Within the previous sections two alternative control approaches have been conceived. The resulting block diagrams summarizing them are given in Figures 4.6 and 4.7. LQR with integral control and subsequent output feedback approximation (denoted as 'LQR w. I') as shown in Figure 4.6 is the preferred solution in terms of tuning and simplicity of the resulting implementation. Therefore, several variants with subsets of steering actuators as outlined in Table A.4 of Appendix A.6.2 have been developed. The second approach avoiding integral control and using EKF estimation based disturbance feedforward control instead (denoted as 'LQR w. EKF') has been only derived using all steering actuators. Both approaches will be studied in simulations and experiments. In addition, LQR control with subsequent output feedback approximation without additional measures (denoted as 'LQR w/o I') will be considered to a limited extend. This is done in order to demonstrate the need for additional measures to account for wheel side-slip. The corresponding block diagram is identical to Figure 4.6 except for the omitted integral control.
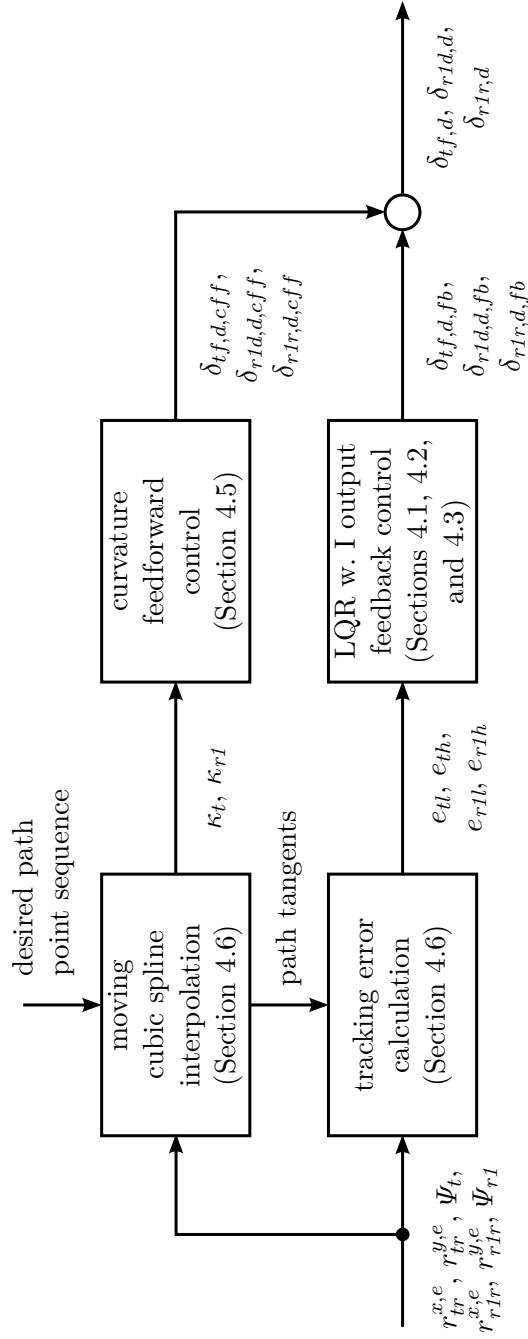
Figure 4.6: Controller block diagram of LQR output feedback with integral control and curvature feedforward (LQR w. I).
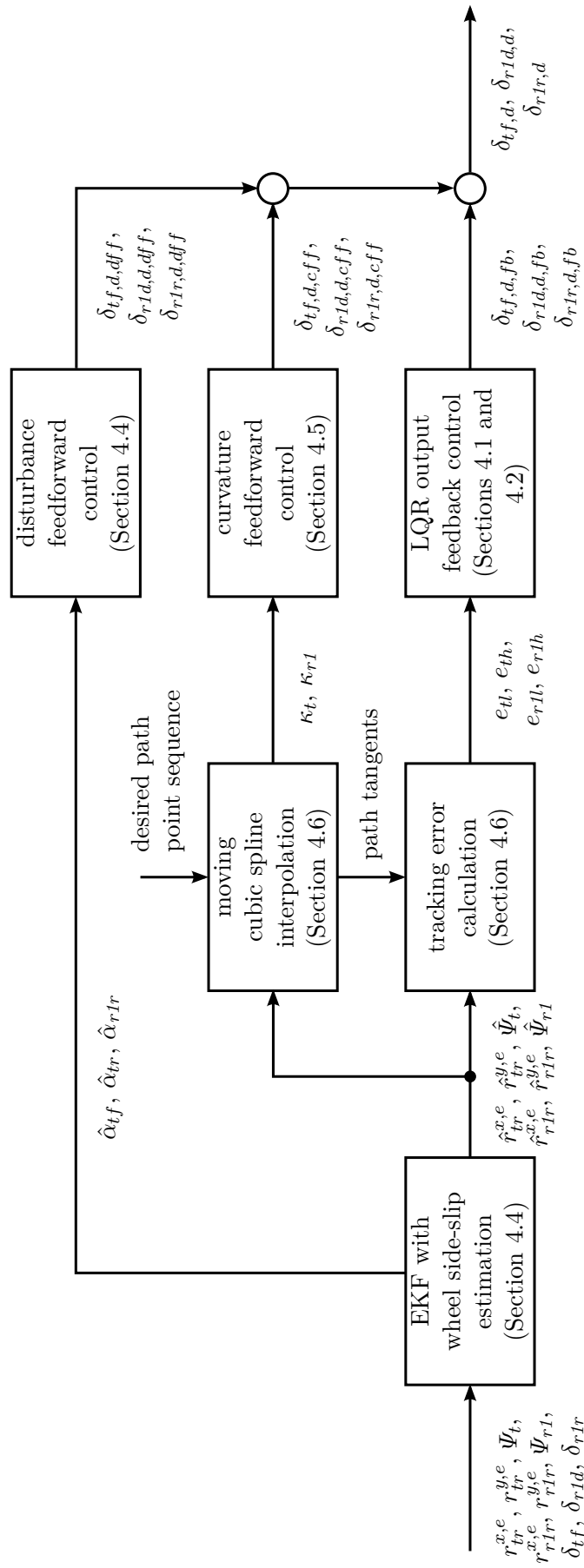
Figure 4.7: Controller block diagram of LQR output feedback with EKF wheel side-slip estimation based disturbance feedforward and curvature feedforward (LQR w. EKF).

5 Results

Within this chapter, the path tracking controllers' performance is studied in simulations and experiments. In a first step the test setup comprising experimental hardware, test field, simulation models, and various path tracking controllers is outlined. Subsequently, initial condition responses, disturbance step responses, steady-state cornering, and curved path tracking scenarios with transient cornering conditions are considered. Finally, the influence of varying parameters is studied.

5.1 Test Setup

5.1.1 Experimental Hardware and Test Field

Experiments have been performed using a John Deere 6210R tractor towing a custom built implement with a multitude of hydraulic steering actuators. A detailed description of this combination is provided in Appendix A.3. For this work's experiments implement wheel steering and front drawbar steering was used. All other implement actuators have been held in mid position and steering coulters were raised. Inner loop implement steering angle control was based on simple proportional control using ISO 11783 hydraulic valve flow commands as plant inputs and analog steering angle measurements as plant outputs. Tractor steering relied on a built-in tractor steering angle controller with a standard ISO 11783 Tractor Implement Automation (TIA) [ISO09] interface. It accepts curvature commands corresponding to desired steering angles and returns measured steering angles in a similar format. Tractor and implement position measurements were obtained with 10 Hz sample rate using John Deere SF 3000 GPS receivers augmented by RTK correction signals. Both tractor and implement were equipped with two GPS receivers each. The additional receivers were used to calculate the machine heading accurately. Obtaining tractor and implement position involves a projection of measurements from the antenna position to ground level which needs to account even for small vehicle roll and pitch angles. To perform this projection the receiver built-in IMU and Terrain Compensation Module (TCM) were used. A rapid prototyping platform providing Controller Area Network (CAN) interfaces and analog inputs was used to run the path tracking controller and the inner loop implement steering angle controllers.

Curved path tracking as well as path acquisition experiments have been performed on a level field of dry loam [LGB14]. Initially, the field was worked with a ripper and slightly compacted by repeated tractor passes. Subsequently, tests have been performed with

continuously shifted desired paths in order to prevent the creation of grooves due to multiple passes. Experiments on dry grassy slopes have been performed to a limited extent. However repeatability of those experiments as required for a sound statistical analysis could not be achieved. This was because changing desired paths also resulted in changing slope angles and maintaining a desired path resulted in creation of deep grooves.

5.1.2 Simulation Model

Simulations have been carried out using the most detailed model derived, which is the nonlinear dynamic tractor-implement model including transient tire forces as compiled in Section 3.1.6. Unless stated otherwise a tractor velocity of $v_{tr}^{x,t} = 3$ m/s and parameters as stated in Appendix A.5 are assumed. Those parameters resemble this work's tractor-implement experimental setup with tire parameters obtained on solid ground (asphalt). Scenarios deviating from those nominal simulation conditions will be considered by parameter variation. This includes changes of tire parameters accounting for loose soil.

Estimators in particular are affected by noisy sensor signals. For that reason all simulations, unless stated otherwise, account for noise by using additive white Gaussian noise models with parameters as stated in Appendix A.5. Steering angle sensor noise was added directly to simulation outputs. For GPS sensor measurements noise has been applied by first obtaining the four antenna positions from the simulated tractor and implement position and orientation. In a second step additive noise has been applied to those antenna position signals. Finally, the resulting noisy antenna position signals are used to calculate tractor and implement position and heading within the controller.

5.1.3 Path Tracking Controllers

Several control approaches as summarized in Section 4.7 have been studied. For future reference those are denoted as follows:

LQR w. I: LQR with subsequent output feedback approximation accounting for disturbances using integral control

LQR w. EKF: LQR with subsequent output feedback approximation accounting for disturbances using EKF based wheel side-slip estimation and disturbance feedforward control

LQR w/o I: LQR with subsequent output feedback approximation resulting in purely proportional control without measures to account for disturbances

Parameters are chosen as outlined in Appendix A.6. A tractor forward velocity of $v_{tr}^{x,t} = 3$ m/s was used for controller design if nothing different is stated. Comparison of different control approaches as stated above was performed using all desired steering angles ($\delta_{tf,d}$,

$\delta_{r1d,d}$, $\delta_{r1r,d}$) as plant inputs. In this case, tractor lateral error e_{tl} as well as implement lateral and heading error e_{r1l} and e_{r1h} are the controlled outputs. For 'LQR w. I' experiments with subsets of actuators and controlled variables have been performed. The resulting variants denoted by ① to ⑤ are summarized in Table A.4 of Appendix A.6. Less formally speaking those variants depict the following objectives:

①: Use all three steering inputs to control tractor lateral position as well as implement lateral position and heading.

②: Use tractor wheel steering and implement drawbar steering to control tractor and implement lateral position.

③: Use tractor wheel steering and implement wheel steering to control tractor and implement lateral position.

④: Use tractor wheel steering to control implement lateral position.

⑤: Use tractor wheel steering to control tractor lateral position, i.e. the implement is trailing the tractor in an uncontrolled manner.

Identical discrete time path tracking controllers have been used for simulations and experiments. The associated sample times are provided in Appendix A.6 as well. Desired paths are as outlined in Appendix A.4.

5.2 Initial Condition Responses

The first scenarios investigated in experiments as well as simulations are initial condition responses starting with a 1 m lateral offset from a desired path. The resulting lateral errors and measured steering angles are shown in Figures 5.1 and 5.2. In case of LQR w. EKF tractor and implement position as well as heading measurements are subject to additional filtering within the EKF (cf. Figure 4.7). In order to allow for better comparison with other control approaches the associated tracking errors as seen from unfiltered sensor signals are included and marked by (u). The influence of filtering in the given scenarios however is marginal.

Observation

From simulations and experimental results of Figure 5.1 can be seen that for LQR w. EKF lateral errors e_{tl} and e_{r1l} settle with a small overshoot of less than 10 cm. In experiment $|e_{tl}|$ remains below 50 cm after 6.6 m and below 10 cm after 10.6 m. For $|e_{r1l}|$ this is the case after 8.3 m and 14.4 m. LQR w. I in contrast exhibits a larger overshoot for e_{tl} and e_{r1l} which is typical for integral control. In experiments the overshoot was 25 cm and 20 cm respectively. In simulations it was even more pronounced. $|e_{tl}|$ remains below 50 cm after 5.9 m and below 10 cm after 15.4 m. For $|e_{r1l}|$ this is after 4.5 m and 17.5 m. Lateral

errors hence start diminishing quicker, yet settling takes longer. Differences in implement heading e_{r1h} were less pronounced for both approaches.

Considering variants of LQR w. I as shown in Figure 5.2 the variant ① was already discussed with Figure 5.1. ⑤ depicts the case of an uncontrolled implement. Here e_{r1l} initially exhibits an increase. This is due to the tractor hitch point first moving away from the desired path. This behavior is as expected knowing the transfer function from $\delta_{tf,d}$ to e_{r1l} is non-minimum phase. For ⑤ in experiments $|e_{r1l}|$ is below 50 cm after 10.8 m and below 10 cm after 14 m. Implement wheel steering (variant ③) results in a performance similar to variant ①. Wheel steering does not negatively influence implement heading. Variant ② with implement drawbar steering in contrast exhibits a worse performance with $|e_{r1l}|$ staying below 50 cm after 8.6 m and below 10 cm after 19.9 m. Variant ④ using tractor steering to control the implement lateral error took a very long time to settle in experiments and did not settle in simulations.

Regarding measured steering angles as shown in Figures 5.1 and 5.2 it can be seen that those are initially subject to steering angle rate limits.

Interpretation

Trying to achieve zero steady-state tracking errors via integral control comes at a price in terms of overshooting initial condition responses. In experiments the overshoots were moderate, yet resulted in an increased distance to settle within a 10 cm band of lateral errors, despite a quicker drop below 50 cm lateral errors. In simulations overshooting was more pronounced. This might be due to the rather simple second order lag model depicting steering actuator dynamics. In any case, care must be taken when acquiring a path with integral control. Measured steering angles showed that steering angle rate limits are encountered initially. Accounting for those rate limits in anti-windup therefore still offers possibility for improvement.

LQR w. I variant ④ in particular suffers from difficulties due to the double integrator non-minimum phase transfer function from $\delta_{tf,d}$ to e_{r1l}. In this case it seems advisable to acquire the track by different means, e.g. using tractor lateral error e_{tl} control prior to switching to e_{r1l} as controlled output.

Figure 5.1: Experimental and simulated initial condition responses depicting the acquisition of a straight desired path. Results have been obtained by instantaneously shifting the desired path laterally by 1 m. This was done after tractor and implement lateral errors had settled. Δs_d denotes the desired path arc length covered after the shift occurred. (u) denotes the lateral and heading errors as obtained from raw sensor measurements prior to EKF filtering.
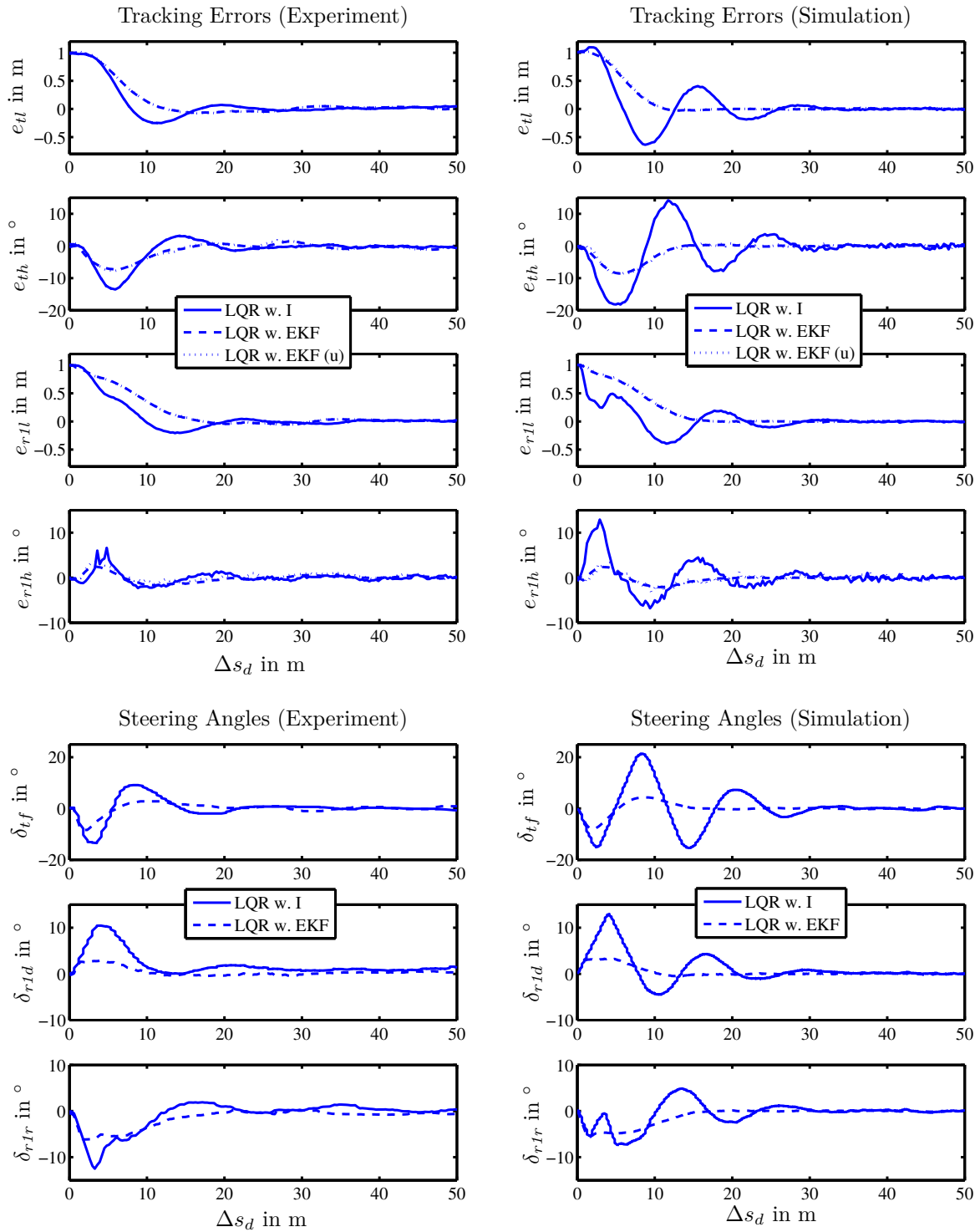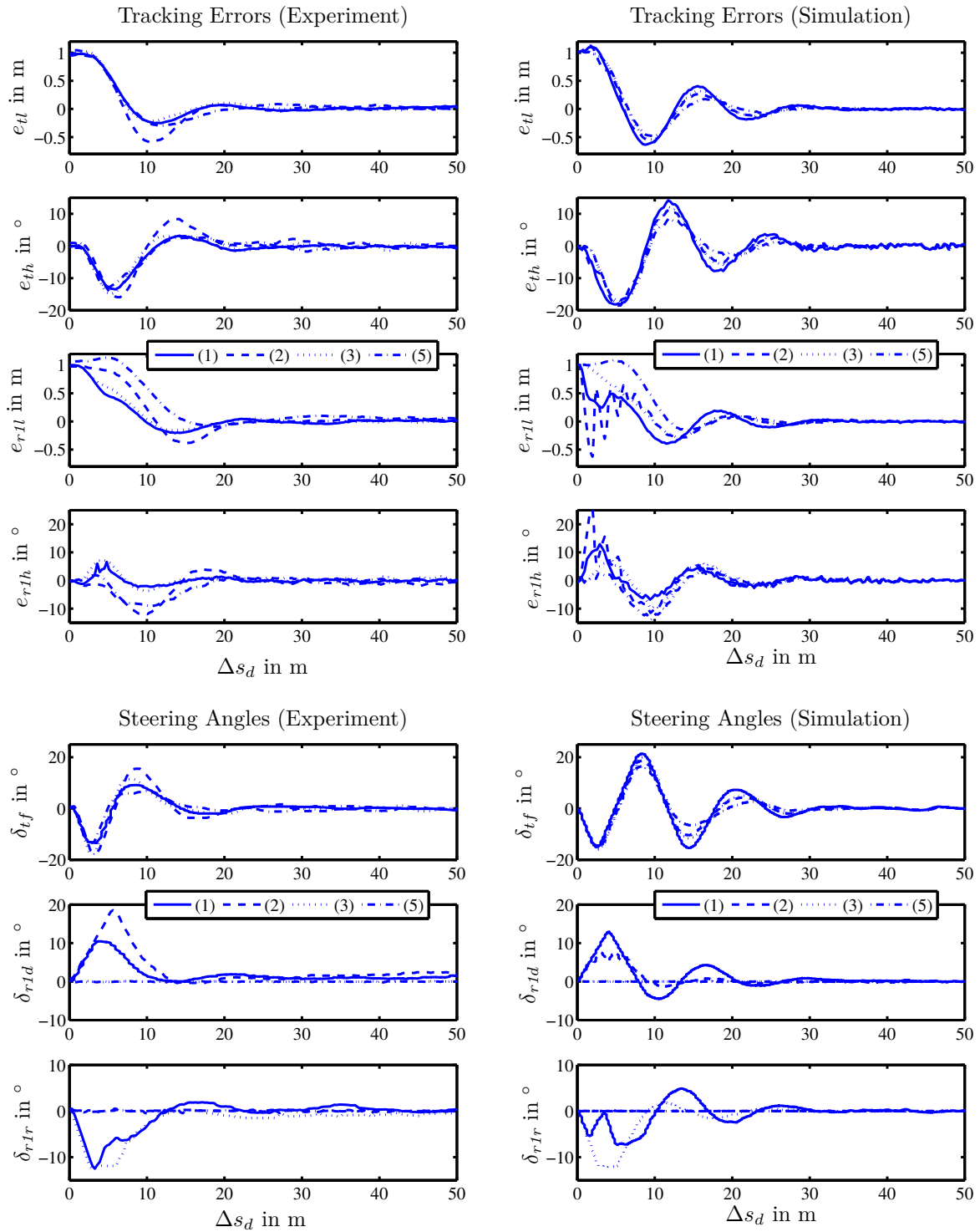
Figure 5.2: Experimental and simulated initial condition responses depicting the acquisition of a straight desired path. Results have been obtained by instantaneously shifting the desired path laterally by 1 m. This was done after tractor and implement lateral errors had settled. Δs_d denotes the desired path arc length covered after the shift occurred.

5.3 Disturbance Step Responses

Path tracking control in agriculture is subject to large disturbances resulting from lateral down-hill forces on sloped terrain. Simulations have been performed to assess the proposed controllers' performance subject to lateral disturbing force steps while tracking a straight desired path. The disturbing forces were chosen to act on tractor and implement c.g. in $\mathbf{e}_{y,t}$ and $\mathbf{e}_{y,r1}$ direction. Absolute values depict down-hill forces caused by an instantaneous side slope angle change from $0°$ to $20°$ considering m_t and m_{r1} respectively. The associated disturbance step responses are depicted in Figure 5.3. For LQR w. EKF in particular simulated wheel side-slip angles and the respective EKF estimates are shown Figure 5.4.

Observation

By first considering LQR w/o I in Figure 5.3 it becomes apparent that purely proportional output feedback results in large steady state lateral errors of 35 cm and 38 cm for the tractor and the implement. The implement heading error is very small. The tractor heading error is an uncontrolled output and remains nonzero for all control approaches. As a consequence the tractor is pointing slightly up-hill exhibiting a lateral velocity $v_t^{y,t}$ in steady state. LQR w. EKF uses the same proportional feedback control law yet is now accompanied by disturbance feedforward. With this measure steady-state e_{tl}, e_{r1l}, and e_{r1h} become very small. From Figure 5.4 can be seen that the EKF wheel side-slip angle estimates used for disturbance feedforward and the actual values within the simulation model coincide in steady-state. LQR w. I as an approach to account for disturbances allows to obtain vanishing e_{tl}, e_{r1l}, and e_{r1h} as well. This is the case if all three steering inputs are used and three controlled variables can be chosen (variant ①). In case of ③ and implement wheel steering only the remaining implement heading error is caused by the tractor hitch point running offset from the desired path due to a remaining e_{th}. As a consequence the implement is pointing slightly down-hill. Variant ②, with implement drawbar steering only, in contrast, results in a steady-state condition with an up-hill pointing implement and a non-vanishing e_{r1h} of opposite sign. In case of an unsteerable implement zero steady-state error can only be achieved for one controlled output. In case of ④ and ⑤ this is the implement lateral error and the tractor lateral error respectively. Either the tractor is offset 25 cm up-hill or the implement follows 25 cm down-hill.

Interpretation

From large steady-state lateral errors obtained in simulations it appears that purely proportional control is not capable of coping with disturbances that result from wheel side-slip on sloping terrain. This impression was also supported by preliminary experiments on slopes. LQR w. I and LQR w. EKF using either integral control or disturbance feedforward in contrast was found capable of compensating the steady-state influence of wheel side-slip. It is worth noting, however, that wheel side-slip was the only disturbance in those simulations. As a consequence LQR w. EKF encountered ideal conditions. In practice additional disturbances of different origin might contribute to path tracking errors.
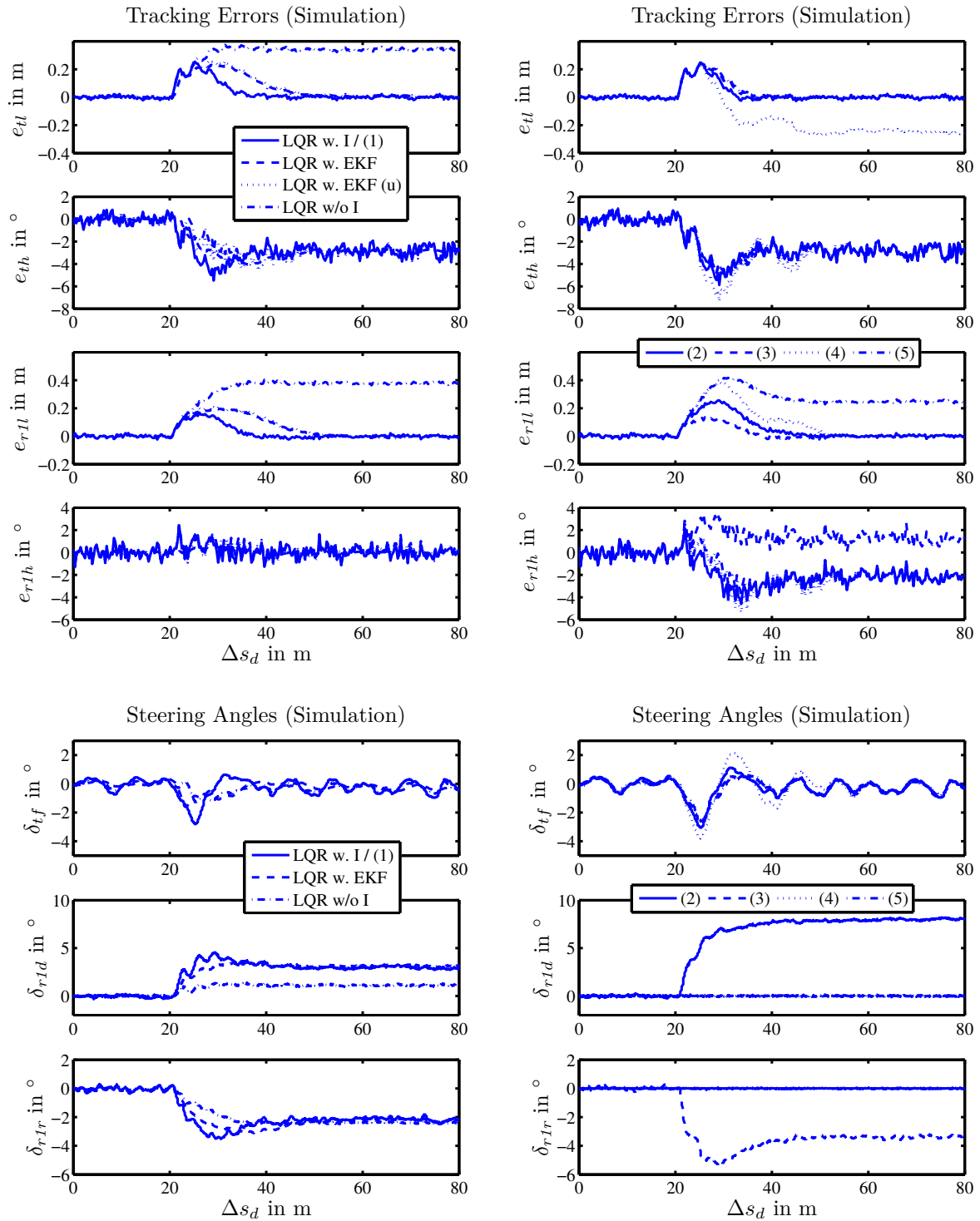
Figure 5.3: Simulated disturbance step responses following lateral tractor and implement force steps. These forces act on tractor and implement c.g. in $\mathbf{e}_{y,t}$ and $\mathbf{e}_{y,r1}$ direction and are chosen to depict an instantaneous side slope angle change from $0°$ to $20°$. Δs_d denotes the desired path arc length covered. The disturbance step was applied at $\Delta s_d = 20$ m. (u) denotes the lateral and heading errors as obtained from raw sensor measurements prior to EKF filtering.

Figure 5.4: Simulation results showing actual wheel side-slip angles α_{tf}, α_{tr}, α_{r1r} and respective EKF estimates $\hat{\alpha}_{tf}$, $\hat{\alpha}_{tr}$, $\hat{\alpha}_{r1r}$ in case o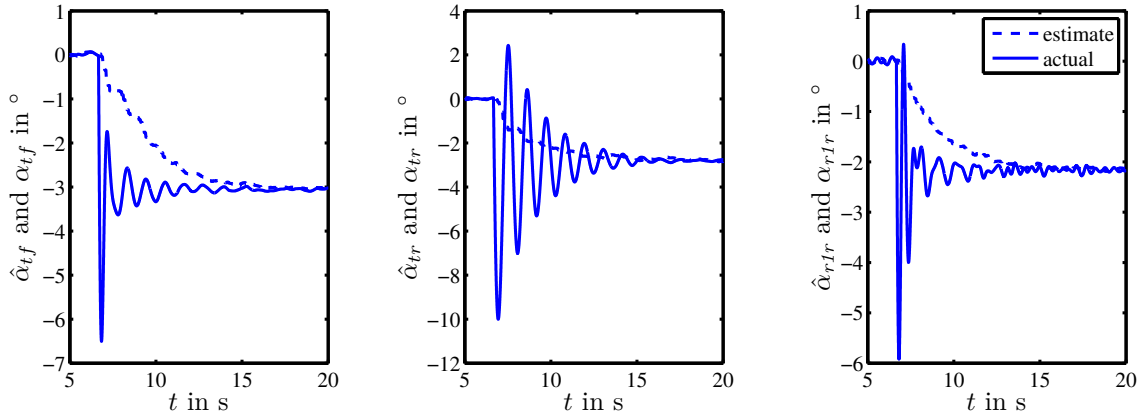f a disturbance step caused by lateral tractor and implement forces. These forces act on tractor and implement c.g. in $\mathbf{e}_{y,t}$ and $\mathbf{e}_{y,r1}$ direction and are chosen to depict an instantaneous side slope angle change from 0° to 20°.

5.4 Steady-State Cornering

All control approaches and steering input variants have been assessed in experiments on a circular desired path with 20 m radius. In each case 3 full left curve circles and 3 full right curve circles served as basis for statistical analysis. Lateral and heading errors for left curves have been multiplied by -1 to obtain always positive lateral errors for radii larger than the desired path radius. Statistical results are depicted in Figure 5.5. For LQR w. EKF in addition side-slip angle estimates obtained from experiments are outlined in Figure 5.6. In comparison simulation results depicting the principle expectation with side-slip as only disturbance are provided in Figure 5.7.

Observation

Results for LQR w/o I as shown in Figure 5.5 again exhibit large lateral errors with 13.1 cm and 12.3 cm mean for tractor and implement respectively. Approaches accounting for wheel side-slip show better results. Tracking errors for LQR w. EKF however are non-zero mean with -2.0 cm, 1.3 cm and -0.4° for e_{tl}, e_{r1l}, and e_{r1h}. The respective SDs are 3.2 cm, 2.2 cm and 0.3° if filtered receiver position and heading signals as seen by the path tracking controller are used. EKF filtering has an only slightly notable influence on the implement heading error. LQR w. I actually achieves zero mean tracking errors for all controlled outputs. In case of all three steering inputs (variant ①) standard deviations for e_{tl}, e_{r1l}, and e_{r1h} are 3.2 cm, 2.0 cm and 0.7°. Lateral errors for variants ② (implement drawbar steering only) and ③ (implement wheel steering only) are comparable with ①. The large implement heading error in case of ③ is inevitable on curves making drawbar steering per se a better choice if e_{r1h} matters. In case of tractor steering only a single controlled output remains. Variant ④ places the implement with zero mean and 3.1 cm

SD the tractor is forced to leave the path with a mean lateral error of 28.2 cm. Variant ⑤ in contrast accounts for tractor path tracking with a SD of 3.3 cm. The implement cuts corners with a lateral error mean of -27.7 cm.

Returning to LQR w. EKF, simulation results for side-slip estimates as depicted in Figure 5.7 raise the expectation of symmetric graphs in case of left and right curves. Wheel side-slip angles are expected to be all positive for left curves and all negative for right curves due to centripetal forces. Actual experimental results as depicted in Figure 5.6 however do not resemble this completely and implement wheel side-slip estimates were found to be of opposite sign. It is worth noting that the remaining difference between actual and estimated wheel side-slip angles in Figure 5.7 could be reduced by increasing the sample time used for EKF propagation, which results in an improved discrete time approximation of the original continuous time model ODEs.

Interpretation

From the experimental results shown above one may conclude that LQR w/o I is not sufficient for curved path tracking and the additional measures to account for disturbances resulting from wheel side-slip are actually necessary. LQR w. I exhibits the advantage that zero steady-state path tracking errors can be achieved regardless of the (constant) disturbances' origin. For LQR w. EKF disturbances from other origins like small steering angle sensor offsets or hardware tolerances may either result in non-zero steady-state tracking errors or wheel side-slip estimates deviating from the actual values. With both LQR w. EKF and LQR w. I the lateral error SDs of 3.2 cm or less are already close to what the given sensor accuracy actually permits (cf. Appendix A.3). In case of LQR w. EKF implement heading information was filtered most. This is a consequence of having a higher heading sensor noise variance than the tractor (see Appendix A.6.5) which in turn results from a shorter distance between both implement GPS receiver antennas. Using a filtered heading information might be beneficial in this case.
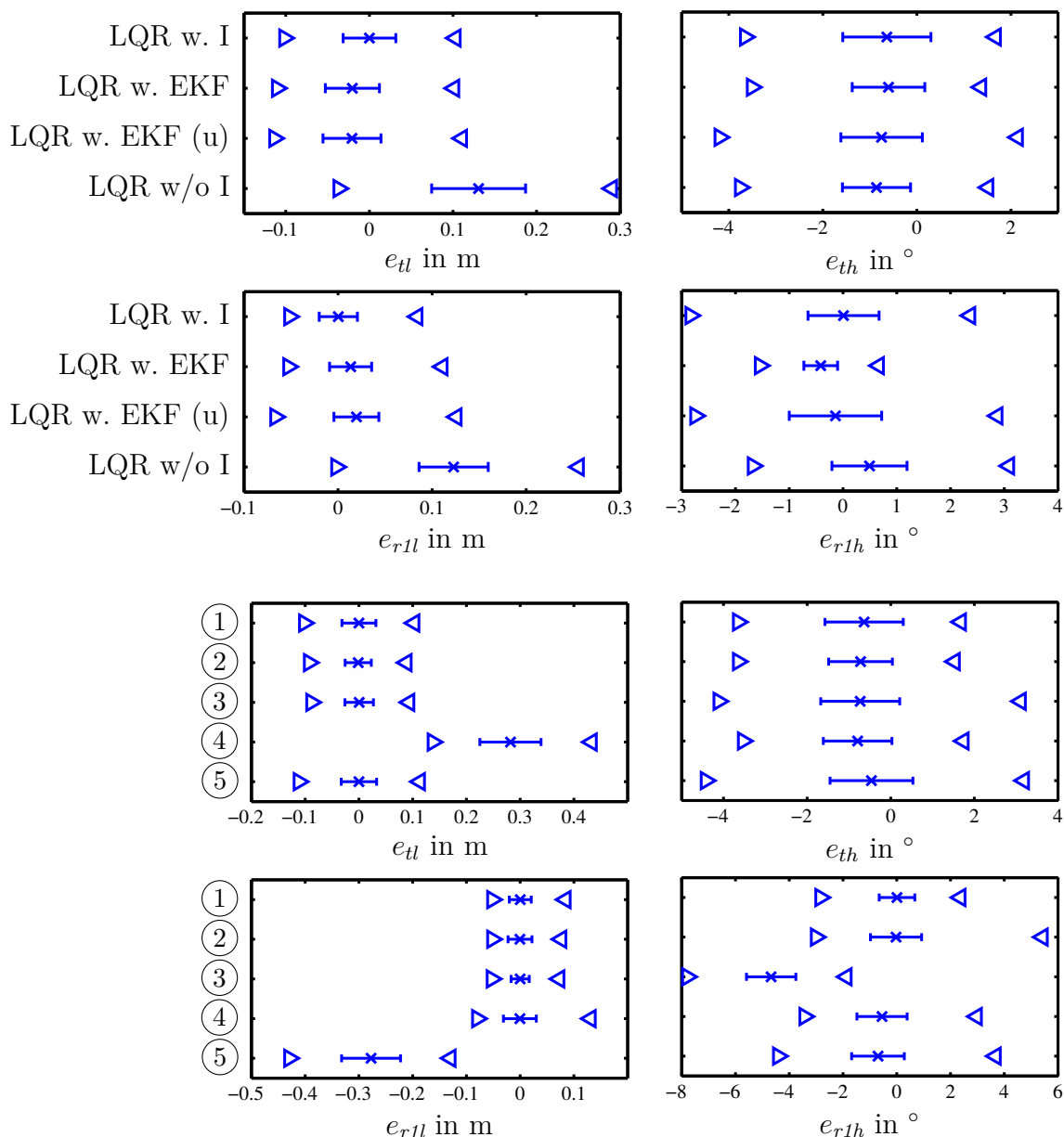
Figure 5.5: Experimental results for tracking a circular path with 20 m radius. Depicted are min-max ranges (▷ ◁), standard deviations (⊢⊣), and mean values (×) of all tracking errors. Each result was obtained from 3 full circles steering left and 3 full circles steering right. Tractor forward velocity was $v_{tr}^{x,t} = 3$ m/s. For analysis lateral and heading errors on left curves have been multiplied by -1, which means positive lateral errors always indicate larger radii. (u) denotes the lateral and heading errors as obtained from raw sensor measurements prior to EKF filtering.

Figure 5.6: Experimental results for tracking a circular path with 20 m radius. Depicted are wheel side-slip angle estimates $\hat{\alpha}_{tf}$, $\hat{\alpha}_{tr}$, $\hat{\alpha}_{r1r}$ while either steering left or right.
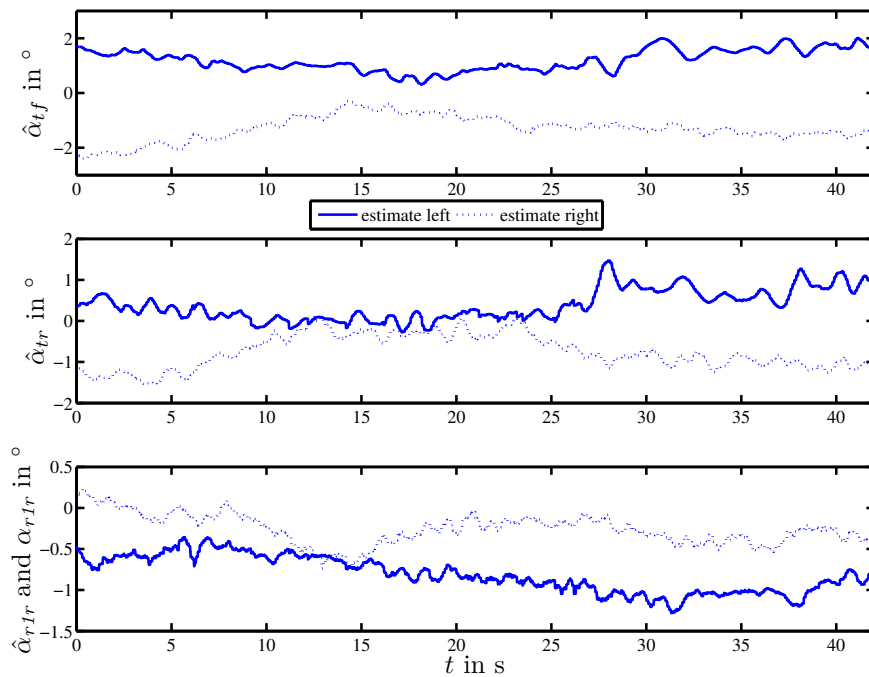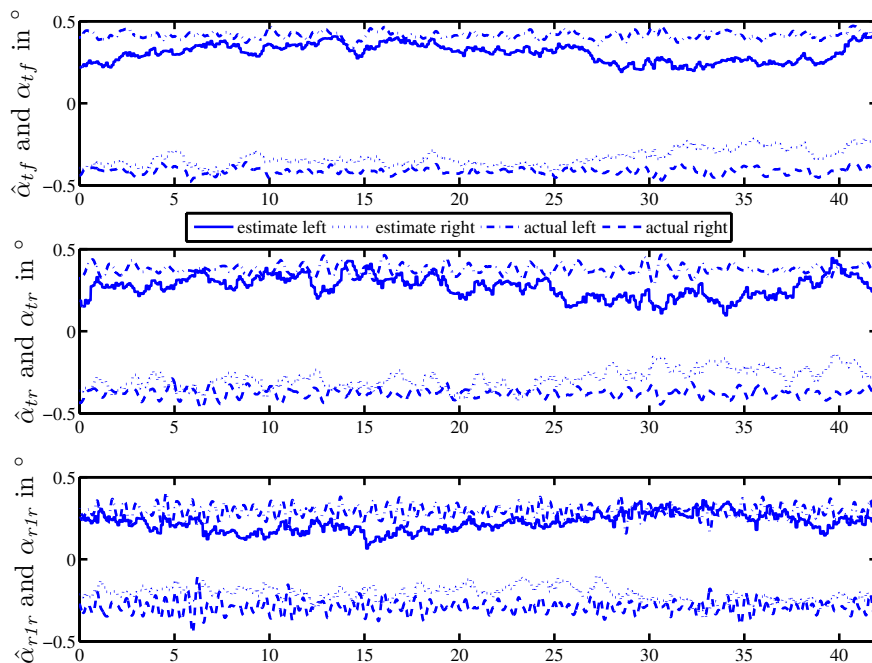

Figure 5.7: Simulation results for tracking a circular path with 20 m radius. Depicted are the wheel side-slip angles α_{tf}, α_{tr}, α_{r1r} and respective EKF estimates $\hat{\alpha}_{tf}$, $\hat{\alpha}_{tr}$, $\hat{\alpha}_{r1r}$ while either steering left or right. Note that the tire parameters used represent the nominal case as identified on asphalt.

5.5 Curved Path Tracking

Curved path tracking has been investigated using the desired paths C1 (max. curvature $1°/m$, curvature change rate $0.1°/m^2$) and C3 (max. curvature $3°/m$, curvature change rate $0.3°/m^2$) consisting of straights, clothoids, and arc segments as defined in Appendix A.4.

Again, experiments were performed on a level field of dry loam. Tractor forward speed was $v_{tr}^{x,t} = 3$ m/s. 6 passes with 3 in each direction have been recorded and used for statistical analysis of tracking errors. Analysis started with the tractor rear axle entering the first curve and ended with the implement axle leaving the last curve. The respective results are summarized in Figures 5.8 and 5.9. For C3 exemplary tracking error and steering angle plots over the arc length covered are given in Figure 5.12.

For comparison and later use in a parameter variation study simulations have been performed using curve C3 and nominal simulation parameters, i.e. those obtained on asphalt. Statistical analysis of those simulation results is provided in Figure 5.10. An exemplary tracking error and steering angle plot is given in Figure 5.13. Finally, in order to assess the influence of curvature feedforward on implement path tracking, simulations have been performed omitting implement curvature feedforward. Tractor curvature feedforward was maintained, as it is already known to be a crucial part in path tracking. The results are summarized in Figure 5.11.

Observation

Results for tracking path C1 as shown in Figure 5.8 outline rather minor differences between LQR w. EKF and LQR w. I. The SDs for controlled outputs e_{tl}, e_{r1l}, and e_{r1h} are 4.1 cm, 3.6 cm, and $0.3°$ $(0.6°$ unfiltered) in one case and 2.9 cm, 1.9 cm, and $0.5°$ in the other. Both results, however, exhibit zero mean tracking errors for the given symmetric path.

Variants ① (all steering inputs), ② (implement drawbar steering only), ③ (implement wheel steering only) for LQR w. I result in very similar lateral errors. Implement heading is an uncontrolled output for ② and ③. In case of drawbar steering the implement heading error is slightly increased. Wheel steering again suffers from introducing a heading error while trying to track the curved path. In case of tractor path tracking only ⑤ with tractor lateral error as controlled output results are comparable to previous variants. The uncontrolled implement however is cutting corners. Variant ④ using tractor steering for implement path tracking control fails to achieve accurate implement control while the tractor is off-track as well.

Path C3 compared to C1 exhibits a larger maximum curvature as well as an increased curvature change rate. Results depicted in Figure 5.9 show a similar pattern, yet SDs for controlled outputs e_{tl}, e_{r1l}, and e_{r1h} are increased. For LQR w. EKF those are 7.1 cm, 7.1 cm, and $0.4°$ $(0.7°$ unfiltered). For LQR w. I one obtains 5.6 cm, 3.1 cm, and $0.5°$.

Considering path C3 in simulations yields results as shown in Figure 5.10. Results obtained for those nominal conditions exhibit tracking errors with zero means. SDs are below those found in experiments on dry loam. For e_{tl}, e_{r1l}, and e_{r1h} one obtains 3.6 cm, 2.7 cm, and 0.1° for LQR w. EKF as well as 3.0 cm, 1.4 cm and 0.5° in case of LQR w. I.

If implement curvature feedforward is omitted as shown in the simulation results of Figure 5.11 the implement path tracking accuracy suffers compared to the previous results of Figure 5.10. The resulting SDs for e_{r1l} and e_{r1h} are 15 cm and 1.8° (LQR w. EKF) as well as 10 cm and 1.3° (LQR w. I).

Finally, tracking errors and steering angle plots as shown in Figures 5.12 and 5.13 unsurprisingly reveal that large lateral errors in simulations as well as experiments coincide with changing curvature. Tractor front wheel and implement drawbar steering angles as shown obtain their largest signal part from curvature feedforward.

Interpretation

This section's results for different curves as well as previous results for steady-state cornering illustrate that comparing different approaches in non-steady state conditions requires the use of identical paths. In those conditions there will not be a single number describing the accuracy of a controller. For LQR w. I on path C1 and C3 lateral errors in experiment remained below 3 cm and 6 cm SD respectively. This was for all variants using a steerable implement. Experimental results for LQR w. EKF ranged slightly above. This however might be due to small differences in transient behavior of side-slip estimation and integral control. Spending increased effort on fine tuning both for a particular scenario might turn the outcome.

In case of three steering inputs implement heading was made a controlled variable. From the above results this effort seems unnecessary if implement drawbar steering is used and the terrain is flat. However, as seen from previous results in Figure 5.3, path tracking on slopes benefits from wheel steering rather than drawbar steering. If path tracking on curves and slopes is intended using two implement steering actuators therefore is advantageous.

Controlling the implement lateral position with tractor steering only (variant ④) exhibited poor performance on the considered curved paths. This might be due to the current state of tractor feedforward control which was designed for tractor and implement driving on one identical path. If controlling unsteered implements was in focus, planning a separate tractor path accounting for the required offsets as done in [KT08] could be beneficial.

From simulation results using path C3 it was seen that curvature feedforward is an important part of accurate implement control.
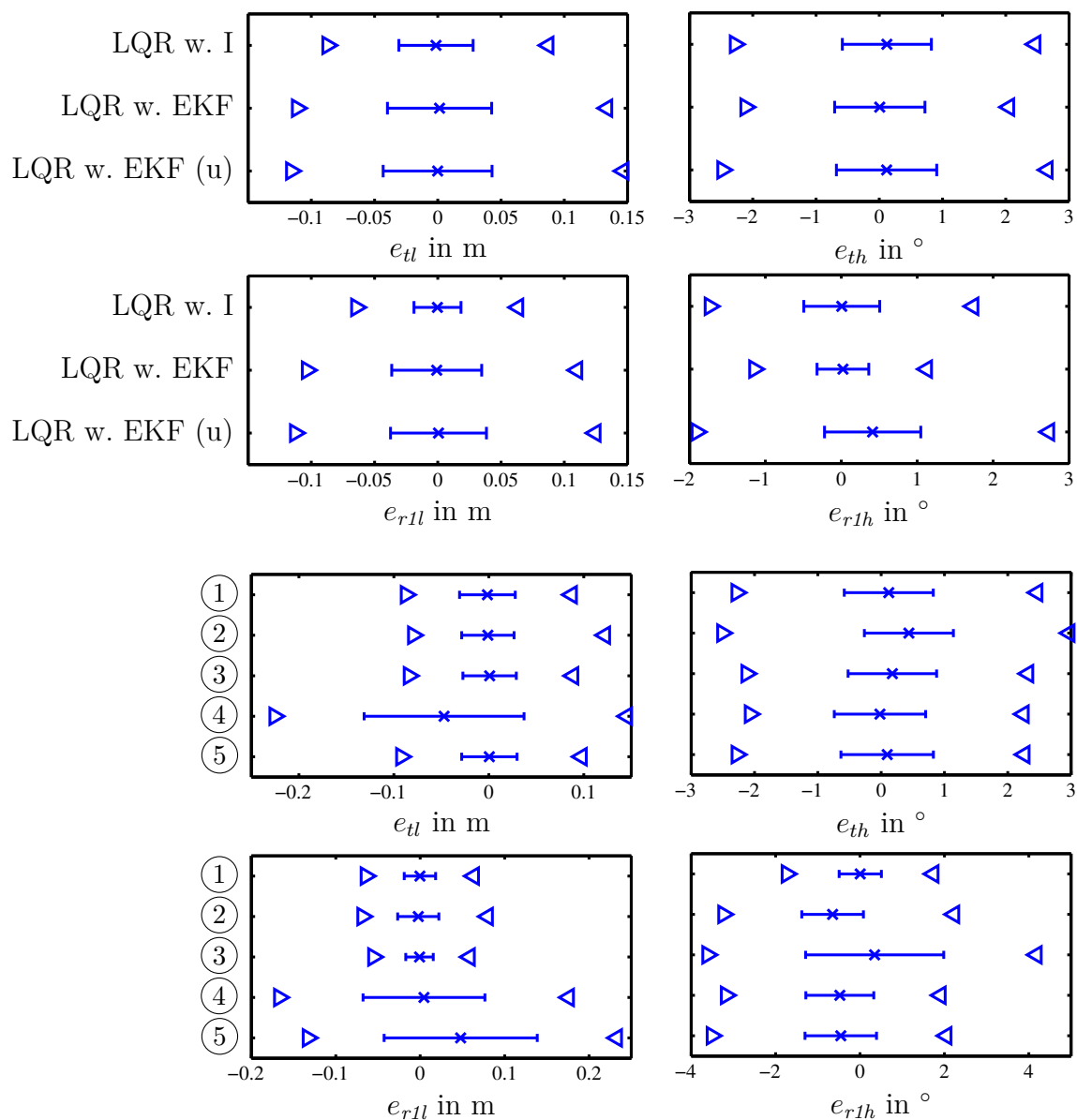
Figure 5.8: Experimental results for tracking path C1. Depicted are min-max ranges (▷ ◁), standard deviations (⊢⊣), and mean values (×) of all tracking errors. Each result was obtained from 6 passes with 3 in each direction. Tractor forward velocity was $v_{tr}^{x,t} = 3$ m/s. (u) denotes the lateral and heading errors as obtained from raw sensor measurements prior to EKF filtering.
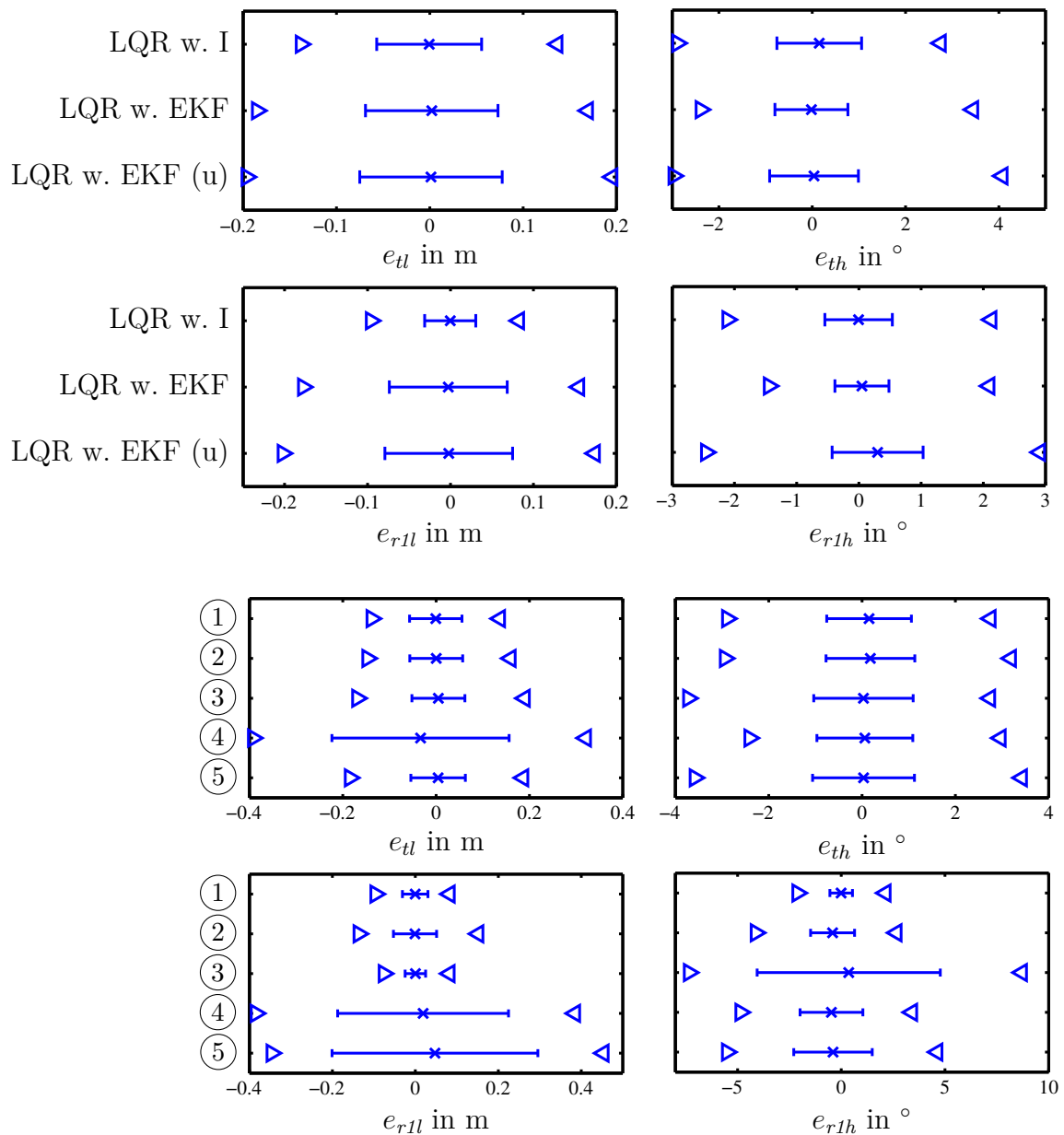
Figure 5.9: Experimental results for tracking path C3. Depicted are min-max ranges (▷ ◁), standard deviations (⊢⊣), and mean values (×) of all tracking errors. Each result was obtained from 6 passes with 3 in each direction. Tractor forward velocity was $v_{tr}^{x,t} = 3$ m/s. (u) denotes the lateral and heading errors as obtained from raw sensor measurements prior to EKF filtering.
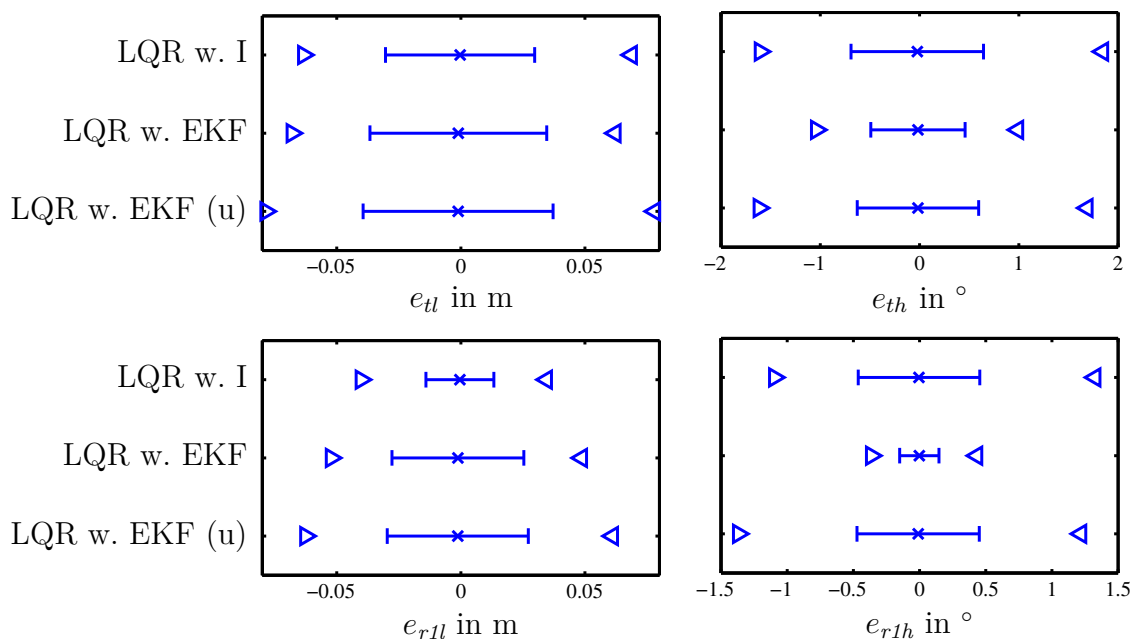
Figure 5.10: Simulation results for tracking path C3. Depicted are min-max ranges ($\triangleright\triangleleft$), standard deviations ($\vdash\dashv$), and mean values ($\times$) of all tracking errors. Each result was obtained from 6 passes with 3 in each direction. Tractor forward velocity was $v_{tr}^{x,t} = 3$ m/s. (u) denotes the lateral and heading errors as obtained from raw sensor measurements prior to EKF filtering.
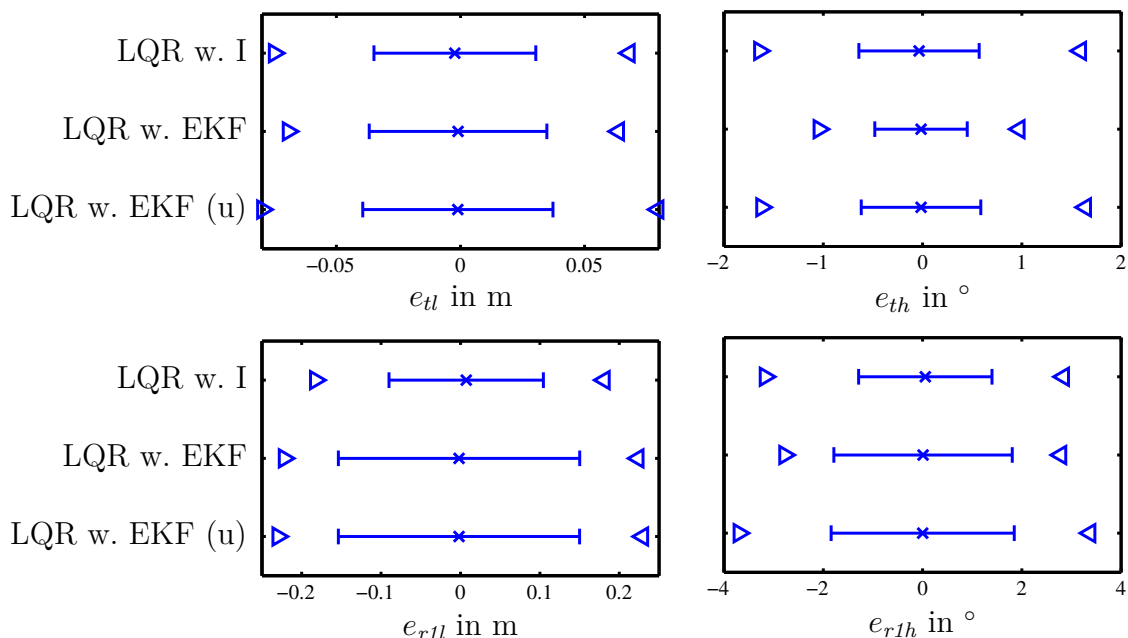
Figure 5.11: Simulation results for tracking path C3 without implement curvature feed-forward. Depicted are min-max ranges ($\triangleright\triangleleft$), standard deviations ($\vdash\dashv$), and mean values ($\times$) of tracking errors. Each result was obtained from 6 passes with 3 in each direction. Tractor forward velocity was $v_{tr}^{x,t} = 3$ m/s. (u) denotes the lateral and heading errors as obtained from raw sensor measurements prior to EKF filtering.
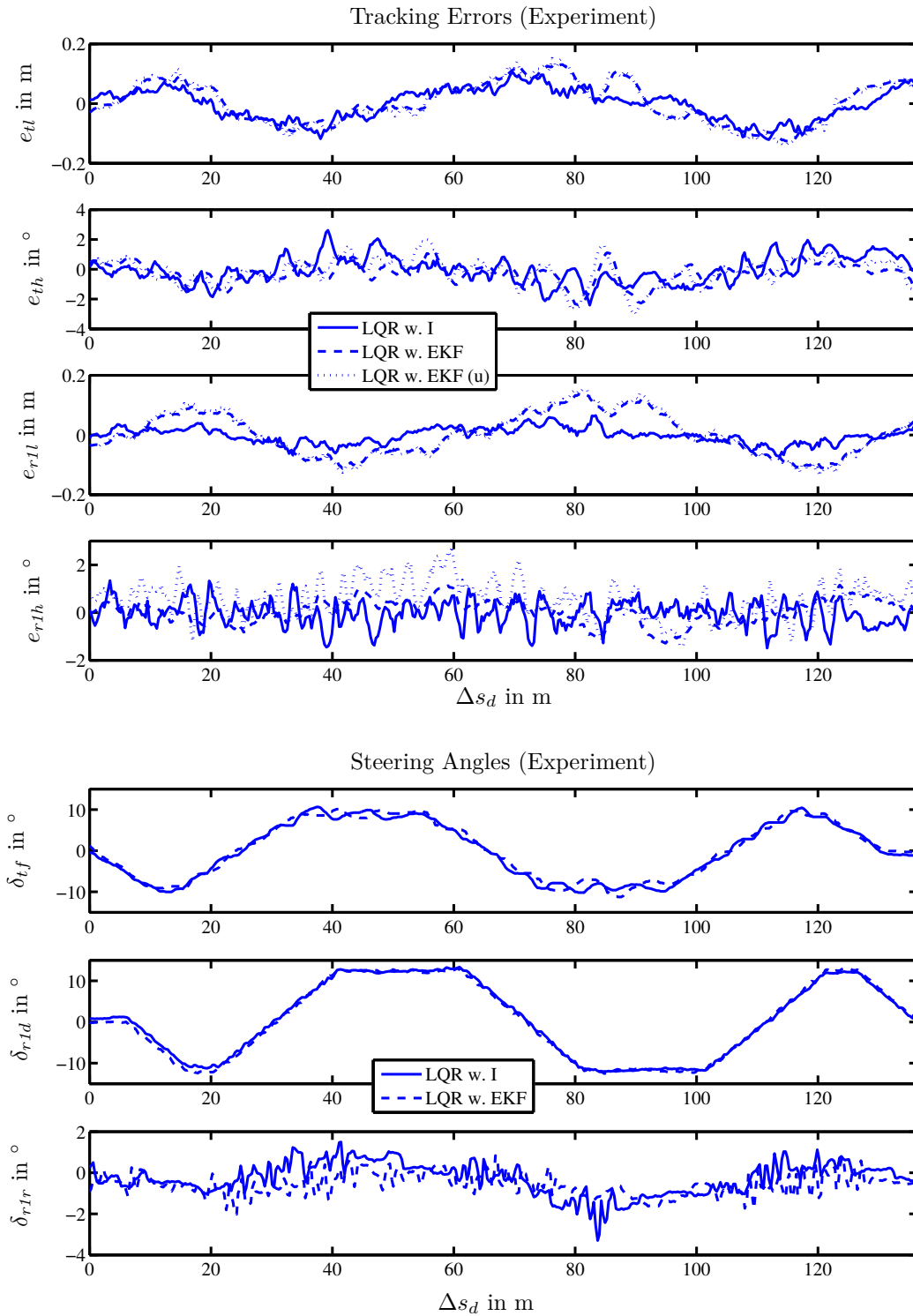
Figure 5.12: Experimental results for tracking path C3. Depicted are tracking errors and measured steering angles over the arc length Δs_d covered. Tractor forward velocity was $v_{tr}^{x,t} = 3$ m/s. (u) denotes the lateral and heading errors as obtained from raw sensor measurements prior to EKF filtering.

Figure 5.13: Simulation results for tracking path C3. Depicted are tracking errors and measured steering angles over arc length Δs_d covered. Tractor forward velocity was $v_{tr}^{x,t} = 3$ m/s. (u) denotes the lateral and heading errors as obtained from raw sensor measurements prior to EKF filtering.
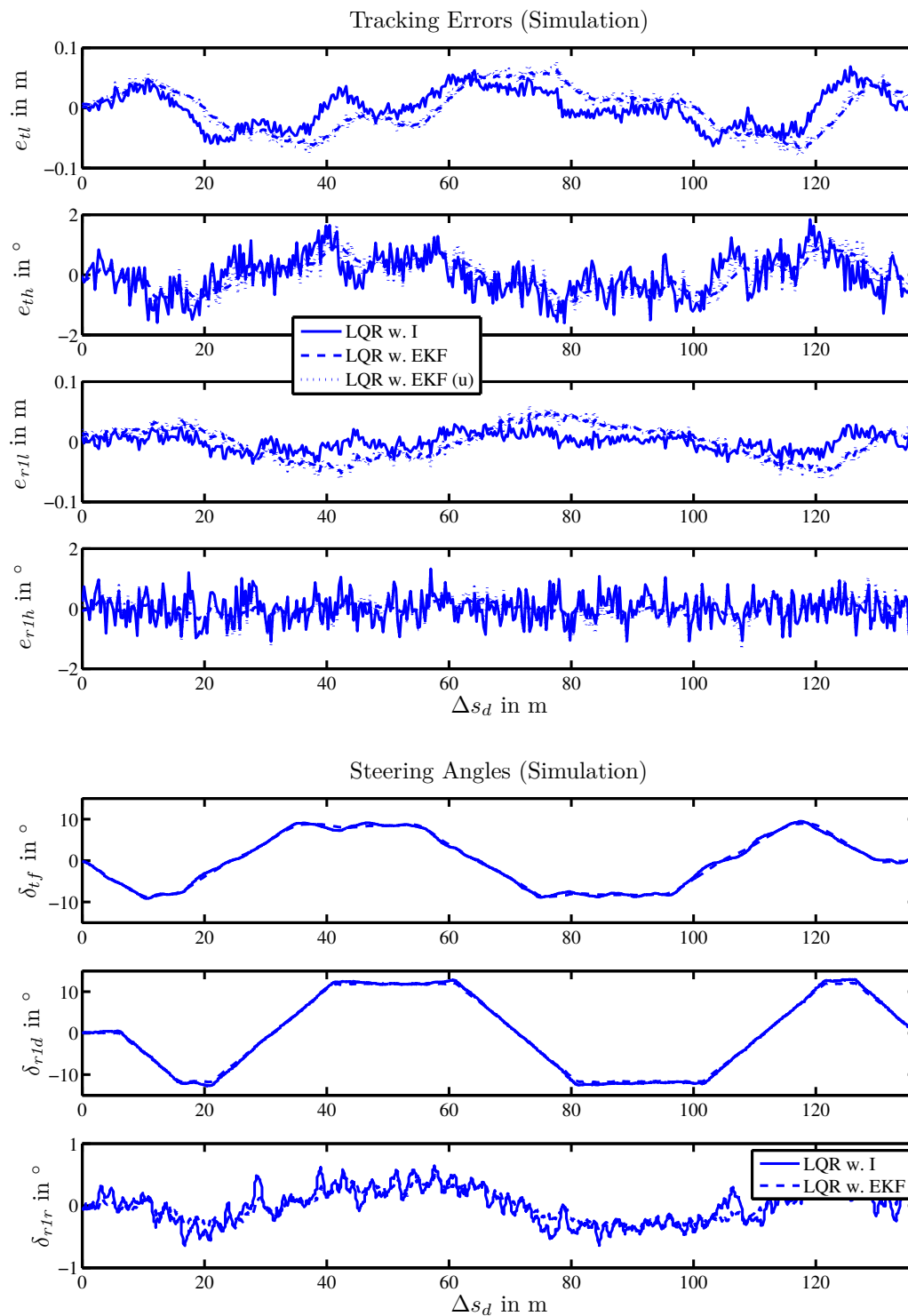
5.6 Parameter Variation Study

Tractor longitudinal velocity $v_{tr}^{x,t}$ has a pronounced influence on the system under control, as seen in Chapter 3. Controller design so far assumed a fixed velocity of 3 m/s. Similarly, experiments and simulations were performed at this nominal velocity. In this section the influence of a varying tractor velocity is studied. For that reason step response and curved path tracking experiments have been performed while $v_{tr}^{x,t}$ was either matching or deviating from the nominal value used for controller design. The results are outlined in Figure 5.14 and 5.15.

In addition simulations were performed to study the influence of varying model parameters. The nominal simulation model with parameters as stated in Appendix A.6.1 is used as a reference. Simulations were performed using path C3 and $v_{tr}^{x,t} = 3$m/s. The system remained stable for all variations performed. The resulting changes in tracking errors are summarized in Figures 5.16, 5.17, and 5.18. The resulting SDs are presented relative to the nominal results as shown in Figure 5.10. Simulations resulted in zero mean tracking errors and mean values are not stated for that reason. As a remark it should be noted that comparison of absolute values Δ SD between tractor and implement must be considered with care, because those differ significantly in terms of inertial and tire properties.

Observation

Comparing LQR w. EKF with LQR w. I, as done in Figure 5.14, reveals that step responses for LQR w. EKF are little susceptible to changes in tractor forward velocity. LQR w. I in contrast exhibits a tendency towards oscillations if the tractor forward velocity deviates widely from $v_{tr}^{x,t} = 3$m/s as used for controller design. Recalculating the controller by using identical weights and only changing the velocity parameter, however, allows to prevent those oscillations and obtain a very short settling distance. Similar observations can be made from tracking error statistics in Figure 5.15. Recalculating the controller using the correct velocity resulted in very small tracking errors.

Reducing the cornering stiffnesses by 50% in simulation as shown in Figure 5.16 had a strong deteriorating influence in transient path tracking conditions of path C3. This was true for all considered cases. Varying $C_{\alpha,tf}$ had the most influence on both tractor and implement lateral errors. Varying $C_{\alpha,r1r}$ only influenced the implement itself. Comparing LQR w. EKF and LQR w. I exhibits similar tendencies with slight differences in reaction to changes of $C_{\alpha,tf}$ and $C_{\alpha,tr}$.

Varying the tire relaxation lengths by 50%, as depicted in Figure 5.17, had a very small influence of less than 5% on tracking error SDs. This was true in all cases, even when changes were combined.

Varying the tractor mass as shown in Figure 5.18 influenced both the tractor and the implement lateral errors. Varying the implement mass, in contrast, mostly affected the implement itself. Varying the moments of inertia by 50% had little influence for I_t and almost no influence for I_{r1}. Shifting the tractor c.g. towards the rear axle appeared to be beneficial, shifting it to the front deteriorated results. This is, however, without considering changes in cornering stiffnesses due to wheel load transfer. Shifting the implement c.g. was less influential.

Interpretation

The most important conclusion from above observations is, that LQR w. I must account for changing velocities. In practical applications this could be achieved, for instance, by adjusting the controller in a gain scheduling manner.

For all other plant parameters varied the closed loop remained stable in simulations. For integral control in particular this at least suggests that the controller is robust and remains stable in a parameter range not too small for practical applications. This means, once the overall controller gain is set for a particular field and tractor-implement combination, moderate parameter changes will not require controller readjustment.

Simulations of transient conditions while tracking path C3 unsurprisingly showed that cornering stiffnesses have a large influence on path tracking accuracy. While there are few possibilities of altering soil conditions to increase cornering stiffness, lowering tire inflation pressure (cf. Table 2.1) or using dual tires are design measures that could be taken to improve the system.
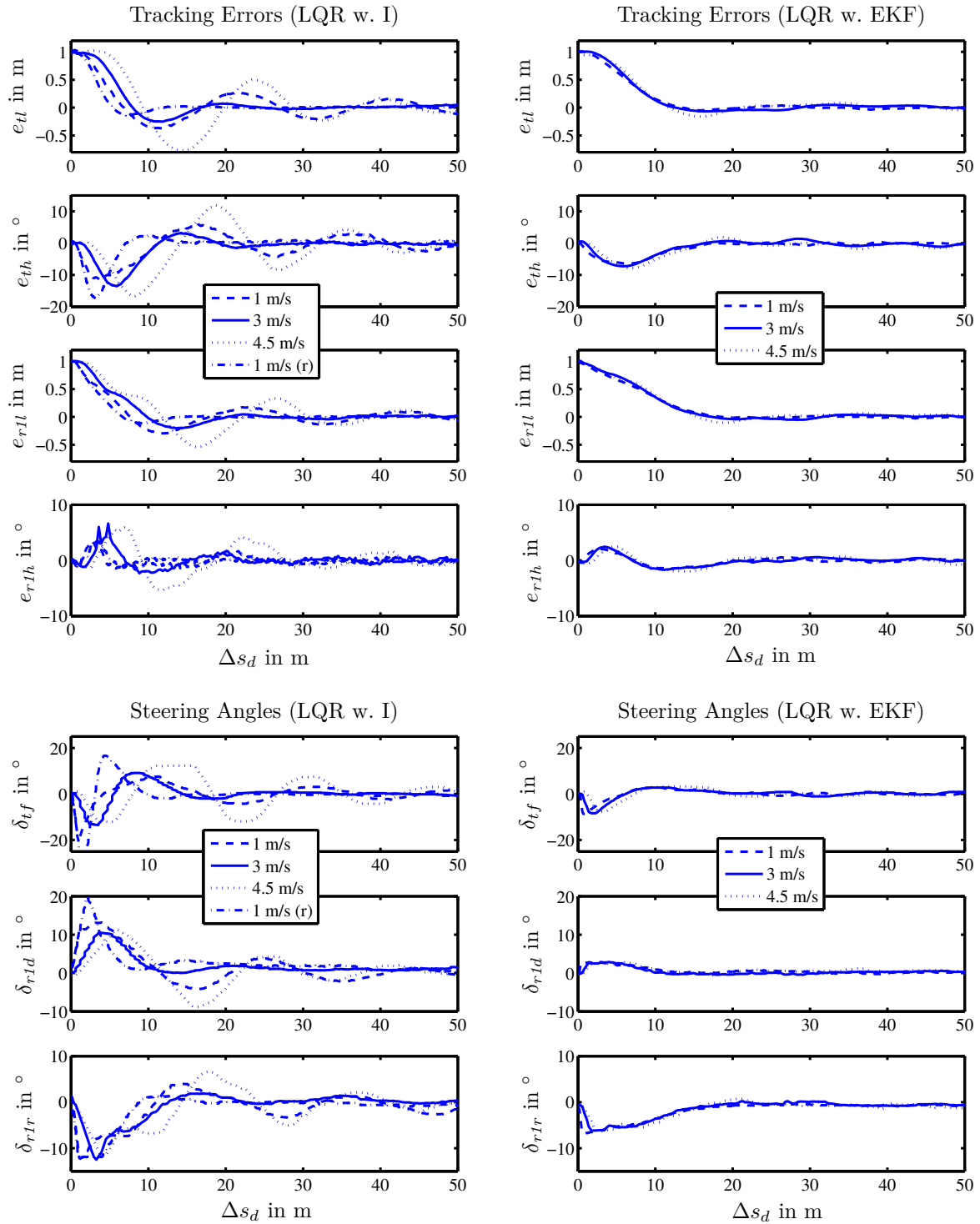
Figure 5.14: Experimental initial condition responses depicting the acquisition of a straight desired path using various tractor forward velocities $v_{tr}^{x,t}$. Results have been obtained by instantaneously shifting the desired path laterally by 1 m. This was done after tractor and implement lateral errors had settled. Controller design assumed $v_{tr}^{x,t} = 3$ m/s for all results except the last denoted by (r). In this case the controller was recalculated using identical weights yet assuming $v_{tr}^{x,t} = 1$ m/s. Δs_d denotes the desired path arc length covered after the shift occurred.
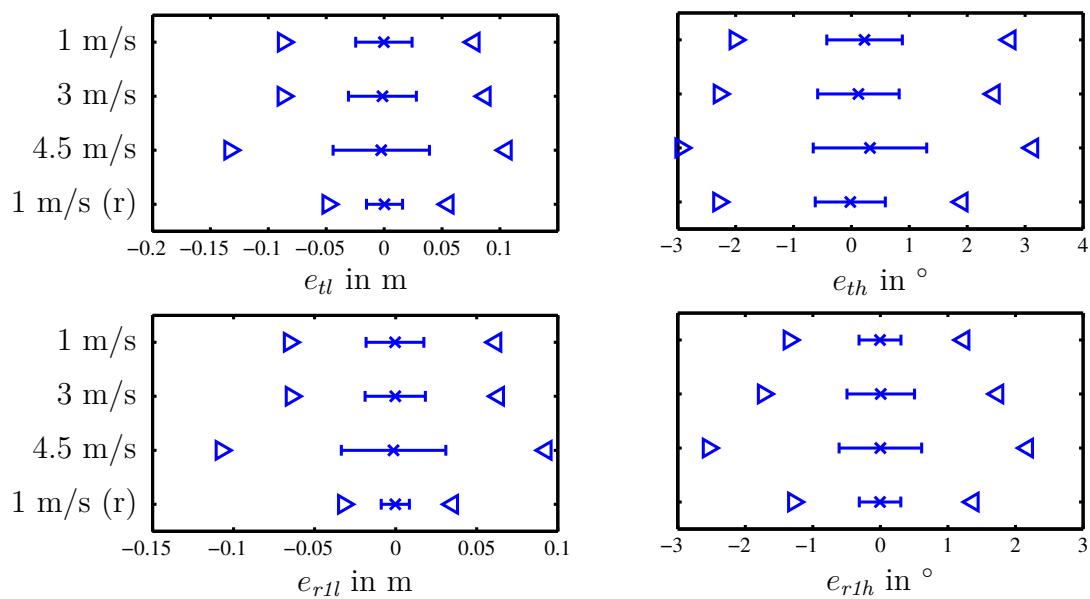
Figure 5.15: Experimental results for tracking path C1 using various tractor forward velocities $v_{tr}^{x,t}$. Depicted are min-max ranges ($\triangleright \triangleleft$), standard deviations ($\vdash\dashv$), and mean values ($\times$) of tracking errors. Each result was obtained from 6 passes with 3 in each direction. Controller design assumed $v_{tr}^{x,t} = 3$ m/s for all results except the last denoted by (r). In this case the controller was recalculated using identical weights yet assuming $v_{tr}^{x,t} = 1$ m/s.
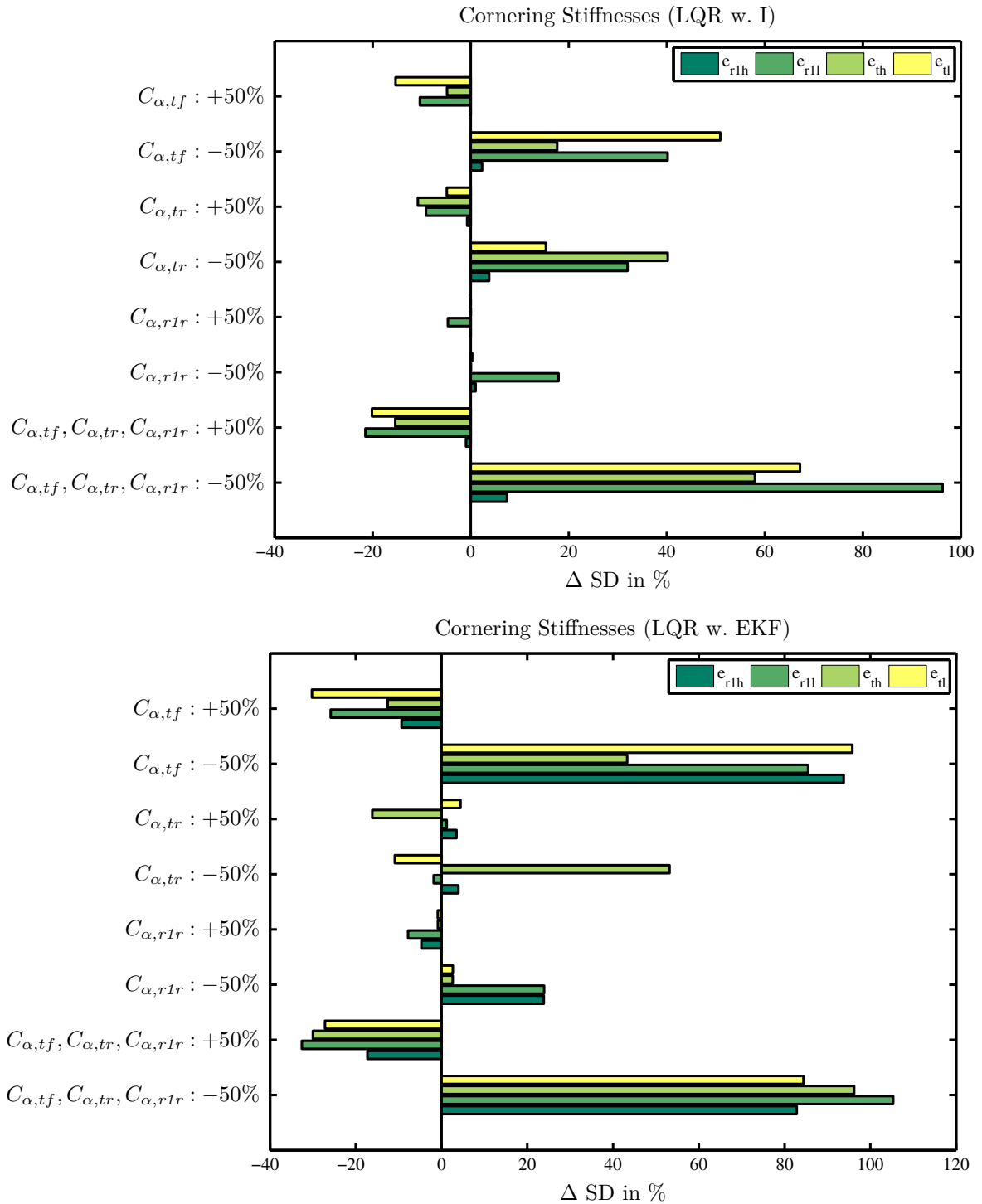
Figure 5.16: Simulation results for tracking path C3 with varying simulation model parameters. Δ SD denotes the resulting change in tracking error standard deviations relative to nominal results as presented in Figure 5.10.
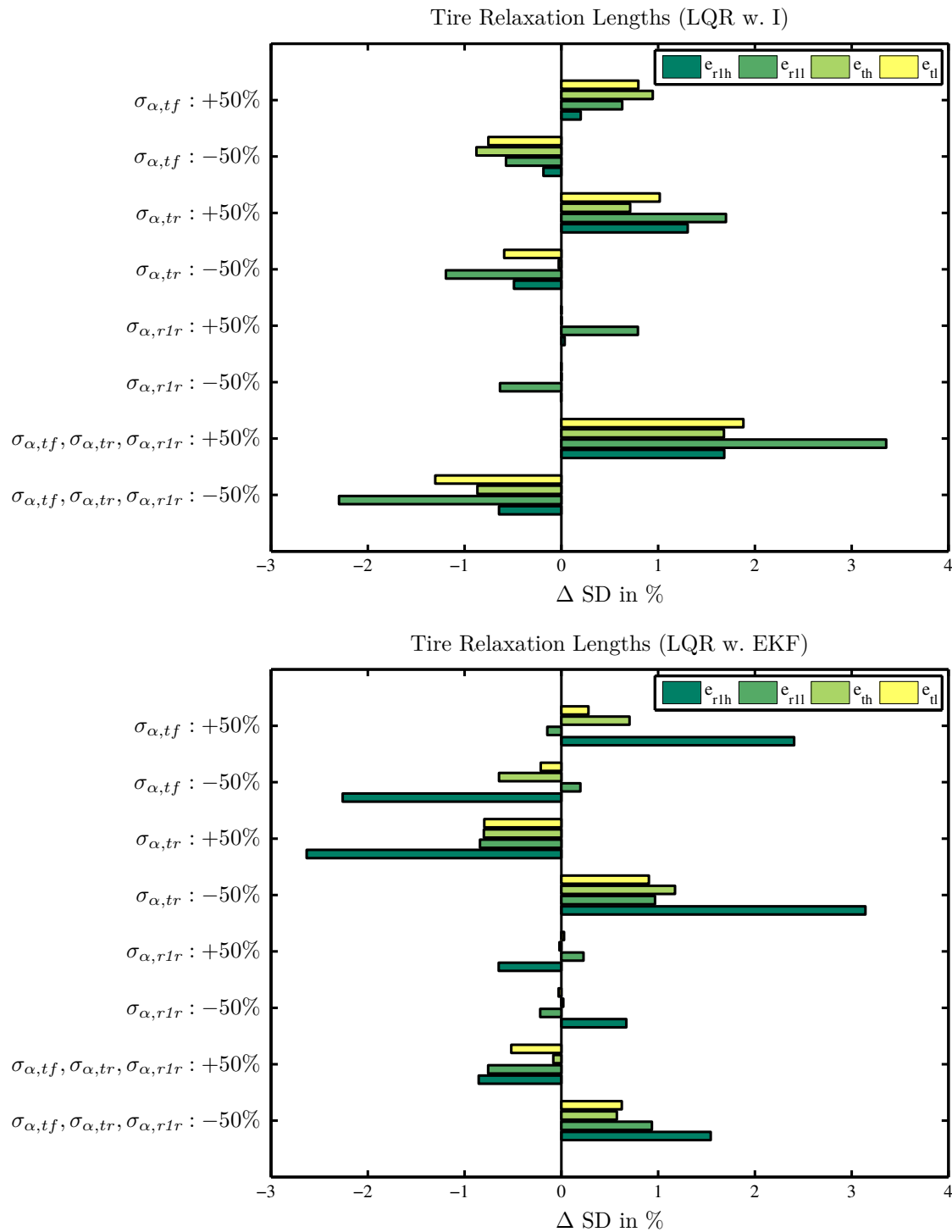
Figure 5.17: Simulation results for tracking path C3 with varying simulation model parameters. Δ SD denotes the resulting change in tracking error standard deviations relative to nominal results as presented in Figure 5.10.
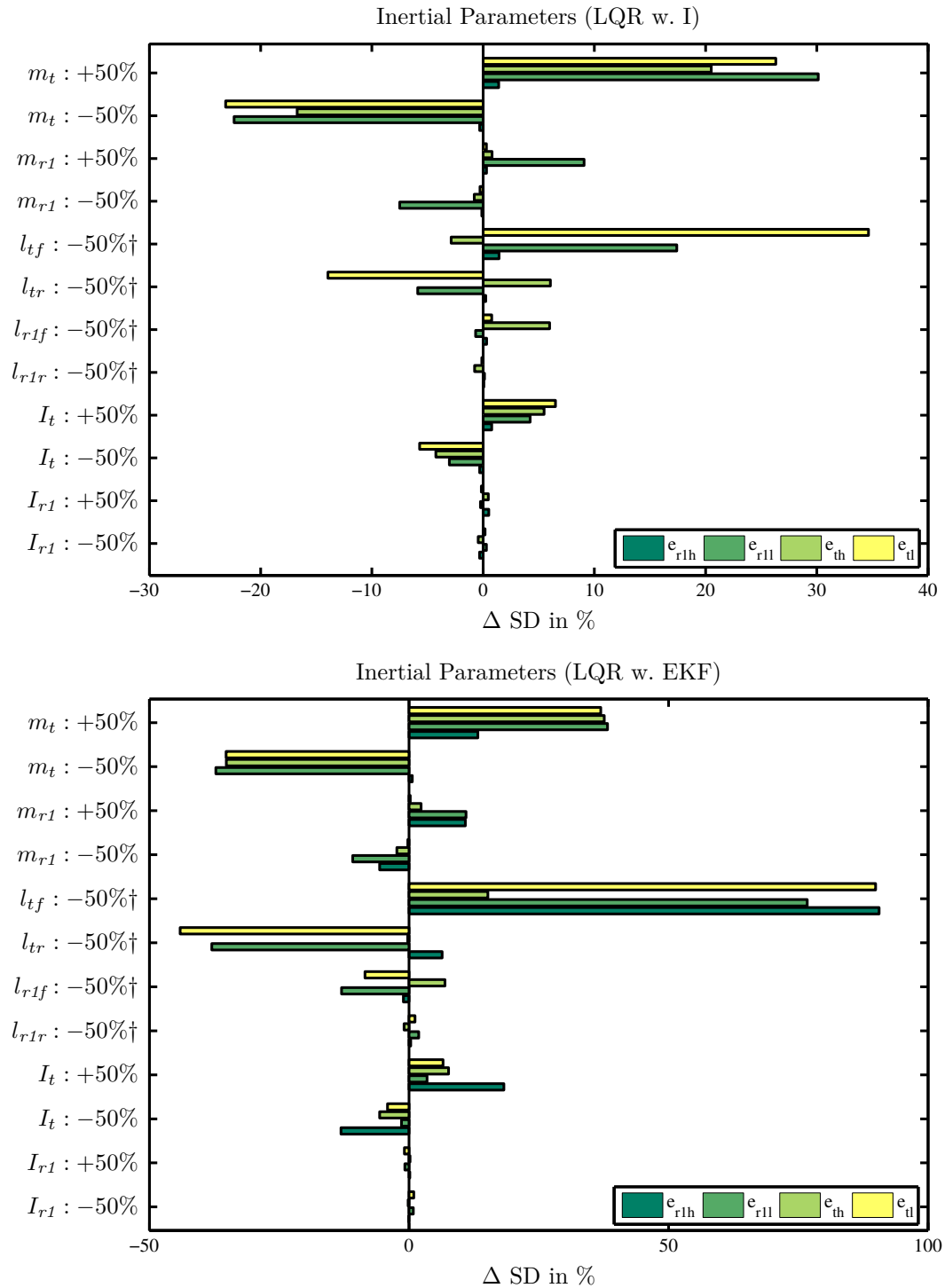
Figure 5.18: Simulation results for tracking path C3 with varying simulation model parameters. Δ SD denotes the resulting change in tracking error standard deviations relative to nominal results as presented in Figure 5.10. In case of †
the total tractor wheel base l_t and the implement length l_{r1} are maintained by lengthening the respective opposite.

6 Conclusion and Future Work

In order to meet a growing world population's demand for food and energy, agricultural methods are required to become more efficient and sustainable. Accurate GPS based guidance of agricultural machinery became an important part of this development. Today's solutions allow for accurate path tracking control of tractors. However, the actual position of an implement attached to the tractor and performing the agricultural tasks is neglected in most cases. To further increase the accuracy of agricultural methods, the focus is now shifting towards implement path tracking control using actively steered implements, i.e. implements equipped with steering actuators. In order to address the emerging interest in those new tractor-implement combinations, this work contributed new plant models and new path tracking control approaches.

Multiple tractor-implement models of different complexity have been developed. A tractor towing a wheel and drawbar steered implement has been used as an example throughout the work. In any case, however, the derivation of the equations of motion was performed in a systematic way using computer algebra software. Considering other implement actuators therefore is simple and can be achieved by modifying the constraints stated prior to automated derivation. All models derived are given in terms of explicit differential equations in order to allow for controller design and further system analysis. Simple kinematic models based on a single-track tractor-implement description in plain motion have been developed. Those models are based on geometric properties as well as constraints regarding tractor and implement wheel velocities. As a consequence parameterizing the kinematic models to describe a particular tractor-implement combination is an easy task comprising mostly of the measurement of vehicle dimensions. For that reason, using kinematic models for controller or estimator design seemed very desirable. A more complex representation of tractor-implement combinations was found by using dynamic models, yet again reduced to a single-track description. These models account for forces and moments causing the vehicle motion. The required parameters comprise tractor and implement inertial properties as well as tire parameters. Parameterization therefore is more involved and applicability to model based controller design is very limited due to numerous implement variants. The derived dynamic models have been used for further analysis and numerical simulation only. Derivation of dynamic models in particular was aggravated by lengthy equations resulting from steering actuators between tractor and implement. Within this work a new way of modeling was proposed. For the example of a steered drawbar it was assumed that an arbitrary kind of actuator and a steering angle controller are in place. The actuator was assumed capable of providing any moment required to steer the drawbar. With this assumption the steerable drawbar could be modeled as a rheonomic or

time dependent constraint and derivation of equations of motion was done systematically using Lagrangian mechanics and computer algebra software. Some well-chosen coordinate transformations during the derivation allowed to express the equations in such a way that linearization was possible for small deviations from a desired path which in turn allowed for further analysis.

In preparation of controlling the MIMO system consisting of a tractor and a steerable implement, a comprehensive overview of current path tracking control approaches has been provided. Research on on-road and off-road path tracking control using passenger cars, tractor-trailer and tractor-implement combinations has been taken into account. The control approaches considered comprise classical Proportional-Integral-Derivative (PID) control, Linear-Quadratic Regulators (LQRs), Model Predictive Control (MPC), Robust H_∞ Control, various nonlinear control methods, Sliding Mode Control (SMC), geometric approaches, and Fuzzy Logic Control (FLC). Each approach was discussed and assessed regarding this work's objectives as outlined in Section 1.2. In particular the required applicability to a multitude of implements and steering actuators as well as the resulting effort for setup and tuning performed by the user narrowed down the list of approaches that seemed suitable for this work. Following this initial assessment LQR control was used as a starting point. Weighting matrices have been chosen in such a way that only steering inputs and tracking errors (lateral and angular deviations from a desired path) are considered for tuning. The relative weight of steering inputs and tracking errors provided a tuning parameter for the overall controller gain. This was the only controller parameter that had to be found from experiments. Choosing the relative weights for different tracking errors allowed for emphasizing a particular objective. It was shown that the chosen approach is not only suitable for implement lateral position control but also for implement orientation control, which has been introduced as a new feature within this work. In this optional case the implement does not only track the desired path but also remains aligned with the desired path's direction. To overcome the additional implementation and tuning effort for state estimation the state feedback controller resulting from LQR design was approximated using a static output feedback. The chosen method is based on mode preservation and aims for an output feedback approximating the dominant eigenvalues of a controlled system with state feedback. From simulations and experiments it was found that LQR without additional measures resulted in unsatisfactory steady-state tracking errors on slopes and in curves. For that reason two variants overcoming this problem have been conceived and implemented. The first variant was a LQR controller augmented by integral control to account for constant disturbances (LQR w. I). The second variant relied on Extended Kalman Filter (EKF) based wheel side-slip estimation using the side-slip estimates for subsequent disturbance feedforward control (LQR w. EKF). In comparison LQR w. EKF exhibits an increased implementation and parameterization effort making LQR w. I the preferred approach. By considering theoretical limitations it was shown

that, in general, a second implement steering actuator is required to achieve tractor and implement lateral position control as well as implement orientation control with zero steady-state errors in the case of constant disturbances. For all controller variants it was shown that implement path tracking can be improved by adding a feedforward control law based on the path's curvature. Suitable feedforward control laws for steerable implements have been newly derived within this work.

As final part of this thesis numerous simulations and experiments have been carried out. Experiments have been performed using a mid-size tractor and a custom built implement demonstrator with numerous steering actuators. Simulations have been carried out using a non-linear dynamic model of this experimental setup. Initial condition responses in both simulations and experiments indicated that LQR w. I in particular is prone to overshooting behavior in the presence of actuator limits and rate limits. The first of which had been considered in anti-windup measures already. Considering the latter, however, might still offer room for improvement. Simulations with lateral down-hill forces on slopes and experiments on circular paths both indicated that LQR w. I as well as LQR w. EKF are capable of achieving sufficiently small steady-state tracking errors despite the presence of constant disturbances and wheel side-slip. As an example, experiments on a circular path of 20 m radius using tractor front wheel steering, implement wheel steering, and implement drawbar steering, while driving with a tractor forward velocity of 3 m/s, resulted in 3.2 cm, 2.0 cm and 0.7° SD for tractor lateral error, implement lateral error, and implement heading error in case of LQR w. I. Each error was zero mean. Similarly, errors for LQR w. EKF have been 3.2 cm, 2.2 cm and 0.3° SD with -2.0 cm, 1.3 cm and -0.4° mean. LQR w/o I in contrast resulted in errors with 13.1 cm, 12.3 cm, and -0.5° mean. Similar experiments considering transient conditions on paths consisting of straights, clothoids, and arc segments exhibited similar results with lateral errors below 3 cm SD for LQR w. I, if curvature change rate was moderate ($0.1°/m^2$). Increased curvature change rates of $0.3°/m^2$ resulted in increased tracking errors below 6 cm SD. Tracking errors for LQR w. EKF were slightly increased. This however could be due to small differences in the transient behavior of side-slip estimation and integral control. Parameter variation studies have been carried out using simulations and experiments. Experimental variation of tractor forward velocity indicated, that LQR w. I in particular must account for velocity changes. This could be done using gain scheduling techniques for instance. Their implementation however is subject to future work. Additional simulations have been carried out with tire and inertial parameters varied by $\pm 50\%$. The resulting closed loops remained stable for both LQR w. I and LQR w. EKF. Decreased tire cornering stiffness parameters however unsurprisingly exhibited a strong influence on path tracking accuracy in transient conditions.

Future work might address both the modeling and the control of tractor-implement combinations. Replacing the rather simple linear model for lateral tire forces by a more detailed description accounting for lateral and longitudinal forces would allow one to consider path tracking during driving and breaking scenarios. By giving up the assumption of a single-track model one could consider scenarios with different friction coefficients for different wheels. In terms of controller design, gain scheduling based on tractor forward velocity could be the next step. Anti-windup measures may be improved by accounting for steering actuator rate limits as well as by addressing actuator limits in a refined way, e.g. by continuing tractor integral control despite saturated implement actuators and vice versa.

A Appendix

A.1 Dynamic Equations of Motion

A.1.1 Tractor

To illustrate this work's approach of deriving the dynamic equations of motion for a tractor and a steered implement this section provides a concise example using the tractor single track model of Figure 2.2. The approach utilizes Lagrangian mechanics and follows a proposal by [Gen97], who considered a tractor and unsteered tractor-trailer combinations. His method is modified to account for applied forces and moments in a more convenient way.

The tractor in plain motion exhibits 3 DoFs and hence 3 generalized coordinates are chosen to be:

$$q_1 = r_t^{x,e}, \qquad\qquad q_2 = r_t^{y,e}, \qquad\qquad q_3 = \Psi_t. \qquad (A.1)$$

Obviously, the vehicle position and orientation as well as linear and angular velocities can be stated in terms of generalized coordinates:

$$r_t^{x,e} = q_1, \qquad\qquad r_t^{y,e} = q_2, \qquad\qquad \Psi_t = q_3, \qquad (A.2)$$

$$v_t^{x,e} = \dot{r}_t^{x,e} = \dot{q}_1, \qquad v_t^{y,e} = \dot{r}_t^{y,e} = \dot{q}_2, \qquad \omega_t^{z,e} = \dot{\Psi}_t = \dot{q}_3. \qquad (A.3)$$

In case the wheel's kinetic energy is neglected the tractor's kinetic energy is [Gre88]:

$$T = \frac{1}{2}I_t\left(\omega_t^{z,e}\right)^2 + \frac{1}{2}m_t\left(\left(v_t^{x,e}\right)^2 + \left(v_t^{y,e}\right)^2\right) \qquad (A.4)$$

$$= \frac{1}{2}I_t\dot{q}_3^2 + \frac{1}{2}m_t\left(\dot{q}_1^2 + \dot{q}_2^2\right). \qquad (A.5)$$

With potential energy $V = 0$ the Lagrangian function is:

$$L = T - V = T. \qquad (A.6)$$

In order to obtain equations of motion in a rather general form arbitrary applied forces $F_t^{x,e}$ and $F_t^{y,e}$ acting on the tractor c.g. as well as an applied moment $M_t^{z,e}$ are assumed. These earth-fixed components are related to their respective tractor-fixed components via:

$$\begin{bmatrix} F_t^{x,e} \\ F_t^{y,e} \end{bmatrix} = \underbrace{\begin{bmatrix} \cos(\Psi_t) & -\sin(\Psi_t) \\ \sin(\Psi_t) & \cos(\Psi_t) \end{bmatrix}}_{\mathbf{T}_{t,e}} \begin{bmatrix} F_t^{x,t} \\ F_t^{y,t} \end{bmatrix}, \tag{A.7}$$

$$M_t^{z,e} = M_t^{z,t}. \tag{A.8}$$

Lagrange's equations of motion (2nd kind) [Gre88] are:

$$\frac{d}{dt}\left(\frac{\partial L}{\partial \dot{q}_i}\right) - \frac{\partial L}{\partial q_i} = Q_i, \quad i = 1, 2, 3. \tag{A.9}$$

The generalized forces Q_i are chosen to account for the applied forces as well as applied moments and are given by [Gre88]:

$$Q_i = F_t^{x,e}\gamma_{t,i}^{x,e} + F_t^{y,e}\gamma_{t,i}^{y,e} + M_t^{z,e}\beta_{t,i}^{z,e}, \tag{A.10}$$

with $\gamma_{t,i}^{x,e}$, $\gamma_{t,i}^{y,e}$ and $\beta_{t,i}^{z,e}$ denoting linear and angular velocity coefficients defined as [Gre88]:

$$\gamma_{t,i}^{x,e} = \frac{\partial \dot{r}_t^{x,e}}{\partial \dot{q}_i} = \frac{\partial r_t^{x,e}}{\partial q_i}, \qquad \gamma_{t,i}^{y,e} = \frac{\partial \dot{r}_t^{y,e}}{\partial \dot{q}_i} = \frac{\partial r_t^{y,e}}{\partial q_i}, \qquad \beta_{t,i}^{z,e} = \frac{\partial \omega_t^{z,e}}{\partial \dot{q}_i}. \tag{A.11}$$

Inserting (A.5), (A.6), (A.10), and (A.11) in (A.9) yields:

$$\frac{d}{dt}\left(m_t\dot{q}_1\right) = F_t^{x,e}\cdot 1 + F_t^{y,e}\cdot 0 + M_t^{z,e}\cdot 0, \tag{A.12}$$

$$\frac{d}{dt}\left(m_t\dot{q}_2\right) = F_t^{x,e}\cdot 0 + F_t^{y,e}\cdot 1 + M_t^{z,e}\cdot 0, \tag{A.13}$$

$$\frac{d}{dt}\left(I_t\dot{q}_3\right) = F_t^{x,e}\cdot 0 + F_t^{y,e}\cdot 0 + M_t^{z,e}\cdot 1. \tag{A.14}$$

Reintroducing the original coordinates (A.1) leads to the unsurprising result:

$$\frac{d}{dt}\left(m_t\dot{r}_t^{x,e}\right) = F_t^{x,e}, \tag{A.15}$$

$$\frac{d}{dt}\left(m_t\dot{r}_t^{y,e}\right) = F_t^{y,e}, \tag{A.16}$$

$$\frac{d}{dt}\left(I_t\dot{\Psi}_t\right) = M_t^{z,e}. \tag{A.17}$$

These equations of motion in earth-fixed coordinates would be sufficient for simulation based on numerical integration. For vehicle modeling in general however a vehicle-fixed representation is advantageous. This is due to the fact that many properties, like tire

forces for instance, are more suitably described relative to the vehicle. Linearization and subsequent system analysis in particular benefit from a vehicle-fixed representation. For that reason [Gen97] proposes a trick based on introducing vehicle-fixed velocities $v_t^{x,t}$ and $v_t^{y,t}$ prior to evaluating the time derivatives in (A.15) and (A.16). Hence inserting

$$\begin{bmatrix} \dot{r}_t^{x,e} \\ \dot{r}_t^{y,e} \end{bmatrix} = \begin{bmatrix} v_t^{x,e} \\ v_t^{y,e} \end{bmatrix} = \underbrace{\begin{bmatrix} \cos(\Psi_t) & -\sin(\Psi_t) \\ \sin(\Psi_t) & \cos(\Psi_t) \end{bmatrix}}_{\mathbf{T}_{t,e}} \begin{bmatrix} v_t^{x,t} \\ v_t^{y,t} \end{bmatrix} \tag{A.18}$$

in (A.15) and (A.16) and utilizing (A.7) results in:

$$\begin{bmatrix} \cos(\Psi_t) & -\sin(\Psi_t) \\ \sin(\Psi_t) & \cos(\Psi_t) \end{bmatrix} \begin{bmatrix} m_t \dot{v}_t^{x,t} - m_t \dot{\Psi}_t v_t^{y,t} \\ m_t \dot{v}_t^{y,t} + m_t \dot{\Psi}_t v_t^{x,t} \end{bmatrix} = \begin{bmatrix} \cos(\Psi_t) & -\sin(\Psi_t) \\ \sin(\Psi_t) & \cos(\Psi_t) \end{bmatrix} \begin{bmatrix} F_t^{x,t} \\ F_t^{y,t} \end{bmatrix}. \tag{A.19}$$

Finally multiplying with $\mathbf{T}_{t,e}^{-1}$ and solving for the highest order derivatives yields the desired tractor-fixed equations of motion:

$$\dot{v}_t^{x,t} = \frac{1}{m_t} F_t^{x,t} + \dot{\Psi}_t v_t^{y,t}, \tag{A.20}$$

$$\dot{v}_t^{y,t} = \frac{1}{m_t} F_t^{y,t} - \dot{\Psi}_t v_t^{x,t}, \tag{A.21}$$

$$\ddot{\Psi}_t = \frac{1}{I_t} M_t^{z,t}. \tag{A.22}$$

A.1.2 Tractor and Implement

In order to provide a complete picture, the equations of motion (3.19) of a tractor towing a wheel and drawbar steered implement as described in Section 3.1.2 are provided in detail. Computer algebra software has been used to obtain these equations. Exports to simulation software and this document have been automated to avoid the introduction of typographical errors.

$$
\underbrace{\begin{bmatrix} m_{1,1} & m_{1,2} & m_{1,3} & m_{1,4} \\ m_{2,1} & m_{2,2} & m_{2,3} & m_{1,4} \\ m_{3,1} & m_{3,2} & m_{3,3} & m_{3,4} \\ m_{4,1} & m_{4,2} & m_{4,3} & m_{4,4} \end{bmatrix}}_{\mathbf{M}} \begin{bmatrix} \dot{v}_t^{x,t} \\ \dot{v}_t^{y,t} \\ \ddot{\Psi}_t \\ \ddot{\delta}_{thr} \end{bmatrix} + \underbrace{\begin{bmatrix} r_1 \\ r_2 \\ r_3 \\ r_4 \end{bmatrix}}_{\mathbf{r}} = \mathbf{0} \tag{A.23}
$$

$$m_{1,1} = m_{r1} + m_t, \tag{A.24}$$

$$m_{1,2} = 0, \tag{A.25}$$

$$m_{1,3} = -\sin(\delta_{thr})l_{r1d}m_{r1} - \sin(\delta_{thr} + \delta_{r1d})l_{r1f}m_{r1}, \tag{A.26}$$

$$m_{1,4} = \sin(\delta_{thr})l_{r1d}m_{r1} + \sin(\delta_{thr} + \delta_{r1d})l_{r1f}m_{r1}, \tag{A.27}$$

$$m_{2,1} = 0, \tag{A.28}$$

$$m_{2,2} = m_{r1} + m_t, \tag{A.29}$$

$$m_{2,3} = -\cos(\delta_{thr})l_{r1d}m_{r1} - \cos(\delta_{thr} + \delta_{r1d})l_{r1f}m_{r1} - (l_{tr} + l_{thr})m_{r1}, \tag{A.30}$$

$$m_{2,4} = \cos(\delta_{thr})l_{r1d}m_{r1} + \cos(\delta_{thr} + \delta_{r1d})l_{r1f}m_{r1}, \tag{A.31}$$

$$m_{3,1} = -\sin(\delta_{thr})l_{r1d}m_{r1} - \sin(\delta_{thr} + \delta_{r1d})l_{r1f}m_{r1}, \tag{A.32}$$

$$m_{3,2} = -\cos(\delta_{thr})l_{r1d}m_{r1} - \cos(\delta_{thr} + \delta_{r1d})l_{r1f}m_{r1} - (l_{tr} + l_{thr})m_{r1}, \tag{A.33}$$

$$
\begin{aligned}
m_{3,3} = {} & 2\cos(\delta_{thr})(l_{tr} + l_{thr})l_{r1d}m_{r1} + 2\cos(\delta_{r1d})l_{r1d}l_{r1f}m_{r1} \\
& + 2\cos(\delta_{thr} + \delta_{r1d})(l_{tr} + l_{thr})l_{r1f}m_{r1} + (l_{tr} + l_{thr})^2 m_{r1} + l_{r1d}^2 m_{r1} + l_{r1f}^2 m_{r1} \\
& + I_{r1} + I_t,
\end{aligned}
\tag{A.34}
$$

$$
\begin{aligned}
m_{3,4} = {} & -\cos(\delta_{thr})(l_{tr} + l_{thr})l_{r1d}m_{r1} - 2\cos(\delta_{r1d})l_{r1d}l_{r1f}m_{r1} \\
& - \cos(\delta_{thr} + \delta_{r1d})(l_{tr} + l_{thr})l_{r1f}m_{r1} - l_{r1d}^2 m_{r1} - l_{r1f}^2 m_{r1} - I_{r1},
\end{aligned}
\tag{A.35}
$$

$$m_{4,1} = \sin(\delta_{thr})l_{r1d}m_{r1} + \sin(\delta_{thr} + \delta_{r1d})l_{r1f}m_{r1}, \tag{A.36}$$

$$m_{4,2} = \cos(\delta_{thr})l_{r1d}m_{r1} + \cos(\delta_{thr} + \delta_{r1d})l_{r1f}m_{r1}, \tag{A.37}$$

$$
\begin{aligned}
m_{4,3} = {} & -\cos(\delta_{thr})(l_{tr} + l_{thr})l_{r1d}m_{r1} - 2\cos(\delta_{r1d})l_{r1d}l_{r1f}m_{r1} \\
& - \cos(\delta_{thr} + \delta_{r1d})(l_{tr} + l_{thr})l_{r1f}m_{r1} - l_{r1d}^2 m_{r1} - l_{r1f}^2 m_{r1} - I_{r1},
\end{aligned}
\tag{A.38}
$$

$$m_{4,4} = 2\cos(\delta_{r1d})l_{r1d}l_{r1f}m_{r1} + l_{r1d}^2 m_{r1} + l_{r1f}^2 m_{r1} + I_{r1}, \tag{A.39}$$

$$r_1 = (l_{r1f}m_{r1}\ddot{\delta}_{r1d} - F_{r1}^{y,r1})\sin(\delta_{thr} + \delta_{r1d}) + (l_{r1d}m_{r1}\dot{\Psi}_t^2 - 2l_{r1d}m_{r1}\dot{\Psi}_t\dot{\delta}_{thr}$$
$$+ l_{r1d}m_{r1}\dot{\delta}_{thr}^2)\cos(\delta_{thr}) + (l_{r1f}m_{r1}\dot{\Psi}_t^2 - 2l_{r1f}m_{r1}\dot{\Psi}_t\dot{\delta}_{r1d} - 2l_{r1f}m_{r1}\dot{\Psi}_t\dot{\delta}_{thr} + l_{r1f}m_{r1}\dot{\delta}_{r1d}^2$$
$$+ 2l_{r1f}m_{r1}\dot{\delta}_{r1d}\dot{\delta}_{thr} + l_{r1f}m_{r1}\dot{\delta}_{thr}^2 - F_{r1}^{x,r1})\cos(\delta_{thr} + \delta_{r1d}) + \dot{\Psi}_t^2(l_{tr} + l_{thr})m_{r1}$$
$$- v_t^{y,t}\dot{\Psi}_t m_{r1} - v_t^{y,t}\dot{\Psi}_t m_t - F_t^{x,t}, \tag{A.40}$$

$$r_2 = (-l_{r1d}m_{r1}\dot{\Psi}_t^2 + 2l_{r1d}m_{r1}\dot{\Psi}_t\dot{\delta}_{thr} - l_{r1d}m_{r1}\dot{\delta}_{thr}^2)\sin(\delta_{thr}) + (-l_{r1f}m_{r1}\dot{\Psi}_t^2 + 2l_{r1f}m_{r1}\dot{\Psi}_t\dot{\delta}_{r1d}$$
$$+ 2l_{r1f}m_{r1}\dot{\Psi}_t\dot{\delta}_{thr} - l_{r1f}m_{r1}\dot{\delta}_{r1d}^2 - 2l_{r1f}m_{r1}\dot{\delta}_{r1d}\dot{\delta}_{thr} - l_{r1f}m_{r1}\dot{\delta}_{thr}^2 + F_{r1}^{x,r1})\sin(\delta_{thr} + \delta_{r1d})$$
$$+ (l_{r1f}m_{r1}\ddot{\delta}_{r1d} - F_{r1}^{y,r1})\cos(\delta_{thr} + \delta_{r1d}) + (v_t^{x,t}\dot{\Psi}_t m_{r1}) + (v_t^{x,t}\dot{\Psi}_t m_t) - F_t^{y,t}, \tag{A.41}$$

$$r_3 = (-2l_{r1d}l_{r1f}m_{r1}\dot{\Psi}_t\dot{\delta}_{r1d} + l_{r1d}l_{r1f}m_{r1}\dot{\delta}_{r1d}^2 + 2l_{r1d}l_{r1f}m_{r1}\dot{\delta}_{r1d}\dot{\delta}_{thr} - l_{r1d}F_{r1}^{x,r1})\sin(\delta_{r1d})$$
$$+ (-2(l_{tr} + l_{thr})l_{r1d}m_{r1}\dot{\Psi}_t\dot{\delta}_{thr} + (l_{tr} + l_{thr})l_{r1d}m_{r1}\dot{\delta}_{thr}^2 + l_{r1d}m_{r1}\dot{\Psi}_t v_t^{y,t})\sin(\delta_{thr})$$
$$+ (-2(l_{tr} + l_{thr})l_{r1f}m_{r1}\dot{\Psi}_t\dot{\delta}_{thr} - 2(l_{tr} + l_{thr})l_{r1f}m_{r1}\dot{\Psi}_t\dot{\delta}_{r1d} + (l_{tr} + l_{thr})l_{r1f}m_{r1}\dot{\delta}_{thr}^2$$
$$+ 2(l_{tr} + l_{thr})l_{r1f}m_{r1}\dot{\delta}_{thr}\dot{\delta}_{r1d} + (l_{tr} + l_{thr})l_{r1f}m_{r1}\dot{\delta}_{r1d}^2 + l_{r1f}m_{r1}\dot{\Psi}_t v_t^{y,t}$$
$$- F_{r1}^{x,r1}(l_{tr} + l_{thr}))\sin(\delta_{thr} + \delta_{r1d}) + (-l_{r1d}l_{r1f}m_{r1}\ddot{\delta}_{r1d} + l_{r1d}F_{r1}^{y,r1})\cos(\delta_{r1d})$$
$$- \cos(\delta_{thr})l_{r1d}m_{r1}\dot{\Psi}_t v_t^{x,t} + (-((l_{tr} + l_{thr})l_{r1f}m_{r1}\ddot{\delta}_{r1d}) - l_{r1f}m_{r1}\dot{\Psi}_t v_t^{x,t}$$
$$+ (F_{r1}^{y,r1}(l_{tr} + l_{thr})))\cos(\delta_{thr} + \delta_{r1d}) - (l_{tr} + l_{thr})m_{r1}\dot{\Psi}_t v_t^{x,t} - (\ddot{\delta}_{r1d}l_{r1f}^2 m_{r1})$$
$$+ (F_{r1}^{y,r1}l_{r1f}) - (\ddot{\delta}_{r1d}I_{r1}) - M_{r1}^{z,r1} - M_t^{z,t}, \tag{A.42}$$

$$r_4 = (2l_{r1d}l_{r1f}m_{r1}\dot{\Psi}_t\dot{\delta}_{r1d} - l_{r1d}l_{r1f}m_{r1}\dot{\delta}_{r1d}^2 - 2l_{r1d}l_{r1f}m_{r1}\dot{\delta}_{r1d}\dot{\delta}_{thr} + l_{r1d}F_{r1}^{x,r1})\sin(\delta_{r1d})$$
$$+ ((l_{tr} + l_{thr})l_{r1d}m_{r1}\dot{\Psi}_t^2 - l_{r1d}m_{r1}\dot{\Psi}_t v_t^{y,t})\sin(\delta_{thr}) + ((l_{tr} + l_{thr})l_{r1f}m_{r1}\dot{\Psi}_t^2$$
$$- l_{r1f}m_{r1}\dot{\Psi}_t v_t^{y,t})\sin(\delta_{thr} + \delta_{r1d}) + (l_{r1d}l_{r1f}m_{r1}\ddot{\delta}_{r1d} - l_{r1d}F_{r1}^{y,r1})\cos(\delta_{r1d})$$
$$+ \cos(\delta_{thr})l_{r1d}m_{r1}\dot{\Psi}_t v_t^{x,t} + \cos(\delta_{thr} + \delta_{r1d})l_{r1f}m_{r1}\dot{\Psi}_t v_t^{x,t} + (\ddot{\delta}_{r1d}l_{r1f}^2 m_{r1})$$
$$- (F_{r1}^{y,r1}l_{r1f}) + (\ddot{\delta}_{r1d}I_{r1}) + M_{r1}^{z,r1}. \tag{A.43}$$

A.2 Linearized System Descriptions

A.2.1 Dynamic Models

The dynamic model with transient tire forces as complied in Section 3.1.6 is given by:

$$\dot{\mathbf{x}} = \mathbf{A}\mathbf{x} + \mathbf{B}\mathbf{u}, \tag{A.44}$$

$$\mathbf{y} = \mathbf{C}\mathbf{x}, \tag{A.45}$$

with

$$\mathbf{x} = \left[e_{tl}, e_{th}, v_t^{y,t}, \dot{\Psi}_t, \alpha_{re,tf}, \alpha_{re,tr}, \alpha_{re,r1r}, \delta_{thr}, \dot{\delta}_{thr}, \delta_{tf}, \dot{\delta}_{tf}, \delta_{r1d}, \dot{\delta}_{r1d}, \delta_{r1r}, \dot{\delta}_{r1r} \right]^{\mathrm{T}}, \tag{A.46}$$

$$\mathbf{u} = \left[\delta_{tf,d}, \delta_{r1d,d}, \delta_{r1r,d} \right]^{\mathrm{T}}, \tag{A.47}$$

$$\mathbf{y} = \left[e_{tl}, e_{th}, e_{r1l}, e_{r1h} \right]^{\mathrm{T}}, \tag{A.48}$$

and structure matrices

$$[\mathbf{A}] = \begin{bmatrix}
0 & \star & \star & \star & 0 & 0 & 0 & 0 & 0 & 0 & 0 & 0 & 0 & 0 & 0 \\
0 & 0 & 0 & \star & 0 & 0 & 0 & 0 & 0 & 0 & 0 & 0 & 0 & 0 & 0 \\
0 & 0 & 0 & \star & \star & \star & \star & 0 & 0 & 0 & 0 & \star & \star & 0 & 0 \\
0 & 0 & 0 & 0 & \star & \star & \star & 0 & 0 & 0 & 0 & \star & \star & 0 & 0 \\
0 & 0 & \star & \star & \star & 0 & 0 & 0 & 0 & \star & 0 & 0 & 0 & 0 & 0 \\
0 & 0 & \star & \star & 0 & \star & 0 & 0 & 0 & 0 & 0 & 0 & 0 & 0 & 0 \\
0 & 0 & \star & \star & 0 & 0 & \star & \star & \star & 0 & 0 & \star & \star & \star & 0 \\
0 & 0 & 0 & 0 & 0 & 0 & 0 & 0 & \star & 0 & 0 & 0 & 0 & 0 & 0 \\
0 & 0 & 0 & 0 & \star & \star & \star & 0 & 0 & 0 & 0 & \star & \star & 0 & 0 \\
0 & 0 & 0 & 0 & 0 & 0 & 0 & 0 & 0 & 0 & \star & 0 & 0 & 0 & 0 \\
0 & 0 & 0 & 0 & 0 & 0 & 0 & 0 & 0 & \star & \star & 0 & 0 & 0 & 0 \\
0 & 0 & 0 & 0 & 0 & 0 & 0 & 0 & 0 & 0 & 0 & 0 & \star & 0 & 0 \\
0 & 0 & 0 & 0 & 0 & 0 & 0 & 0 & 0 & 0 & 0 & \star & \star & 0 & 0 \\
0 & 0 & 0 & 0 & 0 & 0 & 0 & 0 & 0 & 0 & 0 & 0 & 0 & 0 & \star \\
0 & 0 & 0 & 0 & 0 & 0 & 0 & 0 & 0 & 0 & 0 & 0 & 0 & \star & \star
\end{bmatrix}, \qquad
[\mathbf{B}] = \begin{bmatrix}
0 & 0 & 0 \\
0 & 0 & 0 \\
0 & \star & 0 \\
0 & \star & 0 \\
0 & 0 & 0 \\
0 & 0 & 0 \\
0 & 0 & 0 \\
0 & 0 & 0 \\
0 & \star & 0 \\
0 & 0 & 0 \\
\star & 0 & 0 \\
0 & 0 & 0 \\
0 & \star & 0 \\
0 & 0 & 0 \\
0 & 0 & \star
\end{bmatrix}, \tag{A.49}$$

$$[\mathbf{C}] = \begin{bmatrix}
\star & 0 & 0 & 0 & 0 & 0 & 0 & 0 & 0 & 0 & 0 & 0 & 0 & 0 & 0 \\
0 & \star & 0 & 0 & 0 & 0 & 0 & 0 & 0 & 0 & 0 & 0 & 0 & 0 & 0 \\
\star & \star & 0 & 0 & 0 & 0 & 0 & \star & 0 & 0 & 0 & \star & 0 & 0 & 0 \\
0 & \star & 0 & 0 & 0 & 0 & 0 & \star & 0 & 0 & 0 & \star & 0 & 0 & 0
\end{bmatrix}. \tag{A.50}$$

Similarly, the dynamic model neglecting transient tire forces with state, input and output vectors:

$$\mathbf{x} = \left[e_{tl}, e_{th}, v_t^{y,t}, \dot{\Psi}_t, \delta_{thr}, \dot{\delta}_{thr}, \delta_{tf}, \dot{\delta}_{tf}, \delta_{r1d}, \dot{\delta}_{r1d}, \delta_{r1r}, \dot{\delta}_{r1r} \right]^{\mathrm{T}}. \tag{A.51}$$

$$\mathbf{u} = \left[\delta_{tf,d}, \delta_{r1d,d}, \delta_{r1r,d} \right]^{\mathrm{T}}, \tag{A.52}$$

$$\mathbf{y} = \left[e_{tl}, e_{th}, e_{r1l}, e_{r1h} \right]^{\mathrm{T}}, \tag{A.53}$$

has the structure matrices

$$[\mathbf{A}] = \begin{bmatrix}
0 & \star & \star & \star & 0 & 0 & 0 & 0 & 0 & 0 & 0 & 0 \\
0 & 0 & 0 & \star & 0 & 0 & 0 & 0 & 0 & 0 & 0 & 0 \\
0 & 0 & \star & \star & \star & \star & \star & 0 & \star & \star & \star & 0 \\
0 & 0 & \star & \star & \star & \star & \star & 0 & \star & \star & \star & 0 \\
0 & 0 & 0 & 0 & 0 & \star & 0 & 0 & 0 & 0 & 0 & 0 \\
0 & 0 & \star & \star & \star & \star & \star & 0 & \star & \star & \star & 0 \\
0 & 0 & 0 & 0 & 0 & 0 & 0 & \star & 0 & 0 & 0 & 0 \\
0 & 0 & 0 & 0 & 0 & 0 & \star & \star & 0 & 0 & 0 & 0 \\
0 & 0 & 0 & 0 & 0 & 0 & 0 & 0 & 0 & \star & 0 & 0 \\
0 & 0 & 0 & 0 & 0 & 0 & 0 & 0 & \star & \star & 0 & 0 \\
0 & 0 & 0 & 0 & 0 & 0 & 0 & 0 & 0 & 0 & 0 & \star \\
0 & 0 & 0 & 0 & 0 & 0 & 0 & 0 & 0 & 0 & \star & \star
\end{bmatrix}, \qquad
[\mathbf{B}] = \begin{bmatrix}
0 & 0 & 0 \\
0 & 0 & 0 \\
0 & \star & 0 \\
0 & \star & 0 \\
0 & 0 & 0 \\
0 & \star & 0 \\
0 & 0 & 0 \\
\star & 0 & 0 \\
0 & 0 & 0 \\
0 & \star & 0 \\
0 & 0 & 0 \\
0 & 0 & \star
\end{bmatrix}, \tag{A.54}$$

$$[\mathbf{C}] = \begin{bmatrix}
\star & 0 & 0 & 0 & 0 & 0 & 0 & 0 & 0 & 0 & 0 & 0 \\
0 & \star & 0 & 0 & 0 & 0 & 0 & 0 & 0 & 0 & 0 & 0 \\
\star & \star & 0 & 0 & \star & 0 & 0 & 0 & \star & 0 & 0 & 0 \\
0 & \star & 0 & 0 & \star & 0 & 0 & 0 & \star & 0 & 0 & 0
\end{bmatrix}. \tag{A.55}$$

A.2.2 Kinematic Models

The linearized kinematic model as derived in Section 3.2.6 in detail is:

$$\dot{\mathbf{x}} = \mathbf{A}\mathbf{x} + \mathbf{B}\mathbf{u}, \tag{A.56}$$

$$\mathbf{y} = \mathbf{C}\mathbf{x}, \tag{A.57}$$

with

$$\mathbf{x} = \left[e_{tl}, e_{th}, \delta_{thr}, \delta_{tf}, \dot{\delta}_{tf}, \delta_{r1d}, \dot{\delta}_{r1d}, \delta_{r1r}, \dot{\delta}_{r1r}\right]^{\mathrm{T}}, \tag{A.58}$$

$$\mathbf{u} = \left[\delta_{tf,d}, \delta_{r1d,d}, \delta_{r1r,d}\right]^{\mathrm{T}}, \tag{A.59}$$

$$\mathbf{y} = \left[e_{tl}, e_{th}, e_{r1l}, e_{r1h}\right]^{\mathrm{T}}, \tag{A.60}$$

$$\mathbf{A} = \begin{bmatrix}
0 & v_{tr}^{x,t} & 0 & 0 & 0 & 0 & 0 & 0 & 0 \\
0 & 0 & 0 & \frac{v_{tr}^{x,t}}{l_t} & 0 & 0 & 0 & 0 & 0 \\
0 & 0 & \frac{-v_{tr}^{x,t}}{l_{r1d}+l_{r1}} & \frac{v_{tr}^{x,t}(l_{thr}+l_{r1d}+l_{r1})}{(l_{r1d}+l_{r1})l_t} & 0 & \frac{-v_{tr}^{x,t}}{l_{r1d}+l_{r1}} & \frac{-l_{r1}}{(l_{r1d}+l_{r1})} & \frac{v_{tr}^{x,t}}{l_{r1d}+l_{r1}} & 0 \\
0 & 0 & 0 & 0 & 1 & 0 & 0 & 0 & 0 \\
0 & 0 & 0 & \frac{-1}{T_{tf}^2} & \frac{-2D_{tf}}{T_{tf}} & 0 & 0 & 0 & 0 \\
0 & 0 & 0 & 0 & 0 & 0 & 1 & 0 & 0 \\
0 & 0 & 0 & 0 & 0 & \frac{-1}{T_{r1d}^2} & \frac{-2D_{r1d}}{T_{r1d}} & 0 & 0 \\
0 & 0 & 0 & 0 & 0 & 0 & 0 & 0 & 1 \\
0 & 0 & 0 & 0 & 0 & 0 & 0 & \frac{-1}{T_{r1r}^2} & \frac{-2D_{r1r}}{T_{r1r}}
\end{bmatrix}, \tag{A.61}$$

$$\mathbf{B} = \begin{bmatrix}
0 & 0 & 0 \\
0 & 0 & 0 \\
0 & 0 & 0 \\
0 & 0 & 0 \\
\frac{-1}{T_{tf}^2} & 0 & 0 \\
0 & 0 & 0 \\
0 & \frac{1}{T_{r1d}^2} & 0 \\
0 & 0 & 0 \\
0 & 0 & \frac{1}{T_{r1r}^2}
\end{bmatrix}, \tag{A.62}$$

$$\mathbf{C} = \begin{bmatrix}
1 & 0 & 0 & 0 & 0 & 0 & 0 & 0 & 0 \\
0 & 1 & 0 & 0 & 0 & 0 & 0 & 0 & 0 \\
1 & -l_{r1}-l_{r1d}-l_{thr} & l_{r1d}+l_{r1} & 0 & 0 & l_{r1} & 0 & 0 & 0 \\
0 & 1 & -1 & 0 & 0 & -1 & 0 & 0 & 0
\end{bmatrix}. \tag{A.63}$$

A.3 Experimental Setup

All experiments in this work have been performed using a test setup consisting of a John Deere 6210R tractor and a custom built implement as show in Figure A.1. Four GPS receivers augmented by RTK correction signals have been used to obtain tractor and implement position as well as orientation during path tracking control. The IMUs served parameter identification purposes in [Pfr13] only.
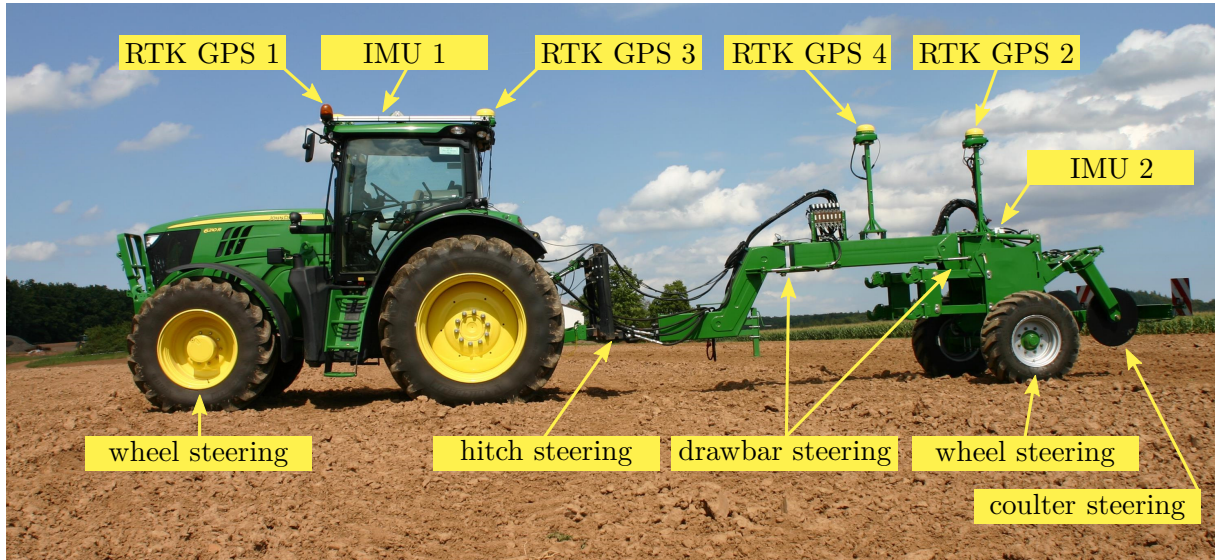
Figure A.1: Experimental setup consisting of a John Deere 6210R tractor towing a custom built actively steered implement with a multitude of hydraulic steering actuators. RTK GPS 1 and 2 are the main sensors used for path tracking. A second GPS receiver on tractor and implement is used to precisely distinguish between machine heading and direction of travel. The IMUs serve as additional sensors for parameter identification purposes only.

Tractor

The tractor used is a series production John Deere 6210R tractor. Front and rear tires have been low pressure models Michelin XeoBib VF 600/60 R30 (1.0 bar) and Michelin XeoBib VF 710/60 R42 (0.9 bar). The built-in ISO 11783 TIA [ISO09] interface was used to steer the tractor. This interface uses curvature commands as a wheel base independent representation of the desired steering angles. Tractor input and output signals have been as follows.

Signals	T_s	Resolution	Type
Wheel-based Machine Speed	100 ms	0.001 m/s	Output
Guidance Curvature Command	100 ms	0.25 1/km	Input
Guidance Curvature Estimated	100 ms	0.25 1/km	Output

Implement

A custom built implement with a multitude of hydraulic steering actuators was used for all tests. The implement was equipped with Petlas 405/70-20 tires with 1.4 bar pressure. ISO 11783 capable hydraulic valves have been used to drive the actuators. Analog angle sensors provided the measured joint angles to an inner loop steering angle controller. This steering angle controller was implemented on the rapid control prototyping platform also used for path tracking control.

Signals	T_s	Resolution	Type
Valve Flow Commands (5 valves)	20 ms	0.1 l/min	Input
Front Drawbar Steering Angle	1 ms	0.11°	Output
Rear Drawbar Steering Angle	1 ms	0.11°	Output
Wheel Steering Angle	1 ms	-	Output
Coulter Steering Angle	1 ms	-	Output
Hitch Steering Position	1 ms	-	Output

GPS Receivers

Tractor as well as implement position and orientation have been obtained using John Deere SF 3000 receiver position measurements augmented by RTK correction signals. The horizontal accuracy of these position measurements is 2 cm (2 SD, 15 min pass-to-pass) and 1.5 cm (2 SD, 24 h absolute) [Dee11b]. Tractor and implement heading were found using two receiver position measurements each. For each receiver the Terrain Compensation Module (TCM) was activated, i.e. the receiver built-in IMU has been used to project the antenna position along the vehicle vertical axis to ground level.

Signals	T_s	Resolution	Type
Latitude	100 ms	$3.90625 \cdot 10^{-10}$ °	Output
Longitude	100 ms	$3.90625 \cdot 10^{-10}$ °	Output
Altitude	100 ms	$4.8828 \cdot 10^{-4}$ m	Output

IMUs

Parameter identification performed by [Pfr13] relied on two additional IMUs (Honeywell 6DF-1N6-C2-HWL) [Hon13] providing lateral acceleration and angular rate measurements.

Signals	T_s	Resolution	Type
Linear accelerations (3 axes)	40 ms	0.0151 m/s^2	Output
Angular rates (3 axes)	40 ms	0.0114 °/s	Output

A.4 Path Descriptions

Curved path tracking as outlined in Section 5.5 was performed using desired paths consisting of straight lines, clothoids and arc segments as depicted in Figures A.2 and A.3. Point sequences with distances of 0.15 m between subsequent points were used to represent the desired paths within the controller.
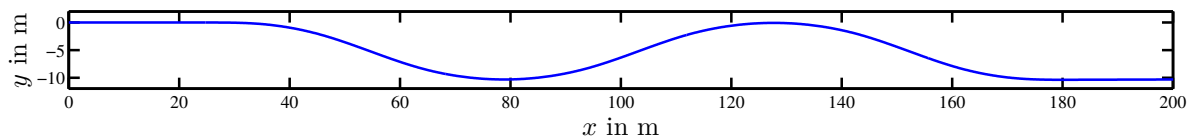
Figure A.2: Path C1 with max. curvature $1°/m$, curvature change rate $0.1°/m^2$, and curvature changing sign when path tangent reaches $\Psi_d = \pm 20°$.
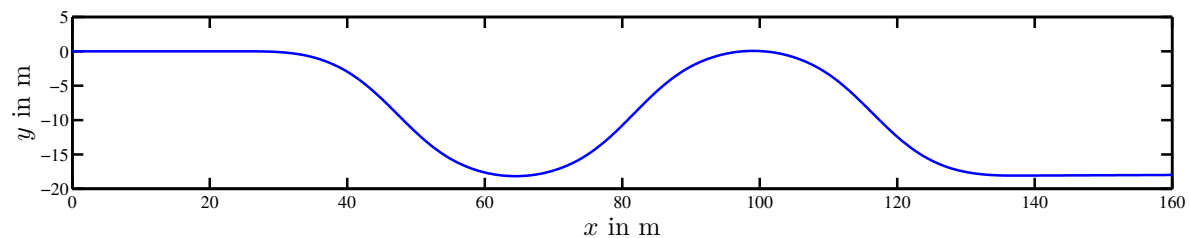
Figure A.3: Path C3 with max. curvature $3°/m$, curvature change rate $0.3°/m^2$, and curvature changing sign when path tangent reaches $\Psi_d = \pm 45°$.

A.5 Simulation Model Parameter Summary

Simulations in Chapter 5 have been performed using the parameters as given in Tables A.1, A.2, and A.3. These parameters were chosen to depict the experimental setup as described in Appendix A.3. Tractor and implement ODEs have been solved using an ODE4 (Runge-Kutta) fixed-step solver with 1 ms sample time. Measurement sample times of GPS antenna positions, tractor steering angle, and tractor wheel speed as provided to the discrete time controller have been 100 ms. Implement steering angle measurements were obtained using 20 ms sample times.

Table A.1: Tractor model parameters.

Parameter	Value	Unit	Description	Origin
$C_{\alpha,tf}$	3.54	kN/°	Combined front wheel cornering stiffness	Quasi steady-state cornering identification [Pfr13]
$C_{\alpha,tr}$	7.23	kN/°	Combined rear wheel cornering stiffness	Quasi steady-state cornering identification [Pfr13]
$\sigma_{\alpha,tf}$	0.40	m	Front wheel relaxation length	Sine sweep steering identification [Pfr13]
$\sigma_{\alpha,tr}$	1.61	m	Rear wheel relaxation length	Sine sweep steering identification [Pfr13]
m_t	9088	kg	Mass	Vehicle scale measurement
I_t	21782	kg m^2	Moment of inertia	Sine sweep steering identification [Pfr13]
l_t	2.8	m	Tractor wheel base	Total station measurement
l_{tf}	1.77	m	Distance between c.g. and front axle	Axle load from vehicle scale measurement
l_{tr}	1.03	m	Distance between c.g. and rear axle	Axle load from vehicle scale measurement
l_{thr}	1.81	m	Distance between rear axle and hitch point	Total station measurement
T_{tf}	0.19	s	Front wheel steering time constant	Small step response identification
D_{tf}	0.80		Front wheel steering damping ratio	Small step response identification
$\delta_{tf,min}$	-28	°	Minimum front wheel steering angle	Angle sensor measurement
$\delta_{tf,max}$	+28	°	Maximum front wheel steering angle	Angle sensor measurement
$\dot{\delta}_{tf,min}$	-23	°/s	Minimum front wheel steering angle rate	Large step response identification
$\dot{\delta}_{tf,max}$	+21	°/s	Maximum front wheel steering angle rate	Large step response identification

Table A.2: Implement model parameters.

Parameter	Value	Unit	Description	Origin
$C_{\alpha,r1r}$	3.47	kN/°	Combined wheel cornering stiffness	Quasi steady-state cornering identification [Pfr13]
$\sigma_{\alpha,r1r}$	0.61	m	Wheel relaxation length	Sine sweep steering identification [Pfr13]
m_{r1}	2418	kg	Mass	Vehicle scale measurement
I_{r1}	5316	kg m^2	Moment of inertia	Sine sweep steering identification [Pfr13]
l_{r1d}	1.76	m	Distance between hitch point and drawbar joint	Total station measurement
l_{r1}	2.44	m	Distance between drawbar joint and axle	Total station measurement
l_{r1f}	2.13	m	Distance between drawbar joint and c.g.	Axle load from vehicle scale measurement
l_{r1r}	0.31	m	Distance between implement c.g. and axle	Axle load from vehicle scale measurement
T_{r1d}	0.12	s	Drawbar steering time constant	Small step response identification
D_{r1d}	0.55		Drawbar steering damping ratio	Small step response identification
T_{r1r}	0.10	s	Wheel steering time constant	Small step response identification
D_{r1r}	0.49		Wheel steering damping ratio	Small step response identification
$\delta_{r1d,min}$	-34	°	Minimum drawbar steering angle	Angle sensor measurement
$\delta_{r1d,max}$	+34	°	Maximum drawbar steering angle	Angle sensor measurement
$\dot{\delta}_{r1d,min}$	-10	°/s	Minimum drawbar steering angle rate	Large step response identification
$\dot{\delta}_{r1d,max}$	+10	°/s	Maximum drawbar steering angle rate	Large step response identification
$\delta_{r1r,min}$	-12	°	Minimum wheel steering angle	Angle sensor measurement
$\delta_{r1r,max}$	+12	°	Maximum wheel steering angle	Angle sensor measurement
$\dot{\delta}_{r1r,min}$	-14	°/s	Minimum wheel steering angle rate	Large step response identification
$\dot{\delta}_{r1r,max}$	+19	°/s	Maximum wheel steering angle rate	Large step response identification

Table A.3: Sensor noise model parameters.

Parameter	Value	Unit	Description	Origin
Sensors				
$[l_{GPS1}^{x,t}, l_{GPS1}^{y,t}, l_{GPS1}^{z,t}]^{\mathrm{T}}$	$[1.526, 0, 3.187]^{\mathrm{T}}$	$[\mathrm{m}, \mathrm{m}, \mathrm{m}]^{\mathrm{T}}$	GPS 1 antenna lever arm from center of tractor rear axle on ground level	Total station measurement
$[l_{GPS3}^{x,t}, l_{GPS3}^{y,t}, l_{GPS2}^{z,t}]^{\mathrm{T}}$	$[-0.132, 0, 3.245]^{\mathrm{T}}$	$[\mathrm{m}, \mathrm{m}, \mathrm{m}]^{\mathrm{T}}$	GPS 3 antenna lever arm from center of tractor rear axle on ground level	Total station measurement
$[l_{GPS2}^{x,r1}, l_{GPS2}^{y,r1}, l_{GPS2}^{z,r1}]^{\mathrm{T}}$	$[0.004, 0, 2.939]^{\mathrm{T}}$	$[\mathrm{m}, \mathrm{m}, \mathrm{m}]^{\mathrm{T}}$	GPS 2 antenna lever arm from center of implement axle on ground level	Total station measurement
$[l_{GPS4}^{x,r1}, l_{GPS4}^{y,r1}, l_{GPS4}^{z,r1}]^{\mathrm{T}}$	$[1.350, 0, 3.032]^{\mathrm{T}}$	$[\mathrm{m}, \mathrm{m}, \mathrm{m}]^{\mathrm{T}}$	GPS 4 antenna lever arm from center of implement axle on ground level	Total station measurement
$\mathrm{SD}(r_{GPS}^{x,e})$	0.0075	m	GPS antenna position measurement noise SD	GPS receiver specification [Dee11b]
$\mathrm{SD}(r_{GPS}^{y,e})$	0.0075	m	GPS antenna position measurement SD	GPS receiver specification [Dee11b]
$\mathrm{SD}(\delta_{tf})$	0.02	°	Tractor front wheel angle sensor noise SD	Estimated
$\mathrm{SD}(\delta_{r1d})$	0.05	°	Implement front drawbar angle sensor noise SD	60 s sensor measurement in standstill
$\mathrm{SD}(\delta_{r1r})$	0.02	°	Implement front wheel angle sensor noise SD	60 s sensor measurement in standstill
$\mathrm{SD}(v_{tr}^{x,t})$	0.01	m/s	Tractor forward speed measurement noise SD	Estimated

A.6 Controller Parameter Summary

This section summarizes the controller parameters as used in both simulations and experiments of Chapter 5.

A.6.1 Plant Parameters

Controller design is based on a kinematic model description. The respective parameters are a subset of dynamic model simulation parameters as stated in Appendix A.5. The parameter subset comprises geometric parameters (l_t, l_{thr}, l_{r1d}, l_{r1}) and steering actuator related parameters (T_{tf}, D_{tf}, T_{r1d}, D_{r1d}, T_{r1r}, D_{r1r}). Numerical values are as stated in Appendix A.5.

A.6.2 LQR Weights

Output and input weighting matrices $\mathbf{Q}$ and $\mathbf{R}$ depend on the chosen control approach and variant. LQR control without additional measures to account for robustness as well as LQR combined with EKF estimation based disturbance feedforward use the weights as given in the following paragraph. In the case of integral control additional weights have to be chosen which is done subsequently.

Standard LQR

Output and input weighting matrices $\mathbf{Q}$ and $\mathbf{R}$ are given by:

$$\mathbf{Q} = \mathrm{diag}(q_{e,tl}, q_{e,th}, q_{e,r1l}, q_{e,r1h}), \tag{A.64}$$

$$\mathbf{R} = \mathrm{diag}(r_{\delta,tf}, r_{\delta,r1d}, r_{\delta,r1r}). \tag{A.65}$$

Individual entries are normalized using typical signal ranges, resulting in:

$$q_{e,tl} = q_{e,tl,N}/(1\mathrm{m})^2, \qquad q_{e,r1l} = q_{e,r1l,N}/(1\mathrm{m})^2, \tag{A.66}$$

$$q_{e,th} = q_{e,th,N}/(10°)^2, \qquad q_{e,r1h} = q_{e,r1h,N}/(10°)^2, \tag{A.67}$$

$$r_{\delta,tf} = r_{\delta,tf,N}/(10°)^2, \qquad r_{\delta,r1d} = r_{\delta,r1d,N}/(10°)^2, \qquad r_{\delta,r1r} = r_{\delta,r1r,N}/(10°)^2. \tag{A.68}$$

The normalized weights as chosen in simulations and experiments are:

$$q_{e,tl,N} = 100, \qquad q_{e,th,N} = 1, \qquad q_{e,r1l,N} = 100, \qquad q_{e,r1h,N} = 100 \tag{A.69}$$

$$r_{\delta,tf,N} = 80, \qquad r_{\delta,r1d,N} = 80, \qquad r_{\delta,r1r,N} = 80 \tag{A.70}$$

LQR with Integral Control

Weights for LQR with integral control are chosen in a similar way, yet account for additional error integral outputs. The output and input weighting matrices $\mathbf{Q}$ and $\mathbf{R}$ therefore are:

$$\mathbf{Q} = \text{diag}(q_{e,tl}, q_{e,th}, q_{e,r1l}, q_{e,r1h}, q_{int,e,tl}, q_{int,e,r1l}, q_{int,e,r1h}), \tag{A.71}$$

$$\mathbf{R} = \text{diag}(r_{\delta,tf}, r_{\delta,r1d}, r_{\delta,r1r}). \tag{A.72}$$

The entries are normalized using:

$$q_{e,tl} = q_{e,tl,N}/(1\text{m})^2, \qquad\qquad q_{e,r1l} = q_{e,r1l,N}/(1\text{m})^2, \tag{A.73}$$

$$q_{e,th} = q_{e,th,N}/(10°)^2, \qquad\qquad q_{e,r1h} = q_{e,r1h,N}/(10°)^2, \tag{A.74}$$

$$q_{int,e,tl} = q_{int,e,tl,N}/(1\text{m}\cdot\text{s})^2, \qquad q_{int,e,r1l} = q_{int,e,r1l,N}/(1\text{m}\cdot\text{s})^2, \tag{A.75}$$

$$q_{int,e,r1h} = q_{int,e,r1h,N}/(10°\cdot\text{s})^2, \tag{A.76}$$

$$r_{\delta,tf} = r_{\delta,tf,N}/(10°)^2, \qquad\qquad r_{\delta,r1d} = r_{\delta,r1d,N}/(10°)^2, \tag{A.77}$$

$$r_{\delta,r1r} = r_{\delta,r1r,N}/(10°)^2. \tag{A.78}$$

LQR with integral control was considered using variants of input and controlled output combinations. In those cases $\mathbf{Q}$ and $\mathbf{R}$ are found by omitting rows and columns containing unconsidered steering actuators and error integrals. Normalized weights for all variants as found in simulations and experiments are shown in Table A.4.

Table A.4: Normalized input and output weights of LQR with integral control.

	Tractor steering, implement wheel and drawbar steering	Tractor steering, implement drawbar steering	Tractor steering, implement wheel steering	Tractor steering (implement control)	Tractor steering (tractor control)
Variant	①	②	③	④	⑤
Inputs	$\delta_{tf,d}$	$\delta_{tf,d}$	$\delta_{tf,d}$	$\delta_{tf,d}$	$\delta_{tf,d}$
	$\delta_{r1d,d}$	$\delta_{r1d,d}$	$\delta_{r1r,d}$		
	$\delta_{r1r,d}$				
Controlled outputs	e_{tl}	e_{tl}	e_{tl}	e_{r1l}	e_{tl}
	e_{r1l}	e_{r1l}	e_{r1l}		
	e_{r1h}				
$q_{e,tl,N}$	100	100	100	1	100
$q_{e,th,N}$	1	1	1	1	1
$q_{e,r1l,N}$	100	100	100	100	1
$q_{e,r1h,N}$	100	1	1	1	1
$q_{int,e,tl,N}$	100	100	100	-	100
$q_{int,e,r1l,N}$	100	100	100	100	-
$q_{int,e,r1h,N}$	100	-	-	-	-
$r_{\delta,tf,N}$	80	80	80	80	80
$r_{\delta,r1d,N}$	80	80	-	-	-
$r_{\delta,r1r,N}$	80	-	80	-	-

A.6.3 Output Feedback Approximation Weights

Output feedback as outlined in Section 4.2 relies on weights emphasizing the approximation of a subset of state feedback closed-loop eigenvalues $\bar{\lambda}_i$. Elements w_i of the weighting matrix

$$\mathbf{W} = \mathrm{diag}\,(w_1, \ldots, w_n) \tag{A.79}$$

are chosen as follows: for the considered open-loop systems with m inputs and n states $2m$ states result from steering actuator dynamics. Accordingly an equal number of $2m$

less dominant eigenvalues is neglected in the output feedback approximation, resulting in the weights:

$$w_i = \begin{cases} 100 & \text{for } n - 2m \text{ eigenvalues } \bar{\lambda}_i \text{ closest to the origin,} \\ 1 & \text{others.} \end{cases} \tag{A.80}$$

A.6.4 Anti-Windup Thresholds

Anti-windup as described in Section 4.3 uses the thresholds outlined in Table A.5.

Table A.5: Anti-windup threshold parameters.

Parameter	Value	Unit	Description
Desired steering angle thresholds holding integration			
$\delta_{tf,d,th,max}$	+27	°	Desired tractor front wheel steering angle upper threshold
$\delta_{tf,d,th,min}$	−27	°	Desired tractor front wheel steering angle lower threshold
$\delta_{r1d,d,th,max}$	+30	°	Desired implement drawbar steering angle upper threshold
$\delta_{r1d,d,th,min}$	−30	°	Desired implement drawbar steering angle lower threshold
$\delta_{r1r,d,th,max}$	+12	°	Desired implement wheel steering angle upper threshold
$\delta_{r1r,d,th,min}$	−12	°	Desired implement wheel steering angle lower threshold
Error thresholds holding integration			
$e_{tl,th,max}$	+1.2	m	Tractor lateral error upper threshold
$e_{tl,th,min}$	−1.2	m	Tractor lateral error lower threshold
$e_{r1l,th,max}$	+1.2	m	Implement lateral error upper threshold
$e_{r1l,th,min}$	−1.2	m	Implement lateral error lower threshold
$e_{r1h,th,max}$	+45	°	Implement heading error upper threshold
$e_{r1h,th,min}$	−45	°	Implement heading error lower threshold
Error integration limits in case a particular error and error integral are both positive or negative			
$e_{tl,max}$	+0.2	m	Tractor lateral error integration upper limit
$e_{tl,min}$	−0.2	m	Tractor lateral error integration lower limit
$e_{r1l,max}$	+0.2	m	Implement lateral error integration upper limit
$e_{e1l,min}$	−0.2	m	Implement lateral error integration lower limit
$e_{r1h,max}$	+4	°	Implement heading error integration upper limit
$e_{e1h,min}$	−4	°	Implement heading error integration lower limit
Error integral limits			
$e_{tl,int,max}$	+5	m · s	Tractor lateral error integral upper limit
$e_{tl,int,min}$	−5	m · s	Tractor lateral error integral lower limit
$e_{r1l,int,max}$	+5	m · s	Implement lateral error integral upper limit
$e_{r1l,int,min}$	−5	m · s	Implement lateral error integral lower limit
$e_{r1h,int,max}$	+20	°· s	Implement heading error integral upper limit
$e_{r1h,int,min}$	−20	°· s	Implement heading error integral lower limit

A.6.5 Extended Kalman Filter Parameters

If an EKF is used for disturbance estimation and feedforward additional plant parameters are required. Those comprise of the process and measurement noise covariance matrices $\mathbf{Q}[k]$ and $\mathbf{R}[k]$ as stated in Section 4.4. Numerical values used within this work are stated in Tables A.6 and A.7. Furthermore, initial values for state estimate $\hat{\mathbf{x}}[k]$ and estimation error covariance matrix $\hat{\mathbf{P}}[k]$ must be provided. The latter are summarized in Table A.8. $\hat{\mathbf{x}}[0]$ is initialized using the current tractor position and orientation measurements as well as all current steering angle measurements. All other initial states are set to zero.

Table A.6: Elements of process noise covariance matrix $\mathbf{Q}[k]$.

Parameter	Value	Unit	Description
$q_{1,1}[k]$	0.0005^2	m^2	$r_{tr}^{x,e}$ process noise variance
$q_{2,2}[k]$	0.0005^2	m^2	$r_{tr}^{y,e}$ process noise variance
$q_{3,3}[k]$	0.01^2	$(°)^2$	Ψ_t process noise variance
$q_{4,4}[k]$	0.01^2	$(°)^2$	δ_{thr} process noise variance
$q_{5,5}[k]$	0.01^2	$(°)^2$	δ_{tf} process noise variance
$q_{6,6}[k]$	0.05^2	$(°/s)^2$	$\dot{\delta}_{tf}$ process noise variance
$q_{7,7}[k]$	0.01^2	$(°)^2$	δ_{r1d} process noise variance
$q_{8,8}[k]$	0.05^2	$(°/s)^2$	$\dot{\delta}_{r1d}$ process noise variance
$q_{9,9}[k]$	0.01^2	$(°)^2$	δ_{r1r} process noise variance
$q_{10,10}[k]$	0.05^2	$(°/s)^2$	$\dot{\delta}_{r1r}$ process noise variance
$q_{11,11}[k]$	0.01^2	$(°/s)^2$	α_{tf} process noise variance
$q_{12,12}[k]$	0.01^2	$(°/s)^2$	α_{tr} process noise variance
$q_{13,13}[k]$	0.01^2	$(°/s)^2$	α_{r1r} process noise variance

Table A.7: Elements of measurement noise covariance matrix $\mathbf{R}[k]$.

Parameter	Value	Unit	Description
$r_{1,1}[k]$	0.0075^2	m^2	$r_{tr}^{x,e}$ measurement noise variance
$r_{2,2}[k]$	0.0075^2	m^2	$r_{tr}^{y,e}$ measurement noise variance
$q_{3,3}[k]$	0.37^2	$(°)^2$	Ψ_t measurement noise variance
$r_{4,4}[k]$	0.0075^2	m^2	$r_{r1r}^{x,e}$ measurement noise variance
$r_{5,5}[k]$	0.0075^2	m^2	$r_{r1r}^{y,e}$ measurement noise variance
$r_{6,6}[k]$	0.45^2	$(°)^2$	Ψ_{r1} measurement noise variance
$r_{7,7}[k]$	0.02^2	$(°)^2$	δ_{tf} measurement noise variance
$r_{8,8}[k]$	0.05^2	$(°)^2$	δ_{r1d} measurement noise variance
$r_{9,9}[k]$	0.02^2	$(°)^2$	δ_{r1r} measurement noise variance

Table A.8: Initial estimation error covariance matrix $\hat{\mathbf{P}}[0]$.

Parameter	Value	Unit	Description
$\hat{p}_{1,1}[0]$	0.0075^2	m^2	$r_{tr}^{x,e}$ initial estimation error variance
$\hat{p}_{2,2}[0]$	0.0075^2	m^2	$r_{tr}^{y,e}$ initial estimation error variance
$\hat{p}_{3,3}[0]$	0.37^2	$(°)^2$	Ψ_t initial estimation error variance
$\hat{p}_{4,4}[0]$	4^2	$(°)^2$	δ_{thr} initial estimation error variance
$\hat{p}_{5,5}[0]$	0.02^2	$(°)^2$	δ_{tf} initial estimation error variance
$\hat{p}_{6,6}[0]$	2^2	$(°/s)^2$	$\dot{\delta}_{tf}$ initial estimation error variance
$\hat{p}_{7,7}[0]$	0.05^2	$(°)^2$	δ_{r1d} initial estimation error variance
$\hat{p}_{8,8}[0]$	5^2	$(°/s)^2$	$\dot{\delta}_{r1d}$ initial estimation error variance
$\hat{p}_{9,9}[0]$	0.02^2	$(°)^2$	δ_{r1r} initial estimation error variance
$\hat{p}_{10,10}[0]$	2^2	$(°/s)^2$	$\dot{\delta}_{r1r}$ initial estimation error variance
$\hat{p}_{11,11}[0]$	0.01^2	$(°/s)^2$	α_{tf} initial estimation error variance
$\hat{p}_{12,12}[0]$	0.01^2	$(°/s)^2$	α_{tr} initial estimation error variance
$\hat{p}_{13,13}[0]$	0.01^2	$(°/s)^2$	α_{r1r} initial estimation error variance

A.6.6 Curvature Feedforward Parameters

Path curvature feedforward control as described in Section 4.5 uses curvature values obtained some velocity dependent distance ahead of the current tractor and implement position. This is to compensate for delays introduced by steering actuator dynamics. In this work the distance is obtained by multiplying tractor and implement forward speed with time constants 0.35 s and 0.19 s respectively.

A.6.7 Sample Times

Input and output signals as well as internal controller calculations are subject to various sample times which are partly predetermined by standardized CAN messages. GPS position and orientation measurements as well as tractor wheel speed and steering angle measurements are obtained every 100 ms. Implement steering angles are measured every 20 ms. Internally the inner loop steering angle controller and the EKF use a 20 ms sample time. Path tracking control is performed with 40 ms sample time. Desired tractor steering angle output signals are sent every 100 ms. Implement hydraulic valve flow commands for inner loop steering angle control are updated every 20 ms.

A.7 Robust Controllers

Robust controllers as considered here follow a definition by [DG75] which is briefly summarized.

A linear time-invariant system is assumed and described by:

$$\dot{\mathbf{x}} = \mathbf{A}\mathbf{x} + \mathbf{B}\mathbf{u} + \mathbf{E}\mathbf{d}, \tag{A.81}$$

$$\mathbf{y} = \mathbf{C}\mathbf{x} + \mathbf{D}\mathbf{u} + \mathbf{F}\mathbf{d}, \tag{A.82}$$

$$\mathbf{y}_c = \mathbf{C}_c\mathbf{x} + \mathbf{D}_c\mathbf{u} + \mathbf{F}_c\mathbf{d}, \tag{A.83}$$

$$\mathbf{e} = \mathbf{y}_c - \mathbf{r}, \tag{A.84}$$

with system states $\mathbf{x} \in \mathbb{R}^n$, inputs $\mathbf{u} \in \mathbb{R}^m$, disturbances $\mathbf{d} \in \mathbb{R}^{m_d}$, measured outputs $\mathbf{y} \in \mathbb{R}^p$, controlled outputs $\mathbf{y}_c \in \mathbb{R}^{p_c}$, reference inputs $\mathbf{r} \in \mathbb{R}^{p_c}$, and errors $\mathbf{e} \in \mathbb{R}^{p_c}$. [DG75] distinguishes between measured outputs $\mathbf{y}$ and controlled outputs $\mathbf{y}_c$. The first may be used to stabilize the system. The latter are required to track reference inputs $\mathbf{r}$.

It is assumed:

$$\text{rank}\,\mathbf{C}_c = p_c, \qquad\qquad \text{rank}\,\mathbf{B} = m, \qquad\qquad \text{rank}\begin{bmatrix} \mathbf{E} \\ \mathbf{F}_c \end{bmatrix} = m_d. \tag{A.85}$$

Perturbations are denoted by $\mathbf{M} \in \Omega_\epsilon$ indicating that elements $m_{k,l}$ of $\mathbf{M}$ are subject to

$$m_{k,l} \in \Omega_\epsilon \text{ with } \Omega_\epsilon = \{m_{k,l} | \, |m_{k,l}| < \epsilon\}. \tag{A.86}$$

Robust Controller Definition

Suppose there exists a controller stabilizing the system (A.81) to (A.84) and an asymptotic regulation takes place ($\mathbf{e} \to 0$ for $t \to \infty$). Now assume there are disturbed plant parameters $\mathbf{A} + \delta\mathbf{A}$, $\mathbf{B} + \delta\mathbf{B}$, $\mathbf{C} + \delta\mathbf{C}$ and $\epsilon > 0$ is chosen such that the closed-loop system remains stable for all $\delta\mathbf{A} \in \Omega_\epsilon$, $\delta\mathbf{B} \in \Omega_\epsilon$, $\delta\mathbf{C} \in \Omega_\epsilon$. Then if asymptotic regulation still takes place for all $\delta\mathbf{A} \in \Omega_\epsilon$, $\delta\mathbf{B} \in \Omega_\epsilon$, $\delta\mathbf{C} \in \Omega_\epsilon$ the controller is said to be a robust controller.

Robust Controller Existence

[DG75] provide necessary and sufficient conditions for the existence of a robust controller for system (A.81) to (A.84). They consider reference inputs $\mathbf{r}$ and disturbances $\mathbf{d}$ in a general framework allowing for constant, sinusoidal or ramp signals for instance. Here conditions are abbreviated by only considering constant reference inputs and disturbances.

Necessary and sufficient for the existence of a linear time-invariant robust controller for (A.81) to (A.84), such that the controlled system is stabilizable and $\mathbf{e} \to 0$ as $t \to \infty$ for

all measureable or unmeasureable constant disturbances **d** as well as constant reference inputs **r**, is that all subsequent conditions hold:

- The system $(\mathbf{A}, \mathbf{B})$ is stabilizable.

- The system $(\mathbf{C}, \mathbf{A})$ is detectable.

- $m \geq p_c$, i.e. the number of inputs at least equals the number of controlled outputs.

- The transmission zeros of $\mathbf{C}_c (s\mathbf{I} - \mathbf{A})^{-1} \mathbf{B} + \mathbf{D}_c$ do not coincide with $s = 0$.

- **y** contains the actual output $\mathbf{y}_c$, i.e. there is a nonsingular **T** with $\begin{bmatrix} \mathbf{y}_c \\ \tilde{\mathbf{y}} \end{bmatrix} = \mathbf{T}\mathbf{y}$.

Robust Controller Structure

A robust controller is found in a two-step approach. In a first step the plant (A.81) to (A.84) is extended by introducing suitable controller dynamics which is determined by the class of reference input and disturbance that must be considered. [FW75] coined the term 'internal model principle' for this property of a controller. In a second step the extended plant is stabilized using an arbitrary suitable control approach.

To obtain the extended plant [DG75] introduces the 'servo-compensator':

$$\dot{\mathbf{x}}_s = \mathbf{A}_s \mathbf{x}_s + \mathbf{B}_s \mathbf{e} \tag{A.87}$$

which models the classes of reference inputs **r** and disturbances **d** considered. In case of constant reference inputs and disturbances this results in p_c integrators for p_c controlled outputs and the respective block diagonal matrices simply are:

$$\mathbf{A}_s = \mathrm{blockdiag}(\underbrace{0, \ldots, 0}_{p_c \text{ times}}) \qquad \mathbf{B}_s = \mathrm{blockdiag}(\underbrace{1, \ldots, 1}_{p_c \text{ times}}). \tag{A.88}$$

The overall extended plant model is then given by:

$$\underbrace{\begin{bmatrix} \dot{\mathbf{x}} \\ \dot{\mathbf{x}}_s \end{bmatrix}}_{\dot{\mathbf{x}}_e} = \underbrace{\begin{bmatrix} \mathbf{A} & \mathbf{0} \\ \mathbf{B}_s \mathbf{C}_c & \mathbf{A}_s \end{bmatrix}}_{\mathbf{A}_e} \underbrace{\begin{bmatrix} \mathbf{x} \\ \mathbf{x}_s \end{bmatrix}}_{\mathbf{x}_e} + \underbrace{\begin{bmatrix} \mathbf{B} \\ \mathbf{B}_s \mathbf{D}_c \end{bmatrix}}_{\mathbf{B}_e} \mathbf{u} + \underbrace{\begin{bmatrix} \mathbf{E} & \mathbf{0} \\ \mathbf{B}_s \mathbf{F}_c & -\mathbf{B}_s \end{bmatrix}}_{\mathbf{E}_e} \begin{bmatrix} \mathbf{d} \\ \mathbf{r} \end{bmatrix}, \tag{A.89}$$

$$\underbrace{\begin{bmatrix} \mathbf{y} \\ \mathbf{x}_s \end{bmatrix}}_{\mathbf{y}_e} = \underbrace{\begin{bmatrix} \mathbf{C} & \mathbf{0} \\ \mathbf{0} & \mathbf{I} \end{bmatrix}}_{\mathbf{C}_e} \underbrace{\begin{bmatrix} \mathbf{x} \\ \mathbf{x}_s \end{bmatrix}}_{\mathbf{x}_e} + \underbrace{\begin{bmatrix} \mathbf{D} \\ \mathbf{0} \end{bmatrix}}_{\mathbf{D}_e} \mathbf{u} + \underbrace{\begin{bmatrix} \mathbf{F} & \mathbf{0} \\ \mathbf{0} & \mathbf{0} \end{bmatrix}}_{\mathbf{F}_e} \begin{bmatrix} \mathbf{d} \\ \mathbf{r} \end{bmatrix}. \tag{A.90}$$

The final step of robust controller design is stabilizing this extended plant by using an arbitrary control approach and input **u**. Within this work LQR control and subsequent static output feedback approximation is used, resulting in a stabilizing control law:

$$\mathbf{u} = \mathbf{K}_y \mathbf{y}_e. \tag{A.91}$$

A.8 Path Tracking Control Literature Survey

Literature on path tracking control of tractor-trailer or tractor-implement combinations is summarized Table A.9.

Table A.9: Summary of literature on path tracking control of tractor-trailer or tractor-implement combinations.

Source	Terrain	Controller Design Model	Actuators	Controlled Variables	Control Approach	Validation
[ABL04]	not stated	kinematic tractor-trailer model in forward and backward motion	tractor front wheels	all system states	nonlinear control based on Lyapunov stability analysis	simulation
[Aut08]	off-road	not stated	tractor front wheels, implement coulters	tractor and implement lateral error	not stated	product
[BOV09]	off-road	kinematic tractor and implement model	tractor front wheels, implement drawbar	tractor and implement lateral error	linear MPC	experiment
[BOV12, Bac13]	off-road	kinematic tractor and implement model with multiplicative factor accounting for tractor front wheel side-slip	tractor front wheels, implement drawbar	tractor and implement lateral error	nonlinear MPC with EKF based full state feedback, pure pursuit geometric path tracking	experiment
[Bel99]	off-road	kinematic tractor and implement model with biases for tractor heading and steering angle	tractor front wheels	not stated	LQR assuming ideal state feedback	simulation
[Bev01]	off-road	model with velocity dependent gains, delays and damping ratios found by system identification, biases for tractor heading and steering angle, implement hitch angle, and some sensor signals	tractor front wheels	implement lateral error	LQR with EKF based full state feedback	simulation, experiment

Table A.9: Summary of literature on path tracking control of tractor-trailer or tractor-implement combinations.

Source	Terrain	Controller Design Model	Actuators	Controlled Variables	Control Approach	Validation
[CLTM10]	off-road	kinematic tractor and implement model extended by wheel side-slip angles	tractor front wheels	implement lateral error	nonlinear control based on Lyapunov stability analysis, step 1: control law considering the implement a virtual vehicle with the direction of travel at the hitch point being the input, step 2: calculation of tractor steering angle causing this direction of travel, side-slip angles are estimated using a nonlinear observer	experiment
[CT95b]	on-road	dynamic tractor and trailer model	tractor front wheels, trailer brakes	projected tractor lateral error at look-ahead distance, trailer hitch angle	LQR and frequency shaped LQR penalizing large lateral accelerations (both using tractor steering only and assuming ideal state feedback), nonlinear control based on input-output linearization using steering angle and differential trailer tire force inputs, backstepping control of differential trailer tire force using trailer wheel brake torque inputs	simulation
[CT00]	on-road	dynamic tractor and trailer model	tractor front wheels, trailer brakes	tractor lateral error, trailer hitch angle	nonlinear control based on input-output linearization using steering angle and differential trailer tire force inputs, backstepping control of differential trailer tire force using trailer wheel brake torque inputs	simulation
[Dee13]	off-road	none	tractor front wheels, one arbitrary hydraulic implement actuator	tractor and implement lateral error	decentralized control, no details stated, one implement controller gain parameter for line acquisition and one for on-line tracking	product

Table A.9: Summary of literature on path tracking control of tractor-trailer or tractor-implement combinations.

Source	Terrain	Controller Design Model	Actuators	Controlled Variables	Control Approach	Validation
[Der08, DB09]	off-road	dynamic tractor and three-point hitched implement model	tractor front wheels	tractor lateral error	PID control with MRAC for inner loop yaw rate controller adapting either feedforward or feedback gain	simulation, experiment
[GB08]	off-road	dynamic tractor and three-point hitched implement model	tractor front wheels	tractor lateral error	PD control with gain adapted according to EKF estimate of steering angle to yaw rate steady state gain	experiment
[HWTT03]	on-road	dynamic tractor and trailer model	tractor front wheels	tractor lateral error at look-ahead distance	robust H_∞ control (†), robust H_∞ control with gain scheduling, linear parameter varying control (†), others identical to [TT03]	simulation, experiment († only)
[KS10]	off-road	kinematic and dynamic tractor and implement model	tractor front wheels	all system states	LQR assuming ideal state feedback	simulation
[KT08, Dee11a]	off-road	geometric properties of tractor and implement	tractor front wheels	implement lateral error	commercial tractor path tracking controller fed with tractor lateral and heading error offsets to steer the implement, offset calculation based on slope angle, desired path and implement position measurements	product
[MM03]	on-road	dynamic tractor and trailer model	tractor front wheels	tractor lateral error at look-ahead distance	robust H_∞ control with disturbance feedforward	experiment
[Rek01]	off-road	dynamic tractor model, three-point hitched implement implicitly considered by adapted parameters	tractor front wheels	not stated	LQR with adaption based on EKF/LMS parameter estimation	experiment

Table A.9: Summary of literature on path tracking control of tractor-trailer or tractor-implement combinations.

Source	Terrain	Controller Design Model	Actuators	Controlled Variables	Control Approach	Validation
[RT07]	on-road	dynamic model of tractor and three trailers	manual tractor front wheel steering, automatic trailer front wheel steering for all or a subset of trailers	all system states, weights are chosen to minimize rearward amplification of trailer lateral accelerations for sinusoidal tractor steering inputs	LQR assuming ideal state feedback	simulation
[RZG12]	on-road	geometric properties of tractor and trailer	manual tractor front wheel steering, automatic trailer front wheel steering	trailer lateral error	geometry based feedforward control	simulation, experiment
[TWH⁺98]	on-road	dynamic tractor and trailer model	tractor front wheels	projected tractor lateral error at look-ahead distance	linear PD control with disturbance feedforward	simulation
[TT03]	on-road	dynamic tractor and trailer model	tractor front wheels	projected tractor lateral error at look-ahead distance	SMC, input-output linearization with cornering stiffness adaption or robust switching feedback, SMC plus backstepping to consider steering actuator dynamics, linear PD control (†), linear PD control with disturbance feedforward (†), input-output linearization with disturbance feedforward (†)	simulation, experiment († only)
[Tri10]	off-road	no details stated, geometric properties of tractor and implement	tractor front wheels	implement lateral error	no details stated, one controller gain parameter	product
[Tri07]	off-road	no details stated, geometric properties of tractor and implement	tractor front wheels, implement coulters	tractor and implement lateral error	decentralized control, no details stated, one implement controller gain parameter	product

Table A.9: Summary of literature on path tracking control of tractor-trailer or tractor-implement combinations.

Source	Terrain	Controller Design Model	Actuators	Controlled Variables	Control Approach	Validation
[Wag10]	on-road	dynamic tractor model with two trailers	tractor front wheels, trailer wheels	lateral error of tractor and either trailer heading or trailer lateral errors	MIMO controller with input-output linearizing feedforward and subsequent linear control of difference between desired and actual generalized vehicle coordinates, separate PD controllers for lateral errors at each axle	not stated

A.9 Path Tracking Control Patent Survey

Patents related to path tracking control of tractors and implements are summarized in Table A.10.

Table A.10: Summary of patents on tractor and implement steering and path tracking control.

Number	Date	Assignee	Title	Summary
EP1243171A3	2002-03-16	Deere & Company	Steuervorrichtung für eine Fahrzeuganbauschnittstelle	Rotation of three-point hitch to reduce turning radius with hitched implements
EP2025536B1	2008-08-07	Josef Kotte Landtechnik GmbH & Co. KG	Trailer with tow bar and angle sensor	Roll and pitch compensated hitch angle sensor
EP2243688A2	2009-04-20	Claas Selbstfahrende Erntemaschinen GmbH	Korrigierte Zwangslenkung für gelenkte Anhänger/Auflieger an mehrachsgelenkten land oder forstwirtschaftlichen Zugfahrzeugen	Forced steering for trailers used with front and rear axle steered tractors
EP2220924B1	2012-01-18	Deere & Company	System and method for variable steering on an implement	Implement steering depending on conditions e.g. tools ground engaging or not
US5240079	1993-08-31	A.I.L. Inc.	Guidance control system for farm tractor/implement combination having improved turnaround capability	Guidance of hitched and towed implements in row crops
US5476147	1995-12-19	Fixemer, R.A.	Guidance system for an agricultural implement	Side-shift steering for bedded crops
US5511623	1996-04-30	Orthman Manufacturing Inc.	Quick hitch guidance device	Rotateable three-point quick hitch
US5646845	1997-07-08	Caterpillar Inc.	System and method for controlling an autonomously navigated vehicle	GPS based vehicle speed and steering control
US5764511	1998-06-09	Caterpillar Inc.	System and method for controlling slope and cut of work implement	GPS based grader blade control
US6052647	2000-04-18	Stanford University	Method and system for automatic control of vehicles based on carrier phase differential GPS	Precise vehicle position control with carrier phase differential GPS
US6070673	2000-06-06	Case Corporation	Location based tractor control	GPS tillage depth control
US6434462B1	2002-08-13	Deere & Company	GPS control of a tractor-towed implement	GPS based control of an unsteered towed implement

Table A.10: Summary of patents on tractor and implement steering and path tracking control.

Number	Date	Assignee	Title	Summary
US7147241B2	2006-12-12	One Pass Implements Inc.	Steering device for towed implements	Wheel steering device for implement lateral control
US20080147281A1	2008-06-19	Deere & Company	Tracking system configured to determine a parameter for use in guiding an implement attached to a working machine	Towed implement geometric parameter identification using GPS
US7460942B2	2008-12-02	Hemisphere GPS LLC	Soil cultivation implement control apparatus and method	Implement position control of three-point hitched implement with side shift actuator
US7490678B2	2009-02-17	A.I.L. Inc.	GPS controlled guidance system for farm tractor/implement combination	Implement position control using rotatable three-point hitch
US7509199B2	2009-03-24	Deere & Company	System and method for calculating instantaneous placement corrections to achieve towed implement placement on curved paths	Unsteered implement lateral position control
US20120240546A1	2012-09-27	Deere & Company	Tractor implement combination	Control of wheel and drawbar steered implement
US20130110358A1	2013-05-02	Deere & Company	Arrangement for automatically steering a combination of a self-propelled vehicle and an implement for cultivating a field	Tractor and implement position control with separate paths and a side-shifted three point hitched implement
US20130186657A1	2013-07-25	Deere & Company	Combination of tractor and implement	Headland turns with steerable implements

Bibliography

[ABL04]   A. Astolfi, P. Bolzern, and A. Locatelli. Path-tracking of a tractor-trailer vehicle along rectilinear and circular paths: a Lyapunov-based approach. *Robotics and Automation, IEEE Transactions on*, 20(1):154–160, 2004.

[ACF07]   G. Antonelli, S. Chiaverini, and G. Fusco. A fuzzy-logic-based approach for mobile robot path tracking. *IEEE Transactions on Fuzzy Systems*, 15:211–221, 2007.

[Ada09]   J. Adami. *Nichtlineare Regelungen (in German)*. Springer, Heidelberg, DE, 2009.

[Aut08]   AutoFarm GPS Precision Farming, Fremont, US-CA. *Brochure: AF Tracker Implement Steering System*, 2008. `http://www.gpsfarm.com/LinkClick.aspx?fileticket=HZGDoAYG6Ow%3D&tabid=101` (Aug. 02, 2013).

[Aut12]   AutoFarm GPS Precision Farming, Fremont, US-CA. *Brochure: GeoSteer*, 2012. `http://www.gpsfarm.com/LinkClick.aspx?fileticket=NQSQqvFKrRc=&tabid=173` (Aug. 02, 2013).

[Bac13]   J. Backman. *Navigation System for Modular Agricultural Machines using Optimal Control Methods and Industrial Standard Network*. Ph.D. thesis, Aalto University, Espoo, FI, 2013.

[Bel99]   T. Bell. *Precision Robotic Control of Agricultural Vehicles on Realistic Farm Trajectories*. Ph.D. thesis, Stanford University, Stanford, US-CA, 1999.

[Bev01]   D.M. Bevly. *High Speed, Dead Reckoning, and Towed Implement Control for Automatically Steered Farm Tractors Using GPS*. Ph.D. thesis, Stanford University, Stanford, US-CA, 2001.

[BGW90]   R.R. Bitmead, M. Gevers, and V. Wertz. Adaptive Optimal Control: the thinking man's GPC. In M.J. Grimble, editor, *Series in Systems and Control Engineering*. Prentice Hall, Englewood Cliffs, US-NJ, 1990.

[BIT03]   A. Ben-Israel and Greville T.N.E. Generalized inverses: Theory and application. In *CMS books in mathematics*, volume 15. Springer, New York, US-NY, 2nd edition, 2003.

[BL74]   G. Bengtsson and S. Lindahl. A design scheme for incomplete state or output feedback with applications to boiler and power system control. *Automatica*, 10:15–30, 1974.

[Bot93]   H.-H. Bothe. *Fuzzy Logic (in German)*. Springer, Berlin, DE, 1993.

164

[BOV09]   J. Backman, T. Oksanen, and A. Visala. Parallel guidance system for tractor-trailer system with active joint. In E.J. van Henten, D. Goense, and C Lokhorst, editors, *Precision agriculture '09*, pages 615–622. Wageningen Academic Publishers, Wageningen, NL, 2009.

[BOV12]   J. Backman, T. Oksanen, and A. Visala. Navigation system for agricultural machines: Nonlinear model predictive path tracking. *Computers and Electronics in Agriculture*, (82):32–43, 2012.

[Bru11]   J. Bruinsma. The resources outlook: By how much do land, water and crop yields need to increase by 2050? In P. Conforti, editor, *Looking Ahead in World Food and Agriculture: Perspectives to 2050*, chapter 6, pages 233–278. Food and Agriculture Organization of the United Nations, Rome, IT, 2011.

[CLTM10] C. Cariou, R. Lenain, B. Thuilot, and P. Martinet. Path following of a vehicle-trailer system in presence of sliding: Application to automatic guidance of a towed agricultural implement. In *IEEE/RSJ International Conference on Intelligent Robots and Systems (IROS)*, pages 4976–4981. Taipei, TW, 2010.

[CT95a]   C. Chen and M. Tomizuka. Dynamic modeling of articulated vehicles for automated highway systems. In *American Control Conference*, pages 653–657. Seattle, US-WA, 1995.

[CT95b]   C. Chen and M. Tomizuka. Steering and braking control of tractor-semitrailer vehicles in automated highway systems. In *American Control Conference*, pages 658–662. Seattle, US-WA, 1995.

[CT00]   C. Chen and M. Tomizuka. Lateral control of commercial heavy vehicles. *Vehicle System Dynamics: International Journal of Vehicle Mechanics and Mobility*, 33:391–420, 2000.

[Dav70]   E.J. Davison. On pole assignment in linear systems with incomplete state feedback. *IEEE Transactions on Automatic Control*, pages 348–351, 1970.

[DB09]   J.B. Derrick and D.M. Bevly. Adaptive steering control of a farm tractor with varying yaw rate properties. *Journal of Field Robotics*, 26(6–7):519–536, 2009.

[DD11]   D.E. Davison and E.J. Davison. Optimal servomechanism control of plants with fewer inputs than outputs. In *Preprints of the 18th IFAC World Congress*, pages 11332–11337. 2011.

[Dee11a]   Deere & Company, Moline, US-IL. *iGuide Operator's Manual*, 2011. OMPFP10808 ISSUE J0 `http://stellarsupport.deere.com/en_US/support/pdf/om/en/ompfp10808_iGuide.pdf` (Aug. 02, 2013).

[Dee11b]   Deere & Company, Moline, US-IL. *StarFire 3000 Specification: System Positional Accuracy*, 2011. Revision F (Feb. 28, 2011).

[Dee12]   Deere & Company, Moline, US-IL. *AutoTrac Controller Operator's Manual*,
           2012. OMPFP12060 ISSUE B2, `http://stellarsupport.deere.com/en_`
           `US/support/pdf/om/en/ompfp12060_ATC.pdf` (Aug. 02, 2013).

[Dee13]   Deere & Company, Moline, US-IL. *Active Implement Guidance Operator's*
           Manual, 2013. OMPFP12957 ISSUE L2, `http://stellarsupport.deere.`
           `com/en_US/support/pdf/om/en/ompfp12957_aig.pdf` (Aug. 02, 2013).

[Der08]   J.B. Derrick. *Adaptive Control of a Farm Tractor with Varying Yaw Proper-*
           ties Accounting for Actuator Dynamics and Nonlinearities. Master's thesis,
           Auburn University, Auburn, US-AL, 2008.

[DG75]   E.J. Davison and A. Goldenberg. Robust control of a general servomechanism
           problem: The servo compensator. *Automatica*, 11:461–471, 1975.

[DGKF89]   J.C. Doyle, K. Glover, P.P. Khargonekar, and B.A. Francis. State-space so-
           lutions to standard H_2 and H_∞ control problems. *IEEE Transactions on*
           Automatic Control, 34:831–847, 1989.

[DIN94]   DIN 70000: Fahrzeugdynamik und Fahrverhalten: Begriffe, ISO 8855 Ausgabe
           1991, modifiziert, Januar 1994.

[Ell94]   J.R. Ellis. *Vehicle Handling Dynamics.* Mechanical Engineering Publications
           Limited, London, UK, 1994.

[Foe94]   O. Foellinger. *Regelungstechnik (in German).* Huethig, Heidelberg, DE, 8th
           edition, 1994.

[FPEN10]   G.F. Franklin, J.D. Powell, and A. Emami-Naeini. *Feedback Control of Dy-*
           namic Systems. Pearson, Upper Saddle River, US-NJ, 6th (international)
           edition, 2010.

[FW75]   B.A. Francis and W.M. Wonham. The internal model principle for linear
           multivariable regulators. *Applied Mathematics and Optimization*, 2:170–194,
           1975.

[GAP+05]   M. Gobbi, M. Aiolfi, M. Pennati, G. Previati, F. Levi, M. Ribaldone, and
           G. Mastinu. Measurement of the forces and moments acting on farm tractor
           pneumatic tyres. *Vehicle System Dynamics*, 43:412–433, 2005.

[GB08]   E. Gartley and D.M. Bevly. Online estimation of implement dynamics for
           adaptive steering control of farm tractors. *Mechatronics, IEEE/ASME Trans-*
           actions on, 13(4):429–440, 2008.

[Gen97]   G. Genta. Motor vehicle dynamics: Modeling and simulation. In *Series on*
           Advances in Mathematics for Applied Sciences, volume 43. World Scientific
           Publishing, Singapore, 1997.

[GKN+74]   A. Gelb, J.F. Kasper, R.A. Nash, C.F. Price, and A.A. Sutherland. *Applied*

Optimal Estimation. MIT Press, Cambridge, US-MA, 1974.

[Gre88] D.T. Greenwood. *Principles of Dynamics.* Prentice Hall, Upper Saddle River, US-NJ, 2nd edition, 1988.

[Hip06] P. Hippe. Windup in control. In M.J. Grimble and Johnson M.A., editors, *Advances in Industrial Control.* Springer, Berlin, DE, 2006.

[Hon13] Honeywell Sensing and Control, Golden Valley, US-MN. *6DF Series 6 Degrees of Freedom Inertial Measurement Unit, 6-D Motion Variant,* 000741-2-en edition, Jan. 2013.   `http://www.honeywellscportal.com/honeywell-sensing-inertial-measurement-unit-6df-productsheet-000741-2-en.pdf?name=6DF-1N6-C2-HWL` (May 13, 2014).

[HT94] T. Hessburg and M. Tomizuka. Fuzzy logic control for lateral vehicle guidance. *IEEE Control Systems,* 14:55–63, 1994.

[HT95] T. Hessburg and M. Tomizuka. An adaption method for fuzzy logic controllers in lateral vehicle guidance. *Mechatronics,* 5:873–898, 1995.

[HWTT03] P. Hingwe, J. Wang, M. Tai, and M. Tomizuka. *Lateral Control of Heavy Vehicles for Automated Systems: Final Report for MOU 313.* Research report, University of California, Berkeley, US-CA, 2003.

[Ise07] R. Isermann. *Mechatronische Systeme (in German).* Springer, Berlin, DE, 2nd edition, 2007.

[ISO09] ISO 11783-7:2009(E) Tractors and machinery for agriculture and forestry – Serial control and communications data network – Part 7: Implement messages application layer, May 2009.

[KS10] M. Karkee and B.L. Steward. Study of the open and closed loop characteristics of a tractor and a single axle towed implement system. *Terramechanics,* 47:379–393, 2010.

[KT08] G. Kormann and R. Thacher. Development of a passive implement guidance system. In *Agricultural and biosystems engineering for a sustainable world. International Conference on Agricultural Engineering.* Hersonissos, Crete, 2008.

[Lee90a] C.C. Lee. Fuzzy Logic in Control Systems: Fuzzy Logic Controller – Part I. *IEEE Transactions on Systems, Man, and Cybernetics,* 20:404–418, 1990.

[Lee90b] C.C. Lee. Fuzzy Logic in Control Systems: Fuzzy Logic Controller – Part II. *IEEE Transactions on Systems, Man, and Cybernetics,* 20:419–435, 1990.

[LGB14] LGB – Landesamt für Geologie und Bergbau, Rheinland-Pfalz, Mainz, DE. *Bodenflächendaten der landwirtschaftlichen Nutzfläche – BFD5L,* 2014. `http://mapclient.lgb-rlp.de/?app=lgb&view_id=18` (Apr. 26, 2014).

[Lun08]   J. Lunze. *Regelungstechnik 1 (in German)*. Springer, Heidelberg, DE, 7th edition, 2008.

[Lun10]   J. Lunze. *Regelungstechnik 2 (in German)*. Springer, Heidelberg, DE, 6th edition, 2010.

[Mac02]   J.M. Maciejowski. *Predictive Control with Constraints*. Pearson Education Ltd., Harlow, GB-ESS, 2002.

[Mac04]   U. Mackenroth. *Robust Control Systems*. Springer, Berlin, DE, 2004.

[Mam96]   S. Mammar. H_∞ robust automatic steering of a vehicle. In *IEEE Intelligent Vehicles Symposium*, pages 19–24. Tokyo, JP, 1996.

[May82]   P.S. Maybeck. Stochastic models, estimation, and control volume 2. In R. Bellman, editor, *Mathematics in Science and Engineering*, volume 141-2. Academic Press, New York, US-NY, 1982.

[Mer04]   R.v.d. Merwe. *Sigma-Point Kalman Filters for Probabilistic Inference in Dynamic State-Space Models*. Ph.D. thesis, Oregon Health and Science University, Portland, US-OR, 2004.

[MG90]   D.C. McFarlane and K. Glover. Robust controller design using normalized coprime factor plant descriptions. In M. Thoma and A. Wyner, editors, *Lecture Notes in Control and Information Sciences*, volume 138. Springer, Berlin, DE, 1990.

[MM03]   S. Martini and V. Murdocco. Lateral control of tractor-trailer vehicles. In *IEEE Conference on Control Applications*, pages 269–273. Istanbul, TR, 2003.

[MSC12]   MSC Software Corporation, Santa Ana, US-CA. *Adams/Car Data Sheet*, 2012. http://www.mscsoftware.com/sites/default/files/ds_adams-car_ltr_w.pdf (Aug. 06, 2013).

[MW04]   M. Mitschke and H. Wallentowitz. *Dynamik der Kraftfahrzeuge (in German)*. Springer, Berlin, DE, 4th edition, 2004.

[Nai02]   D.S. Naidu. *Optimal Control Systems*. CRC Press, Boca Raton, US-FL, 2002.

[OIU96]   R.T. O'Brien, P.A. Iglesias, and T.J. Urban. Vehicle lateral control for automated highway systems. *IEEE Transactions on Control Systems Technology*, 4:266–273, 1996.

[Pac06]   H. Pacejka. *Tyre and Vehicle Dynamics*. Butterworth-Heinemann, Oxford, UK, 2nd edition, 2006.

[Pfr13]   C. Pfrang. *Dynamic Model Parameter Identification for a Farm Tractor Towing a Steerable Implement*. Diploma thesis, University of Kaiserslautern, Kaiserslautern, DE, 2013.

[PKE07] H. Pota, J. Katupitiya, and R. Eaton. Simulation of a tractor-implement model under the influence of lateral disturbances. In *46th IEEE Conference on Decision and Control*, pages 596–601. New Orleans, US-LA, 2007.

[PTVF07] W.H. Press, S.A. Teukolsky, W.T. Vetterling, and B.P. Flannery. *Numerical Recipies*. Cambridge, Cambridge, UK, 3rd edition, 2007.

[Raj06] R. Rajamani. *Vehicle Dynamics and Control*. Springer, New York, US-NY, 1st edition, 2006.

[Rek01] A.K.W Rekow. *System Identification, Adaptive Control and Formation Driving of Farm Tractors*. Ph.D. thesis, Stanford University, Stanford, US-CA, 2001.

[RT07] K. Rangavajhula and H.-S.J. Tsao. Active trailer steering control of an articulated system with a tractor and three full trailers for tractor-track following. *International Journal of Heavy Vehicle Systems*, 14:271–293, 2007.

[RZG12] T. Reich, X. Zhang, and M. Geimer. Driver assistance system for long timber vehicles. *ATZ offhighway*, April:78–87, 2012.

[SAG97] V.L. Syrmos, C.T. Abdallah, and K. Grigoriadis. Static output feedback – a survey. *Automatica*, 33:125–137, 1997.

[Sch05] V. Schlotter. *Einfluss dynamischer Radlastschwankungen und Schräglaufwinkeländerungen auf die horizontale Kraftübertragung von Ackerschlepperreifen (in German)*. Ph.D. thesis, Universität Stuttgart, Stuttgart, DE, 2005.

[SIM11] SIMPACK AG, Gilching, DE. *Brochure: SIMPACK AUTOMO-TIVE*, 2011. `http://www.simpack.com/fileadmin/simpack/doc/flyer/Automotive_Flyer.pdf` (Aug. 06, 2013).

[SKEP09] K.W. Siew, J. Katupitiya, R. Eaton, and H. Pota. Simulation of an articulated tractor-implement-trailer model under the influence of lateral disturbances. In *IEEE/ASME International Conference on Advanced Intelligent Mechatronics (AIM 2009)*, pages 951–956. Singapore, 2009.

[SL91] J.-J.E Slotine and W. Li. *Applied Nonlinear Control*. Prentice-Hall, Upper Saddle River, US-NJ, 1991.

[Sni09] J.M. Snider. *Automatic Steering Methods for Autonomous Automobile Path Tracking*. Report CMU-RI-TR-09-08, Robotics Institute, Carnegie Mellon University, Pittsburgh, US-PA, 2009.

[Top12] Topcon Precision Agriculture. *System 350 X30 Console Operator's Manual, Guidance and auto steering*, 2012. P/N AGA4084-EN Rev. 1.5.1 `http://ag.topconpositioning.com/sites/default/files/AGA4084_X30_Guidance_`

`and_Autosteering_OpM_V1-5-1.pdf` (Aug. 02, 2013).

[Tri01]   Trimble Navigation Limited, Sunnyvale, US-CA. *AgGPS Autopilot Opera-tion Manual*, 2001. P/N 43099-00-ENG Rev. A `http://trl.trimble.com/docushare/dsweb/Get/Document-270852/AutoPilot.pdf` (Aug. 02, 2013).

[Tri07]   Trimble Navigation Limited, Sunnyvale, US-CA. *AgGPS TrueTracker Implement Steering System User Guide*, 2007. P/N 54065-30-E03 Revision A `http://trl.trimble.com/docushare/dsweb/Get/Document-392919/AgGPSTrueTracker_1A_UserGuide_54065-30-E03.pdf` (Aug. 02, 2013).

[Tri10]   Trimble Navigation Limited, Sunnyvale, US-CA. *AgGPS FmX with the AgGPS TrueGuide System Quick Reference Card*, 2010. P/N 93020-87-E03 Revision A `http://trl.trimble.com/docushare/dsweb/Get/Document-466299/93020-87-E03_AgGPSFMXwithTrueGuide_3A_LR.pdf` (Aug. 02, 2013).

[TT03]   M. Tai and M. Tomizuka. *Robust Lateral Control of Heavy Duty Vehicles: Final Report.* Research report, University of California, Berkeley, US-CA, 2003.

[TWH+98] M. Tai, J.-Y. Wang, P. Hingwe, C. Chen, and M. Tomizuka. *Lateral Control of Heavy Duty Vehicles for Automated Highway Systems.* Research report, University of California, Berkeley, 1998.

[Wag10]   S. Wagner. Entwurf einer modellbasierten Steuerung zur hochgradig spurtreuen Fuehrung n-gliedriger, mehrachsgelenkter Fahrzeuge (in German). *mechatronik mobil*, 1:3–11, 2010.

[Wen11]   J. Wendel. *Integrierte Navigationssysteme (in German).* Oldenbourg, München, DE, 2011.

[Won67]   W.M. Wonham. On pole assignment in multi-input controllable linear systems. *IEEE Transactions on Automatic Control*, 12:660–665, 1967.

[Won08]   J.Y. Wong. *Theory of Ground Vehicles.* Wiley, Hoboken, US-NJ, 4 edition, 2008.

[WOS+10] U. Wuster, M. Ortlechner, B. Schick, E. Drenth, and J. Crawley. Simulations-basierte Homologation von Bremsen für LKW-Anhänger (in German). *ATZ*, 9:656–660, 2010.

List of Advised Theses

The following theses have been advised by the author and contributed to this work:

- Deepak Devendran, *Path Tracking Control of Tractors and Steerable Implements Using State Feedback and Observers*, Projektarbeit, 2012

- Immanuel Deepan Morais, *Feedforward Control of Tractors and Steerable Implements on Curved Paths*, Projektarbeit, 2013

- Christoph Pfrang, *Dynamic Model Parameter Identification for a Farm Tractor Towing a Steerable Implement*, Diplomarbeit, 2013

- Daniel Magar, *Modeling of Longitudinal and Lateral Dynamics of a Tractor and a Towed Implement*, Diplomarbeit, 2014

Curriculum Vitae

Roland Werner, geboren am 29.06.1983 in Erlangen

Berufstätigkeit

seit 06/2014	Controls Engineer, John Deere GmbH & Co. KG, Kaiserslautern
01/2011 – 05/2014	Wissenschaftlicher Mitarbeiter,
	Lehrstuhl für Mechatronik in Maschinenbau und Fahrzeugtechnik,
	Technische Universität Kaiserslautern
10/2009 – 12/2010	Ingenieur, ITK Engineering AG, Martinsried b. München

Hochschulbildung

10/2003 – 08/2009	Studium der Elektrotechnik, Elektronik und Informationstechnik,
	Friedrich-Alexander-Universität Erlangen-Nürnberg,
	Abschluss: Diplom-Ingenieur
	Diplomarbeit: Modellierung und Simulation eins Herz-Kreislauf-Unterstützungssystems bei der Fontan-Zirkulation
	Studienarbeit: Iterativ lernende Regelung eines hydraulischen Zylinderantriebs

Schulbildung und Zivildienst

07/2002 – 04/2003	Zivildienst, ASB Herzogenaurach
10/1993 – 06/2002	Gymnasium Herzogenaurach, Abschluss: Abitur

Veröffentlichungen

- R. Werner, G. Kormann, and S. Mueller. Dynamic modeling and path tracking control for a farm tractor towing an implement with steerable wheels and steerable drawbar. In *2nd Commercial Vehicle Technology Symposium*, pages 241-–250. Kaiserslautern, DE, 2012.

- R. Werner, G. Kormann, and S. Mueller. Path tracking control of tractors and steerable implements based on kinematic and dynamic modeling. In *11th International Conference on Precision Agriculture*. Indianapolis, US-IN, 2012.

- R. Werner, G. Kormann, and S. Mueller. Systematic model based path tracking control of actively steered implements in simulation and experiment. In *IFAC Agricontrol*. Espoo, FI, 2013.

Kaiserslautern, 21.05.2015

Wachstum durch Innovation — EFRE

Rheinland**P**falz